UNIVERSITY OF SOUTHAMPTON

Numerical Simulation of Complex Microelectrode Geometries

John Neil Angus, B.Sc.

Submitted for the degree of Ph.D.
Chemistry Department, Faculty of Science, March 2002

UNIVERSITY OF SOUTHAMPTON

ABSTRACT

FACULTY OF SCIENCE

CHEMISTRY

Doctor of Philosophy

NUMERICAL SIMULATION OF COMPLEX MICROELECTRODE GEOMETRIES

by John Neil Angus

The Boundary Element Method (BEM), a numerical method developed in engineering fields, is capable of modelling complex geometrical domains. In this thesis, the BEM is described from an electrochemical perspective and applied to simulation of electrochemical systems.

The properties of the BEM for electrochemical simulation are compared to the most common numerical methods used in electrochemistry and engineering fields; the Finite Difference Method, and the Finite Element Method respectively. The mathematical relation of these three methods is highlighted through a Weighted Residual formulation.

Steady state diffusion at a generator-collector double microband for a diffusion limited reaction is used to validate a two-dimensional BEM model, and investigate mesh discretisation effects. Optimisation of the mesh and implementation of higher order boundary elements are reported.

The two-dimensional steady state model is applied to simulate a variety of microband systems, including Inter-Digitated Arrays, realistic (imperfect) electrode geometries and a novel generator-collector microband array.

An advanced variation of the BEM, the Dual Reciprocity Method (DRM), is described and applied to model a channel flow cell. Due to instability, the method is found inadequate to simulate this system. The details required to extend the DRM for transient systems are also described.

The three-dimensional BEM is implemented and validated. The ability to model any three-dimensional domain has significant potential for simulation of complex geometrical systems in electrochemistry. The extension of the BEM to model multiple species and electrochemical mechanisms, and the future direction and relevance of the BEM as an electrochemical simulation method are discussed.

Acknowledgements

I would like to thank Guy, for his advice and friendly, sociable approach. To those with whom I have worked in the lab; Stuart E, Stuart A, Pete and Terry, thanks for the laughs and happy times. Also to Jon, in addition, I will fondly remember the conferences and travels.

I feel I owe a particular debt of gratitude to my parents, Jan and Donald, for being so supportive throughout my university years. You are the most generous of people and I am fortunate to have you as parents. I would also like to thank my brothers, Ian and James, for many happy memories.

Finally, to Amy, there is not enough space to acknowledge all of your contributions whilst I was studying. Suffice to say thankyou for the fun and relaxation, the consideration and understanding.

Contents

List of Figures viii

List of Tables x

List of Symbols xi

Standard Abbreviations xvi

Introduction **1**

Theoretical Electrochemistry 1

Numerical Methods 2

Why use the Boundary Element Method? 3

Background of the Boundary Element Method 5

1 Numerical Simulation of Electrochemical Processes **7**

1.1 Characteristics of Electrochemical Systems 7

1.1.1 Electrochemical Techniques 7

1.1.2 Electrode Geometry 8

1.1.3 Mechanism 9

1.2 Mathematical Modelling of the Electrochemical System 10

1.2.1 Mass Transport 10

1.2.2 Domains 11

1.2.3 Fick's Second Law 12

1.2.4 Governing Partial Differential Equation 14

1.2.5 Solution of Partial Differential Equations 17

1.2.6 Current 18
1.2.7 Analytical Solution of the Diffusion Equation in One Dimension 19
1.2.8 Simple Simulation of the Diffusion Equation in One Dimension 21
1.2.9 Dimensionless Parameters 26
1.3 Review of Simulation Techniques 29
1.3.1 Finite Difference Method 29
1.3.2 Random Walk 31
1.3.3 Weighted Residual Methods 32
1.4 Comparison of Finite Difference, Finite Element and Boundary Element Methods 34
1.4.1 Introduction 34
1.4.2 Domain Discretisation 36
1.4.3 Optimisation for Electrochemical Geometries 38
1.4.4 Formulations of the Methods 42
1.4.5 Application of the methods to typical electrochemical partial differential equations 46
1.4.6 Summary 47

2 The Application of the Boundary Element Method in Electrochemistry 48

2.1 Fundamentals of the Boundary Element Method 50
2.1.1 The Fundamental Solution 51
2.2 BEM Implementation in Two Dimensions 54
2.2.1 2D Fundamental Solution and its Derivative 60
2.2.2 Singular Integration 60
2.2.3 Numerical Integration 61
2.2.4 Formation of Influence Coefficient Matrices 63
2.2.5 Boundary Solution 63
2.2.6 Internal Points 64

2.2.7 Application to a Simple Case 65
2.3 Domain Meshing 68
2.4 Computational Aspects 70
2.4.1 Matrix Solving Routines 70
2.5 Validation of the Method 73
2.5.1 The Double Microband 73
2.5.2 Discretisation Effects 77
2.5.3 Validation 98
2.6 Microband Arrays 100
2.6.1 Arrays of Generator-Collector Pairs 101
2.6.2 Arrays of Collectors Surrounding a Central Generator 106
2.7 Raised and Recessed Double Electrodes 109
2.7.1 Discretisation of the Domain 110
2.7.2 The Effect of Electrode Height 112
2.8 Novel Raised Band Configurations 116
2.8.1 Multiple Bands 118
2.9 Double Microband Scan 120
2.10 Refinements and Limitations 123
2.10.1 Linear Elements 123
2.10.2 Limitations 128

3 Chapter Three - The Dual Reciprocity Method 130

3.1 Introduction 130
3.1.1 Historical Background 131
3.1.2 The DRM Applied to Electrochemistry 131
3.2 Dual Reciprocity Method Formulation 133
3.2.1 Governing Partial Differential Equation 133
3.2.2 The f Approximating Function 134

3.2.3 Formation of the Boundary Integral Equation 136

3.3 Application to the Steady State Diffusion-Convection Equation 142

3.4 Program Structure 144

3.4.1 Efficiency and Performance 144

3.4.2 DRM Linear Matrix Solving Routines 144

3.5 Channel Flow Electrodes 147

3.5.1 Governing Partial Differential Equation 148

3.5.2 Simulation Domain and Boundary Conditions 152

3.6 Validation of the Dual Reciprocity Method Applied to Convection 154

3.6.1 Analytical Approximations 154

3.6.2 Semi-Infinite Boundary Distances 156

3.6.3 Internal Points 159

3.6.4 The f Approximating Function 161

3.6.5 Parabolic Flow and High Flow Rates 162

3.7 Conclusions 164

3.7.1 Channel Flow Cell Model 164

3.7.2 General Dual Reciprocity Method 165

4 Conclusion: The Future of BEM in Electrochemistry **167**

4.1 Time-Dependent Systems 169

4.1.1 The DRM Applied to the Diffusion Equation 169

4.2 Three Dimensional Boundary Element Method 173

4.2.1 Three Dimensional BEM Formulation 173

4.2.2 Results 177

4.3 Computational Aspects of Numerical Methods 181

4.4 The Boundary Element Method in Electrochemistry 183

4.4.1 Electrochemical Mechanisms 183

4.4.2 Electrochemical Techniques 184

4.4.3 Distinguishing Features of the Boundary Element Method 185

A The Formulation of Weighted Residual Numerical Methods 188

A.1 Numerical Methods 188

A.2 Notation 189

A.3 Approximate Solutions 190

A.3.1 Linear Independence and Completeness 191

A.4 Method of Weighted Residuals 191

A.4.1 The Collocation Method 192

A.4.2 Galerkin's Method 194

A.4.3 Properties of Approximating Functions and Weighting Functions 194

A.5 The Weak Formulation 196

A.6 The Inverse Formulation 197

A.7 Classification of Approximate Methods 199

List of Figures

1.1 Derivation of Fick's Second Law; flux through a volume 13

1.2 EFD discretisation in one dimension 22

1.3 A simple finite difference approximation 23

1.4 A comparison of FDM, FEM and BEM discretisations 37

1.5 Three dimensional discretisation primitives for FDM, FEM and BEM 39

1.6 Adaptive strategy used in previous electrochemical FEM simulations . 41

1.7 Relation of FDM,FEM and BEM through the Method of Weighted Residuals 43

2.1 A Thin Layer Cell 49

2.2 Summary of the BEM procedure 49

2.3 Heaviside step function and Dirac delta function 52

2.4 Thin layer cell domain 54

2.5 Definition of the internal angle 57

2.6 The outward normal 58

2.7 The procedure for numerical integration 59

2.8 Gaussian quadrature 62

2.9 Internal points mesh 65

2.10 The double microband domain 73

2.11 A convergence test for the double microband model, using equal sized elements 79

2.12 The effect of α on exponential spacing 81

2.13 Fixed Ratio and Fixed Shape exponential mesh types 82

2.14 The effect of using an exponential mesh over various boundary sections 83

2.15 Local mesh refinement 87

2.16 Concentration profile for fixed concentration boundary condition . . . 90

2.17 Concentration map for fixed concentration boundary condition 91

2.18 Concentration profile for zero flux boundary condition 92

2.19 Thin Layer Cell comparison for a Double Microband 93

2.20 Concentration map for fixed concentration boundary condition 94

2.21 Concentration and flux variation as a function of element number, fixed concentration semi-infinite boundary condition 96

2.22 Concentration and flux variation as a function of element number, zero flux semi-infinite boundary condition 97

2.23 Validation of the double microband BEM method 99

2.24 Multiple electrode domain: generator-collector pairs 102

2.25 Current response with increasing generator-collector pairs 102

2.26 The variation of the ratio of average generator current to double microband current with gap distance 105

2.27 The variation of the ratio of average generator current to an infinite array (IDA) current with gap distance 105

2.28 Multiple electrode domain: central generator surrounded by collectors 106

2.29 Current response with increasing surrounding collector electrodes . . 107

2.30 The variation of the ratio of the generator current and triple microband current with gap distance 108

2.31 A description of the two types of raised/recessed electrodes simulated 109

2.32 The far field domain parameters used in section 2.7 111

2.33 The effect of raised or recessed electrode geometries 113

2.34 The effect of varying gap distance for type 'All' double micrband . . . 114

2.35 The relation of current to gap distance relative to an inlaid DMB . . 115

2.36 A description of electrode type 'sides' 116

2.37 The variation of current with increasing electrode height for three configurations of double raised microbands 117

2.38 The variation of current with increasing electrode height for three configurations of four raised microbands 119

2.39 The scanning probe domain 120

2.40 Current response of the scanning probe 121

2.41 Concentration maps of the scanning probe domain 121

2.42 Different boundary element types 124

2.43 A comparison of constant and linear element discretisation 126

2.44 Definition of the outward normal for linear elements 128

2.45 A comparison of the effect linear and constant element types 129

3.1 DRM domain discretisation 138

3.2 A schematic showing the difference in source point, s and DRM summation point, k 139

3.3 Structure of the DRM formulation 145

3.4 A typical channel flow cell 147

3.5 The parabolic flow profile 149

3.6 The channel microband domain 152

3.7 Current response for increasing semi-infinite boundary length 156

3.8 Internal domain point distribution 159

3.9 Current response for increasing the number of internal points 160

4.1 Boundary element types for three-dimensional surface discretisation . 173

4.2 A typical mesh discretisation for the planar diffusion test case 177

4.3 Simple discretisation of the cube domain used for the planar diffusion test case 178

List of Tables

1 Greek Symbols xi

2 Roman Symbols xii

2.1 Definition of the domain boundary for the Thin Layer Cell model shown in figure 2.4 54

2.2 Concentration and flux values for the simplest possible two dimensional domain, figure 2.4 66

2.3 A description of the steps in a constant element Boundary Element Method program 71

2.4 Boundary conditions for the double microband simulation 78

2.5 The effect of section ratio discretisation 84

2.6 Current values with increasing the number of elements over the electrodes only 84

2.7 The effect of exponential spacing over both electrodes only 85

2.8 A comparison of equal and exponential mesh spacing over the electrodes 86

2.9 The effect of local mesh refinement over insulator and generator boundary sections 87

2.10 Parameters used in figures 2.21 and 2.22. 95

2.11 Parameters used for multiple electrode simulations 101

2.12 The current at each electrode of generator-collector arrays 103

2.13 Selected electrode currents for large values of N_{pairs} 104

2.14 The dimensionless current at electrodes for the array in figure 2.28 . . 108

2.15 Parameters used for raised and recessed microband simulations 111

2.16 Components of the total flux at different configurations of raised microbands, from figure 2.37 118

3.1 Summary of proposed f functions 136

3.2 Optimal f functions 137

3.3 Increasing semi-infinite boundary distance for the channel flow model 157

3.4 Local point distribution variation 161

3.5 Behaviour of f approximating functions 162

4.1 The coordinates of nodes covering two faces of the cube modelled . . 179

4.2 The concentration and flux values at triangle element centroids 180

List of Symbols

Mathematical Notation

A matrix is defined as sans-serif typeface, such as A, a vector is bold typeface, for instance, $\boldsymbol{b}$.

Greek Symbols

Table 1: Greek Symbols

Symbol	Meaning	Usual Dimensions	Section References
α	a) exponential expansion coefficient		2.5.2
	b) coefficient used in the DRM		3.2.1, 3.2.3
Γ	boundary		2.2
Γ_j	boundary along element j		2.2
δ	Dirac delta function		2.1
η	local coordinate system for linear element integration		2.10.1
θ	a) internal angle	radians	2.2
	b) time marching parameter		4.1.1
λ	finite difference coefficient		1.2.8
ν	dimensionless flow rate		3.2.1
ξ_1, ξ_2	source point coordinates		2.2, 3.2.1
τ	dimensionless time		1.2.9
Φ	potential	V	1.2.1
ϕ	basis function for linear elements		2.10.1
Ω	internal domain		2.2
ω	quadrature weighting coefficient		2.2.3

Roman Symbols

Table 2: Roman Symbols

Symbol	Meaning	Usual Dimensions	Section References
A	combined unknown boundary value coefficients		2.2.5, 2.4, 3.4.2
A	area; usually of an electrode	cm^2	1.2
$\boldsymbol{B}$	combined known boundary value coefficients		2.2.5, 2.4, 3.4.2
B	the boundary terms of the Inverse Formulation		2.1
b	partial differential equation function, known in engineering fields as a *forcing* function		3.2.1
$\hat{\mathsf{C}}$	matrix of approximate particular solution vectors		3.2.3
C	a) concentration b) collector electrode	$mol\ cm^{-3}$	1.2.1, 3.5.1 2.6
C_A	concentration of species A	$mol\ cm^{-3}$	1.2.1, 2.2
C_A^*	concentration of species A in bulk solution	$mol\ cm^{-3}$	1.2.6, 1.2.9
$\boldsymbol{c}$	concentration vector		2.2.4, 3.2.1
$\hat{\boldsymbol{c}}$	approximate particular solution vector		3.2.1
c_A	dimensionless concentration of species A		1.2.9
c_A^*	dimensionless concentration of species A in bulk solution		1.2.9
$\hat{c}$	particular solution to a partial differential equation		3.2.1, 3.2.3
D	domain integrals matrix		3.2.3
D_A	diffusion coefficient of species A	$cm^2\ s^{-1}$	1.2.1, 3.5.1
d	a) geometry coefficient b) length of channel in a channel flow cell	 cm	 2.2, 3.2.3 3.5
e^-	an electron		1.2
F	particular solutions matrix		3.2.3
F	a) the Faraday; charge on one mole of electrons	$C\ mol^{-1}$	1.2.1
	b) flux	$mol\ cm^{-2}\ s^{-1}$	1.2.1

continued on the following page

Table 2: *continued*

Symbol	Meaning	Usual Dimensions	Section References
f	approximation function for DRM		3.2.1, 3.2.2, 3.6.4
G	generator electrode		2.6
g	a) gap between electrodes		2.5.1
	b) integer counter for gaussian integration		2.2.3
H	Heaviside step function		2.1
h	a) height of probe above substrate		2.9
	b) half height of the channel flow cell		3.5.2, 3.5
h_e	electrode height (depth if negative)		2.7.2
h_i	length of the insulating block above an electrode		2.8
I	number of DRM internal points		3.2.3
i	a) current	A	1.2.6
	b) integer counter for coordinate, x, starting at zero		1.2.8
i_{avg}	average current of *either* the collector or generator electrodes at an array		2.6
i_{coll}	current at the collector electrode		2.5.3
i_{dmb}	double microband current		2.5.1
i_{gen}	current at the generator electrode		2.5.3
i_{norm}	normalised current		1.2.9, 2.5.1, 3.5.2
i_{tmb}	triple microband current		2.6.2
J	Jacobian		4.2
j	a) integer counter for time, t, starting at zero		1.2.9
	b) field point		2.2, 3.2.3
k	a) homogeneous chemical reaction rate	depends on order	1.2.4
	b) heterogeneous chemical reaction rate	cm s^{-1}	1.2.4
	c) dual reciprocity method field point		3.2.3
L	W influence coefficient matrix incorporating the diagonal term		2.2.4, 3.2.3
$\mathcal{L}(f)(s)$	Laplace transform		1.2.7
L	length of microband electrode	cm	1.2.9

continued on the following page

Table 2: *continued*

Symbol	Meaning	Usual Dimensions	Section References
L_s	length of a source point element		2.2.2
l	a) characteristic length of a microelectrode		1.2.9
	b) dimensionless length of 1D domain		2.1
l_e	length element e		
l_{sj}	W influence coefficient term incorporating the diagonal term		2.2.4, 3.2.3
$\hat{l}_{sj}$	W influence coefficient term		2.2.4, 3.2.3
M	q^* influence coefficient matrix		2.2.4, 3.2.3
m_{sj}	q^* influence coefficient term		2.2.4, 3.2.3
N	total number of boundary elements		2.2, 3.2.3
N_{int}	number of internal points for a DRM domain		3.5.2
N_{pairs}	number of repetitive pairs in a multiple electrodes domain		2.6
NE_{elec}	number of elements over each electrode		2.5.1
$NE_{section}$	number of elements along a boundary section		2.5.2
NI	number of numerical integration points		2.2.3
n	a) number of electrons		1.2.6
	b) outward normal		2.2
n_x , n_y	directional cosines		2.2.1
p	perpendicular distance from source point to the plane passing through a three-dimensional element		4.2
p_1, p_2	flow rate normalising parameters		3.5.1
P_s	Peclet number		3.5.1
$\hat{\mathsf{Q}}$	matrix of approximate particular solution derivative vectors		3.2.3
$\boldsymbol{q}$	flux vector		2.2.4, 3.2.3
$\hat{\boldsymbol{q}}$	approximate particular solution vector		3.2.3
$\hat{q}$	derivative of $\hat{c}$ with respect to the outward normal		2.2, 3.2.3
q_A	dimensionless flux of species A		2.2
q^*	derivative of the weighting function W		2.2, 3.2.3

continued on the following page

Table 2: *continued*

Symbol	Meaning	Usual Dimensions	Section References
R	a) gas constant	J mol^{-1} K^{-1}	1.2.1
	b) residual error		1.4.4
r	distance from source to field points		2.2.1, 3.2.2
s	source point		2.2
T	temperature	K	1.2.1
t	time	s	1.2
v_0	flow rate at the centre of a channel flow cell when considering a parabolic flow profile	cm s^{-1}	3.5.1
v	velocity	cm s^{-1}	1.2.1
v_f	flow rate normalising parameter	cm^3 s^{-1}	3.5.1
v_x	flow rate profile	cm s^{-1}	3.5.1
W	weighting function used in the Method of Weighted residuals		2.1, 2.1.1, 2.2.1, 3.2.3
w	width of electrode	m	1.2.9
w_{dmb}	width of substrate DMB electrode		2.9
w_p	width of probe		2.9
$\boldsymbol{x}$	unknown boundary value vector		2.2.5, 2.4, 3.4.2
X, Y, Z	dimensional cartesian coordinates	m	1.2.9, 2.5.1, 3.5.1
x, y, z	cartesian coordinates		1.2
x_{coll}	collector electrode coordinate		2.5.1, 2.5.2
x_{ds}	downstream boundary in a channel flow cell		3.5, 3.5.2
x_{fbr}	far boundary, right coordinate		2.5.1, 2.5.2
x_{fbl}	far boundary, left coordinate		2.5.1, 2.5.2
x_{gen}	generator electrode coordinate		2.5.1, 2.5.2
x_{gap}	gap coordinate		2.5.1, 2.5.2
x_{local}, y_{local}	dimensions of local internal point distribution mesh		3.6.3
x_{us}	upstream boundary in a channel flow cell		3.5, 3.5.2
x_w	width of microband electrode		2.5.1, 2.5.2, 3.5, 3.5.2
y_{wall}	wall coordinate		2.5.1, 2.5.2
z	charge on a species		1.2.1

Standard Abbreviations

Abbreviation	Definition	Section References
ATPS	Augmented Thin Plate Spline	3.2.2
BC	Boundary Condition	1.2.2
BEM	Boundary Element Method	1.4, 2
BIE	Boundary Integral Equation	2.1, 2.2, 3.2.3, 4.1.1, 4.2
CGS	Conjugant Gradient Squared	3.4.2
DMB	Double Microband	2.5.1
DRM	Dual Reciprocity Method	3
FDM	Finite Difference Method	1.2.8, 1.4
FEM	Finite Element Method	1.4
GMRES	Generalised Minimum Residual	3.4.2
IDA	Interdigitated Array	2.6
RBF	Radial Basis Function	3.2.2
RDE	Rotating Disc Electrode	3.5
SECM	Scanning Electrochemical Microscope	2.9
TLC	Thin Layer Cell	2
TMB	Triple Microband	2.6.2
TPS	Thin Plate Spline	3.2.2

Introduction

The aim of the work presented in this thesis was to investigate the applicability and possible benefits of the Boundary Element Method to simulate electrochemical systems.

This technique has primarily been developed through engineering research; the presentation contained herein is intended to explain the theory and implementation of the Boundary Element Method in terms that are familiar to an audience with an electrochemistry background.

To facilitate understanding the significance of the Boundary Element Method for electrochemistry the technique is placed within the context of alternative simulation methods. Further, conclusions are drawn on which simulation techniques will be most useful for future electrochemical simulation development.

Theoretical Electrochemistry

An electrochemical experiment is described by an experimental technique and a theoretical model. A description of experimental techniques is beyond the scope of this thesis; details may be found in various standard texts.[1,2] The model usually consists of an equation or set of equations which describe the system. Solving these equations provides a comprehensive theoretical description. A solution may be obtained either analytically, by derivation, or approximately by use of an analytical approximation or numerical method. It is only possible to derive analytical solutions for relatively simple systems, thus approximations are required for many electrochemical models.

An approximate analytical solution involves derivation of a semi-analytical solution through the use of defined approximations. It is important to distinguish the definition of this term from that of an analytical solution. An analytical solution may be derived from a simplified set of equations, which have been obtained using an approximation of the original equations which describe the model. This solution is exact for the *simplified* equations. An approximate analytical solution uses approximations as part of the derivation, and is not exact.

Approximate numerical methods reduce the degrees of freedom of the concentration field (and any other fields) described by the original equations to a finite number; the manner in which this is achieved depends on the particular method. This concept is explained in detail in section 1.4 on page 34. The application of a numerical method is referred to as a simulation.

Numerical Methods

Electrochemical simulation is an important tool for modelling electrochemical systems, enabling a solution to theoretical models that are analytically intractable. There are a wide variety of numerical methods, ranging from simple direct approximation of the original equations[1] to complex integral equation techniques[3] and statistical methods.[4] Simple numerical methods were applied to electrochemistry[5] as far back as the 1960's, significant breadth of application and more advanced techniques[6] occurred during the 1980s, with the advent of inexpensive computers. There has been continued development of electrochemical simulation techniques[7] throughout the 1990s. A variety of free[7,8] and commercial[9] software is now available.

The equations used to describe an electrochemical system are often related to equations in models used in physical science and engineering disciplines. Frequently, developments in approximate numerical methods in related fields may be applied to electrochemistry. However, transferring application of numerical methods is often complex, due to the unique nature of electrochemical problems. The equations describing an electrochemical system often include mixed boundary conditions and boundary singularities, chemical reaction terms, possibly leading to non-linear equations, and multiple coupled partial differential equations. Thus electrochemical simulations represent a challenging class of models for application of numerical methods.

The following section describes the reasons why the BEM was chosen for this work. A detailed explanation of fundamental concepts and relevant terms of numerical methods applied to electrochemistry, some of which are mentioned in the following section, is given in section 1.2 on page 10.

Why use the Boundary Element Method?

Initial work completed at the beginning of the period of study involved development of three-dimensional Finite Difference Methods[10]. Investigations into suitable algorithms and mesh optimisations were undertaken.

The Finite Difference Method is well understood within the electrochemistry field.[2,6,7] It approximates an electrochemical domain at a series of points, known as a mesh*. Recent research has developed two-dimensional simulations for a variety of mechanisms and different electrochemical techniques. Optimised conformal mappings, which alter the distribution of mesh points, are available for common electrode geometries. Three dimensional Finite Difference was a natural progression considering this wealth of accessible literature.

The necessity for a three dimensional simulation is caused by a lack of symmetry in the domain which prevents description by lower dimensional models. For example, specific electrode shapes or orientations, such as two microbands on opposite sides of a thin channel or domains incorporating extra features in addition to a basic electrode geometry; for instance, a Scanning Electrochemical Microscope[11] imaging a substrate.

The transition from two to three dimensions dramatically increases the number of points required to discretise a domain. The maximum number that may be simulated is limited, in practice, by the speed of computation. Assuming the code written is efficient this is dependent upon the computer hardware available. To obtain accurate results there must be a sufficient density of points near boundary singularities.[12] These occur where there is an abrupt change in boundary conditions, such as the edge of a microdisc, and the value of concentration flux approaches infinity. The problem of the large number of points required to describe a domain

**Mesh* is a general term for how a domain is approximated by a numerical method.

was addressed in two ways: Firstly, the maximum number of points that may be simulated in reasonable time was increased by the use of parallel computing.[13–15] Secondly, exponential spacing[16] and conformal mappings[17] were investigated to determine optimal positioning of mesh points.

A successful transient three dimensional simulation of a simple redox reaction after a potential step at a microdisc was completed.[18] This was validated with a two dimensional version. Further investigations were made to extend the work to more complex domains, however it was found that the implementation of conformal maps for domains which contained several areas requiring high mesh densities[†] was problematic.

The most significant limitation of the Finite Difference Method is the inherent inflexibility of mesh optimisations; they are specific to a particular domain and often cannot be adapted. A new optimisation is usually time-consuming to implement and is always required to obtain accurate results for complex electrochemical geometries. Additionally, their implementation requires significant simulation and programming knowledge, limiting the usefulness of a completed simulation to electrochemists who do not have experience in this particular field.

For these reasons, the conclusion was reached that Finite Difference Methods are unsuited to some two dimensional and all three dimensional electrochemical simulations. An alternative numerical method was thus required, and a range of techniques which had been applied in electrochemistry as well as related scientific and engineering fields were assessed. Two methods were of note for two different reasons.

Firstly, the Finite Element Method[19] (FEM); this had previously been applied in electrochemistry,[20,21] but had not become as popular as Finite Difference, due to a more advanced formulation. However, it was the most popular approximate numerical method in engineering, where it originated, with a wide range of literature and introductory texts. FEM approximates the domain with a series of primitive shapes[‡], for example triangles. Optimisation of the mesh is required for boundary singularities, however, due to the FEM formulation (see below) optimisation is far

[†]For some electrochemical models other features in addition to boundary singularities must also be considered during mesh optimisation, for example reaction layers.

[‡]The most common shapes used for FEM are triangles or quadrilaterals in two dimensions and tetrahedrons in three dimensions.

more flexible than FDM.

Secondly, the Boundary Element Method[22] (BEM); also developed in engineering, this method offered particular advantages for simulation of complex geometries due to its inherent reduction in dimensionality of the domain mesh. Thus a three dimensional domain is described by a mesh of surface primitives[§]. This also may require optimisation for boundary singularities, however, as for FEM, due to its formulation this optimisation is extremely flexible.

Details on both the FEM and BEM formulations are given in section 1.4.4 on page 42, a comparison of optimisations is given in section 1.4.3 on page 38.

The Boundary Element Method was chosen as it appeared the most elegant solution to simulating complex systems. Additionally, it was relatively unknown within the electrochemistry field, and exhibited the potential to model electrochemical systems that had proved intractable using established methods.

The terms *complex system* or *complex geometry* are used throughout this thesis in the context of electrochemical systems or electrode geometries that are difficult to simulate using numerical methods. This is not intended to reflect the complexity of other considerations.

Background of the Boundary Element Method

The basic principles of numerical methods date back to the pre-computer era. Finite Difference Methods in particular may be traced to the early part of the twentieth century. With the development of computer technology in the 1950's and 1960's there was a significant growth in research of numerical methods. Integral equation techniques, which led to the Finite Element Method and later Boundary Element Method, originated at this time.[3] Boundary Element Methods were developed in the 1970's and 1980's in mechanical engineering.[23] The amount of research was significantly smaller than in Finite Element, which by this time had become the most popular numerical method in engineering. A significant growth in research of

[§]For BEM the most common primitives are line segments in two dimensions and triangles and quadrilaterals in three dimensions.

Boundary Element Methods occurred in the 1990's. Towards the end of the decade some of the advanced formulations of FEM, such as adaptive meshing,[24] were incorporated into BEM.[25] There is a perception within engineering fields that Boundary Element Methods are more complex than equivalent Finite Element Methods.[3,26] The paucity of accessible introductory and advanced texts is a hindrance to the uptake of the BEM, although this is improving as the method becomes more mainstream.[27–29]

At the time of writing Boundary Element research continues to be a dynamic and stimulating field, with a wide range of useful application.

Chapter 1

Numerical Simulation of Electrochemical Processes

1.1 Characteristics of Electrochemical Systems

The behaviour of an electrochemical system is defined by the electrochemical technique used, its mass transport regime and the mechanism of reactions occurring. In this introductory section basic electrochemistry concepts are defined to place the numerical modelling which forms the basis of this work in context.

1.1.1 Electrochemical Techniques

Electrochemical experiments may be divided into those which are *potentiostatic* (controlled potential) and *galvanostatic* (controlled current). For potentiostatic techniques the waveform applied will typically be either a *potential step* or a *potential sweep*. More complicated waveforms are used; for example, a square wave or staircase shape, however only the potential step waveform is considered in this work.

A *transient* state exists while the behaviour of the system is dependent upon time. A *steady state* is reached when no changes occur to the flux of a species at the electrode

surface. The mathematical basis for these states is described in section 1.2.4 on page 17.

The Boundary Element Method simulations in this work were of a steady state potential step experiment. In practice this is obtained at long times after a step in the potential from a value where no reaction occurs to a value which is sufficient that the reaction is diffusion controlled. For example, for a 1 μm radius microdisc, the current typically reaches 110% of its steady state limiting value at times greater than approximately 0.1s. Transient Boundary Element Method simulations are also possible.[22]

1.1.2 Electrode Geometry

Many electrode geometries are used within the electrochemistry field.[1,2] Which geometry is chosen depends upon the application; for instance, microelectrodes used in the laboratory for kinetic analysis, or Thin Layer Cells used in industry for bulk electrolysis.

Analytical theories have been developed for geometries which are relatively simple to model, such as the Thin Layer Cell and Rotating Disc Electrode.[1] However, more complex geometries are usually intractable. Numerical approximation methods are a useful alternative to solve these problems. The complexity often arises due to a lack of symmetry of the system. This may be inherent to the system, for example a Scanning Electrochemical Microscope,[11] or due to manufacturing techniques causing variations from the expected geometry.

A class of electrodes which are of particular interest for electroanalytical research are microelectrodes.[30,31] These are generally defined as electrodes with a dimension smaller than the diffusion length of converted species. Typically this is less than 30 μm. This small size, known as a *characteristic length*, leads to useful properties such as high rates of steady state diffusion, decreased distortion from iR drop and lower charging currents.

This study is concerned with the simulation of complex microelectrode geometries.

1.1.3 Mechanism

In addition to the electrochemical reactions taking place at the electrode, chemical processes are often of central importance when considering an electrochemical system. Reactions occurring in solution are called *homogeneous*; for example, the decay of an unstable species, or reaction of the product with another species. Those reactions occurring on the surface of the electrode (including electron transfer and ion transfer) are *heterogeneous*.

1.2 Mathematical Modelling of the Electrochemical System

Typically in electrochemistry mathematical models describe the concentration distribution of species in an electrochemical system, from which the current may be obtained. The distribution is affected by a number of processes, including mass transport, homogeneous and heterogeneous reactions. A mathematical description of all processes present is necessary to understand the cases simulated in this study.

1.2.1 Mass Transport

Mass transport is a fundamental part of all electrochemical systems. It consists of three components: diffusion, migration and convection. Mathematically, it is described by the Nernst-Planck equation,[1] which in one dimension is

$$F(x,t) = -D\frac{\partial C(x,t)}{\partial x} - \frac{zF}{RT}\frac{\partial \Phi(x,t)}{\partial x} + vC(x,t)(x,t) \tag{1.1}$$

where	$F(x,t)$	$mol\ cm^{-2}\ s^{-1}$	flux of species at distance x from the electrode at time t
	D	$cm^2\ s^{-1}$	the diffusion coefficient of species
	$C(x,t)$	$mol\ cm^{-3}$	concentration of species at time t and position x
	z	*no units*	the charge on species
	F	$Cmol^{-1}$	the faraday constant
	R	$Jmol^{-1}K^{-1}$	the gas constant
	T	K	temperature
	$\Phi(x,t)$	V	potential at a distance x from the electrode at time t
	$v(x,t)$	$cm\ s^{-1}$	velocity of a volume element at a distance x from the electrode at a time t

The negative signs in the Nernst-Planck equation are due to the direction of flux opposing the direction of increasing potential and of increasing concentration.

Diffusion of a species is driven by differences in chemical potential. If a concentration gradient is present species will, on average, move to areas of lower concentration. Note that molecules continue moving randomly at all times, including once equi-

librium is reached. A simple example is the classic bromine experiment[32] where a gas jar of brown bromine species may clearly be distinguished diffusing through an adjoining jar until, after a short time, equal concentration is achieved throughout.

Migration is the movement of charged species due to an external electric field, in the presence of a potential gradient. The presence of the field is caused by the drop in potential between electrodes in a cell. Experimentally the effect of migration may be rendered negligible by addition of excess supporting electrolyte. If the concentration of species under investigation is at least two orders of magnitude lower than that of the electrolyte then the majority of movement of ions due to migration, and thus current transfer, may be attributed to the supporting electrolyte species.

Convection consists of two components. Forced convection is created by an external mechanical force, for example stirring, pumping or gas bubbles. Natural convection is due to thermal gradients or density differences. It is an undesirable feature of an electrochemical system as it is difficult to predict. This effect becomes significant after approximately 30 seconds, which means most electrochemical experiments, having shorter timescales, are not affected. Convection may be eliminated by careful experimental design, however a class of electroanalytical systems, known as hydrodynamic methods, use forced convection as a significant component of mass transport.

The example system used in subsequent sections is a potential step experiment which drives the oxidation of a redox species R, in the presence of an excess electrolyte solution. Electron transfer is assumed to be fast, so the system is mass transport controlled. Homogeneous reactions are ignored and convection is assumed to be negligible. The potential is initially set so that no reaction occurs. It is then stepped to a positive value, such that all species R on the surface of the electrode immediately reacts. The concentration of the oxidised form is irrelevant to the current measured, thus only R is modelled.

1.2.2 Domains

A domain is the physical description of the geometry of the electrochemical system. It consists of boundary and interior areas. *Boundary Conditions* are prescribed

values of concentration and flux at the boundary. A boundary condition of fixed concentration is also known as a *Dirichlet* condition, of fixed flux a *Neumann* condition. Mixed boundaries where both concentration and flux are prescribed are known as *Robin* conditions. *Initial Conditions* describe concentration and flux values over the whole domain, for a time dependent system, at time $t = 0$.

1.2.3 Fick's Second Law

When convection and migration are neglected equation 1.1, the Nernst-Planck equation, applied to species R simplifies to

$$F_R(x,t) = -D_R \frac{\partial C_R(x,t)}{\partial x} \tag{1.2}$$

where F_R is the flux of species R, D_R is the diffusion coefficient, C_R is concentration of species R, x is distance and t is time.

This is Fick's first law of diffusion which states that the rate of diffusion at a given point is proportional to the concentration gradient at that point.

Consider the variation of concentration in the region x to $x+dx$, shown in figure 1.1 on the next page. If the number of moles entering the region of cross sectional area A, per unit time, is

$$N_{in} = F_R(x,t)A \tag{1.3}$$

and an analogous equation, N_{out}, is used for the number of moles leaving the region, the net change is

$$\frac{\partial C_R(x,t)}{\partial t} = \frac{N_{in}}{A\,dx} - \frac{N_{out}}{A\,dx} = \frac{F_R(x,t) - F_R(x+dx,t)}{dx} \tag{1.4}$$

where
	C_R	is concentration of species R
	N_{in}	is flux in
	N_{out}	is flux out
	A	is area
	F_R	is flux of species R

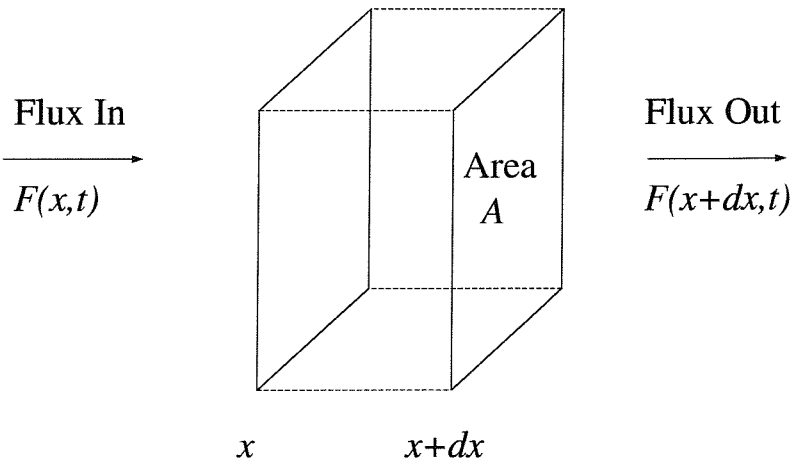

Figure 1.1: The flux of species R through a volume of area A and width dx. The total flux through this volume, assuming one dimensional diffusion in the x direction, is $F(x,t) - F(x+dx,t)$.

Substituting equation 1.2 for x and $x + dx$

$$\frac{\partial C_R(x,t)}{\partial t} = \frac{1}{dx}\left[-D_R\frac{\partial C(x,t)}{\partial x} - \left(-D_R\frac{\partial C_R(x+dx,t)}{\partial x}\right)\right] \tag{1.5}$$

An expression for the flux at $x+dx$ may be found using the approximation theorem[33]

$$\frac{\partial C_R(x+dx)}{\partial x} = \frac{\partial}{\partial x}\left[C_R(x) + \frac{\partial C_R(x)}{\partial x}\right] \tag{1.6}$$

substituting equation 1.6 into equation 1.5 gives

$$\frac{\partial C_R(x,t)}{\partial t} = \frac{1}{dx}\left[-D_R\frac{\partial C_R(x,t)}{\partial x} + D_R\frac{\partial}{\partial x}\left(C_R(x,t) + \frac{\partial C_R(x,t)}{\partial x}\right)\right] \tag{1.7}$$

rearranging gives

$$\frac{\partial C_R(x,t)}{\partial t} = D_R\frac{\partial^2 C_R(x,t)}{\partial x^2} \tag{1.8}$$

where C_R is concentration of species R, D_R is the diffusion coefficient, x is distance and t is time. This equation is known as Fick's Second Law.

This describes the planar diffusion of species R in one dimension. Analogous expressions for diffusion in two or three dimensions or using alternative coordinate systems, such as radial or spherical, may also be derived.[34]

1.2.4 Governing Partial Differential Equation

Fick's Second Law is a type of partial differential equation. The three dimensional version of equation 1.8 is

$$\frac{\partial C_R(x,y,z,t)}{\partial t} = D_R\frac{\partial^2 C_R(x,y,z,t)}{\partial x^2} + D_R\frac{\partial^2 C_R(x,y,z,t)}{\partial y^2} + D_R\frac{\partial^2 C_R(x,y,z,t)}{\partial z^2} \quad (1.9)$$

where D_R is the diffusion coefficient of species R and is assumed to be in an isotropic medium. This type of equation is the fundamental starting point for mathematical models of many electrochemical systems. By solving, or approximately solving this equation the electrochemical terms of interest, concentration and flux, may be found.

Some properties of equation 1.9 are now defined, as understanding of terms relating to differential equations is required for later explanations. This equation is *second order* because the highest derivative is two. It is also *linear* as the C_R terms are all to the first power and no products, such as $C\partial C/\partial x$ occur. If each term of the partial differential equation contains the dependent variable (in this case C_R) or one of its derivatives, the equation is said to be *homogeneous*.[35] Note this concept is separate and unrelated to homogeneous reactions.

Multiple Species

Each species in an electrochemical mechanism has a governing partial differential equation. For example, a redox couple, shown here as a reduction

$$O + e^- \rightleftharpoons R \quad (1.10)$$

where O, R are different chemical species and e^- is an electron.

This reaction, which is used throughout this thesis, is described by two governing partial differential equations. For a one dimensional, diffusion only, system these would be

$$\frac{\partial C_R(x,t)}{\partial t} = D_R \frac{\partial^2 C_R(x,t)}{\partial x^2} \tag{1.11}$$

$$\frac{\partial C_O(x,t)}{\partial t} = D_O \frac{\partial^2 C_O(x,t)}{\partial x^2} \tag{1.12}$$

where C_R is concentration of species R, D_R is the diffusion coefficient of species R, x is distance and t is time.

Hydrodynamics

Convection terms describe the rate of flow of a volume element of solution. They are significant in hydrodynamic experiments such as rotating disc electrodes and channel flow systems. For example, a three dimensional diffusion model with convective flow in the x direction only may be cast as follows

$$\frac{\partial C_R(x,y,z,t)}{\partial t} = D_R \frac{\partial^2 C_R(x,y,z,t)}{\partial x^2} + D_R \frac{\partial^2 C_R(x,y,z,t)}{\partial y^2} + D_R \frac{\partial^2 C_R(x,y,z,t)}{\partial z^2} - v_x \frac{\partial C_R(x,y,z,t)}{\partial x} \tag{1.13}$$

where C_R is concentration of species R, D_R is the diffusion coefficient, ν_x is a velocity coefficient, x, y, z are cartesian coordinates and t is time. The fourth term on the right hand side describes convection.

Homogeneous Reactions

Chemical reactions in the mechanism lead to extra terms in the partial differential equations to account for the production or loss of species. This often gives a set of coupled equations which are linked through homogeneous reaction terms. For

example, an E_rC_i reaction

$$A + e^- \rightleftharpoons B \tag{1.14}$$

$$B \xrightarrow{k} C \tag{1.15}$$

where A, B, C are different chemical species, e^- is an electron and k a chemical rate constant. E signifies an electron transfer reaction, C a chemical reaction, of which r is reversible and i irreversible.

The partial differential equation of species A will be unchanged, however the equation for species B includes the homogeneous term; there is also a corresponding equation for species C

$$\frac{\partial C_A(x,t)}{\partial t} = D_A \frac{\partial^2 C_A(x,t)}{\partial x^2} \tag{1.16}$$

$$\frac{\partial C_B(x,t)}{\partial t} = D_B \frac{\partial^2 C_B(x,t)}{\partial x^2} - kC_B(x,t) \tag{1.17}$$

$$\frac{\partial C_C(x,t)}{\partial t} = D_C \frac{\partial^2 C_C(x,t)}{\partial x^2} + kC_B(x,t) \tag{1.18}$$

where C_A, C_B, C_C are concentrations of species A, B and C respectively and k the chemical rate constant.

The inclusion of homogeneous reaction terms may change the type of the partial differential equation, for example, for a second order E_rC_{2i} reaction

$$A + e^- \rightleftharpoons B \tag{1.19}$$

$$2B \xrightarrow{k} C \tag{1.20}$$

the governing equations are

$$\frac{\partial C_A(x,t)}{\partial t} = D_A \frac{\partial^2 C_A(x,t)}{\partial x^2} \tag{1.21}$$

$$\frac{\partial C_B(x,t)}{\partial t} = D_B \frac{\partial^2 C_B(x,t)}{\partial x^2} - 2kC_B^2(x,t) \tag{1.22}$$

$$\frac{\partial C_C(x,t)}{\partial t} = D_C \frac{\partial^2 C_C(x,t)}{\partial x^2} + kC_B^2(x,t) \tag{1.23}$$

The partial differential equations of species B and C are now non-linear. This will lead to additional problems when attempting to solve this set of equations.

Transient and Steady State

A partial differential equation which contains a time derivative, such as Fick's second law, is called a transient equation. For a system at a steady state the concentration profile does not change with time. Thus the time derivative term of the differential equation is equal to zero. If only diffusion is considered this gives the steady state diffusion equation, known as the Laplace equation, which for one dimension is

$$\frac{\mathrm{d}^2 C_R(x)}{\mathrm{d}x^2} = 0 \tag{1.24}$$

1.2.5 Solution of Partial Differential Equations

A solution to a partial differential equation is any function that satisfies the equation in question for a specified integral. The integral limits are defined by the domain. For a one dimensional diffusion equation this would be the x coordinates of two end points. Often this requires the function to be continuous on the boundary of the region and to have derivatives in the interior of the region.

A partial differential equation will have many solutions as integration introduces an arbitrary constant. A function involving this arbitrary constant is called a *general*

solution. A solution where a specific value of the constant is used is known as a *particular solution*.

The unique solution of a partial differential equation is obtained by considering additional conditions that are specific to the problem. In the case of an electrochemistry domain, some *boundary conditions* are known in advance, and if the problem is time dependent, *initial conditions* when $t = 0$ will also be known. These types of partial differential equation problems are known as boundary value and initial value problems respectively.

This was a brief definition of some important terms found in partial differential equations related to electrochemistry problems. The reader is directed to mathematical texts[35,36] for rigorous definitions.

1.2.6 Current

The current at an electrode may be obtained from the flux (the concentration gradient) at the electrode surface.[1]

$$i(t) = nFAD_R \left.\frac{\partial C_R(x,t)}{\partial x}\right|_{x=0} \tag{1.25}$$

where	i	A	current
	n	n/a	number of electrons
	F	$Cmol^{-1}$	faraday constant
	A	cm^2	area
	D_R	$mol\ cm^2\ s^{-1}$	the diffusion coefficient of species R
	C_R	$mol\ cm^{-3}$	concentration of species R
	x	m	distance
	t	s	time

Using the analytical solution to the diffusion equation in one dimension (derived in the next section) and substituting its derivative into equation 1.25 gives the Cottrell equation

$$i(t) = \frac{nFD_R^{\frac{1}{2}}AC_R^*}{\pi^{\frac{1}{2}}t^{\frac{1}{2}}} \tag{1.26}$$

where C_R^* is the bulk solution concentration of species R and other parameters are

defined in the previous equation.

1.2.7 Analytical Solution of the Diffusion Equation in One Dimension

For a limited number of electrochemical systems a solution to the partial differential equation and boundary conditions that describe the model may be derived. This is called an analytical solution. For the one dimensional diffusion equation, equation 1.8, an analytical solution may be derived.[34,37] This gives the concentration of species C_R at any time, anywhere in the domain. Various methods of solving partial differential equations are available,[35,38] a common method found in electrochemistry is the Laplace Transform.[39]

The Laplace Transform technique consists of three steps

1. Perform a Laplace Transform on the original partial differential equation taking into account initial conditions.
2. Solve the resulting ordinary differential equation in Laplace space considering the boundary conditions.
3. Convert back to real space using the inverse transform, which may be found in tables or using a numerical approximation.

A Laplace Transform converts a function, f, to an ordinary differential equation with the Laplace space variable, s

$$\mathcal{L}(f)(s) = \int_{t=0}^{\infty} \mathrm{e}^{-st} f(t)\, dt \tag{1.27}$$

where $\mathcal{L}(f)(s)$ is the Laplace Transform of $f(x)$.

Applying this to equation 1.8, the diffusion equation, gives

$$\int_{t=0}^{\infty} \mathrm{e}^{-st} \frac{\partial C_R(x,t)}{\partial t}\, dt = D_R \frac{\partial^2 \bar{C}_R(x,s)}{\partial x^2} \tag{1.28}$$

where the bar indicates a Laplace transform. Integration by parts gives

$$s\int_{t=0}^{\infty} \mathrm{e}^{-st}C_R(x,t)\,dt + \left[\mathrm{e}^{-st}C_R(x,t)\right]_0^{\infty} = D_R\frac{\partial^2\bar{C}_R(x,s)}{\partial x^2} \tag{1.29}$$

therefore

$$s\bar{C}_R(x,s) - C_R(x,0) = D_R\frac{\partial^2\bar{C}_R(x,s)}{\partial x^2} \tag{1.30}$$

Using the initial conditions

$$s\bar{C}_R(x,s) - C_R^*(x,s) = D_R\frac{\partial^2\bar{C}_R(x,s)}{\partial x^2} \tag{1.31}$$

rearranging gives

$$D_R\frac{\partial^2\bar{C}_R(x,s)}{\partial x^2} - s\bar{C}_R(x,s) = -C_R^* \tag{1.32}$$

where C_R^* is constant. The solution of the above equation may be found in tables[40]

$$\bar{C}_R(x,s) = \frac{C_R^*}{s} + A(s)\exp\left[-\left(\frac{s}{D_R}\right)^{\frac{1}{2}}x\right] + B(s)\exp\left[\left(\frac{s}{D_R}\right)^{\frac{1}{2}}x\right] \tag{1.33}$$

The coefficients A and B may be found by applying boundary conditions. At large distances from the electrode ($x = \infty$) then $C_R(\infty,t) = C_R^*$, where C_R^* is the bulk solution value. In Laplace space

$$\mathcal{L}(C_R^*) = \frac{C_R^*}{s} \tag{1.34}$$

equation 1.33 becomes

$$\frac{C_R^*}{s} = \frac{C_R^*}{s} + B(s)\exp\left[-\left(\frac{s}{D_R}\right)^{\frac{1}{2}}x\right] \tag{1.35}$$

therefore at $x = \infty$, B(s) must equal zero, which gives

$$\bar{C}_R(x,s) = \frac{C_R^*}{s} + A(s)\exp\left[-\left(\frac{s}{D_R}\right)^{\frac{1}{2}} x\right] \tag{1.36}$$

The boundary conditions at the electrode allow evaluation of A. At $x = 0$ then $C(0,t) = 0$ so in Laplace space

$$\mathcal{L}(0) = 0 \tag{1.37}$$

thus

$$A(s) = -\frac{C_R^*}{s} \tag{1.38}$$

so the solution in Laplace space is

$$\bar{C}_R(x,s) = \frac{C_R^*}{s} - \frac{C_R^*}{s}\exp\left[-\left(\frac{s}{D_R}\right)^{\frac{1}{2}} x\right] \tag{1.39}$$

Using tabulated results[41] the inverse transform gives

$$C_R(x,t) = C_R^* \mathrm{erf}\left[\frac{x}{2(D_R t)^{\frac{1}{2}}}\right] \tag{1.40}$$

The function may be verified by substituting known boundary conditions. At $x = \infty$, $\mathrm{erf}(\infty) = 1$ so $C_R = C_R^*$. At $x = 0$, $\mathrm{erf}(0) = 0$ so $C_R = 0$.

This gives a solution which is a function of space and time. The values of concentration may be directly found at any given point in space and time.

1.2.8 Simple Simulation of the Diffusion Equation in One Dimension

For any systems other than the most basic models an analytical solution is often impractical. An alternative is to find an approximate solution by utilising a numer-

ical simulation. The simplest possible simulation, Explicit Finite Difference (EFD) is outlined here, for the one dimensional diffusion equation.

Finite Difference

The concept of a domain has been introduced in section 1.2.2 on page 11, and a simulation domain for a one dimensional system is shown in figure 1.2. This example uses the point collocation method, readers are referred to the text by Britz[6] for alternative views of the EFD technique. Concentration values are calculated at a series of discrete points; figure 1.2. This illustrates the concept of discretisation, where a domain is divided into separate points or sections.

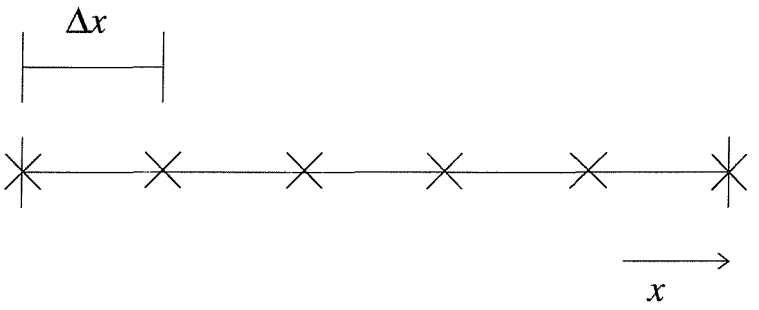

Figure 1.2: Discretisation of a one dimensional domain into equally spaced collocation points.

The differentials present in equation 1.8 may be approximated, giving a value for concentration at each point, figure 1.3 on the next page. The points are separated by equal size intervals, ΔX, so the X coordinate is given by $X = i\Delta X$, where i is an integer, starting at zero. Unequal size intervals may also be used allowing efficiency savings, see section 1.4.3 on page 38. Time may also be discretised in the same manner giving $t = j\Delta t$.

The rate of change of concentration with respect to distance, that is the concentration gradient, may be represented using a two point approximation.[6] There are three possible equations:

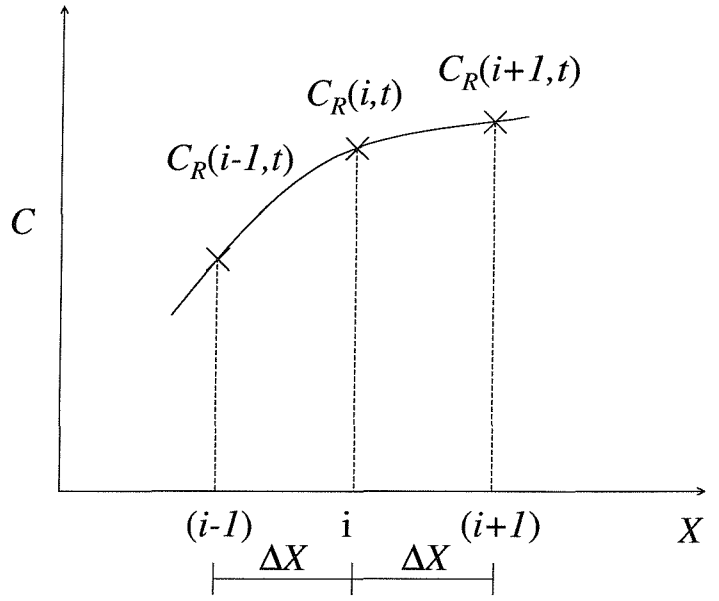

Figure 1.3: The concentration profile at time t may be discretised into distinct points. Variation of concentration between points is assumed to be linear. Thus problems may be caused if the flux (rate of change of concentration) relative to ΔX is too large.

backward difference

$$\frac{\partial C_R(i,j)}{\partial x} = \frac{C_R(i,j) - C_R(i-1,j)}{\Delta X} \tag{1.41}$$

forward difference

$$\frac{\partial C_R(i,j)}{\partial x} = \frac{C_R(i+1,j) - C_R(i,j)}{\Delta X} \tag{1.42}$$

or a central difference

$$\frac{\partial C_R(i,j)}{\partial x} = \frac{C_R(i+1,j) - C_R(i-1,j)}{2\Delta X} \tag{1.43}$$

where C_R is concentration of species R, ΔX is the distance increment, i is the spatial integer counter, j is the temporal integer counter and X is distance.

Recalling a second order derivative may also be written

$$\frac{\partial^2 C_R(i,j)}{\partial X^2} = \frac{\partial}{\partial X}\left(\frac{\partial C_R(i,j)}{\partial X}\right) \tag{1.44}$$

then combining equations 1.42 and 1.41 and differentiating gives

$$\frac{\partial^2 C_R(i,j)}{\partial x^2} = \frac{C_R(i+1,j) - 2C_R(i,j) + C_R(i-1,j)}{\Delta X^2} \tag{1.45}$$

where C_R is concentration of species R, ΔX is the distance increment, i is the spatial integer counter, j is the temporal integer counter and X is distance.

This gives an approximation for C_R at each timestep. To link timesteps the same approximating functions may be used to discretise the temporal term. If a forward or backward difference approximation is used for the timestep, the method is known as *explicit* as it uses the previous timesteps result. If we use a central difference the method is known as *implicit*, as we are using the values of C at a current, unknown, timestep.

The simplest method, which may be directly extended to two and three dimensions, is explicit finite difference. Substituting a backward difference approximation, equation 1.41, for the temporal derivative and equation 1.45 for the spatial term into the diffusion equation, equation 1.8, gives the explicit finite difference approximation in one dimension

$$\frac{C_R(i,j+1) - C_R(i,j)}{\Delta t} = D_R\left(\frac{C_R(i+1,j) - 2C_R(i,j) + C_R(i-1,j)}{\Delta X^2}\right) \tag{1.46}$$

where C_R is concentration of species R, ΔX is the distance increment, Δt is the time increment, i is the spatial integer counter and j is the time integer counter.

This equation may be used to simulate concentration at discrete points in space and time. Any point may be calculated either by ensuring it coincides with a simulated point or interpolating between points.

Transient and Steady State Simulations The Explicit Finite Difference method applied to the diffusion equation is a transient simulation. At long times the con-

centration will approach a near-steady-state equal to the true steady state value. There are also alternative simulation methods which calculate the steady state directly, see section 1.3 on page 29.

Stability

The Explicit Finite Difference equation may be written in terms of a stability coefficient, λ, which is defined as

$$\lambda = \frac{D_R \Delta t}{\Delta X^2} \tag{1.47}$$

where Δt is the time increment and ΔX is the distance increment. Equation 1.46 becomes

$$C_R(i, j+1) = \lambda C_R(i+1, j) + (1 - 2\lambda) C_R(i, j) + \lambda C_R(i-1, j) \tag{1.48}$$

where C_R is concentration of species R, λ is the stability coefficient, i is the spatial integer counter and j is the time integer counter.

The stability coefficient relates space and time increments, and effectively puts a limit on the maximum timestep interval that is permissible while maintaining stability. If this limit is exceeded the simulation starts to oscillate, giving incorrect results.

For one dimensional EFD[6] then $\lambda \leq 0.5$. It is possible, from this simple example, to directly comprehend the effect of the stability coefficient. Substituting the maximum λ value into equation 1.48 one may see that the second term on the right hand side, $C_R(i, j)$, is equal to zero, giving

$$C_R(i, j+1) = \frac{C_R(i+1, j) - C_R(i-1, j)}{2} \tag{1.49}$$

Thus the new concentration value, $C_R(i, j+1)$, cannot exceed the average of the old concentrations on either side.

An analytical theory predicting the theoretical stability of different finite difference

schemes, known as Von Neumann analysis, has been published for a variety of schemes.[42]

The stability limitation means that large numbers of timesteps are required to reach near steady state times. This is often prohibitive due to the computing resources available. Thus more efficient finite difference models are required. Finite difference approximations which are theoretically stable for all values of λ are reviewed in section 1.3.1 on page 29. Although they may be theoretically stable many of these approximations still exhibit some instability, often due to additional factors such as large kinetic parameters.

Stability is a problem for most numerical simulation techniques, not just finite difference. However as the simulation formulation becomes more complex, so does the theoretical treatment required to prove stability. Often analytical stability theory is unavailable, requiring numerical validation of the model to achieve a degree of confidence of the accuracy of the model under certain conditions.

1.2.9 Dimensionless Parameters

When working with electrochemical models it is often advantageous to normalise parameters to remove dependence of the model on specific values. For example removing the diffusion coefficient, D_R, enables the same model to be applied to any species R. The details of normalisation for the one dimensional diffusion equation are outlined below.

Concentration is normalised with respect to the bulk solution concentration value.

$$c = \frac{C}{C^*} \tag{1.50}$$

where c is dimensionless concentration, C is dimensional concentration and C^* is bulk concentration.

Distance parameters such as X are normalised with respect to a characteristic length, l. For example, for a microdisc system the radius of the disc is used, for a

microband the width of the band.

$$x = \frac{X}{l} \tag{1.51}$$

where x is dimensionless distance, X is dimensional distance and l is the length of the domain.

Time is usually normalised with respect to the diffusion coefficient, D_R, and a characteristic length

$$\tau = \frac{D_R t}{l^2} \tag{1.52}$$

where τ is dimensionless time, D_R is the diffusion coefficient, t is dimensional time and l is the length of the domain.

Substituting these parameters into the diffusion equation gives the dimensionless form of the diffusion equation

$$\frac{\partial c(x,\tau)}{\partial \tau} = \frac{\partial^2 c(x,\tau)}{\partial x^2} \tag{1.53}$$

where c is dimensionless concentration, τ is dimensionless time and x is dimensionless distance.

Note the original parameters are also known as dimensional parameters.

Dimensionless Current

The equation describing current at an electrode, equation 1.25, may be cast in dimensionless form by normalising with respect to a characteristic current. For example, for the microband electrode

$$i_{\text{norm}} = \frac{nFwlD_R \int_0^w \left.\frac{\partial C_R(X,Y,t)}{\partial Y}\right|_{Y=0} \mathrm{d}X}{(nFD_R l C^*)} \tag{1.54}$$

where			
	i_{norm}		dimensionless current
	n	n/a	number of electrons
	F	$Cmol^{-1}$	Faraday constant
	A	m^2	area of electrode
	D_R	$cm^2\ s^{-1}$	diffusion coefficient of species R
	C_R	$mol\ cm^{-3}$	concentration of species R
	C_R^*	$mol\ cm^{-3}$	concentration of bulk solution of species R
	w	cm	width of microband electrode
	X, Y	m	distance
	l	none	electrode length normalised with respect to the electrode width
	x, y	none	distance normalised with respect to the electrode width
	t	s	time

to give

$$i_{\text{norm}} = \int_0^1 \left.\frac{\partial c_R(x,y,\tau)}{\partial y}\right|_{y=0} \mathrm{d}x \tag{1.55}$$

where parameters are as defined above.

1.3 Review of Simulation Techniques

Electrochemical simulation is a broad and diverse topic. A brief review of some alternative simulation techniques is included, to place the Boundary Element Method within the general electrochemical numerical modelling field.

Finite Difference Methods are by far the most popular simulation techniques in electrochemistry. The main simulation algorithms are summarised here. The optimisations of these FDM techniques, applicable to all algorithms, are covered in section 1.4.3 on page 38.

For all methods mentioned, except random walk[1,43] and BEM,[22,44] interested readers are referred to the excellent review by Speiser,[7] and for FDM basics in particular, the text by Britz.[6]

A detailed comparison of three of these methods, the Finite Difference Method, Finite Element Method and Boundary Element Method is covered in section 1.4 on page 34.

1.3.1 Finite Difference Method

The concept of finite difference approximation, where a differential equation is reduced to a series of algebraic equations, was presented in section 1.2.8 on page 21. A specific finite difference formulation yields an algorithm. Explicit Finite Difference (EFD) is the simplest algorithm for the solution of a partial differential equation, however it is not particularly efficient. Alternative finite difference algorithms are briefly reviewed here.

Hopscotch A slight extension of the EFD algorithm gives the Hopscotch method, which has a degree of implicitness without the complexity of Crank-Nicolson. It it stable for all λ and simple to implement. However it produces disappointing accuracy.[45,46]

Crank-Nicolson (CN) A simple one dimensional semi-implicit scheme,[6] this leads to a tri-diagonal matrix and is theoretically stable for all values[47] of λ. A

method implemented by Heinze[48] and Britz,[49] FIFD (see below) has proved more popular.

Du-Fort Frankel (DFF) or Fast Quasi-Explicit Finite Difference (FQEFD) An improvement to EFD, the Du-Fort Frankel method[50,51] uses concentration values at $C(x, t-\Delta t)$ in addition to $C(x, t)$ to calculate new values at $C(x, t+\Delta t)$. This is found to be stable for varying λ, but has also proved disappointing as it must be started near equilibrium conditions to avoid initial oscillations.[52]

Fast Implicit Finite Difference (FIFD) This is also known as the Backward Difference Method, and was applied to channel flow systems by Compton *et al.*[53,54] It was introduced as FIFD by Rudolph.[55,56] This algorithm uses only values of $C(x, t+\Delta t)$ in addition to $C(x, t)$. Recently it has been modified by Feldberg[57] to simulate large values of the diffusion coefficient, and is still being developed by Rudolph.[58] FIFD is the basis of the commercial electrochemical simulation program, Digisim®,[9] which is capable of simulating general electrochemical mechanisms.

Alternating Direction Implicit (ADI) A semi-implicit two dimensional scheme,[59] ADI is unconditionally stable for all values of λ. It is effectively a two-dimensional CN algorithm. Two half-steps are used, the first half-step is implicit in one axis and explicit in the other. These are then exchanged for the second half-step, when the final concentration values are calculated.[60] ADI has been successfully applied to a number of electrochemical problems, particularly microdiscs, by Unwin *et al*,[61–64] Taylor[65] and Amphlett *et al.*[66]

Recently a three dimensional ADI algorithm has been developed.[10]

Strongly Implicit Procedure (SIP) and Multi Grid Method (MGM) Introduced by Alden *et al*[67,68] SIP is a fully implicit two dimensional method, that allows direct solution of steady state problems. This gives a significant efficiency gain.[69] An initial approximate solution must be given for the concentration values of all mesh points and an iterative solution found. Transient simulations are also possible, and SIP has been found to be more stable than ADI due to its fully implicit nature.[70]

Alden later found the Multi Grid Method,[71] which is also implicit and uses a larger number of mesh points in the finite difference approximation, to have superior convergence properties than SIP for some problems.[72] Additionally, a wider range of conformal mappings are possible as the original partial differential equation modelled is more general.

Matrix Solvers

Of particular note is the generalisation of two dimensional FD methods, with application to wide ranging electrochemical mechanisms, enabled by a number of matrix solving techniques collectively known as Pre-conditioned Krylov Subspace (PKS) solvers. A non-generalised form of Krylov integration technique was originally used by Bard *et al*[73] for SECM simulation.

The finite difference method formulation may be written in matrix form leading to a diagonal sparse matrix. For example, an EFD approximation produces a tri-diagonal matrix. If homogeneous reactions are also included in the formulation, additional diagonal lines appear. The FDM is an efficient way of solving these matrices. Each method produces a specific matrix, and may only be used to solve that matrix.

Pre-conditioned Krylov Subspace methods allow any linear sparse matrix to be solved. Therefore they are a general method which may be used with a finite difference approximation. Although not as efficient as specific solvers, for example SIP, they are much more flexible.

A general electrochemical simulator has been proposed by Alden[74] based on the PKS method, which will allow any mechanism to be simulated. This has been applied to simulation of a wide variety of mechanisms for microdiscs and microbands.[75]

1.3.2 Random Walk

Random Walk methods simulate the possible paths taken by a species, noting where a particle hits a boundary. The number of particles hitting an electrode, per timestep, gives the current. It is more complex, although possible, to calculate a concentration profile.[43] The path taken is determined by moving the particle in

a random direction and care must be taken to ensure a sufficiently random number generation routine. A distinct advantage of the method is that a general three dimensional boundary may be simulated in addition to a moving boundary. Nagy *et al*[43,76] applied the random walk method to growing arrays of hemi-spherical electrodes. There is no mesh or primitive elements to restrict the description of the boundary, however recent research[77] suggests problems due to the assumption of zero flux perpendicular to the boundary, when a curved boundary is modelled. Therefore the advantages of application to general boundary shapes may not be as significant as first thought.

1.3.3 Weighted Residual Methods

Orthogonal Collocation

Orthogonal Collocation[78,79] uses a polynomial of degree N to interpolate between concentration points. The polynomial is forced to be exact at certain points called collocation points. The weighting function used is related to the polynomial function and its order. The space derivatives are therefore replaced, leading to a system of ordinary differential equations of the form

$$\frac{\mathrm{d}C}{\mathrm{d}t} = f(C_i) \tag{1.56}$$

where C is concentration, f a polynomial function, i an integer counter and t is time.

These equations are then integrated on a discrete time grid. Far fewer discretisation steps are required than Finite Difference.[80,81] Care must be taken to use suitable numerical integration to maintain stability.[82] A comparison is given by Bieniasz.[83]

Finite Element Method

This technique divides the domain into a mesh of primitive shapes such as triangles, rather than discrete points as used in OC methods. The concentration variation over each element is calculated. Complex geometries may be simulated although

mesh generation is not simple. The Finite Element Method has been applied to electrochemistry[84,85] and is described in more detail in section 1.4 on the following page.

Boundary Element Method

The Boundary Element Method requires only discretisation of the boundary of the domain into elements. Recently applied to electrochemistry by Fulian *et al*[86] it allows modelling of complex shapes. A detailed description of BEM is given in the next chapter. It is compared to two popular alternative methods in section 1.4 on the next page.

1.4 Comparison of Finite Difference, Finite Element and Boundary Element Methods

1.4.1 Introduction

The two numerical simulation methods, Finite Difference (FDM) and Finite Element (FEM), most widely used in electrochemistry and engineering respectively, are compared to the Boundary Element Method (BEM). This section initially summarises each method after which specific properties of interest to electrochemists are compared.

The formulation of each method are related mathematically, through a Method of Weighted Residuals (MWR) technique in Appendix A on page 188.

Finite Difference

This method has been comprehensively developed within the electrochemistry field[6,7] with many optimisations implemented. Finite difference (FDM) techniques approximate the derivatives of the partial differential equation in question using a form of truncated Taylor expansion. This leads to a mesh of concentration points, represented by a series of algebraic equations, to which boundary conditions are applied to solve the problem. The regular FDM grid is unable to accurately reproduce the geometry of many problems. Hence some form of expanding grid or conformal mapping is applied to increase the number of concentration points in areas of high flux. These have been successfully applied to many problems including both microband[69,87,88] and microdisc geometries[16,89–92] the latter using a two dimensional axisymmetric domain. However the domain mesh is relatively inflexible even if some kind of adaptive grid technique is used and it is difficult to incorporate complex shapes. Three dimensional simulations have been limited to simple geometries. Electrochemical finite difference methods are a broad and varied area of research, a summary of different algorithms is given in section 1.3.1 on page 29.

Finite difference codes can be extremely efficient to run, due to the sparse matrix produced, however for two and particularly three dimensions this is often offset by

the large number of points required to maintain accuracy.

Transient effects and chemical reactions may be included with relative ease once the mesh transformation has been derived.

Finite Element

There has been some application of the Finite Element Method to electrochemical problems although the technique has not proved as popular as FDM. The FEM model involves the approximation of the variables over small elements of the domain, in terms of polynomial interpolation functions. A weighted residual formulation may be written in order to distribute the error introduced by this approximation over each element. This results in matrices which express the properties of each element in terms of a discrete number of nodal values. Assembling these into a global matrix then represents the whole domain. Various shapes of elements may be used to discretise the model, including triangles and quadrilaterals in two dimensions, tetrahedrons and cuboids in three dimensions.

Regular grids in FEM models are insufficient to account for boundary singularities. Expanding grids have been successfully implemented,[93] however altering the geometry of the mesh is not a simple matter. Distortion of the original shape of the elements must be avoided to ensure accuracy. Recent developments of adaptive grid FEM techniques[94–96] allow for various geometries and boundary conditions, while accounting for boundary singularities. Current electrochemical FEM simulations have been limited to two dimensional domains. Three dimensional FEM is possible, but leads to more complex integrals and difficulties in generating suitable element meshes.

The FEM is a powerful technique and has been extensively researched in engineering fields.[19,97] It is also possible to include transient effects and chemical reactions.

Boundary Element

The Boundary Element Method[22,44,98] requires only discretisation of the boundary of the domain. The variables at different boundary points are related by the use of

an analytical function (the fundamental solution) resulting in a series of influence coefficient matrices. Boundary conditions are then applied to solve for all variables at all boundary points. Subsequently, values at internal points may be obtained.

Boundary elements can be of various types, including curvilinear shaped boundaries, enabling a wide range of domains to be accurately modelled. A regular mesh is normally sufficient to model boundary singularities. A distinct advantage of the method is a reduction in dimension by one. Thus a three dimensional model is described using two dimensional surface elements. This greatly simplifies generation of the mesh, although it does lead to more complex integral equations. Many model geometries may be described as only the cartesian coordinates of the surrounding boundary are required as input. Therefore once developed a BEM program is highly flexible in its application.

The BEM was applied to common electrochemistry problems by Fulian *et al*[86,99,100] during the course of this Ph.D.

Time-dependent terms in the partial differential equation may be incorporated,[22,101,102] additionally some coupled chemical reactions (represented by multiple differential equations) may be simulated.[103]

1.4.2 Domain Discretisation

The three types of basic domain discretisation are shown in figure 1.4 on the following page.

Finite Difference Finite Difference meshes divide the domain into a sequence of points (figure 1.4a) and boundary conditions are applied to points on the edge of the domain. The placement of mesh points has been shown to have a significant effect on accuracy.[104] The distribution of points and distances between them are related to the original partial differential equation; any alteration in mesh spacing changes the form of this equation. This causes restrictions on the geometry that may be modelled, in addition to rendering each mesh specific to a particular geometry. However many electrochemical systems may be accurately approximated by an ideal

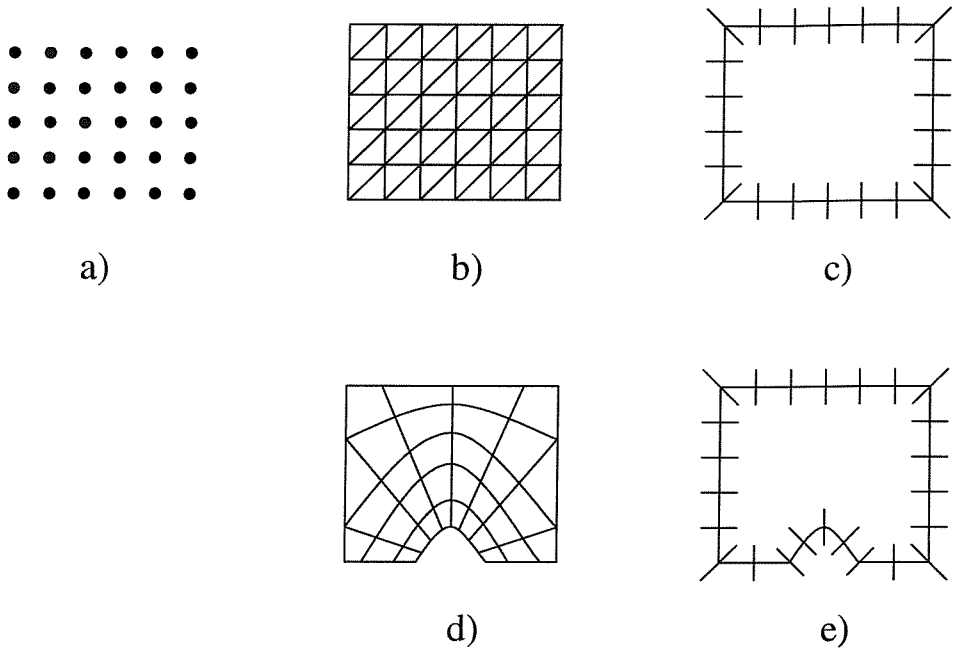

Figure 1.4: Typical two dimensional discretisations for a) Finite Difference, b) Finite Element and c) Boundary Element. The greater flexibility of the latter two methods is demonstrated in more complex domain shapes d) and e). The Boundary Element Method, e), gives the easiest domain discretisation due to a reduction in dimension, allowing description of the domain with line elements.

(simple) geometry, enabling optimised finite difference simulations to successfully model a wide variety of electrochemical problems.[7]

Finite Element The Finite Element domain is described by a mesh of primitive elements. In two dimensions either triangles (shown in figure 1.4b) or quadrilaterals. These cover the entire domain with the nodes on the edges of elements on the boundary having boundary conditions applied to them. The placement of elements does not directly affect the partial differential equation. Thus they may be different sizes and shapes and if for instance, triangles, do not have to be congruent. However, the aspect ratio of the sides of the elements must be reasonably close to unity, to prevent elongated, thin elements which reduce accuracy. These FEM meshes can model a wide variety of domain shapes and are much more flexible than FDM meshes (figure 1.4d).

Boundary Element A Boundary Element mesh requires only discretisation of the boundary of a domain (figure 1.4c), due to a reduction in dimension by the BEM formulation. Thus line elements are used in two dimensions. Complex domain shapes may be more easily modelled due to this simplified discretisation (figure 1.4e).

Three Dimensions

In three dimensions a finite difference mesh is also described simply by a mesh of points. A single point and those neighbours which contribute to calculation of concentration at that point is shown in figure 1.5a on the next page. A very large number of points is generated leading to problems with obtaining a realistic computational time, and difficult optimisation. Finite Element meshes consist of either tetrahedra (figure 1.5b) or cuboid primitives. Meshing is much more complex, especially when optimisation is required. Significantly fewer points are required than with FDM for the same accuracy, although computational time may still be a factor. Due to a reduction in dimension three dimensional primitives for the Boundary Element Method are surfaces,[22] such as triangles or quadrilaterals (figure 1.5c). Meshes are still fairly complex as the elements must still be defined in three dimensional space. However this is markedly simpler than volume meshing.

1.4.3 Optimisation for Electrochemical Geometries

Electrochemical simulations of two dimensions or higher usually have one or more boundary singularities. These are caused by an abrupt change in boundary conditions at the edge of an electrode, for example at the edge of a microdisc. The flux tends to infinity at this point, which is called a singularity. Around this region rapid changes in concentration occur which often require some form of optimisation to be modelled accurately.[12]

If one is simulating homogeneous chemical reactions, it may also be necessary to consider rapid and highly localised changes in concentration caused by the reaction, in a region known as the reaction layer. A reaction layer is analogous to a diffusion layer.[6] The size of the reaction layer may be a different order of magnitude to

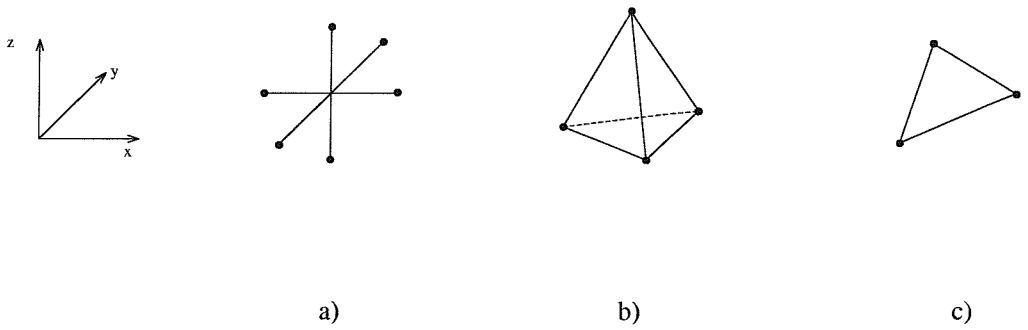

Figure 1.5: The simplest discretisation possible in three dimensional space for each of the three methods compared. a) Finite Difference uses the six neighbouring points, these must be mutually perpendicular unless some sort of conformal mapping is used. b) For FEM the volume may be divided into tetrahedrons; these do not need to be of a specific shape, although they must remain reasonably close to a pyramid shape to maintain accuracy. c) BEM may use a triangular surface, although this must be defined in three dimensional space.

the diffusion layer; additionally it may be some distance away from the electrode surface,[105–107] leading to conflicting optimisation requirements.

Finite Difference

A basic two dimensional finite difference mesh is rectangular; all boundaries are at right angles to one another. To increase the number of points near a boundary singularity several optimisation strategies have been implemented.

Exponential Meshes Exponential meshes increase the density of points[16] in a single dimension at an area or several areas defined by the specific equations used. When applied in two dimensional domains the number of points near the singularity can be significantly increased. This also has the side effect of increasing point density in some regions far away from the singularity - this does not adversely affect accuracy although it does increase computational time.

Local Approximation A special formulation immediately adjacent to the singularity may be implemented[108] (a locally valid series expansion) which reduces computational time.

Conformal Mapping A transformation of coordinate system (known as conformal mapping) may be applied to obtain a high density of points in real space with equally spaced points in transformed space, where the FDM calculation is performed. An ideal conformal map will have points distributed in a similar manner to the diffusion field[109] (in a diffusion only system). A wide variety of conformal maps have been considered[89,110–112] not just limited to rectangular domains but also more challenging geometries.[17,113]

These optimisations are specific to each geometry and to implement any optimisation the finite difference method must be fully understood. Three dimensional conformal mapping is complex, and still an active area of research in both mathematics[114–116] and electrochemistry related fields.[117,118] However limitations due to the inherent inflexibility of the FDM optimisations often mean that the amount of effort involved cannot be justified.

Finite Element

Optimisations include techniques analogous to Finite Difference. Exponential grids have been employed to increase the density of elements near boundary singularities.[93] Alternatively an automatic adaptive mesh routine increases the number of elements in areas of high flux.[94] These may be based on either optimising concentration or flux.

Recently an error-bounding technique has been introduced in addition to adaptive meshing.[119,120] This gives a global error limit, and the actual error is often significantly below this. This has distinct advantages over alternative methods as convergence testing is not required, and the possibility of unforseen problems with a new geometry is removed. This has so far been limited to two dimensions. Adaptive routines used in electrochemistry have relied on a rectangular discretisation strategy. A rectangular mesh of triangles, figure 1.4b on page 37, (two triangles per rectangle) is used as the base discretisation. In areas of high flux existing triangles are divided

to form two new triangles (figure 1.6). However this type of strategy limits domains that may be modelled to rectangular types. An improved technique, allowing more complex meshes, is Delauney triangulation.[121,122] This allows generalised domains to be meshed, while restricting the aspect ratio of triangles used.

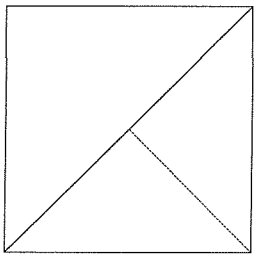

Figure 1.6: The adaptive meshing strategy used in previous electrochemical FEM simulations by Gavaghan *et al.*[95] A rectangle is split in half to form two triangles. One of these triangles is split into two further triangles if required. A similar strategy could be used for three dimensional BEM simulations, however superior alternative techniques, such as Delaunay triangulation are also available.[122]

Higher order approximations over elements may also improve accuracy, allowing an improved description of concentration variations.[97]

Usually semi-infinite boundary conditions are used, with a domain that extends far enough from the area of interest that the influence of the infinite boundary is negligible. Alternatively special infinite elements may be incorporated. These use an approximating function that decays to the specified value at infinity.[19]

Three dimensional optimisations are analogous to the two dimensional techniques already mentioned. However they are more complex and some advanced stategies, such as error-bounding and Delauney triangulation have not been fully developed.

Boundary Element

Boundary Element optimisations include many procedures analogous to previous methods. Exponential element spacing is described in section 2.5.2 on page 80. Adaptive meshes are a current area of research in specialised BEM fields.[123] Thus

far, there has been limited development analogous to FEM error-bounding although this would be a desirable future direction.

Higher order approximations to describe concentration and flux variations over the primitive element may be implemented. Linear elements are described in detail in section 2.10.1 on page 123. Additionally an analytical element may be used adjacent to a boundary singularity. This is a high-order element which optimises the approximation over the element, for a known variation of flux near the singularity.[103] Analytical elements were not considered in this work.

Semi-infinite boundaries are usually used in the same manner as FEM and FDM. A significant optimisation unique to BEM is to model a genuine infinite domain, discretising the object of interest in the same way as a closed domain, but considering the concentration field exterior to this discretised domain. The infinite boundary is incorporated in the BEM formulation and does not require discretisation.[22]

1.4.4 Formulations of the Methods

The system to be modelled is described by a partial differential equation as explained in section 1.2.4 on page 14. The relation of the formulation of each method to this partial differential equation is outlined below. The implementation details of each method will change if the partial differential equation is changed. The relation between the formulations of the three methods is summarised in figure 1.7 on the next page.

FEM and BEM are often derived through a weighted residual approach as this is perhaps the easiest to understand, although both may be derived through alternative formulations. FDM methods are usually derived directly (section 1.2.8 on page 21), however they may also be derived through a weighted residual method allowing a direct relationship between the three methods to be established. The mathematical details of these relationships are covered in Appendix A on page 188. A brief summary of the Method of Weighted Residuals follows.

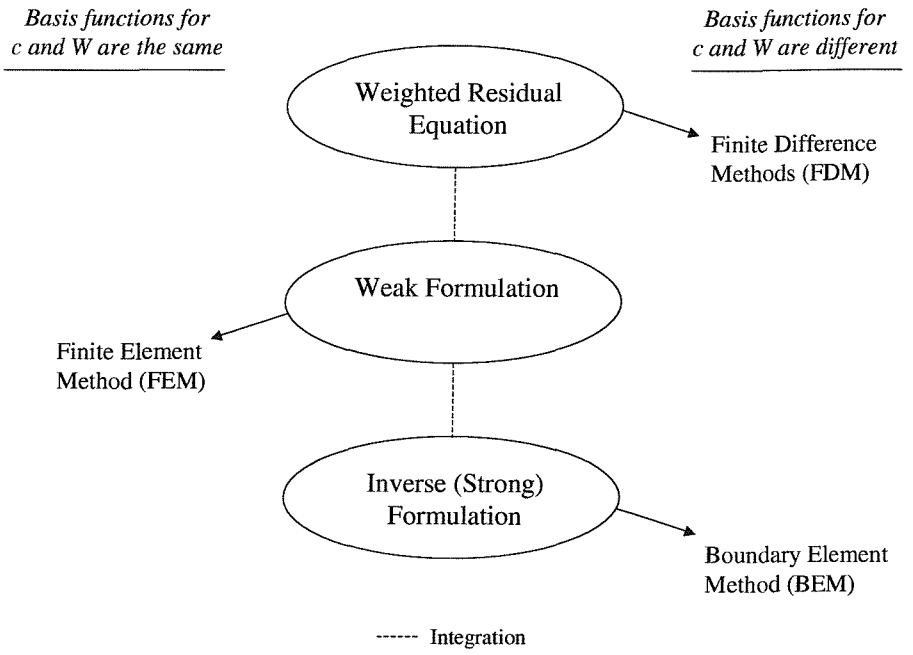

Figure 1.7: The three methods under discussion may be related through a Method of Weighted Residuals (MWR) formulation. The choice of weighting function is of fundamental importance for both the Finite Element Method and Boundary Element Method, however, it is inherent within a finite difference method which is more usually derived directly. c is a concentration field approximation function, W is a MWR weighting function.

Method of Weighted Residuals

Diffusion in one dimension is described by Fick's second law, equation 1.8, which in dimensionless form and dropping the species subscripts is

$$\frac{\partial c(x,t)}{\partial t} = \frac{\partial^2 c(x,t)}{\partial x^2} \tag{1.57}$$

Substituting an *approximation function*, $\hat{c}$, for c in the diffusion equation, equation 1.8, gives a *Residual*, or error function, R, such that

$$R = \frac{\partial^2 \hat{c}(x,t)}{\partial x^2} - \frac{\partial \hat{c}(x,t)}{\partial t} \neq 0 \tag{1.58}$$

where R is the residual, $\hat{c}$ is concentration, x is distance and t is time.

The aim of the weighted residual method is to force R to be zero in an average sense, over the entire domain. To achieve this a weighting function W is used to distribute the error. For equation 1.58 this gives

$$\int_0^d \left(\frac{\partial^2 \hat{c}(x,t)}{\partial x^2} - \frac{\partial \hat{c}(x,t)}{\partial t} \right) W \, \mathrm{d}x = 0 \tag{1.59}$$

where W is an arbitrary weighting function, $\hat{c}$ is the concentration, d is the length of the domain, x is distance and t is time.

This equation is known as a weighted residual, which in this case has been applied to the one dimensional diffusion equation. The same procedure may be used for any partial differential equation by replacing equation 1.57.

Finite Difference

Finite Difference methods are a direct approximation of the diffusion equation, giving concentration and flux values at a series of points. FDM is related to MWR in Appendix A. A large number of FDM algorithms (section 1.3 on page 29) have been derived, many of which have been optimised (section 1.4.3 on page 38) and applied to electrochemistry. Although possessing different properties the basic form of these methods is the same; for example the simplest algorithm, explicit finite difference, may be written as a tri-diagonal matrix. More advanced algorithms have additional diagonal components but always lead to a sparse matrix form.

Concentration values are obtained at each discrete point. The flux may be calculated from adjacent points and the current from the flux at the electrode surface. Two point Taylor approximations[36] are usually used for this calculation, although higher order approximations are possible.

Relatively few three-dimensional formulations have been developed, two examples are EFD and ADI.[10]

Finite Element

FEM methods start from what is known as the weak form of the partial differential equation, where the weighted residual form of the partial differential equation has been integrated by parts. Concentration is replaced with an approximation function often using linear basis functions. The most common FEM methods use the same weighting function as approximation function; these are known as Galerkin techniques. Each element is numerically integrated and the values combined to assemble a global matrix and vector (known from FEM's engineering origin as the *stiffness* matrix and *load* vector). The boundary conditions are then applied and the resulting matrix system solved. The FEM leads to a sparse matrix which may be solved by standard optimised solvers, such as Conjugant Gradient.[124]

All unknown concentration values are thus obtained and flux values may be calculated by substituting any previously unknown concentration values.

Boundary Element

The BEM method starts from the inverse (also known as strong) form of the partial differential equation. The weighted residual form is integrated by parts twice to obtain the inverse form. The weighting function used is a free space Green's function, called the fundamental solution. The fundamental solution is derived from the original partial differential equation, and is therefore specific to that equation. A method to use the same fundamental solution for different partial differential equations is described in Chapter 3 on page 130. The elements are numerically integrated and resulting values assembled into *influence coefficient* matrices. Boundary conditions are then applied and the resulting matrix system solved. The BEM leads to a fully populated matrix which may be solved by standard linear algebra solvers such as LU factorisation.[124]

Concentration and flux values are both obtained directly by the method. Thus current may simply be calculated from the flux value. A full derivation of the BEM for one dimension is contained in Chapter 2 on page 48, which includes details of implementation for two dimensions.

1.4.5 Application of the methods to typical electrochemical partial differential equations

This section highlights some of the applications of the three methods to electrochemistry. It is not intended to be a review of all applications but aims to emphasize the advantages and disadvantages of each method in solving particular classes of electrochemical problems.

For diffusion only systems all three methods perform well, provided FD and FE meshes have sufficient optimisation for boundary singularities. The discussion of additional factors that follows assumes such optimisations have been included.

When convection is introduced this often causes problems for numerical methods due to the nature of the governing partial differential equation changing from parabolic to hyperbolic when convection dominates diffusion at higher flow rates. The FDM performs well as long as a suitable algorithm is chosen,[70] such as Backward Implicit in one dimension and Strongly Implicit in two dimensions. The standard FEM and BEM are often adequate for low flow rates but require special formulations for convection dominated flow. For the former this is known as Streamline-Diffusion Finite Element Method.[120] The latter, the BEM formulation, must usually resort to domain discretisation.[125,126]

The inclusion of homogeneous reactions is perhaps the most challenging of electrochemical systems to simulate. There has been a significant amount of development, for a wide range of mechanisms, of simulations utilising the FDM. This has led to generalised algorithms in one dimension,[55] and more recently in two dimensions,[74,75] which have the potential to simulate any electrochemical mechanism. This is a distinct advantage compared to present development of FEM and BEM. The FEM has been successfully applied to several homogeneous reactions.[96,127–129]

The BEM has been applied to simple homogeneous reactions in the field of chemical engineering,[103] however it is more complex to implement and greater research is required into electrochemical applications.

1.4.6 Summary

In summary, the relative merits of FDM, FEM and BEM have been assessed.

FDM has been most widely applied in electrochemistry. It is reasonably easy to understand and implement, and is capable of simulating a variety of electrochemical reactions, linear, non-linear and coupled. In one dimension any mechanism may be simulated; commerical packages[9] and open source packages[7] are available. In two dimensions a more general class of finite difference type methods, matrix methods, also allows general mechanistic simulations. However these methods are inflexible with regard to the geometry modelled and specific optimisations are usually required. It is often not possible to find a suitable optimisation for complex domains.

The FEM method is more suitable to simulate complex geometries, especially if some kind of adaptive mesh routine is implemented. It may be applied to a wide range of electrochemical reactions and flow effects. Although uptake has not been rapid in electrochemistry, it is now the most popular method in related fields, particularly engineering, and a wide range of literature and texts are available. However, three dimensional simulations are complex and optimisations are required for electrochemical problems.

The BEM method is ideally suited for complex geometries in two or three dimensions. Defining a domain mesh is easier than the alternative methods due to a reduction in dimension by one. However there are some drawbacks. The depth of research and availability of texts is much reduced compared to the two alternative methods. Incorporating multiple species is involved and general techniques are only appropriate for linear systems of equations.

Chapter 2

The Application of the Boundary Element Method in Electrochemistry

In this chapter the concepts of the Boundary Element Method (BEM) are illustrated with a simple electrochemical problem, the simulation of the steady state current in a Thin Layer Cell (TLC). In this system mass transport occurs by planar diffusion. A TLC may be modelled as a steady state generator-collector system, figure 2.1 on the following page, and has an analytically determined current which will be used to validate the Boundary Element Method. The terms generator and collector originate from a description of electrochemical systems in terms of feedback, a concept described in section 2.5.1 on page 76. In practice the steady state would be observed at long times after applying a potential step from a value where no reaction occurs to one where the reaction is diffusion controlled.

Thin Layer Cells are typically operated in either potential step or potential sweep configurations. Uses include adsorption, electrodeposition and spectrochemical studies. TLC theory and mathematical analysis may also be applied to a number of other electrochemical problems.[1]

Initially the fundamental BEM theory is derived in one dimension, then a two dimensional model of a TLC is used to expand upon the implementation of the method. The BEM procedure is summarized in figure 2.2 on the following page.

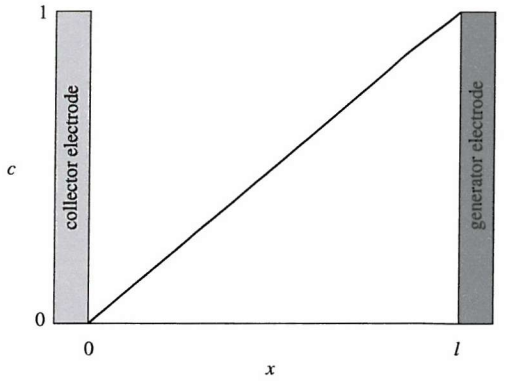

Figure 2.1: Representation of a Thin Layer Cell (TLC). Diffusion is uniformly planar, thus transport in the TLC may be modelled with a one dimensional equation along the x axis. c is concentration of species A.

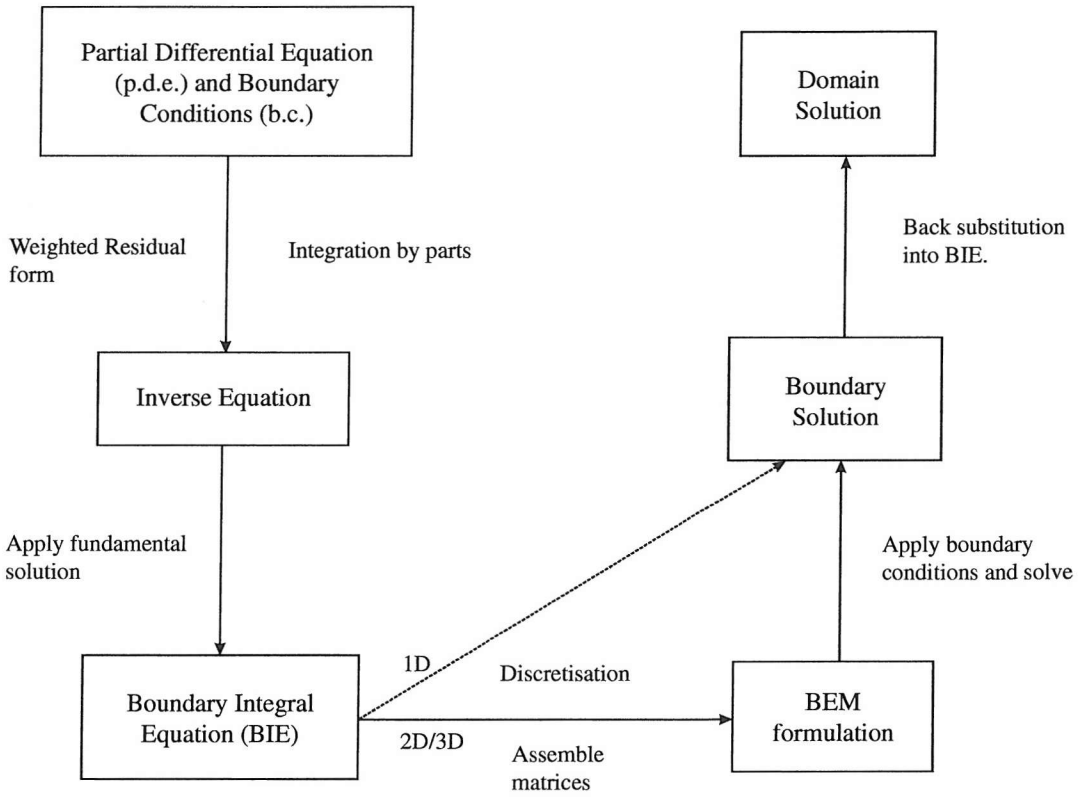

Figure 2.2: A summary of the Boundary Element Method procedure. The one dimensional case may be solved directly from the third stage by applying boundary conditions. For the two and three dimensional cases additional steps are required.

2.1 Fundamentals of the Boundary Element Method

Transport of reactant and product within the Thin Layer Cell system is described by the one dimensional steady state diffusion equation

$$\frac{\mathrm{d}^2 c(x)}{\mathrm{d}x^2} = 0 \tag{2.1}$$

where $c(x)$ is the dimensionless concentration of species A at coordinate x. Note the subscript A is omitted for clarity. This is known as the Laplace equation in one dimension.

The weighted residual form, as described in section 1.4.4 on page 43, is

$$\int_0^l \frac{\mathrm{d}^2 c(x)}{\mathrm{d}x^2} W(x)\,\mathrm{d}x = 0 \tag{2.2}$$

where W is an arbitrary weighting function, 0 and l are the coordinates of the electrodes, see figure 2.1 on the preceding page.

Integrating by parts twice gives

$$\int_0^l \frac{\mathrm{d}^2 c(x)}{\mathrm{d}x^2} W(x)\,\mathrm{d}x = \left[W(x)\frac{\mathrm{d}c(x)}{\mathrm{d}x}\right]_0^l - \left[\frac{\mathrm{d}W(x)}{\mathrm{d}x}c(x)\right]_0^l + \int_0^l \frac{\mathrm{d}^2 W(x)}{\mathrm{d}x^2} c(x)\,\mathrm{d}x \tag{2.3}$$

where c is concentration of species A, W is a weighting function and l is a distance between two electrodes.

This is known as the Inverse Form* of the original partial differential equation. Note the first two terms are boundary only values; calling this part

$$B = \left[W(x)\frac{\mathrm{d}c(x)}{\mathrm{d}x}\right]_0^l - \left[\frac{\mathrm{d}W(x)}{\mathrm{d}x}c(x)\right]_0^l \tag{2.4}$$

*Equation 2.3 is also known as the adjoint form. The Laplacian operator on W is the same as the original operator, the equation is thus self-adjoint.[103]

gives the more compact form

$$\int_0^l \frac{\mathrm{d}^2 c(x)}{\mathrm{d}x^2} W(x)\,\mathrm{d}x = B + \int_0^l \frac{\mathrm{d}^2 W(x)}{\mathrm{d}x^2} c(x)\,\mathrm{d}x \tag{2.5}$$

If we ensure W fulfills certain conditions the differential operator may be simplified or eliminated, leading to a boundary only formulation.

2.1.1 The Fundamental Solution

Obtaining a suitable equation for the weighting function is an important prerequisite of the Boundary Element Method. A special function, called the Dirac delta function, gives one of the properties required.

The Dirac delta function A Heaviside step function, H, has the properties shown in figure 2.3 on the next page,

$$H(x-s) = \begin{cases} 0 & \text{if } x < s \\ 1 & \text{if } x \geq s \end{cases} \tag{2.6}$$

The derivative of the Heaviside step function is the Dirac delta function

$$\delta(x-s) = \begin{cases} 0 & \text{if } x < s \\ \infty & \text{if } x = s \\ 0 & \text{if } x > s \end{cases} \tag{2.7}$$

When used within an integral equation this has a *sifting property* for any function $f(x)$.

$$\int_{-\infty}^{\infty} f(x)\delta(x-s)\mathrm{d}x = f(s) \tag{2.8}$$

The weighting function, $W(x, \xi_1)$, is chosen such that it satisfies the Dirac delta property and is independent of boundary conditions. This type of weighting func-

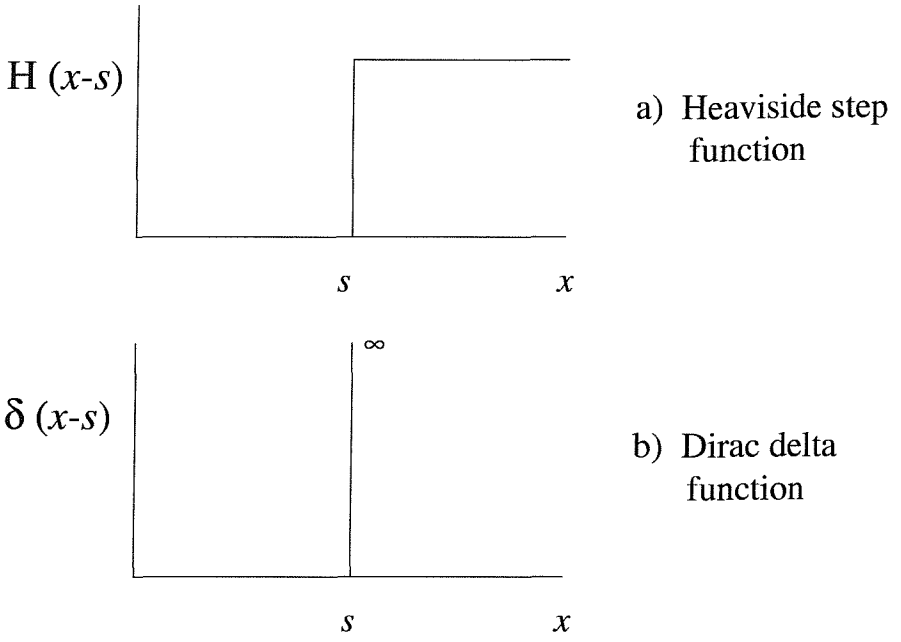

Figure 2.3: Functions used in the derivation of the fundamental solution. The Dirac delta function is the derivative of the Heaviside step function.

tion, of central importance to the Boundary Element Method, is called the fundamental solution. Strictly, it is the fundamental solution to the Laplacian operator. The fundamental solution may be thought of as a generalized Green's function.[22] Physically it represents steady state diffusion of any species from a source point to infinity.

The fundamental solution to the one dimensional Laplace equation is[23]

$$W(x, \xi_1) = \delta(x - s) = \frac{r}{2} \tag{2.9}$$

where $r = |x|$.

The sifting property of the fundamental solution means the final term of the inverse form, equation 2.5, is zero everywhere except at the point where the equation is applied. This point, for historical reasons, is called the source point. The equation

is reduced to

$$\left[W(x,\xi_1)\frac{\mathrm{d}c(x)}{\mathrm{d}x}\right]_0^l - \left[\frac{\mathrm{d}W(x,\xi_1)}{\mathrm{d}x}c(x)\right]_0^l + c(\xi_1) = 0 \tag{2.10}$$

which is known as the Boundary Integral Equation (BIE). This equation is valid anywhere in the domain. As the aim is to obtain a boundary only solution the source point is moved to the boundaries.

This stage is the third box in figure 2.2 on page 49 and is a boundary only formulation. The remaining stages in figure 2.2 do not apply to the one dimensional case; as the boundaries are simply two points, discretisation is not required and the solution may be obtained directly.

This gives two equations, one for each end of the domain, and two unknowns, hence one can solve to find the unknown values.

2.2 BEM Implementation in Two Dimensions

The advantages of the BEM over alternative simulation methods become useful for two and three dimensional problems. A two dimensional model of a Thin Layer Cell, figure 2.4, is considered here to introduce the two dimensional BEM implementation.

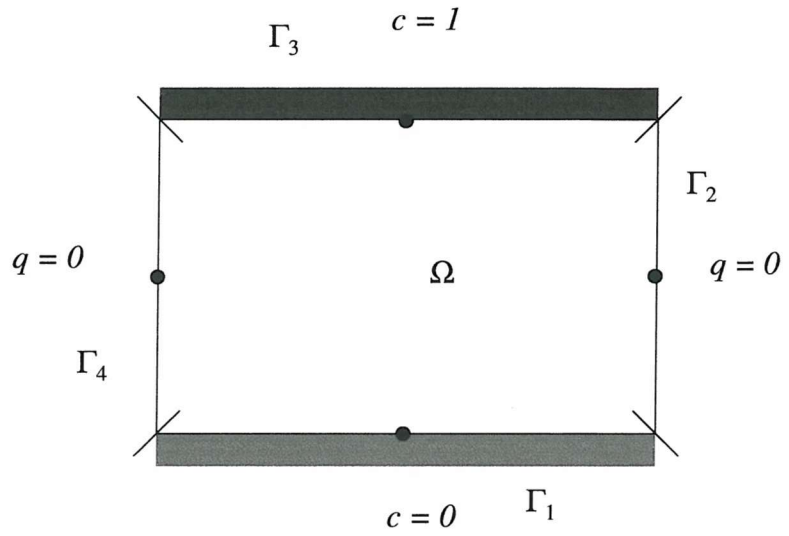

Figure 2.4: A model domain of a Thin Layer Cell. Ω is the internal domain, Γ is the entire boundary, which consists of 2 boundary conditions: Γ_1 and Γ_3 are known concentrations, Γ_2 and Γ_4 are known fluxes. This diagram shows the simplest discretisation of the domain; into four elements. Concentration and flux have a constant value along each element.

The boundary of the TLC domain is described in terms of four regions, table 2.1.

Region	Boundary Condition	Boundary Value	Description
Γ_1	Dirichlet	$c = 0$	generator
Γ_2	Neumann	$q = 0$	insulator
Γ_3	Dirichlet	$c = 1$	collector
Γ_4	Neumann	$q = 0$	insulator

Table 2.1: Definition of the domain boundary for the Thin Layer Cell model shown in figure 2.4

The governing partial differential equation is the two dimensional form of the Laplace

equation

$$\frac{\partial^2 c(x,y)}{\partial x^2} + \frac{\partial^2 c(x,y)}{\partial y^2} = 0 \tag{2.11}$$

The weighted residual form of this is

$$\int \left(\frac{\partial^2 c(x,y)}{\partial x^2} + \frac{\partial^2 c(x,y)}{\partial y^2} \right) W(x,y,\xi_1,\xi_2)\, \mathrm{d}x\, \mathrm{d}y = 0 \tag{2.12}$$

where $c(x,y)$ is the dimensionless concentration, $W(x,y,\xi_1,\xi_2)$ is the fundamental solution and ξ_1, ξ_2 are source point coordinates.

This is integrated by parts, twice, to give the Boundary Integral Equation

$$dc(\xi_1,\xi_2) + \int_\Gamma c(x,y) \frac{\partial W(x,y,\xi_1,\xi_2)}{\partial n}\, \mathrm{d}\Gamma = \int_\Gamma \frac{\partial c(x,y)}{\partial n} W(x,y,\xi_1,\xi_2)\, \mathrm{d}\Gamma \tag{2.13}$$

where	d	is a geometry coefficient caused by moving the source point to the boundary, explained below
	$c(\xi_1,\xi_2)$	is the concentration at the source point
	Γ	is the domain boundary
	$c(x,y)$	is the concentration around the boundary
	$W(x,y,\xi_1,\xi_2)$	is the fundamental solution
	n	the element unit outward normal
	ξ_1,ξ_2	are source point coordinates.

The source point is the point of application of the entire equation. This may be applied anywhere but is chosen to be moved to the boundary. The field point is used to integrate over the boundary, thus is restricted to the boundary only. The fundamental solution is defined as a function of both source and field points.

The BIE consists of three terms. The first is a geometry coefficient term, explained below. The second and third are boundary terms which account for the infiuence of concentration and flux respectively, along the boundary, upon the source point.

The Geometry Coefficient When equation 2.13 is applied at a point on the boundary, the integrals behave differently than inside the domain. This is accounted

for by a geometry coefficient, d, which is defined[22]

$$d = \frac{\theta}{2\pi} \tag{2.14}$$

where θ is the internal angle at the boundary, in radians. The internal angle is illustrated in figure 2.5 on the next page. It is found that

- $d = \frac{1}{2}$ on a smooth boundary
- $d = 1$ if in the interior of the domain

The term 'smooth' is used in the mathematical context meaning that the boundary does not have any sharp corners about the source point. Constant elements, which are used throughout this section, by their definition will always have a smooth boundary and therefore $d = 1/2$. Section 2.10.1 on page 123 describes higher order variations of variables along elements.

The unit outward normal is defined as the direction perpendicular to an element, facing outward, when elements are defined in a consistent manner, figure 2.6 on page 58.

Defining

$$q = \frac{\partial c}{\partial n} \tag{2.15}$$

$$q^* = \frac{\partial W}{\partial n} \tag{2.16}$$

yields a more compact version of equation 2.13, the Boundary Integral Equation,

Internal Angle	Geometry Coefficient	
$\theta = \pi$	$d = \frac{1}{2}$	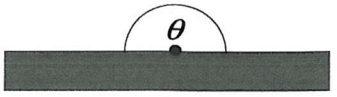
$\theta = \frac{3\pi}{2}$	$d = \frac{1}{3}$	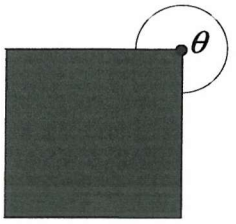
$\theta = 2\pi$	$d = 1$	

Figure 2.5: Examples of internal angles. Definition of the internal angle, θ is given in equation 2.14. Shaded areas are boundaries, the final row is an internal point.

$$dc(\xi_1, \xi_2) + \int_\Gamma c(x, y) q^*(x, y, \xi_1, \xi_2)\, \mathrm{d}\Gamma = \int_\Gamma q(x, y) W(x, y, \xi_1, \xi_2)\, \mathrm{d}\Gamma \qquad (2.17)$$

where

d	is the geometry coefficient
c	is concentration
q	is flux
Γ	is the domain boundary
W	is the fundamental solution
q^*	is the derivative of the fundamental solution
ξ_1,ξ_2	are source point coordinates.
s	a subscript indicating the source point

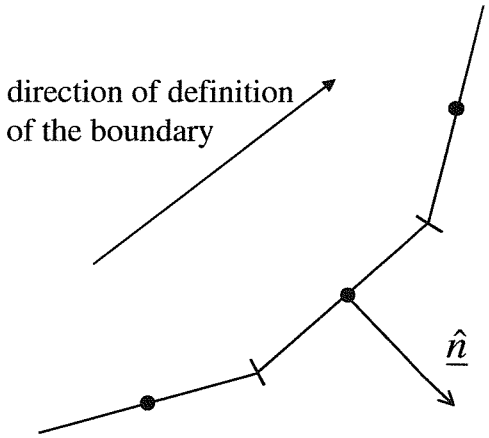

Figure 2.6: The direction of the outward normal is perpendicular to the element facing away from the interior domain. The direction of the definition of the boundary must be consistent.

Discretisation of the boundary A practical way to solve the integrals over the boundary is required. To enable this the boundary is split into sections, called elements, in a process known as discretisation. The simplest possible discretisation of the TLC domain is shown in figure 2.4 on page 54. Concentration and flux values are defined as constant along each element.

The boundary integration is performed by integrating over a small element, then over the next element and proceeding all the way around the boundary, figure 2.7(i-iv) on the next page. Thus the integral terms are represented as the sum of the integrals over these elements.

Each boundary element has one source point at its centre. When the boundary is discretised into N elements there will be N source points, each of which is considered in turn, figure 2.7(1-4) on the following page, leading to a set of N equations 2.18.

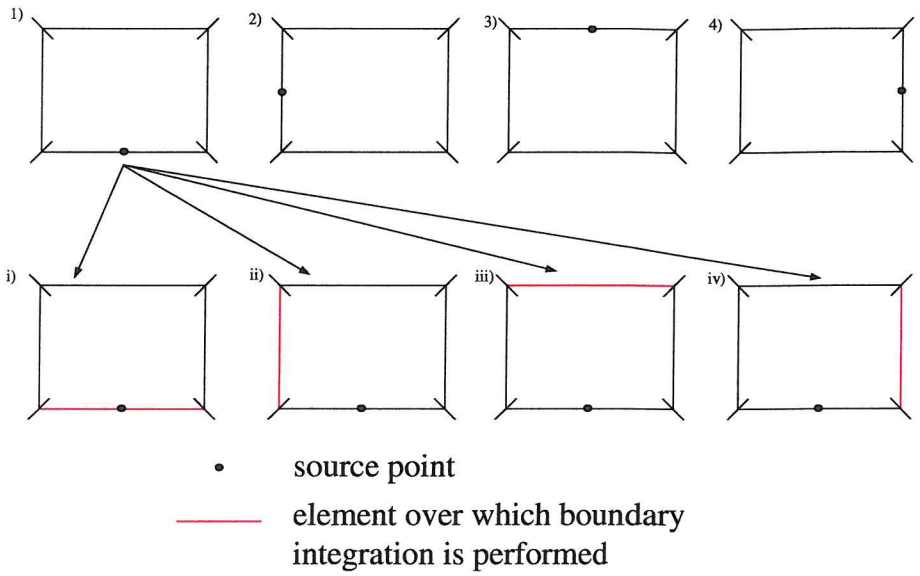

Figure 2.7: Numerical integration is performed over each element in turn, including the element containing the source point. Choice of a clockwise direction is arbitrary.

The discrete BIE is thus

$$\frac{1}{2}c_s(\xi_1,\xi_2) + \sum_{j=1}^{N} c_j(x,y) \int_{\Gamma j} q^*_{sj}(x,y,\xi_1,\xi_2)\, \mathrm{d}\Gamma = \sum_{j=1}^{N} q_j(x,y) \int_{\Gamma j} W_{sj}(x,y,\xi_1,\xi_2)\, \mathrm{d}\Gamma \tag{2.18}$$

where
- c is concentration
- q is flux
- Γ_j is an element boundary
- W is the fundamental solution
- q^* is the derivative of the fundamental solution
- ξ_1,ξ_2 are source point coordinates.
- s is the source point integer counter
- j is the field point integer counter

Any shape boundary may be modelled by constant elements, although a geometric approximation is required to model curved boundaries. More advanced BEM formulations consider higher order variations of concentration and flux along the element. Section 2.10 on page 123 describes elements that more accurately represent boundary values.

2.2.1 2D Fundamental Solution and its Derivative

For two dimensions the fundamental solution is chosen such that

$$\frac{\partial^2 W(x,y,\xi_1,\xi_2)}{\partial x^2} + \frac{\partial^2 W(x,y,\xi_1,\xi_2)}{\partial y^2} = -\delta(x-\xi_1)\delta(y-\xi_2) \tag{2.19}$$

where δ is the Dirac function, ξ_1,ξ_2 are source point coordinates, x,y are field point coordinates.

For the Laplace equation in two dimensions[22] $W(x,y,\xi_1,\xi_2)$ is

$$W(x,y,\xi_1,\xi_2) = -\frac{1}{2\pi}\ln r \tag{2.20}$$

where r is the distance between source and field points

$$r = \left[(x-\xi_1)^2 + (y-\xi_2)^2\right]^{\frac{1}{2}} \tag{2.21}$$

The derivative of W with respect to the outward normal is

$$\frac{\partial W}{\partial n} = -\frac{1}{2\pi r^2}\left[(x-\xi_1)n_x + (y-\xi_2)n_y\right] \tag{2.22}$$

where r is the distance between source and field points and n_x,n_y are directional cosines.

2.2.2 Singular Integration

When integration is performed over an element containing the source point, a singularity occurs at this point. Ordinary numerical integration techniques are not capable of integrating singular elements. There are a variety of ways to approach this problem. For specific types of element an analytical solution may be available. Alternatively many specific types of quadrature may be used, if available; for example the logarithmic behaviour of the two dimensional Laplace fundamental solution may be integrated by logarithmic Gaussian quadrature.[130] If neither of these

approaches is suitable a Telles transformation[131] may be used.

In the case of the two dimensional Laplace fundamental solution, with constant elements, an analytical solution is available, as the integral is symmetrical about the centre point.[22]

$$\int_{\Gamma j} W_{ss}(x, y, \xi_1, \xi_2)\, \mathrm{d}\Gamma = \frac{L_s}{2\pi}\left(1 - \mathrm{In}\left(\frac{L_s}{2}\right)\right) \tag{2.23}$$

where L_s = length of element.

For the derivative of the fundamental solution, since the line element and normal are orthogonal, the dot product is zero, so equation 2.22 is always zero.

2.2.3 Numerical Integration

A standard numerical integration technique,[124] Gaussian quadrature, is used to integrate over non-singular boundary elements.

The integral is approximated as a sum of the values at specific points, figure 2.8 on the following page. The location of these points is dictated by the technique used, and has a significant effect on accuracy.

$$\int f(x)\, \mathrm{d}x \simeq \sum_{g=1}^{NI} f_g(x)\omega_g \tag{2.24}$$

where ω is the quadrature weighting factor, NI is the number of integration points and g is an integer counter.

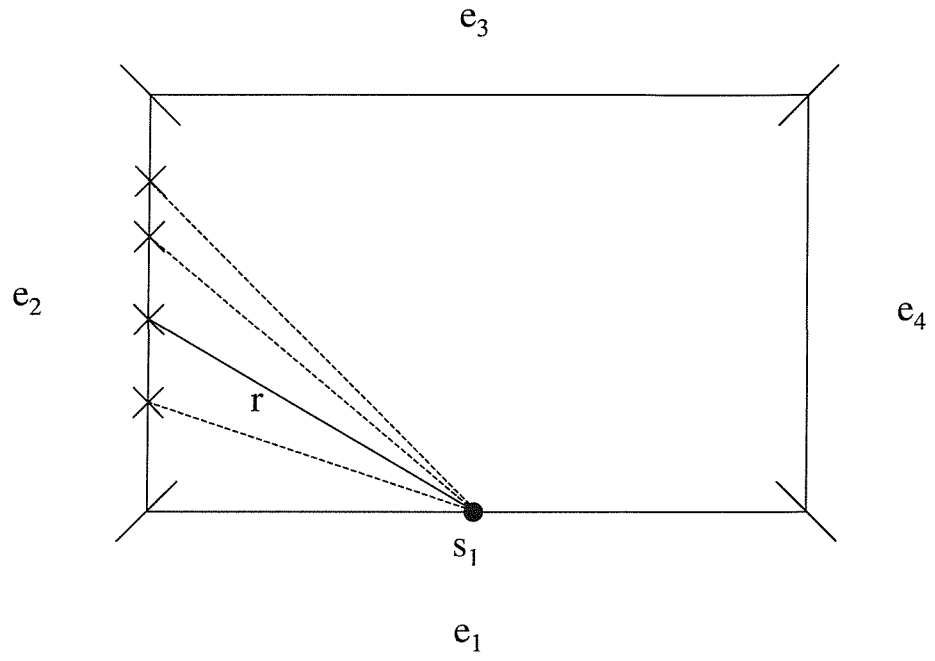

Figure 2.8: Gaussian quadrature integration over element e_2 from source point s_1

Applying Gaussian quadrature to the boundary integrals gives

$$\int_{\Gamma j} W_{sj}(x, y, \xi_1, \xi_2)\, \mathrm{d}\Gamma = \frac{L_j}{2} \sum_{g=1}^{NI} \left(W(x, y, \xi_1, \xi_2)\right)_g \omega_g \tag{2.25}$$

$$\int_{\Gamma j} q^*_{sj}(x, y, \xi_1, \xi_2)\, \mathrm{d}\Gamma = \frac{L_j}{2} \sum_{g=1}^{NI} \left(q^*(x, y, \xi_1, \xi_2)\right)_g \omega_g \tag{2.26}$$

where L_j is the length of the element, NI is the number of integration points, and ω_g are the quadrature weighting factors. Weighting factors are calculated in the range -1 to 1. A local coordinate transform is used leading to the coefficient of $L_j/2$.

Note that singular and numerical integration are the first introduction of numerical approximation in the BEM formulation.

2.2.4 Formation of Influence Coefficient Matrices

The symbols $\hat{l}_{sj}$ and m_{sj} are defined to represent the two types of integrals over the boundary. c and q have been removed from the integrals as they are constant.

$$\hat{l}_{sj} = \int_{\Gamma j} q^*_{sj}(x, y, \xi_1, \xi_2)\, \mathrm{d}\Gamma \tag{2.27}$$

$$m_{sj} = \int_{\Gamma j} W_{sj}(x, y, \xi_1, \xi_2)\, \mathrm{d}\Gamma \tag{2.28}$$

where Γ_j is the length of the element.

Equation 2.18 may be cast in matrix form using the following rules

$$l_{sj} = \hat{l}_{sj} \qquad \text{when } s \neq j \tag{2.29}$$

$$l_{sj} = \hat{l}_{sj} + \frac{1}{2} \qquad \text{when } s = j \tag{2.30}$$

Thus equation 2.18 becomes

$$\sum_{j=1}^{N} L_{sj} c_j = \sum_{j=1}^{N} M_{sj} q_j \tag{2.31}$$

which in matrix notation is

$$\mathsf{L}\boldsymbol{c} = \mathsf{M}\boldsymbol{q} \tag{2.32}$$

where L and M are known as influence coefficient matrices, and are of dimension $N \times N$. They are dependent solely on the geometry of the domain.

2.2.5 Boundary Solution

We now have a system with $2N$ variables of which N are known, as a boundary condition is prescribed for each element. This leaves N unknowns. Equation 2.32 may be resolved by multiplying known boundary values with influence coefficients

to form

$$\mathsf{A}\boldsymbol{x} = \boldsymbol{B} \tag{2.33}$$

where A are the combined unknown boundary value influence coefficients, $\boldsymbol{x}$ the unknown values and $\boldsymbol{B}$ the combined known influence coefficients and boundary values. Equation 2.33 may be solved using standard matrix algebra routines.[124]

At this stage, the penultimate box in figure 2.2 on page 49, all unknown boundary values have been found. Note *both* concentration and flux values have been found directly, in contrast to FDM and FEM techniques when flux must be calculated from concentration values. The final, optional, stage is to calculate any values required for the interior domain.

2.2.6 Internal Points

Concentration and flux values may be obtained anywhere within the domain, once the boundary solution is known, simply by defining the coordinates of the points required. As many points as required may be placed anywhere in the domain. An example distribution of points to obtain a concentration map covering the entire domain is shown in figure 2.9 on the next page. However if a certain area is of particular interest values may be calculated only in this area, unlike domain simulation methods which always require simulation over the entire domain.

As for the boundary, flux values in the interior may be obtained directly. For the two dimensional system these will be vectors consisting of x and y components.

Rearranging equation 2.17 gives an expression for concentration (note that $d = 1$ for internal points).

$$c(\xi_1, \xi_2) = \int_\Gamma q(x,y) W(x,y,\xi_1,\xi_2)\, \mathrm{d}\Gamma - \int_\Gamma c(x,y) q^*(x,y,\xi_1,\xi_2)\, \mathrm{d}\Gamma \tag{2.34}$$

which in compact form is

$$c_s = M_{sj} q_s - L_{sj} c_s \tag{2.35}$$

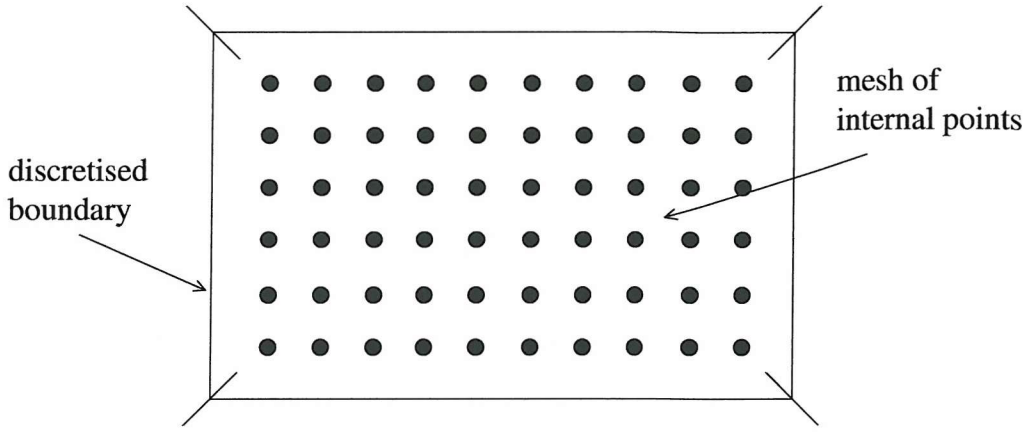

Figure 2.9: Internal points may be placed anywhere in the domain, here an equally spaced mesh is used to observe concentration values. In contrast to the FDM and FEM techniques values may be obtained only where required, not everywhere in the domain. Both concentration and flux values are found directly.

L_s and M_s must be calculated for each point, however, as all boundary values are now known each internal point may be calculated sequentially. A matrix solving step is not required.

The derivatives of equation 2.34 give the flux

$$\left(\frac{\partial c}{\partial x}\right)_s = \int_\Gamma q \left[\frac{\partial W}{\partial x}\right]_s \mathrm{d}\Gamma - \int_\Gamma c \left[\frac{\partial q^*}{\partial x}\right]_s \mathrm{d}\Gamma \tag{2.36}$$

$$\left(\frac{\partial c}{\partial y}\right)_s = \int_\Gamma q \left[\frac{\partial W}{\partial y}\right]_s \mathrm{d}\Gamma - \int_\Gamma c \left[\frac{\partial q^*}{\partial y}\right]_s \mathrm{d}\Gamma$$

2.2.7 Application to a Simple Case

To illustrate the implementation of the Boundary Element Method to electrochemical problems, the method is applied to the simple two dimensional TLC domain, figure 2.4 on page 54.

Results for the model are shown in table 2.2 on the next page. With as few as four

elements, remarkably accurate concentration and flux values are obtained. Doubling the total number of elements to eight gives less than one percent error in concentration and six percent error in flux. Increasing the number of elements further continues to increase accuracy; for example 400 elements gives less than 0.1% error in both concentration and flux near the centre of the sides of the domain. The elements immediately adjacent to the corners of the domain have a significantly higher error, up to 6% for both concentration and flux. However, within three elements this has reduced to under 0.5% error.

Element	Known boundary condition	Analytical		BEM N=4	
		c	q	c	q
1	c	0.000	−1.000	–	−1.175
2	q	50.000	0.000	50.000	–
3	c	1.000	1.000	–	1.175
4	q	50.000	0.000	50.000	–

a)

Internal point coordinates		Analytical			BEM N=4		
x	y	c	q_x	q_y	c	q_x	q_y
0.333	0.333	0.333	0.000	1.000	0.354	−0.095	0.902
0.5	0.5	0.500	0.000	1.000	0.499	0.000	0.900
0.667	0.667	0.667	0.000	1.000	0.650	−0.036	0.962

b)

Table 2.2: Concentration and flux values for the simplest possible two dimensional domain, figure 2.4. N is the total number of elements. *Continued on the following page.*

Element	Known boundary condition	Analytical		BEM N=8	
		c	q	c	q
1	c	0.000	−1.000	–	−1.059
2	c	0.000	−1.000	–	−1.059
3	q	0.250	0.000	0.241	–
4	q	0.750	0.000	0.759	–
5	c	1.000	1.000	–	1.059
6	c	1.000	1.000	–	1.059
7	q	0.750	0.000	0.759	–
8	q	0.250	0.000	0.241	–

c)

Internal Point Coordinates		Analytical			BEM N=8		
x	y	c	q_x	q_y	c	q_x	q_y
0.333	0.333	0.333	0.000	1.000	0.331	0.015	0.999
0.5	0.5	0.500	0.000	1.000	0.500	0.000	1.012
0.667	0.667	0.667	0.000	1.000	0.669	0.014	0.998

d)

Table 2.2: *continued.*

2.3 Domain Meshing

A mesh is a particular discretisation of boundary elements. The input for a BEM program consists of the coordinates of the boundary elements†, plus known boundary conditions and values. These must be specified in a consistent direction to ensure flux is defined identically for all elements. Additionally the coordinates of any internal points may be included if these are desired.

The behaviour of concentration and flux for two different types of domain will not be identical thus one particular mesh is not necessarily valid for both domains.

Finite Difference[12,16,91,92] and Finite Element[132] experience has shown that efforts to increase the number of points near areas of high flux have a considerable effect on accuracy. Expanding grids and conformal maps have proven to be most effective in this regard. Increasing the density of boundary elements may have an analogous effect. This problem may be addressed in a number of ways. For example, empirically, increasing the number of elements near known areas of high flux, or using an automatic adaptive mesh, which calculates an error value at each element. If this is greater than a threshold error, then the element size is reduced.[133–135]

An important feature of modelling microelectrodes is the boundary singularity caused by the abrupt change in boundary conditions at the edge of the electrode. At the point of singularity the magnitude of the flux approaches infinity. Therefore the variation of flux across the electrode contains large flux gradients. There is very little concerning BEM mesh optimisation and discretisation behaviour in the literature. The effect of different discretisation strategies for the BEM applied to microelectrode problems is investigated in sections 2.5.3 on page 98 and 2.7.1 on page 110.

A mesh input routine is required to generate a suitable boundary mesh for the domain to be modelled. It is advantageous if the number of elements over different parts of the boundary are flexible. The mesh generated should be exactly reproducible when the same input is used. To exploit the benefits of the BEM a variety of geometries need to be described. Programming a flexible input routine for the BEM involves considerable effort. Preferably, the routine should also be extensible

†For linear or higher order elements the connections of elements must also be specified.

to unforseen geometries. Two and three dimensional mesh generation is currently an active area of research.[136]

2.4 Computational Aspects

The steps in a typical Boundary Element Method program are described in table 2.4 on the following page. The second and third steps, the core of the method, are shown in more detail using pseudo-code. Any programming language may be used to create a BEM program. However, both the core method and a flexible input routine benefit from the advantages of an object-oriented language[137–139] such as C++[140,141] or Java.[142] Double precision floating point variables were used at all times.

2.4.1 Matrix Solving Routines

Solving the matrix equation, equation 2.33, is the slowest step in the BEM simulation. The size of A is determined by the total number of source points used to discretise the domain. If higher order elements are used, this may increase the number of source points thus enlarging A. For linear elements the number of source points is equal to the number of elements, and although flux components are computed separately, they are combined before the matrix inversion step.

In contrast to FDM and FEM methods there is no banded structure to the matrix, it is always fully populated. Although it takes longer to solve an equation with a fully populated matrix, the discretisation of the domain requires fewer elements than these alternative methods, resulting in much smaller matrices. Matrix solving is an $O(N^3)$ process[‡], so the practical limit on the total number of elements is reached fairly quickly. It is possible to increase the speed of the process[124,143] if specific character traits are present in A.

Some limited investigations were made as to the character of matrix A, as it is important to ascertain the possibility of any errors arising from the matrix solving procedure. For all domains tested A was found to be stable and was not ill-conditioned, and all were diagonally dominant. Both pivoting Gaussian elimination and LU decomposition were used in the simulations herein.

[‡]The Gaussian elimination algorithm has a computational cost which scales with $O(N^3)$ and a memory requirement which scales with $O(N^2)$.

1. Input the boundary geometry, boundary conditions and associated values.

2. Loop source point, $s = 1$ to $s = N$
   Loop element, $j = 1$ to $j = N$
   If integration is non-singular $(s \neq j)$
   Loop gaussian integration $g = 1$ to $g = NI$
   $L(s,j) = L(s,j) + k\left[q^*_{sj}(x,y,\xi_1,\xi_2)\right]_g$ (eqn. 2.27)
   $M(s,j) = M(s,j) + k\left[W^*_{sj}(x,y,\xi_1,\xi_2)\right]_g$ (eqn. 2.28)
   Else integration is singular $(s = j)$
   $L(s,j) =$ analytical solution (eqn. 2.23)
   $M(s,j) = 1/2$

3. Apply boundary conditions to form matrix A and vector $\boldsymbol{B}$.

   Loop source point, $s = 1$ to $s = N$
   Loop element, $j = 1$ to $j = N$
   If bc=known concentration: $A(s,j) = -M(s,j)$
   $B(s) = -L(s,j)c(j)$
   Else bc=known flux: $A(s,j) = L(s,j)$
   $B(s) = M(s,j)q(j)$

4. Standard linear algebraic equation solver, for example, Gaussian Elimination, obtains the unknown values $\boldsymbol{x}$.

5. Order boundary values obtained into vectors $\boldsymbol{c}$ and $\boldsymbol{q}$ which already contain known values. All boundary values are now known.

6. Repeat step 2 for each internal point if any exist, which become the source points, remembering $d_s = 1$. Obtain concentration and flux values from equations 2.34 and 2.36 respectively.

Table 2.3: A description of the steps in a constant element Boundary Element Method program. Symbols used in the table are; N total number of boundary elements, s source point integer counter, j element integer counter, g gaussian integration integer counter, k gaussian integration constant, NI number of integration points, L, M influence coefficient matrices, A, B matrix and vector used for linear algebra solver input, W fundamental solution, q^* derivative of fundamental solution, c concentration, q flux.

For validation of the BEM, section 2.5.3 on page 98, each simulation took less than 0.1 seconds.

Programming was completed in a mixture of C[144] and C++, using Microsoft Visual C++6. Simulations were run on various computers including an IBM® SP2, Silicon Graphics® Origin, and Intel® Pentium® 650MHz.

2.5 Validation of the Method

To investigate the properties of the BEM and validate the accuracy of the method an electrochemical system which is described by the Laplace equation in two dimensions is chosen. A double microband is a suitable system for which previous results are available for comparison.

2.5.1 The Double Microband

The double microband (DMB) consists of two microband electrodes situated in close proximity, figure 2.10. The magnitude of the current is affected by the electrode width, the distance between electrodes, and the geometry surrounding the electrodes.

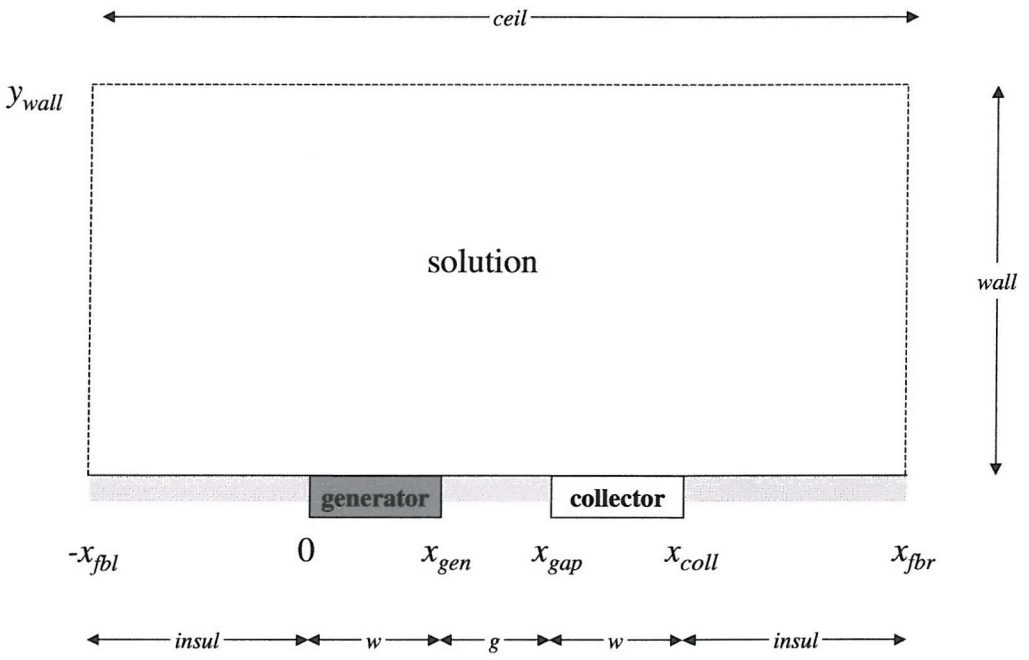

Figure 2.10: The double microband domain. Electrodes are solid coloured, the dotted lines are semi-infinite boundaries and a dashed pattern corresponds to the insulator.

A Note on Boundary Conditions

The double microband system can operate in generation-collection mode where one microband acts as a generator while the other acts as a collector. However, the current obtained at the electrodes will depend on the boundary conditions chosen. Hence it is necessary to distinguish between theoretical, simulated and experimental conditions.

Theory The concentration is equal to bulk concentration *and* flux is equal to zero at an infinite distance from the electrodes; $c = c^*$ *and* $q = 0$.

Simulation The bulk concentration condition *or* zero flux condition apply at a large, but finite, distance from the electrodes; $c = c^*$ *or* $q = 0$.

Experimental We may consider that concentration is equal to the bulk value at a finite distance from the electrodes due to natural convection;[145] $c = c^*$.

In terms of simulation, the current obtained is expected to depend on the far field boundary conditions chosen. For a double microband, inlaid in a flat insulating surrounding material, the steady state reached after a diffusion controlled potential step is considered. One may distinguish three situations corresponding to the three paragraphs above:

Case 1 – A quasi-steady-state, where the current is a function of time; $i = f(1/\ln t)$, when $c = c^*$ *and* $q = 0$ at infinite distance.

Case 2 – A true steady state, when $q = 0$ at a finite distance.

Case 3 – A true steady state, when $c = c^*$ at a finite distance.

The Simulation Model

The electrochemical reaction simulated at the generator electrode is

$$A + e^- \rightarrow B \tag{2.37}$$

where the assumption of equal diffusion coefficients is made to simplify the treatment, $D_A = D_B$. The system is assumed to be diffusion controlled, and only species A is considered. Applying a conservation of matter principle, the concentration of species B is equal to $C_A^* - C_A$, where C_A^* is the concentration of A in bulk solution.

Steady state diffusion gives the Laplace partial differential equation

$$D\frac{\partial^2 C(X,Y)}{\partial X^2} + D\frac{\partial^2 C(X,Y)}{\partial Y^2} = 0 \tag{2.38}$$

Dimensionless Parameters Standard non-dimensional parameters are used[1] and the following variables are defined,

$$c = \frac{C}{C^*}, \quad x = \frac{X}{w}, \quad y = \frac{Y}{w} \tag{2.39}$$

where	c	dimensionless concentration	no units
	C	real concentration	mol cm^{-3}
	C^*	bulk concentration	mol cm^{-3}
	x	dimensionless distance along the x axis	no units
	X	actual distance along x axis	cm
	y	dimensionless distance along the y axis	no units
	Y	actual distance along y axis	cm
	w	width of the generator and collector electrodes	cm

This gives a dimensionless original partial differential equation

$$\frac{\partial^2 c(x,y)}{\partial x^2} + \frac{\partial^2 c(x,y)}{\partial y^2} = 0 \tag{2.40}$$

For simplicity, current is normalised by the steady state current at a Thin Layer Cell, where the distance separating the electrodes in the TLC is equal to the width of the electrodes in the DMB.

$$i_{norm} = \frac{i_{real}}{nFDC^*L} \tag{2.41}$$

where i_{real} is current in A, n is the number of electrons, F the Faraday constant and L the length of the electrodes.

The Feedback Effect

In a generator-collector double microband configuration the collector electrode is placed in close enough proximity to impinge upon the diffusion field of the generator electrode. The collector is set at a potential sufficient to instantaneously convert all of species A which comes into contact with it to species B. The regeneration of species B by the collector leads to an increase in current at the generator. This effect is called positive feedback.

Conversely if a physical object in some way obstructs the natural shape of the diffusion field the amount of species reaching an electrode may be restricted, leading to a reduction in current, known as negative feedback or hindered diffusion.

These phenomena are also seen in other electrochemical systems; for example, Scanning Electrochemical Microscopy (SECM). Depending upon the nature of the substrate (conducting or insulating) positive or negative feedback, respectively, are observed.

A similar feedback effect is of course observed in electrochemical simulations. However, feedback may also occur (erroneously) if a semi-infinite boundary is set too close to the electrodes. If a bulk concentration value is set, positive feedback occurs; with a zero flux condition negative feedback is observed.

This is a common problem with all simulation methods; as part of the validation process, one must ensure that semi-infinite boundaries are at a sufficient distance to have a negligible effect on electrode response.

The positive feedback from concentration boundaries not only affects the magnitude of the current, but will also determine whether two currents are equal and opposite, at steady state, or whether they are slightly different, at quasi-steady-state.

Analytical Solution for the Steady State

In each case, simulation results were compared to the exact solution given by Amatore and Fosset.[146] This was obtained using a specific conformal mapping for the double microband, and solving the steady state diffusion equation in confor-

mal space. The solution is in terms of elliptic integrals which must be numerically integrated.

Current Calculation

The current is simple to calculate from the Boundary Element Method as flux values are obtained directly. Using the dimensionless form of current and discretising the electrode boundary the integral in equation 1.55 becomes a summation of element fluxes giving

$$i_{norm} = \int_0^w \left. \frac{\partial c(x,y)}{\partial y} \right|_{y=0} \mathrm{d}x = \sum_{i=1}^{NE_{elec}} q_i \tag{2.42}$$

where i_{norm} is current, w width of the electrode, $c(x,y)$ concentration, i element number along the electrode, NE_{elec} number of elements along the electrode and q_i the flux at element i.

2.5.2 Discretisation Effects

Discretisation of the domain is an important consideration. Convergence must be shown when increasing the number of elements and optimal parameters for element spacing were investigated. There are singularities at both edges of both electrodes. Exponential grids have proven effective at increasing accuracy in alternative simulation techniques,[7] and their effect within the BEM is considered here. Convergence should also be shown when increasing the distance from the electrode outer edges of the system to the semi-infinite boundary.

Boundary Conditions

The nature of the boundary condition (Dirichlet or Neumann) and its value must be prescribed for each element around the domain. On the generator electrode, as the reaction is diffusion controlled, all species A is instantaneously reduced to species B, giving zero concentration of A. Likewise all of B is instantaneously oxidised back to A at the collector electrode, giving a bulk concentration of A. It is impossible for any

species to cross through the material surrounding the electrodes, thus a boundary condition of zero flux perpendicular to the insulator surface is set. The semi-infinite boundaries, figure 2.10 on page 73, are assumed to be at a far enough distance from the electrodes that the flux is negligible and concentration remains at their bulk value, $c = c^*$. Alternatively one may consider the semi-infinite situation as a zero flux, $q = 0$, condition. Although both conditions are true it is possible to prescribe only one boundary condition. The other is obtained from the simulation and may be compared to the expected value. To test the algorithm, the effect of setting each condition was examined and will be discussed in section 2.5.2 on page 89.

Assuming a zero flux condition for the far field boundaries, the boundary conditions are summarised in table 2.4.

$\frac{\partial c}{\partial n} = 0$	$y = 0$	$-x_{fbl} \leq x < 0$	(2.43a)
		$x_{gen} < x < x_{gap}$	(2.43b)
		$x_{coll} < x \leq x_{fbr}$	(2.43c)
	$y = y_{wall}$	$-x_{fbl} \leq x \leq x_{fbr}$	(2.43d)
	$0 \leq y \leq y_{wall}$	$x = -x_{fbl}$	(2.43e)
		$x = x_{fbr}$	(2.43f)
$c = 0$	$y = 0$	$0 \leq x \leq x_{gen}$	(2.43g)
$c = 1$		$x_{gap} \leq x \leq x_{coll}$	(2.43h)

Table 2.4: Boundary conditions for the double microband simulation. n is the direction normal to the boundary. These conditions would, in practice, require an initial solution of 50% reactant and 50% product if using a two electrode system.

Under these conditions the double microband modelled reaches a steady state as only the electrodes act as source and sink. The simulated collection efficiency should be 100% as the generator current should be identical to the collector current. In the following results only generator currents are shown as all collector currents were within 0.01% of the respective generator current. It should be noted that experimentally this is not the case, as the collection efficiency of the collector is less than 100%. This is due to a proportion of the generated species, B, escaping to the bulk solution, in addition to positive feedback from bulk solution which is transported near to the electrodes by natural convection. For the simulation,

assuming a zero flux far field boundary condition, no matter is allowed to escape giving a 100% collection efficiency.

Equal Spacing

Collector, generator and gap widths were set to the same value, w. The semi-infinite boundaries were initially set at $10w$, then $1000w$.

A simple discretisation with equal length elements and zero flux semi-infinite boundary conditions, Figure 2.11, appears to converge with an error, relative to Amatore's analytical solution,[146] of less than two per cent. This error is due to the proximity of the semi-infinite boundaries, x_{fbl}, x_{fbr} and y_{wall} in figure 2.10 on page 73. See section 2.5.2 on page 89 for additional details.

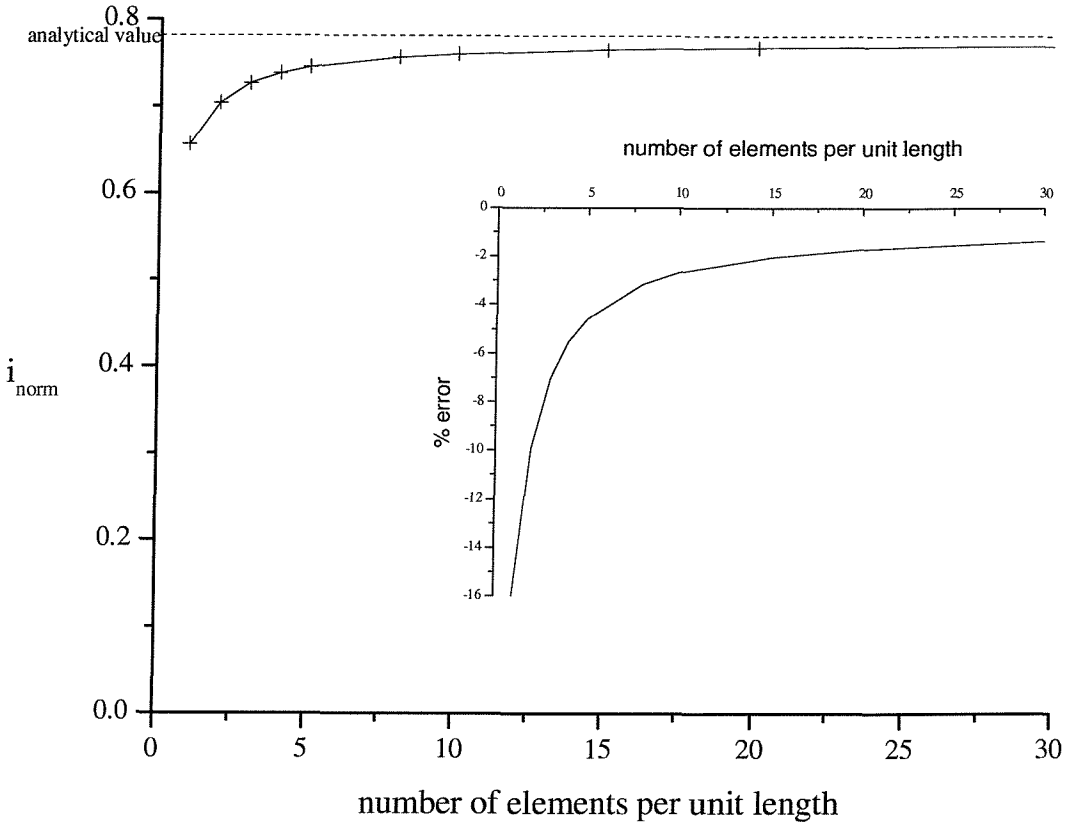

Figure 2.11: A convergence test for the double microband model, using equal sized elements. Parameters used were $w = 1$, $g = 1$, $wall = insul = 10$. Comparison is made with an exact value of 0.7817, calculated using the analytical solution of Amatore and Fosset.[146]

When elements of equal size are used computing limitations prevent positioning the far field boundary far away, as required to reach convergence. Using current computer hardware[§] the number of elements needed give long simulation times, which are impractical. As seen in section 2.4, on page 70, on computational aspects, the time taken to complete a simulation is of $O(N^3)$, where N is the total number of elements. To allow sufficiently large semi-infinite boundary distances different types of mesh discretisation were investigated.

Exponential Mesh Spacing

There has been a significant amount of research undertaken into exponential mesh effects in the electrochemical Finite Difference field.[6,7,66] This has shown that when exponential mesh optimisation is implemented the function used must be continuous and the smallest mesh spacings should be equal. Similar Finite Element investigations[147] have also found that a continuous function must be used. The effect of these properties on the BEM are presented below. An advantage of BEM is that the formulation is unaffected by element spacing, in contrast to FD where the governing partial differential equation is directly affected.

A logarithmic expansion, previously used in Finite Difference simulations,[6,66,104] was applied with two variations in implementation.

$$y = \ln(1 + \alpha x) \tag{2.44}$$

The coefficient α affects the relative size of elements within a section of the boundary, figure 2.12 on the following page.

A large α value increases the number of elements near the edge of the section. If higher densities of elements are required at both ends of a section, for example on an electrode, the distance may be divided by two and a variation of equation 2.44 applied to both halves.

The expansion between different sections of the boundary may be related in one of two ways, shown in figure 2.13 on page 82. Either the smallest size elements

[§]Typical computer used for simulation: Intel® Pentium® III 650MHz, 192Mb Memory.

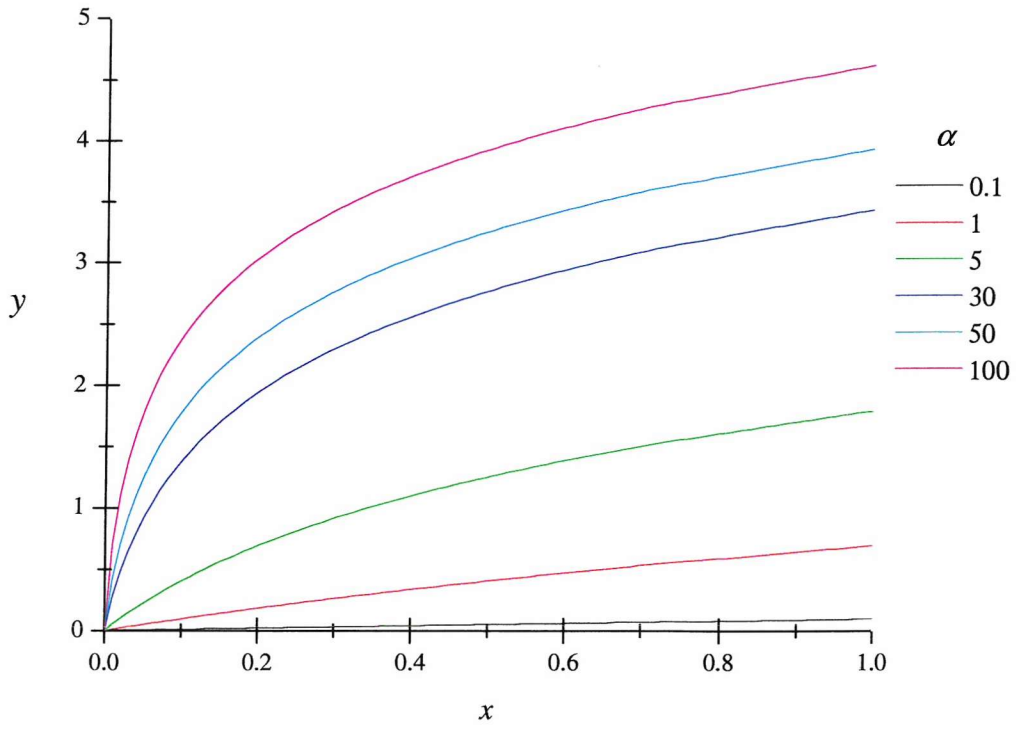

Figure 2.12: The effect of α on exponential spacing. A constant interval of Δy is used to calculate each element length. A small α value corresponds to virtually equal size elements, larger values give significant variation in size.

are identical (fixed ratio) and the number of elements is dependent upon section length or there are the same number of elements within each section (fixed shape) regardless of section length. A consequence of setting the smallest element size is that for a given α value the expansion will probably not fit a given length exactly. Thus the final element size must be truncated. This was done by checking the truncated length with the previous element length to ensure the final element was of comparable size.

Figure 2.14 on page 83 shows the effects of applying exponential spacing to different sections. The number of elements over the electrodes was fixed at ten. The α coefficient was varied from 0.01, which gives virtually equal size elements, to 100 which gives a large variation in size within a section.

As expected accuracy increases when the number of elements near the edge of the microband is increased. However, examining the two components of this - the electrode side and the outer side - shows that increasing the number of elements on the outer side seems to have little effect and the increase in accuracy is due solely to

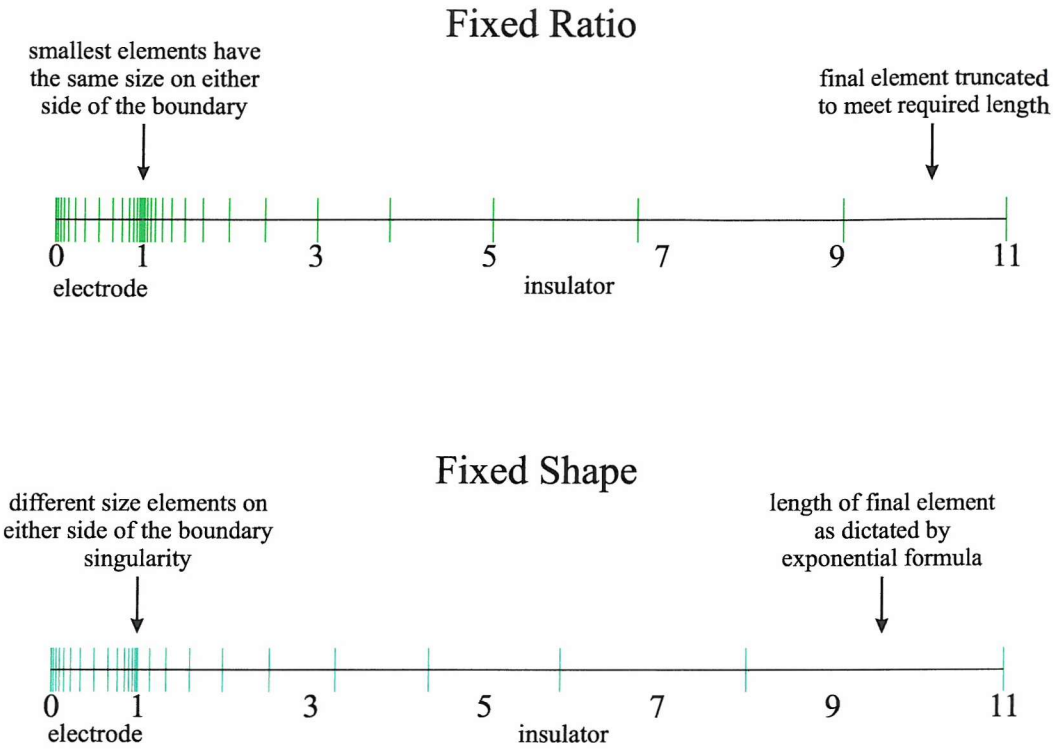

Figure 2.13: Two types of exponential mesh were implemented. In the fixed ratio type expansion the smallest elements in adjacent sections were identical and the final element may be truncated. The fixed shape type expansion fitted a given number of elements exactly to the section length.

the electrode side discretisation. The type of exponential distribution, fixed ratio or fixed shape, affects the discretisation on the insulator relative to the electrode. The element size on the insulator is found to have little effect, thus the difference between types of distribution is negligible.

This is a surprising result as both sides of the singularity could be presumed to have equal influence. Large concentration gradients surround the whole area near the edge of the electrode, including the part of the insulator immediately adjacent.

This behaviour was confirmed by looking at the ratio of number of elements in different sections.

Section Element Ratios

The number of elements over one or more sections of the boundary was fixed, and the effect of increasing and decreasing the number of elements around the fixed section(s)

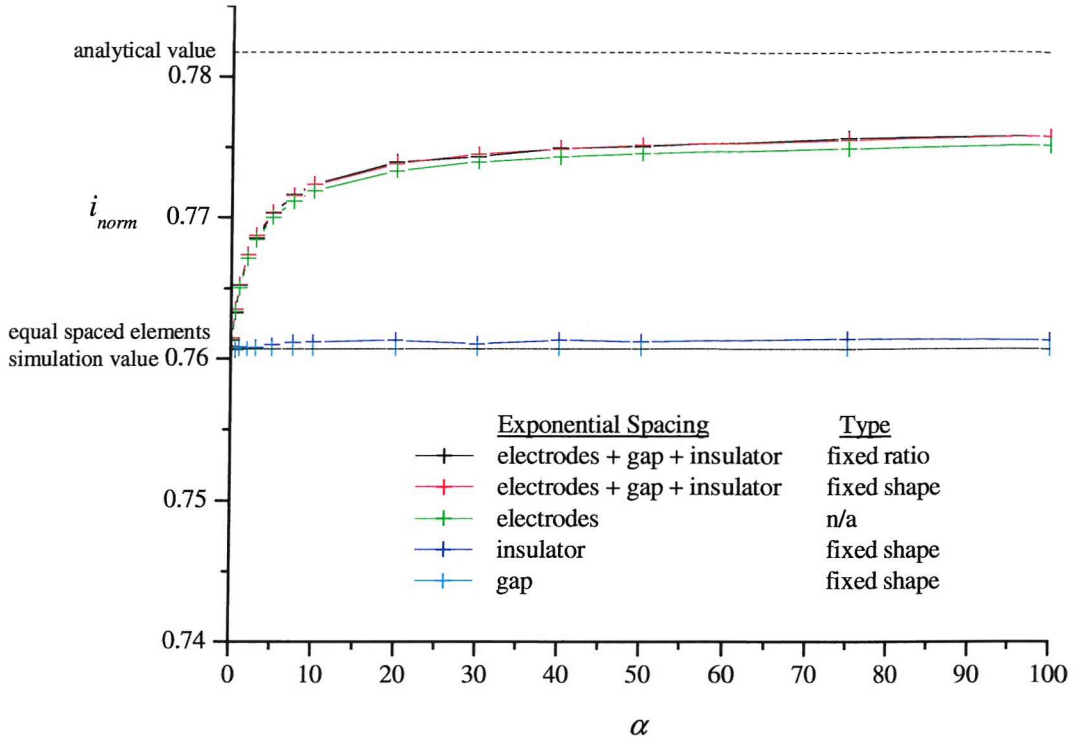

Figure 2.14: The effect of using an exponential mesh over various boundary sections. The expansion type is explained in figure 2.13 on the preceding page. $w = g = 1$, $insul = wall = 10$, $NE_{elec} = NE_{gap} = 10$, $NE_{wall} = 100$, $NE_{ceil} = 200$. NE_{insul} depends upon the exponential mesh used varying from 96 to 19. Two limits are given, the analytical value for this geometry from reference[146] and the value simulated with all equally spaced elements. The number of elements over the semi-infinite boundaries was fixed as varying these had a negligible effect on current response.

observed. Within each boundary section the elements were of equal length.

$$\text{Ratio} = \frac{NE_{variable}}{NE_{fixed}} \tag{2.45}$$

where $NE_{variable}$ number of elements in variable section per unit length

NE_{fixed} number of elements in fixed section per unit length

Table 2.5 on the next page shows that only the number of elements over the electrodes seems to have a discernible effect on the total fluxes at the electrodes. This behaviour may be due to this particular geometry, but as little as one element over each non-electrode section seems to be sufficient.

	Ratio	Fixed Section(s)		
		electrodes	electrodes/gap	electrodes/gap/ insulator
fewer elements in variable section relative to fixed section ↑	0.1	0.7610	0.7610	0.7613
	0.2	0.7608	0.7608	0.7605
	0.3	0.7608	0.7608	0.7605
	0.5	0.7607	0.7607	0.7607
	1	0.7607	0.7607	0.7607
more elements in variable section relative to fixed section ↓	2	0.7607	0.7607	0.7607
	3	0.7607	0.7607	0.7606
	4	0.7607	0.7607	0.7606
	5	0.7607	0.7607	0.7606
	10	0.7607	0.7607	0.7608

Table 2.5: The effect of section ratio discretisation. i_{norm} values are given. The sections of the double microband are defined in figure 2.10 on page 73. Fixed sections each had 10 elements, and the ceiling section had an additional ratio to give equal size elements to the two side sections. $w = g = 1$, $insul$=$wall$=10.

A convergence test was performed increasing the number of elements over the two electrodes, while fixing the number of elements over the rest of the domain. This allows a significant increase in the maximum number of elements over the electrodes before computing limitations become relevant.

Table 2.6 shows convergence to four decimal places with a 0.02% error using 1000 elements.

NE_{elec}	i_{norm}	error /%	NE_{elec}	i_{norm}	error /%
1	0.6612	−15.41	50	0.7786	−0.40
2	0.7088	−9.32	75	0.7796	−0.27
3	0.7317	−6.39	100	0.7801	−0.20
4	0.7437	−4.86	150	0.7807	−0.13
5	0.7510	−3.92	200	0.7809	−0.10
8	0.7623	−2.48	300	0.7812	−0.07
10	0.7662	−1.99	400	0.7813	−0.05
15	0.7713	−1.33	500	0.7814	−0.04
20	0.7739	−1.00	750	0.7815	−0.03
30	0.7765	−0.67	1000	0.7815	−0.02

Table 2.6: Increasing the number of elements over the electrodes only. All other sections have a fixed number of elements. $w = g = 1$, $insul = wall = 1000$, $NE_{insul} = NE_{gap} = NE_{ceil} = NE_{wall} = 10$.

Exponential Discretisation Over Electrodes Only

To simulate a larger number of microband electrodes it is preferable to reduce the number of elements required to maintain accuracy. The effect of an exponential mesh over the electrodes only, with other boundary sections equally spaced and the number of elements fixed, is shown in table 2.7.

α	NE_{elec}	i_{norm}	error /%
0.01	20	0.7739	−1.00
0.1	20	0.7742	−0.96
0.5	22	0.7753	−0.82
1	24	0.7762	−0.71
2	26	0.7773	−0.57
3	26	0.7779	−0.48
5	28	0.7788	−0.38
7.5	30	0.7793	−0.30
10	30	0.7797	−0.26
20	32	0.7804	−0.17
30	32	0.7807	−0.13
40	34	0.7809	−0.10
50	34	0.7810	−0.09
75	34	0.7812	−0.07
100	34	0.7813	−0.05
200	36	0.7814	−0.03
300	36	0.7815	−0.02
500	36	0.7816	−0.02
1000	36	0.7816	−0.01

Table 2.7: The effect of exponential spacing over both electrodes only, all other boundary sections have a fixed number of elements. $w = g = 1$, $insul = wall = 1000$, $NE_{insul} = NE_{gap} = NE_{ceil} = NE_{wall} = 10$.

Significantly increased accuracy is obtained relative to the same number of equally spaced elements. The greater the severity of the exponential mesh (larger α values) the greater the increase in accuracy. An equally spaced mesh with 36 elements gives an error of approximately 0.5% compared to 0.01% for the exponential mesh with the same number of elements. As the α value increases the size of the initial element immediately adjacent to the boundary singularity decreases. At $\alpha = 1000$ the smallest element $l_e = 10^{-4}$. There is a danger with larger α values and therefore smaller l_e values that roundoff errors may cause problems. Matrix solving routines

are particularly susceptible to very small numbers leading to problems with ill-conditioning (see section 2.4.1 on page 70).

An advantage of using an exponential mesh is the significant reduction in the number of elements required for a given accuracy. For the double microband model 54 elements over each electrode produced the same accuracy as 1000 equally spaced elements; table 2.8.

Equal Mesh		Exponential Mesh	
NE_{elec}	error /%	NE_{elec}	error /%
20	1.00	6	0.60
100	0.20	10	0.20
200	0.10	54	0.01
1000	0.02		

Table 2.8: A comparison of equal and exponential mesh spacing over the electrodes. $w = g = 1$, $insul = wall = 1000$, $NE_{insul} = NE_{gap} = NE_{ceil} = NE_{wall} = 10$, $\alpha = 500$.

Local Mesh Refinement

To confirm, contrary to Finite Difference and Finite Element experience, that the continuity of exponential functions is not important in BEM, a local mesh refinement on the insulator, and also on the generator, was simulated as shown in figure 2.15 on the following page.

The number of elements over the *outer* section of the insulator was fixed at 10 while the number on the *local* section was varied. Table 2.9 on the next page shows that local refinement on the insulator has no effect on the simulated current. The simulation was repeated, observing the effect of local refinements on the generator electrode. Here accuracy does improve as the number of elements near the generator edges increases. This emphasises the conclusion that using continuous functions for the expansion of element length is unimportant.

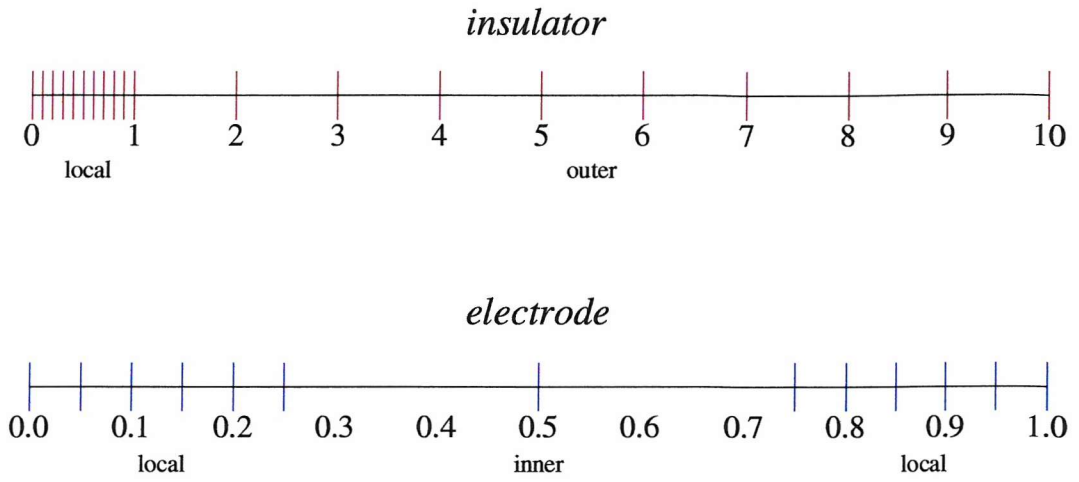

Figure 2.15: Local mesh refinement for a) insulator; section *insul* and b) electrode; section w. Refer to figure 2.10 on page 73 for section definitions. The number of elements on the local mesh was varied while keeping the outer/inner mesh fixed. This tests whether a continuous function is required for mesh refinement.

insulator		generator	
NE_{local}	i_{norm}	NE_{local}	i_{norm}
1	0.760776	1	0.74915
2	0.760773	2	0.758824
4	0.760772	4	0.763577
8	0.760771	5	0.76453
10	0.760771	8	0.765961
12	0.760771	10	0.766439
14	0.760771	12	0.766757
20	0.760771	14	0.766985
25	0.760771	16	0.767155
30	0.760771	20	0.767394
40	0.760771	25	0.767585
50	0.760771	30	0.767713
		40	0.767872
		50	0.767968

Table 2.9: The effect of local mesh refinement over insulator and generator boundary sections respectively. $w = g = 1$, $insul = wall = 10$, $NE_{ceil} = NE_{walls} = NE_{insul} = 100$, $NE_{gap=10}$, $NE_{outer} = 90$, $NE_{inner} = 5$.

Mesh Discretisation Conclusions

The microband current, the parameter used here to assess accuracy, is dependent on the flux at elements over the electrode (refer to equation 1.25). Results show that

two factors contribute to determining accurate fluxes; the number of elements over the electrode and a higher density of elements in areas of high flux. The influence of the number of elements over sections not used to determine current is small. This implies that singular integration is the dominant component of the influence coefficient matrices in the Boundary Element Method. For inlaid generator-collector microband models simply providing sufficient elements over the electrodes is adequate to ensure accuracy. However this domain is a special case, and this discretisation behaviour does not hold for other domains. Investigations of discretisation for raised microbands (see section 2.7.1 on page 110) shows that the mesh must have enough elements to adequately describe local geometric features. A point to emphasize is that for each new type of domain some form of confirmation of discretisation behaviour should be made.

Semi-Infinite Boundary Conditions

Boundary Condition Simulations thus far have used a semi-infinite boundary condition of zero flux, $q = 0$. If the alternative boundary condition of fixed concentration, $c = 1$, is used for simulation, the two electrodes have unequal currents, even for large values of *insul* ($> 10^6 w$). This is due to significant feedback from the far field boundaries increasing the current at the generator electrode. Alternatively one may consider that both the collector electrode and the far field boundaries act as sources, while the generator electrode acts as a sink.

Figure 2.16 on the next page shows concentration profiles for a fixed concentration boundary condition. These behave as one would expect for a double microband at steady state; values smoothly approach $c = 1$ near semi-infinite boundaries. A concentration map, figure 2.17 on page 91, uses bilinear interpolation[148] between internal point values to visualise variation of concentration across the entire xy plane of the simulation domain.

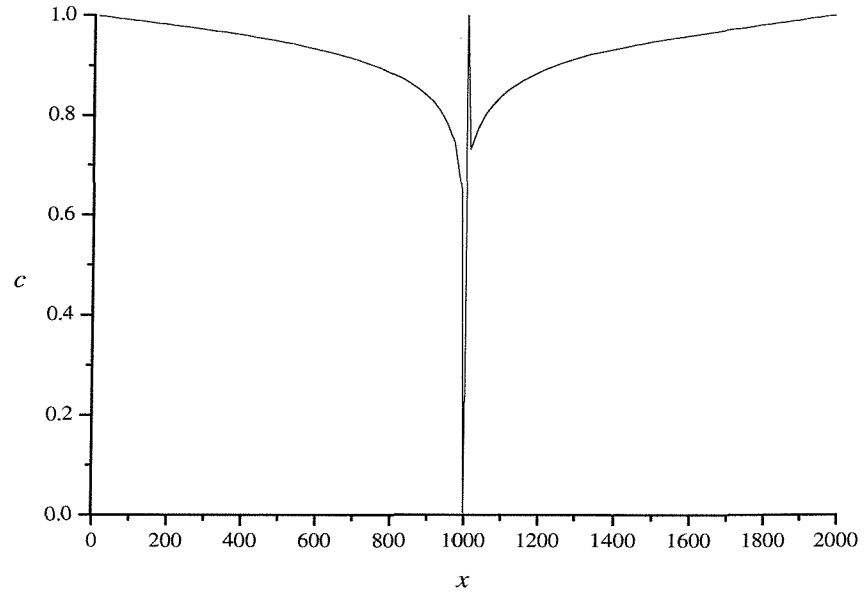

a)

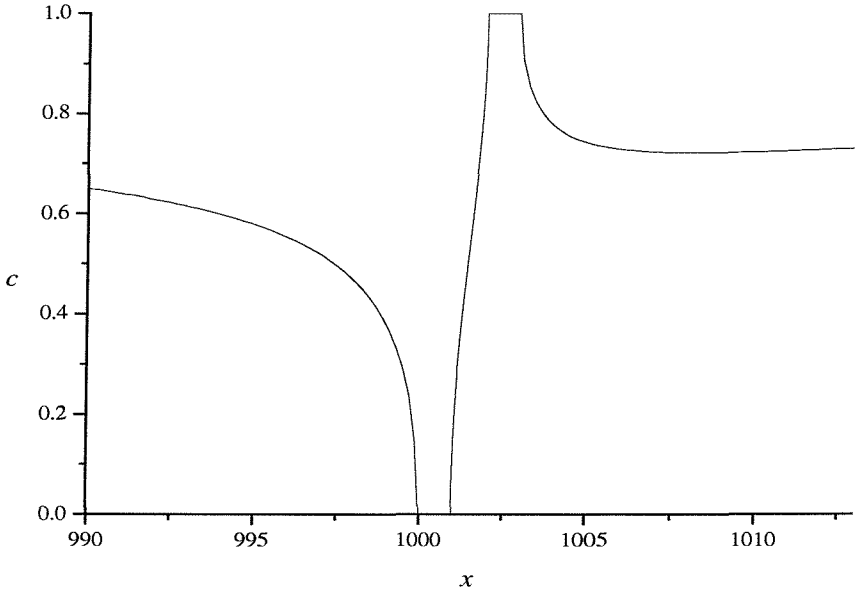

b)

Figure 2.16: The concentration profile along the surface of the microband and surrounding insulator, $y = 0$. The semi-infinite boundary condition was a fixed concentration value equal to one, $c = 1$. a) is the profile of the whole domain, b) the area immediately adjacent to the electrodes. Additional parameters used were $w = g = 1$, $insul = wall = 1000$, $NE_{section} = 50$ with $1 : 1$ ratio spacing between sections. For b) additional elements along two sections $40w$ either side of the electrodes were used.

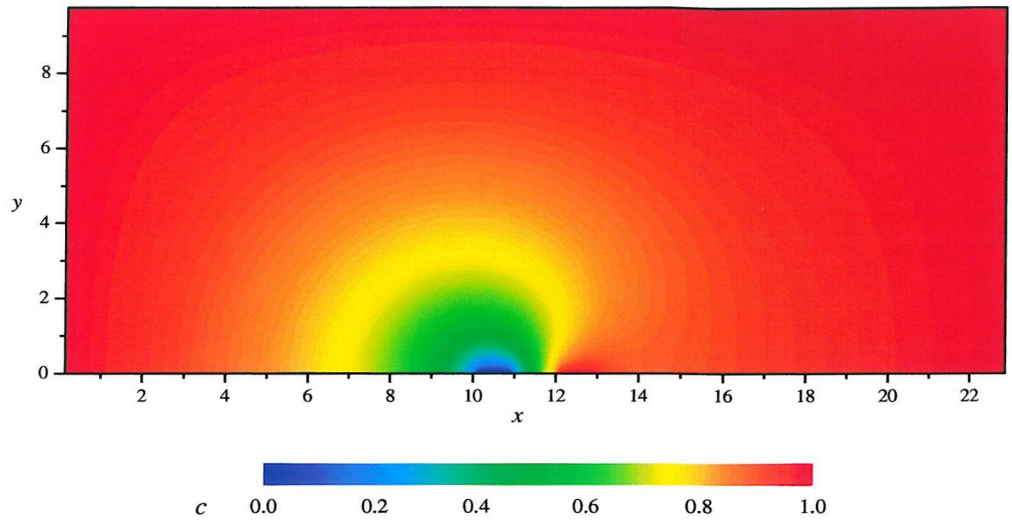

a)

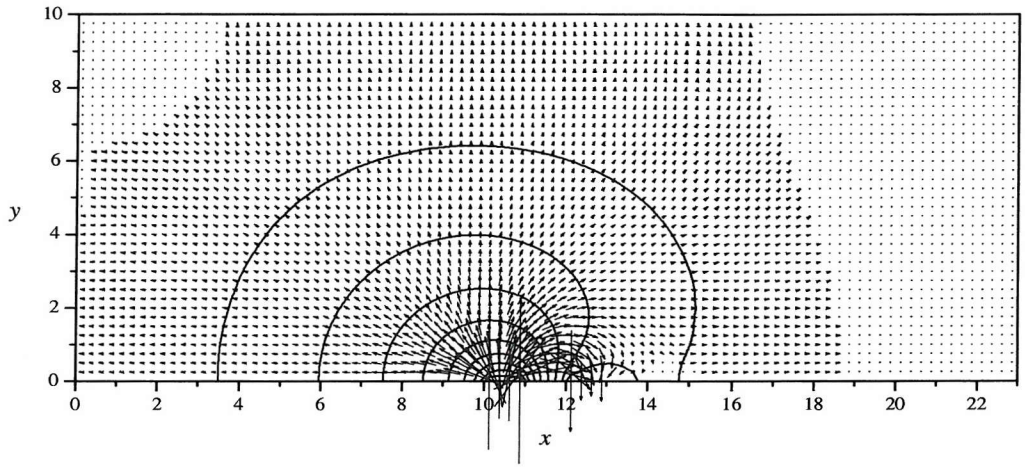

b)

Figure 2.17: a) A concentration map of the entire domain for a fixed concentration, $c = 1$, boundary condition. Values were interpolated between internal points. b) A flux map with concentration contours. The length of the flux arrows are proportional to the flux magnitude. However, the arrow heads are fixed in size. The number of internal points, N_{int}, was 3588 for an equal spaced grid of 92 x 39. Semi-infinite boundaries were set at a distance of $10w$. Additional parameters; $w = g = 1$, $NE_{elec} = 4$ equal spaced around the entire domain.

For the zero flux boundary condition, concentration profiles show that values at the far boundaries converge to $c = 0.5$, figure 2.18.

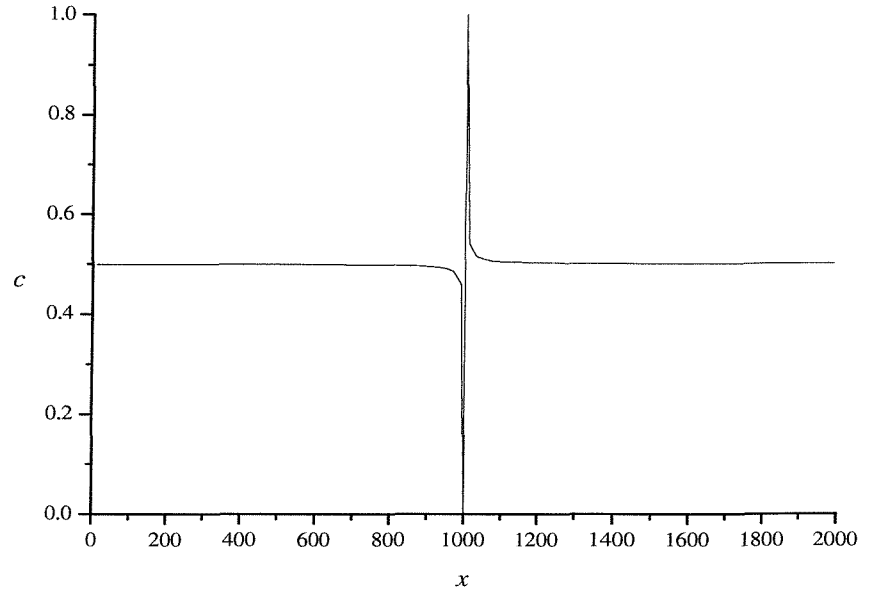

a)

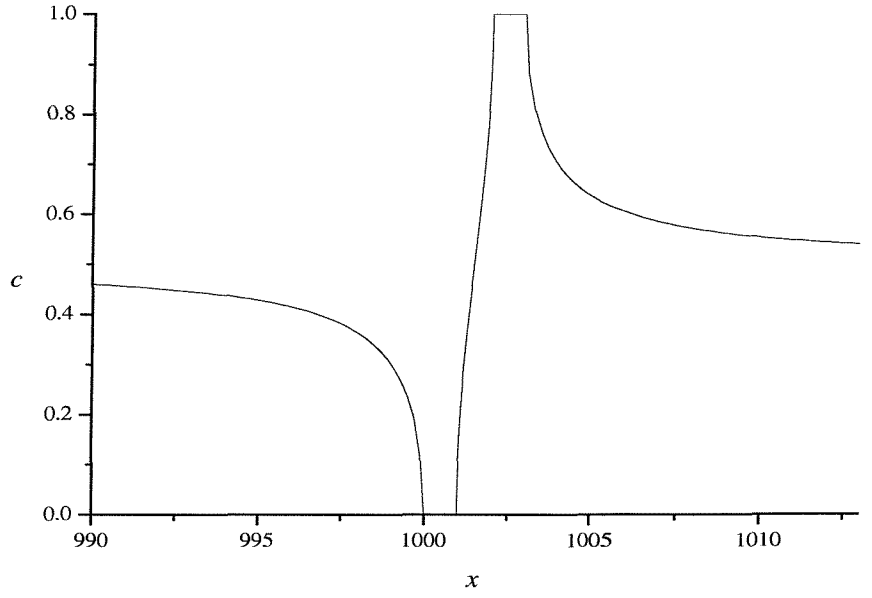

b)

Figure 2.18: The concentration profile along the surface of the microband and surrounding insulator, $y = 0$. The semi-infinite boundary condition was a zero flux condition, $q = 0$. a) is the profile of the whole domain, b) the area immediately adjacent to the electrodes. Parameters are identical to figure 2.16 on page 90.

The double microband system may be compared to a Thin Layer Cell (TLC), fig-

ure 2.19a below, which has planar collector and generator electrodes opposite each other. Species diffuse linearly at a steady state. The DMB at steady state may be thought of in terms of a Thin Layer Cell that is opened out, split in the centre where $c = 0.5$. In regions far from the electrodes, the concentration converges to this value. The contour map for the zero flux boundary condition, figure 2.20 on the following page, supports this interpretation; $c = 0.5$ at distant regions from the electrodes, figure 2.20a on the next page, and the $c = 0.5$ contour line splits the DMB domain in half, 2.20b.

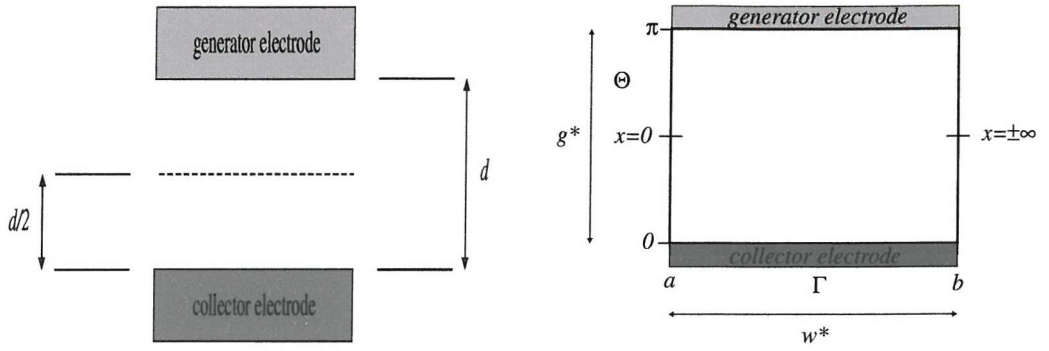

Figure 2.19: a) Schematic of a Thin Layer Cell. Boundary conditions are $c = 0$ along the lower electrode and $c = 1$ along the upper electrode. A concentration of $c = 0.5$ is found at $d/2$. b) The transform space used by Amatore *et al.*[146]

This view of the double microband at steady state in terms of a Thin Layer Cell may be related to a previous finite difference simulation by Amatore and Fosset.[146] They used a conformal mapping to convert a double microband from cartesian coordinates to a transformed space, which was identical to a TLC. The centre of the DMB and infinite boundaries, in transformed space, were located either side of the domain at $x = 0.5$, figure 2.19b on this page.

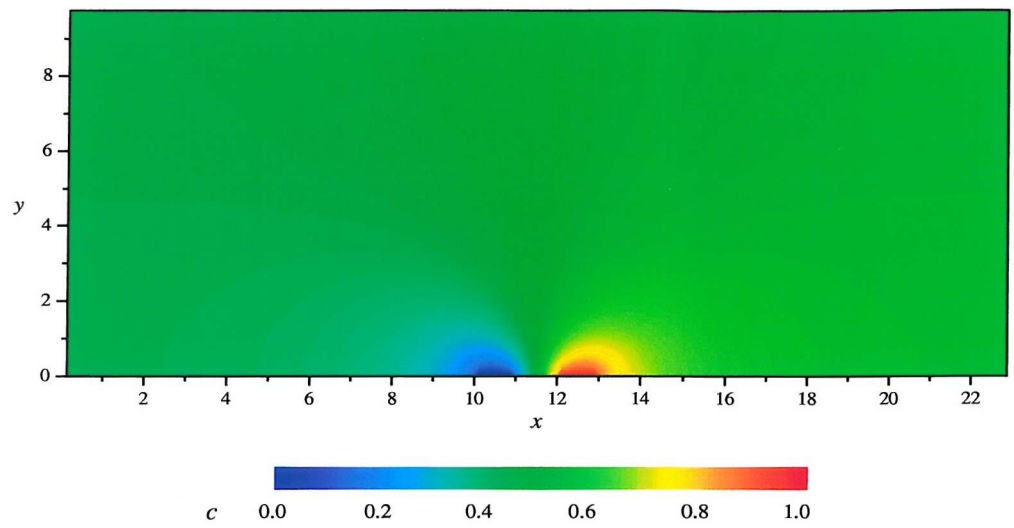

a)

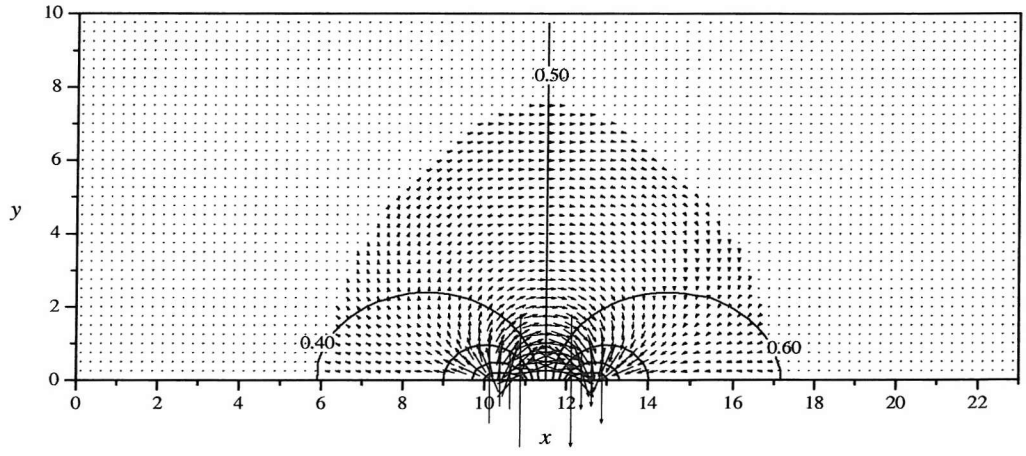

b)

Figure 2.20: a) A concentration map of the entire domain for a zero flux, $q = 0$, boundary condition. Values were interpolated between internal points. b) A flux map with concentration contours. The length of the flux arrows are proportional to the flux magnitude. However, the arrow heads are fixed in size. Parameters are identical to figure 2.17 on page 91.

Boundary Distance If the semi-infinite boundary, x_{fbl}, x_{fbr} and y_{wall} in figure 2.10 on page 73, is not sufficiently far from the generator electrode it will influence the electrode current. If the boundary condition prescribed is concentration, set at the bulk solution value, species A will diffuse from the semi-infinite boundary to react at the generator electrode, creating positive feedback between the boundary and the generator, and the current will be artificially raised. This is analogous to convection bringing the infinite boundary to a finite distance from the electrode.

This effect is observed by comparing the effect of semi-infinite boundary distances of $insul = 10$ and $insul = 1000$ on concentration and flux values, figure 2.21 on the following page. The discretisation used was a constant number of elements along each boundary section, equally spaced within the section. Details are given in table 2.10. Variation of concentration and flux values with element number allows direct comparison of a small and very large semi-infinite boundary distance.

Element number, e_s	Type of boundary	Domain coordinate range	
		x	y
$0-50$	insulator	$-x_{fbl} \leq x < 0$	$y = 0$
$51-100$	generator	$0 \leq x \leq x_{gen}$	
$101-150$	gap	$x_{gen} < x < x_{gap}$	
$151-200$	collector	$x_{gap} \leq x \leq x_{coll}$	
$201-250$	insulator	$x_{coll} < x \leq x_{fbr}$	
$251-300$	far field	$x = x_{fbr}$	$0 \leq y \leq y_{wall}$
$301-350$		$x_{fbr} \leq x \leq -x_{fbl}$	$y = y_{wall}$
$351-400$		$x = -x_{fbl}$	$y_{wall} \leq y \leq 0$

Table 2.10: The correlation between element number, and boundary sections for the simulations used in figures 2.21 and 2.22. A total of 400 elements were used, with 50 over each boundary section. Within sections the elements were equally spaced. Additional simulation parameters are given with the figures.

When the boundary is too close, the flux at the generator electrode increases significantly, while the flux at the collector decreases, figure 2.21c, compared to the large distance, figure 2.21d.

If the semi-infinite boundary condition is set to zero flux, hindered diffusion occurs, reducing the current. The corresponding results for zero flux semi-infinite boundary

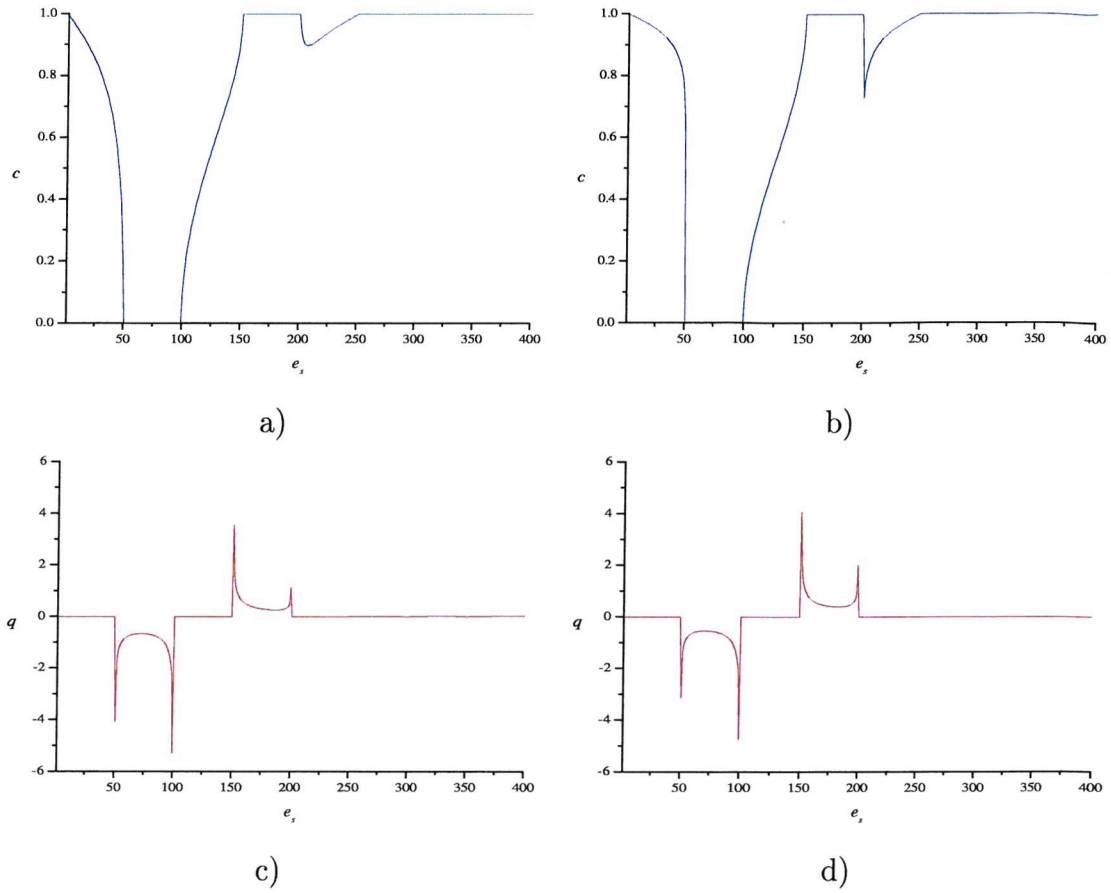

Figure 2.21: The variation of concentration and flux as a function of element number, for a semi-infinite boundary condition of fixed concentration, $c = 1$. A total of 400 elements were used; 50 over each boundary section, with a boundary distance for a) and c) of $insul = 10$ and for b) and d) of $insul = 1000$. c is concentration, q is flux, e_s is element number. Additional parameters; $w = g = 1$, $NE_{elec} = 50$. The relation of element number, e_s, to boundary section is given in table 2.10 on the page before.

condition, figures 2.22a-d on the following page, show the concentration does not converge to $c = 0.5$ at regions near the semi-infinite boundary; figure 2.22a. The flux values are equal at both electrodes, but lower than the correct value.

It was found that the distance from the double microband to the edge of the domain sufficient for there to be negligible effect on the current occurred at distances greater than $1000w$, assuming a zero flux semi-infinite boundary condition.

These results used equal *insul* and *wall* length. When the semi-infinite boundary lengths are altered independently the generator and collector currents diverge, both becoming significantly erroneous.

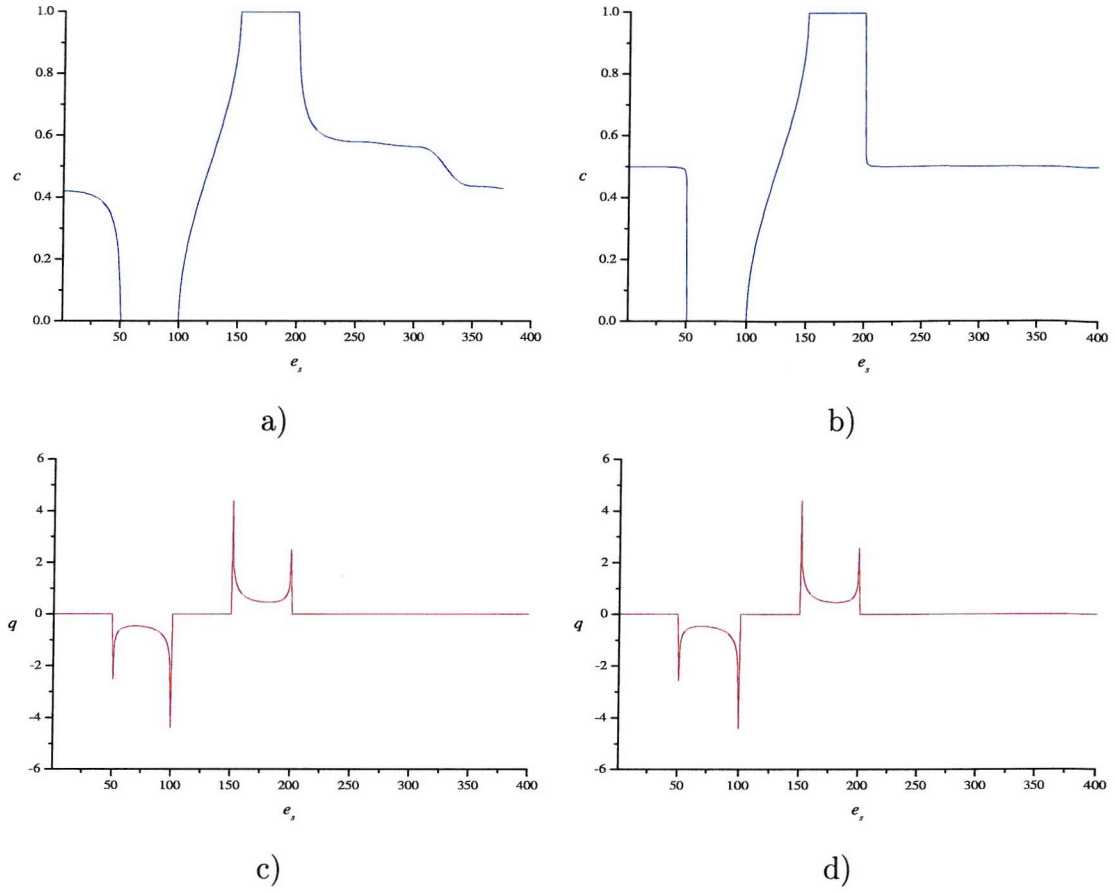

Figure 2.22: The variation of concentration and flux as a function of element number, for a semi-infinite boundary condition of zero flux, $q = 0$. Parameters were identical to figure 2.21 on the preceding page.

This is due to the hemi-cylindrical shape of the diffusion field at long distances from the double microband. Therefore far field boundary lengths must be identical to prevent interference from these boundaries.

Steady States As mentioned at the start of section 2.5.1, it is important to distinguish between definitions of steady state, which depend upon the system under consideration.

Theoretically the double microband should reach a quasi-steady-state at long times after a potential step.[149] At these long timescales, effects such as natural convection should also be taken into account. Natural convection will bring the bulk concentration condition near the electrode and affect the current. The quasi-steady-state current will become a steady state current.

The Boundary Element Method is a mathematical model, which in this case solves the Laplace equation. Thus the method is a simulation of a mathematical steady state. The choice of boundary condition at the semi-infinite boundary is important. A zero flux condition imposes a steady state upon the double microband; when the boundary is at a sufficient distance it may be considered an approximation of an infinite zero flux boundary. A fixed concentration condition allows feedback from the semi-infinite boundary; this is analogous to the boundary layer imposed by natural convection.[145]

2.5.3 Validation

Based on the results presented above the optimal parameters for the inlaid double microband BEM simulation were chosen as follows. A value of $\alpha = 500$ was used as, although higher values are permissible, the risk of errors arising from roundoff problems increases. The number of elements over each electrode was set at $NE_{elec} = 54$ while all other boundary sections are fixed at $NE = 10$. The semi-infinite boundaries were prescribed a zero flux condition, and a distance of $1000w$.

The simulation program was initially validated for a simple heat flow domain by comparing values for individual elements with values in Brebbia *et al.*[22]

Using the parameters outlined above results were compared to Amatore and Fossett's[146] analytical solution, figure 2.23 on the next page. Excellent accuracy is achieved, with less than 0.1 per cent error for all values of g, the gap length between generator and collector electrodes.

As expected the simulated current decays significantly as the gap between the two electrodes increases. This is analogous to the positive feedback approach curves observed in SECM where tip current decreases when the tip moves away from a conducting substrate.

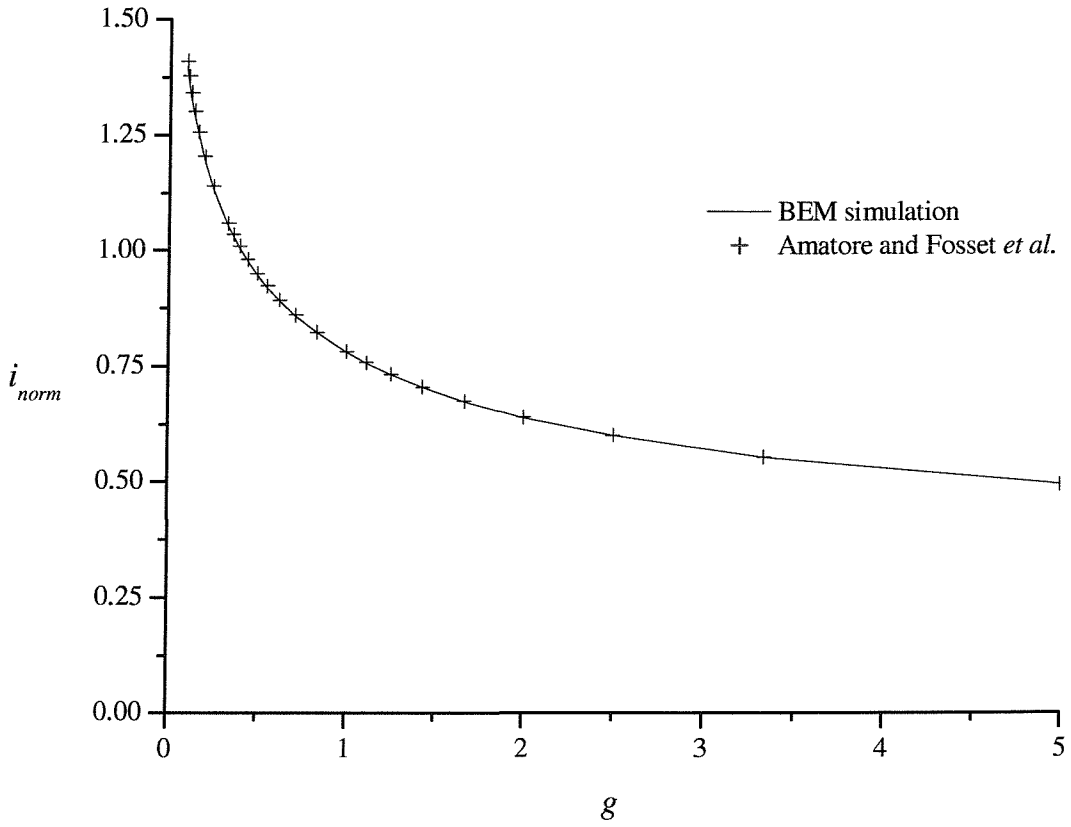

Figure 2.23: Validation of the double microband BEM method. Values are compared to the analytical solution of Amatore and Fosset.[146] Simulation parameters used were $w = g = 1$, $insul = wall = 1000$, $NE_{insul} = NE_{gap} = NE_{ceil} = NE_{wall} = 10$, $\alpha = 500$.

2.6 Microband Arrays

Arrays of microband electrodes have been studied for some years in the laboratory.[150,151] They are now commercially produced[152] and have started to be used for industrial applications. An array may consist of two to ten to many hundreds of separate bands. When a large number of bands is used, the array is considered for theoretical purposes to be of infinite length. An array has two modes of potentiostatic operation: identical potential and generator-collector. The latter mode is more commonly used, these electrodes are also known as Interdigitated Arrays (IDA). In this section the Boundary Element Method is used to investigate the properties of various generator-collector microband array geometries. The simplest system is the double microband electrode (DMB), described in detail in section 2.5.1 on page 73.

The response of a particular cell geometry depends upon the relative size of certain characteristic dimensions with respect to the diffusion layer size. The characteristic dimensions of a microband array are the width of the electrodes, the gap between adjacent electrodes and the overall width of the entire system, which depends upon the previous two dimensions and the number of electrodes.

Previously, finite difference simulations utilising either exponential grids or conformal mapping, and random walk simulations have simulated inlaid double and triple microband systems,[7,146,153] in addition to infinite arrays.[154] However, intermediate numbers of bands cannot practically be simulated by these methods, as the number of mesh points required becomes prohibitive. New conformal mappings are required (if one can be found) for each increase in the number of electrodes or change in electrode geometry. Due to the advantages of the BEM the same computer program may be used to simulate an intermediate number of bands and more realistic geometries.

In the next section inlaid microband arrays are investigated, with two common variations of operation; generator-collector pairs and a central generator surrounded by pairs of collectors. The following section considers deviations from ideal (for simulation) geometries and the effect this has on current response.

For all geometries the reaction simulated is the reduction

$$A + e^- \rightarrow B \tag{2.46}$$

The system is at steady state and assumed to be diffusion controlled.

2.6.1 Arrays of Generator-Collector Pairs

A pair of generator-collector electrodes is the base unit of the array simulated. The electrode system consists of N_{pairs} pairs as shown in figure 2.24 on the next page. The far boundaries are given a boundary condition of zero flux, $q = 0$, to impose a steady state and the optimal discretisation parameters determined in section 2.5.3 on page 98 are used. These are shown in table 2.11

Parameter	Value
w	1
g	1
$insul$	1000
$wall$	1000
α	500
NE_{elec}	10
NE_{gap}	1
NE_{insul}	10
NE_{wall}	10
NE_{ceil}	20

Table 2.11: Parameters used for multiple electrode simulations.

The current response as the number of electrode pairs is increased is shown in figure 2.25 on the following page. The current increases from the value for a double microband to that approaching the value found by Amatore *et al*[155] for an infinite array. Current values for individual electrodes are given in table 2.12 on page 103. The outermost electrode can be seen to have the lowest current, as it is adjacent to only one electrode, rather than surrounded by two as for all other electrodes. The next electrode, one away from the edge, has a higher than average current. This is influenced by the increased flux of species at the edge of the array, as more species have access to the electrode. The same effect is found at the edge of a microelectrode.

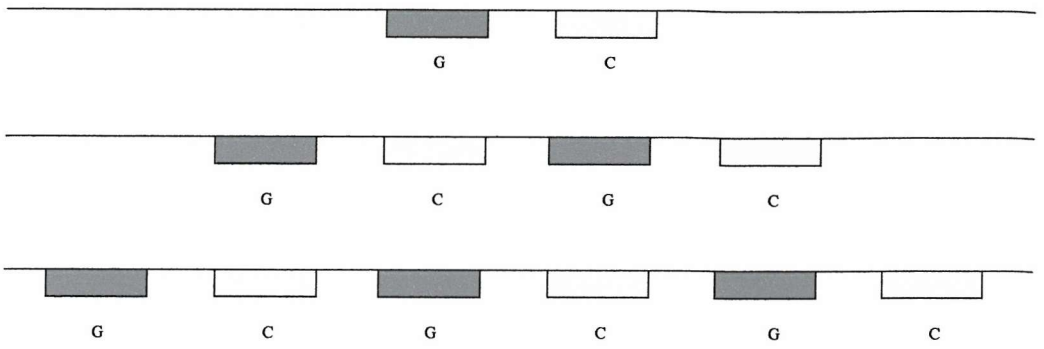

Figure 2.24: A schematic of the first type of multiple electrode domain simulated; generator-collector pairs. G=generator electrode, C=collector electrode. N_{pairs} is the number of generator-collector pairs, therefore the total number of electrodes is $2N_{pairs}$.

The average generator and collector currents are equal, as expected, as the system is at steady state. The individual electrode currents are symmetrical about the centre of the array.

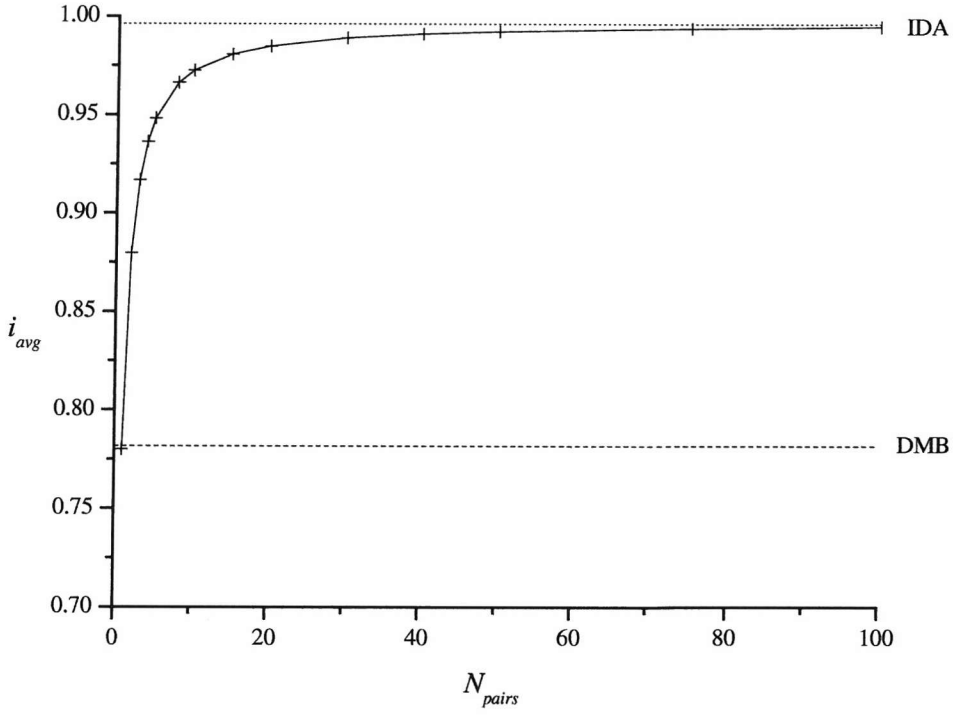

Figure 2.25: Increasing the number of generator-collector pairs, N_{pairs}, from 1 (a double microband, DMB) to 100 (effectively an interdigitated array, IDA). i_{avg} is the average current value at the generator and collector electrodes. The dotted lines are current values calculated by Amatore and Fosset for a DMB[146] and IDA.[155]

Electrode	N_{pairs}						
	1	2	3	4	5	8	10
G1	0.7800	0.7310	0.7197	0.7147	0.7120	0.7082	0.7070
C1	0.7800	1.0283	1.0443	1.0493	1.0517	1.0545	1.0553
G2	–	1.0283	0.9868	0.9790	0.9759	0.9728	0.9720
C2	–	0.7310	0.9868	1.0023	1.0069	1.0108	1.0116
G3	–	–	1.0443	1.0023	0.9946	0.9894	0.9884
C3	–	–	0.7197	0.9790	0.9946	1.0022	1.0033
G4	–	–	–	1.0493	1.0069	0.9948	0.9934
C4	–	–	–	0.7147	0.9759	0.9982	0.9999
G5	–	–	–	–	1.0517	0.9982	0.9959
C5	–	–	–	–	0.7120	0.9948	0.9978

Table 2.12: The current at each electrode of generator-collector arrays. Electrode numbering starts on the left side of the array. N_{pairs} is the number of generator-collector pairs. The current at the collector is equal and opposite to the generator; these values have been omitted.

Electrode currents at larger arrays are shown in table 2.13 on the following page. The current at electrodes more than approximately four away from the edge of the array remains constant. As N_{pairs} increases the influence of edge currents becomes less significant and i_{avg}, the average current, approaches the value for an infinite array.

All the results thus far have used a gap distance of $g = w = 1$. The average current of an array may be normalised by either of the two limits of the number of pairs; a double microband and an infinite array. The double microband normalisation, figure 2.26 on page 105, shows that current is dependent on gap distance. For the alternative normalisation with respect to an infinite array (an InterDigitated Array, IDA), figure 2.27, the difference in current response is most marked at small gap values. As the number of pairs increases the current will approach the values found for an infinite array, giving a staight line ($i_{avg}/i_{IDA} = 1$). Normalising with respect to an infinite array is most logical due to the inherent symmetry of the diffusion field. At any array the diffusion field at the outer electrodes is asymmetrical (assuming a bulk concentration of one species exists). This is most pronounced with a single pair of electrodes, the double microband, and the effect becomes negligible with an increasing number of pairs of electrodes, vanishing completely at an infinite array.

Electrode	N_{pairs}		
	20	50	100
G1	0.7047	0.7033	0.7029
C1	1.0567	1.0574	1.0577
G2	0.9708	0.9702	0.9700
C2	1.0128	1.0134	1.0135
G3	0.9871	0.9866	0.9865
C3	1.0047	1.0052	1.0053
G4	0.9919	0.9914	0.9912
C4	1.0016	1.0021	1.0023
G5	0.9940	0.9935	0.9933
C5	1.0001	1.0006	1.0008
$G(N_{pairs}/2) - 1$	0.9968	0.9973	0.9974
$C(N_{pairs}/2) - 1$	0.9978	0.9974	0.9974
$G(N_{pairs}/2)$	0.9971	0.9973	0.9974
$C(N_{pairs}/2)$	0.9974	0.9974	0.9974
$G(N_{pairs}/2) + 1$	0.9974	0.9974	0.9974
$C(N_{pairs}/2) + 1$	0.9971	0.9973	0.9974

Table 2.13: Selected electrode currents, i_{norm}, for large values of N_{pairs}. Electrodes at the edge and centre are shown. Numbering starts at the left side of the array. N_{pairs} is the number of generator-collector pairs.

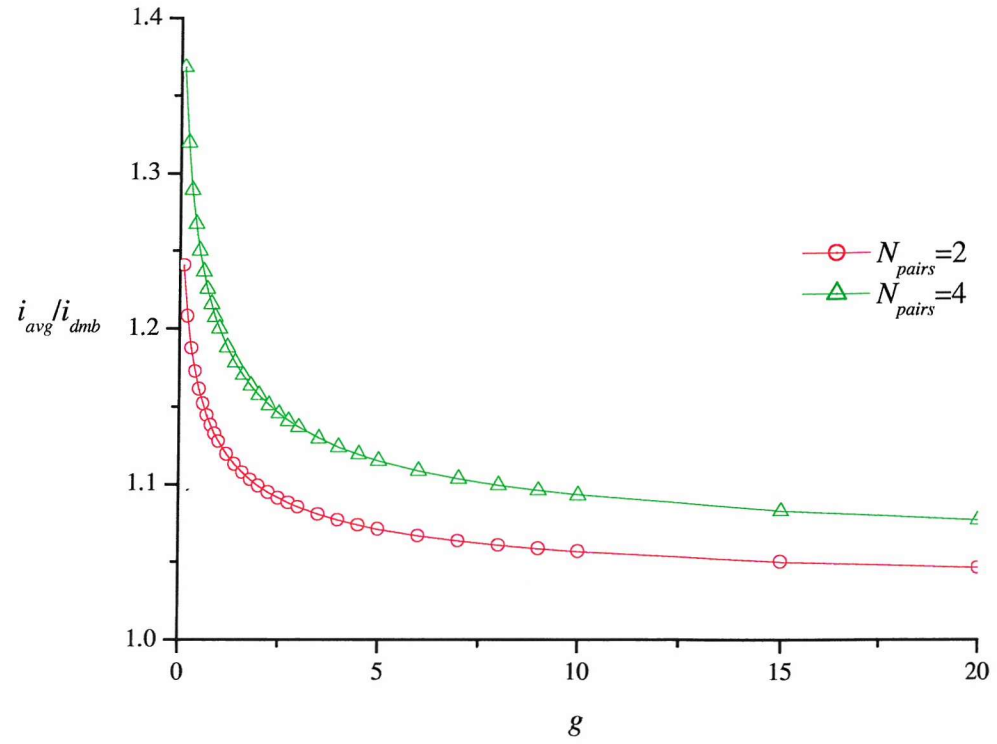

Figure 2.26: The variation of the ratio of average generator current, i_{avg}, to double microband current, i_{dmb}, with gap distance, g. N_{pairs} is the number of generator-collector pairs.

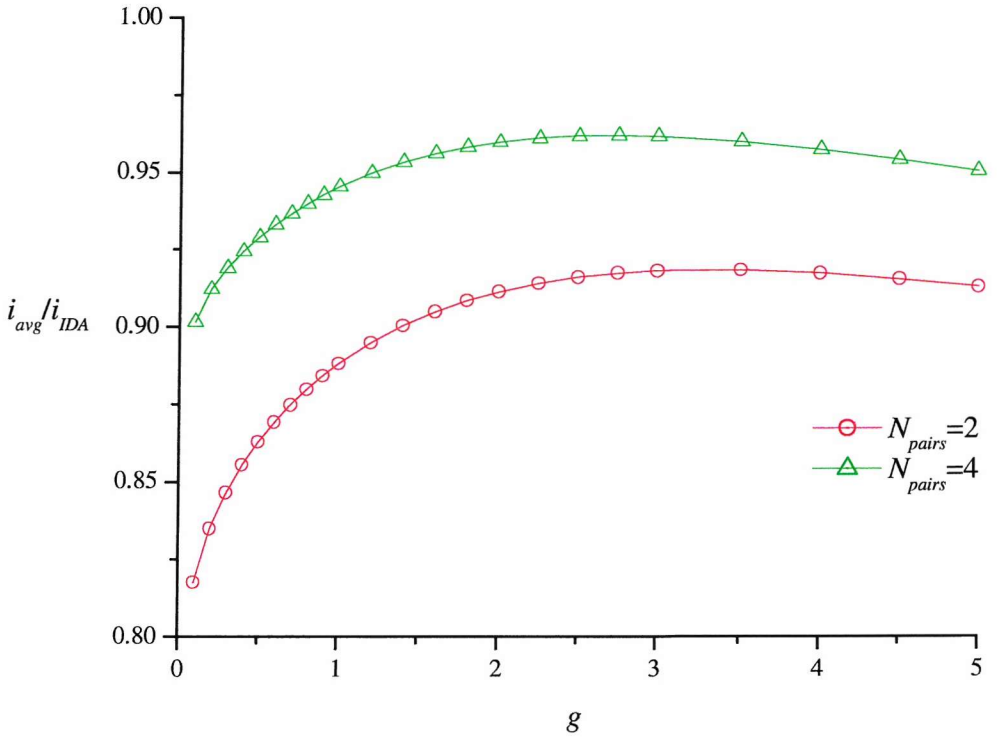

Figure 2.27: The variation of the ratio of average generator current, i_{avg}, to an infinite array (IDA) current, i_{IDA}, with gap distance, g. i_{IDA} is calculated from the empirical equation given by Aoki *et al.*[156]

2.6.2 Arrays of Collectors Surrounding a Central Generator

The second array type studied is based on a generator surrounded by pairs of collector electrodes, figure 2.28. The simplest of these arrays is the triple microband (TMB). As more collector pairs are added the generator current increases rapidly, figure 2.29 on the next page, until after approximately five pairs, when the current starts to plateau. The distance to the extra electrode pairs is large enough and the diffusion field is not greatly affected until eventually the additional feedback becomes negligible. Note the current for a triple microband agrees with the value found by Amatore *et al.*[153]

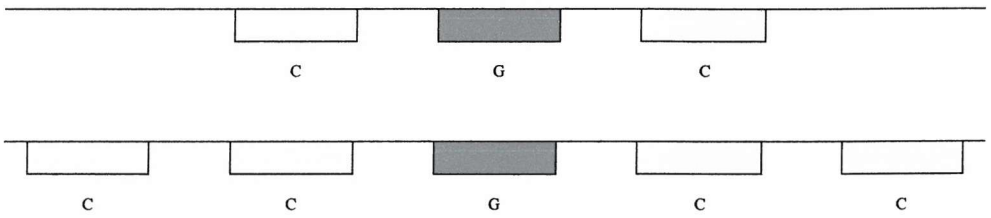

Figure 2.28: A schematic of the second type of multiple electrode domain simulated; a central generator electrode surrounded by collector electrodes. G=generator electrode, C=collector electrode. N_{pairs} is the number of collector electrodes, so the total number of electrodes is $2N_{pairs} + 1$.

Table 2.14 on page 108 gives the current at individual electrodes. The array and diffusion field produced is symmetrical about the centre of the generator electrode, and only half the array is shown. The system is at steady state and, as expected, the sum of the collector currents equals the generator current. The current at the outer electrodes drops off quickly; the probability of species B reaching these electrodes is relatively small due to their distance from the generator combined with the fact many other collector electrodes are placed inbetween.

As found with the previous IDA system, the relation of current to gap distance, figure 2.30 on page 108, is not directly proportional. As the gap distance increases the influence of additional collector electrodes has a greater effect on generator current. This may be due to inner collectors shielding outer electrodes. The magnitude of this effect decays with increasing distance.

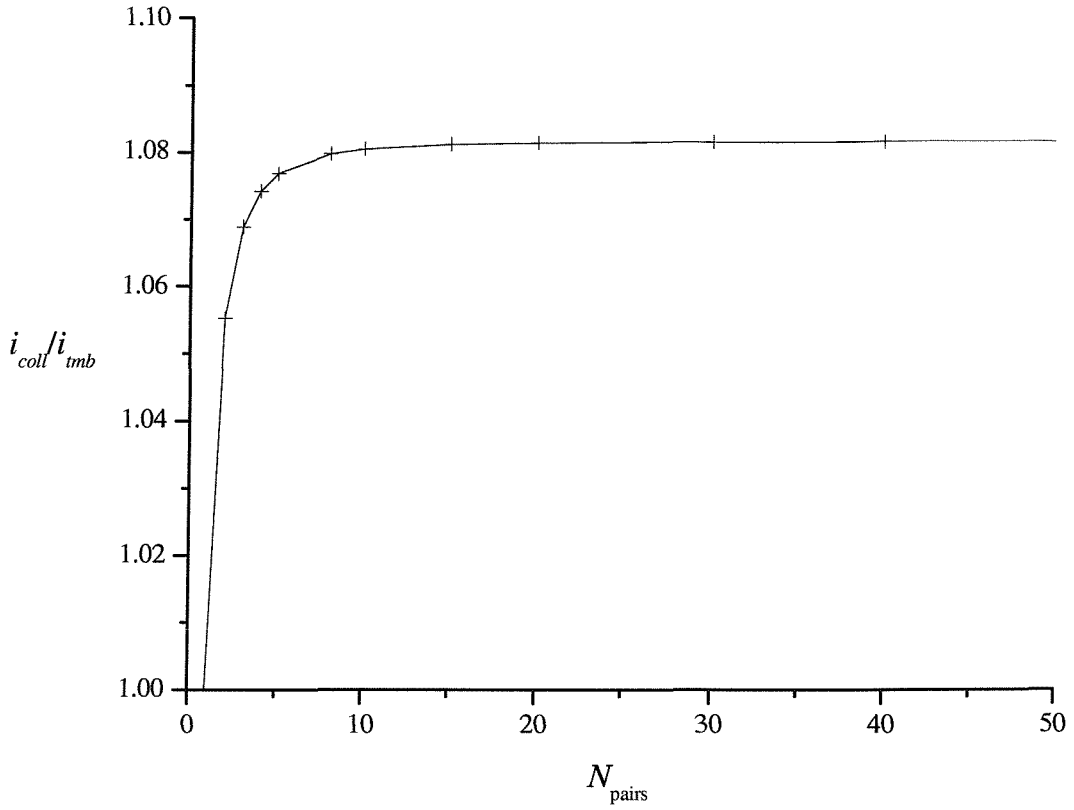

Figure 2.29: The effect of increasing the number of surrounding collector electrodes. The generator electrode current (i_{gen}) is normalised with respect to the current at a triple microband electrode (i_{tmb}), N_{pairs} is half the number of surrounding electrodes.

Experimentally one would expect feedback from the outermost electrodes becomes negligible as their distance from the generator surpasses the radius of the hemicylindrical generator diffusion layer. In practice this layer is of a finite size due to limiting factors, such as natural convection. The steady state BEM method simulates infinite time, and has an infinite diffusion field; in this case reaching a finite boundary set at a sufficiently large distance. Thus simulation of very large generator-collector gap distances will produce some feedback current, but of negligible magnitude.

The TMB current ratio to DMB was also found not to be directly proportional. This is as expected; the TMB has a symmetrical diffusion field whereas the DMB does not.

Electrode	N_{pairs}							
	1	2	3	4	5	10	30	50
G	1.1745	1.2393	1.2554	1.2616	1.2646	1.2689	1.2703	1.2704
C1	0.5872	0.4593	0.4393	0.4324	0.4291	0.4247	0.4233	0.4232
C2	–	0.1604	0.1058	0.0954	0.0913	0.0864	0.0850	0.0849
C3	–	–	0.0825	0.0507	0.0441	0.0380	0.0365	0.0364
C4	–	–	–	0.0523	0.0309	0.0219	0.0204	0.0203
C5	–	–	–	–	0.0369	0.0147	0.0130	0.0129
C6	–	–	–	–	–	0.0110	0.0091	0.0090
C7	–	–	–	–	–	0.0089	0.0067	0.0066
C8	–	–	–	–	–	0.0080	0.0052	0.0051
C9	–	–	–	–	–	0.0082	0.0041	0.0040
C10	–	–	–	–	–	0.0127	0.0034	0.0033
C20	–	–	–	–	–	–	0.0011	0.0009
C30	–	–	–	–	–	–	0.0024	0.0004
C40	–	–	–	–	–	–	–	0.0003
C50	–	–	–	–	–	–	–	0.0011

Table 2.14: The current at electrodes for the second type of array, shown in figure 2.28 on page 106. N_{pairs} is the number of electrodes surrounding the generator.

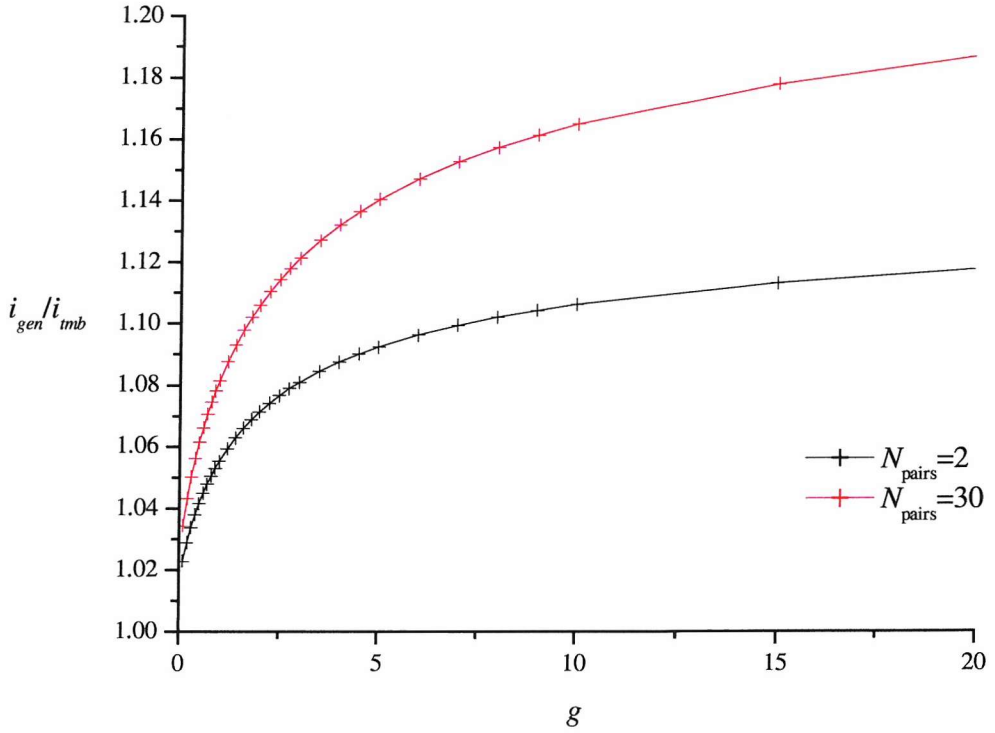

Figure 2.30: The variation of the ratio of the generator current, i_{gen}, and triple microband current, i_{tmb}, with gap distance. The array type is a generator surrounded by collectors.

2.7 Raised and Recessed Double Electrodes

The actual shape of real microband electrodes often differs from the ideal perfectly flat electrode inlaid in an insulating surround. The most common cause of these deviations is the method of manufacture. Lithographic techniques typically lead to slightly raised electrodes, which are electroactive over their entire surface area; figure 2.31a below. Recessed electrodes may also be produced which are electroactive only along the base of the recess. When electrodes produced by sandwiching methods are polished, if one of the electrode and insulator material is softer than the other, the softer surface may be eroded, leading to a raised or recessed electrodes, figure 2.31b.

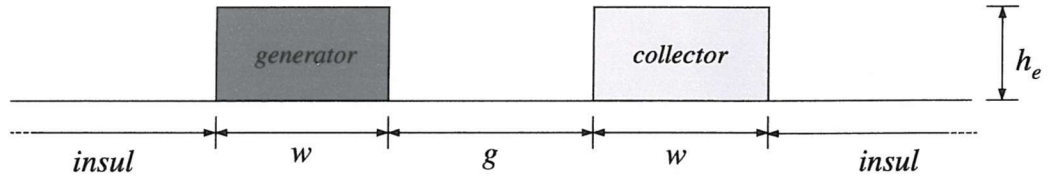

a) 'All'

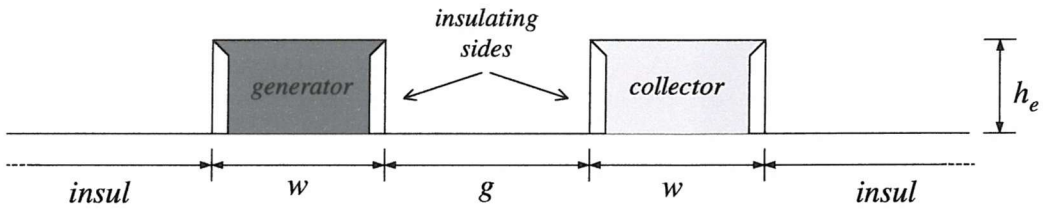

b) 'Top'

Figure 2.31: A description of the two types of electrodes simulated. The electroactive area is shaded, the white area is insulated. Note a positive value of h_e signifies a raised electrode, a negative value a recessed electrode (only raised are shown). A practical example of a raised 'All' electrode may be found in figure 2 of Alden *et al.*[69]

These more complex geometries are difficult to simulate using alternative numerical techniques, particularly if large numbers of electrodes are involved, but are easily dealt with by the Boundary Element Method. It is important to quantify the effect on current response and understand the behaviour of realistic systems.

The following section investigates the steady state chronoamperometric response of raised and recessed rectangular double microband electrodes, as shown in figure 2.31 on the page before. These are the geometries produced by the most common methods of manufacture. The BEM may be used to simulate any shape microband, not necessarily rectangular, as described in section 2.3 on page 68.

2.7.1 Discretisation of the Domain

It is important to determine the discretisation appropriate for each new type of domain shape simulated. Inlaid microband electrodes were investigated in section 2.5.2 using an analytical solution, and in the previous section specific results confirmed values from previously reported alternative simulation techniques. When a novel domain shape is simulated, although a known solution will not be available, there are still some verifications that may be made. These may be based on mathematical modelling requirements, such as convergence with increasing numbers of elements, or on electrochemical knowledge, for instance convergence with increasing semi-infinite boundary distance. Further verifications may be made concerning discretisation optimisation.

For the raised/recessed domain basic tests confirmed convergence, however analysis of different boundary sections showed that, contrary to results for a inlaid system, the number of elements over the gap between electrodes and the number of elements near electrodes on the insulator affected the current. The number of elements a large distance from the electrodes was insignificant.

To obtain sufficient distance of the semi-infinite boundary, *insul*, discretisation optimisation is necessary. It was found that exponential mesh spacing, which ensured the smallest element was the same size as the equally spaced elements over the electrodes (referred to as type FixedRatio in section 2.5.2 on page 80) allowed a large reduction in the number of elements required, with an insignificant change in current. The value of the expansion coefficient, α, was important as values larger than $\alpha \geq 10$ led to oscillations of flux values on the electrodes.

The simulation domain chosen is described in figure 2.32 on the following page. The parameters used for all following simulations are given in table 2.15.

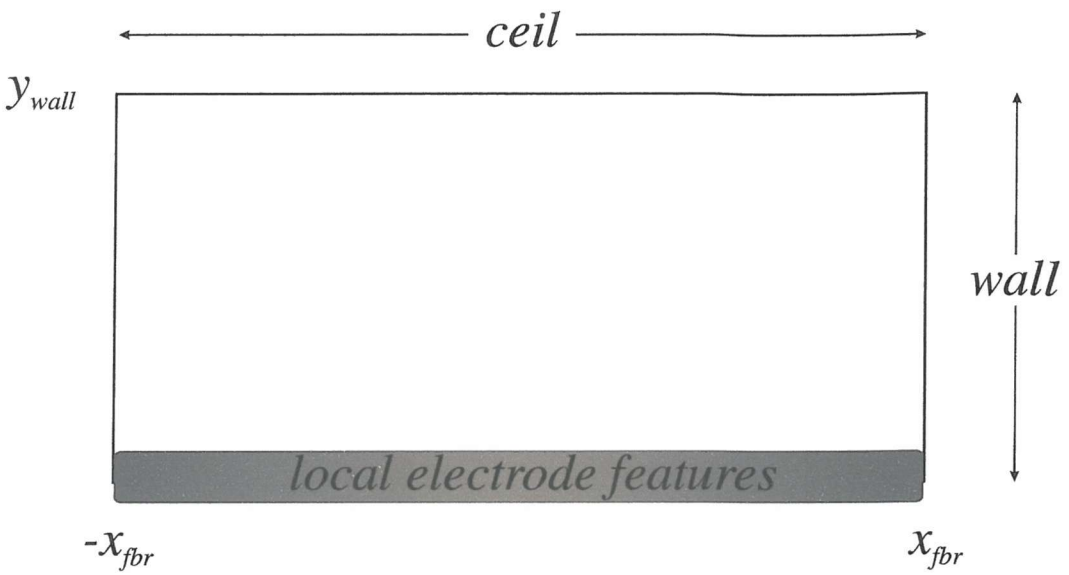

Figure 2.32: The far field domain parameters used for this section. Local electrode features are described in figure 2.31 on page 109. The parameters used are given in table 2.15 below.

Parameter	Value	Element Spacing
w	1	equal(A)
g	1	equal(A)
$insul$	1000	exponential
$wall$	1000	equal(B)
h_e	1	equal(B)
α	3	–

a)

Parameter	Value
NE_{elec}	150[a]
NE_{gap}	50
NE_{insul}	137
NE_{wall}	50
NE_{ceil}	100

[a]50 for electrode type 'Top'.

b)

Table 2.15: Parameters used for raised and recessed microband simulations. Equal(A) and equal(B) signify two different equal spacings.

There has been a limited amount of research into discretisation optimisation and in this area BEM lags behind alternative techniques. FD optimisations are well understood within electrochemistry and FEM optimisations have a much wider range of publication. As described in section 2.5.1 on page 77, the current at an electrode is obtained from the summation of fluxes at each element, equation 2.42, these fluxes being obtained directly through the BEM procedure. A possible explanation for the effects of BEM discretisation found for these systems is that the influence on element flux has two components. Firstly the element singular integration is the dominant factor - hence the number of elements over the electrodes has the greatest

effect. Secondly non-singular integration - geometrical features close to the element have greater influence than distant features and there must be sufficient elements to describe these shapes.

Element discretisation analysis is time consuming, but essential to confirm the veracity of the simulation for a novel electrochemical domain. An attractive solution to reduce the efforts involved are adaptive mesh techniques.[123,133,134] These automatically refine the element mesh based on an error estimation. This would greatly aid discretisation optimisation although electrochemical based tests, such as increasing the distance to semi-infinite boundaries, would still need to be carried out manually.

2.7.2 The Effect of Electrode Height

Two types of electrode were simulated with different electroactive areas, defined in figure 2.31 on page 109. h_e is the dimensionless height/depth of the microband above/below the surrounding flat insulator, where h_e is normalised with respect to the width of the electrode. Positive values describe raised microbands whereas negative values describe recessed microbands.

The current response normalised with the current at a inlaid double microband is shown in figure 2.33 on the next page. A significant deviation from the current at an inlaid DMB is observed, which is most pronounced at small values of h_e. For instance electrodes raised $0.05w$ above the insulator give a 10% increase in current compared to a inlaid DMB.

The system is at steady state and the feedback loop between the two electrodes is the origin of the current response. Raising the microbands exposes the edges which have the greatest effect on flux of species to the electrode. If the entire raised band is electroactive the current is greater than if only the top is electroactive, due to a larger surface area. At higher values of h_e planar diffusion between the two facing electrode sides becomes the dominant factor, giving a current that is directly proportional to h_e. When only the top is electroactive the current reaches a plateau as the electrode is raised away from the insulating surround which no longer inhibits diffusion between the two bands. When the bands are recessed the current

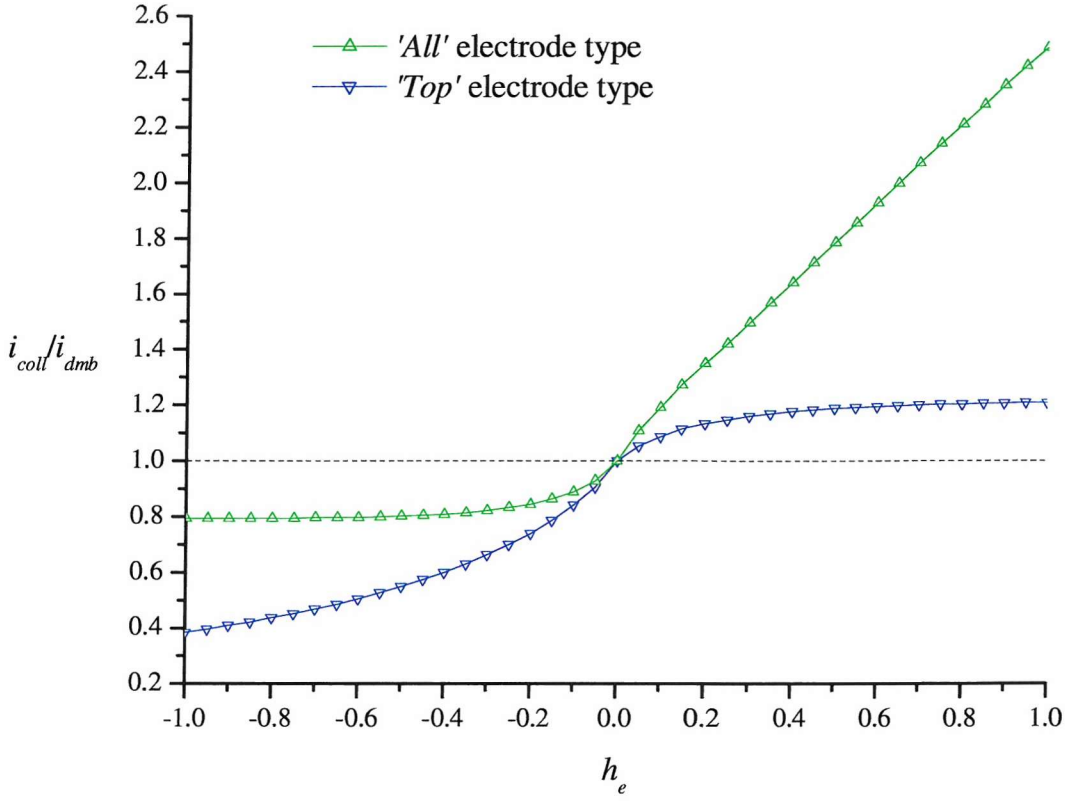

Figure 2.33: The effect of raised or recessed electrode geometries. Current is normalised with the current at a inlaid double microband. h is the height above the insulating surface, thus negative values correspond to recessed electrodes. Electrode types are defined in figure 2.31 on page 109. Parameters used were $w = g = 1$.

is lowered, if the sides of the trough are electroactive the effect is less significant as dominant diffusion occurs between the static sides. If only the base of the recess is electroactive then the current continues to reduce as h_e decreases.

For the generator-collector system short range diffusion is the dominant factor at long times thus the shape of the electrodes and precise dimensions of the surrounding area are of crucial importance in determining an accurate current.

Figure 2.34 on the following page shows the variation of generator current with gap distance for different values of h_e. As expected the current falls with increasing distance between electrodes. This is most pronounced at small gap values. At large gap distances the electrode shape (raised or recessed) has only a relatively small effect on current response.

As seen from figure 2.35 on page 115 the variation of current as a function of gap dis-

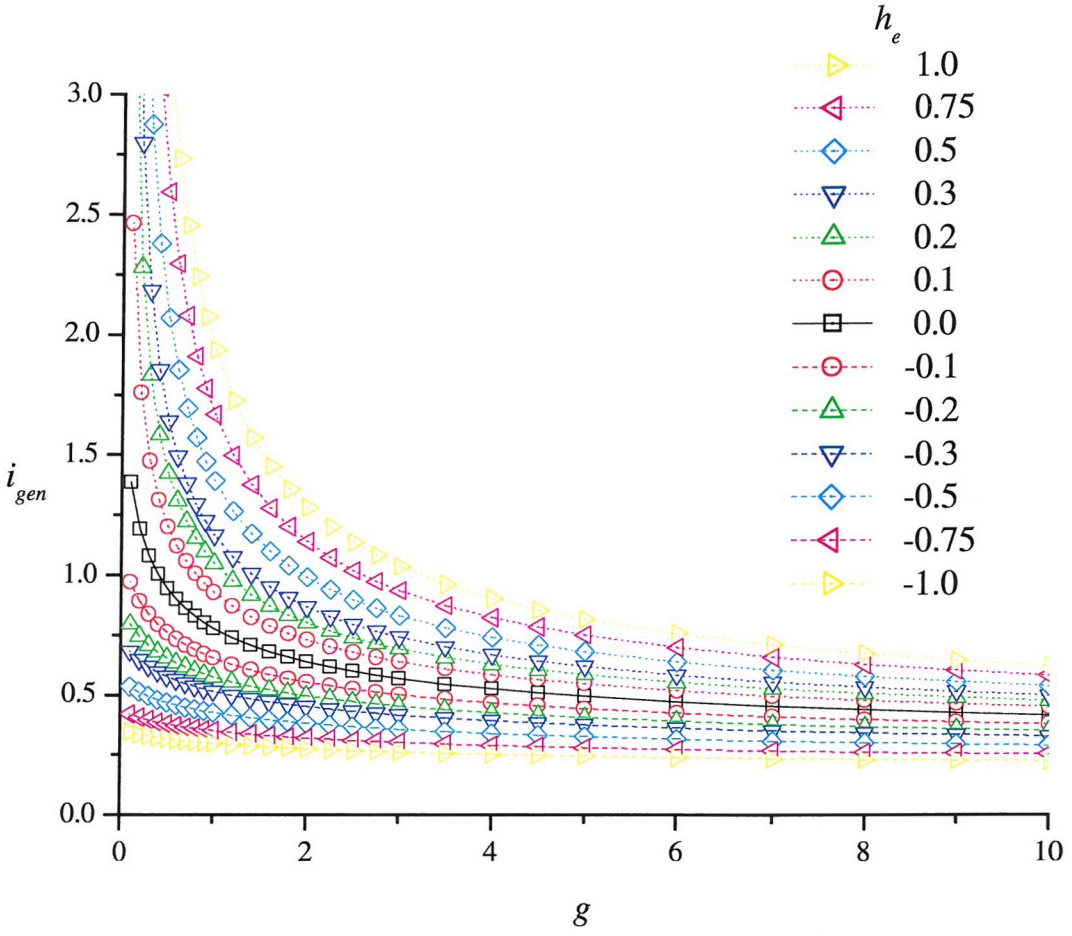

Figure 2.34: The effect of varying gap distance, g on the generator currrent for the 'All' type of electrode. h_e is the height above a flat surface, thus positive h_e is a raised electrode and negative h_e is a recessed electrode. Parameters were as described in table 2.15 on page 111.

tance is not constant, hence each curve in figure 2.34 must be simulated individually. When the width of the electrode is of comparable size to the gap between electrodes the highest contribution to current comes from linear diffusion between the electrode sides. The extra distance species must travel from the far edges of the microbands is substantial. However, as the gap increases this distance, which is fixed, has much less significance. Therefore at large gap values the current approaches that found at a inlaid microband.

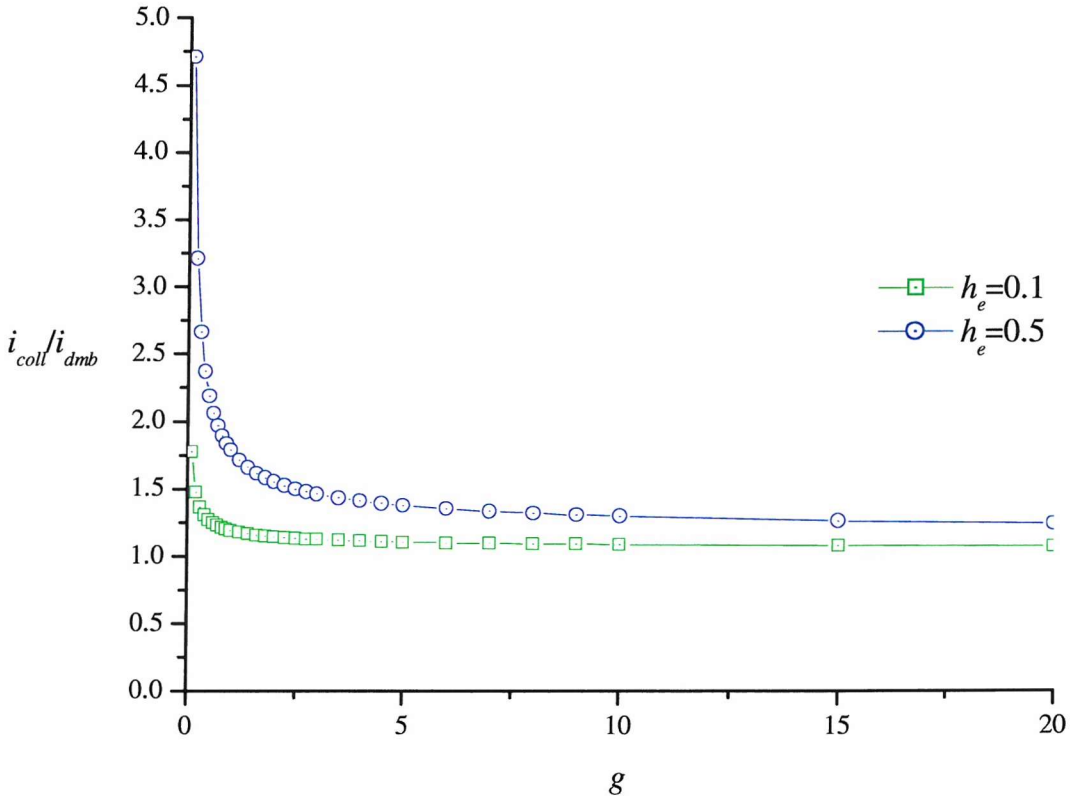

Figure 2.35: The relation of current to gap distance relative to an inlaid DMB. Electrode type 'All'. Parameters were as described in table 2.15 on page 111.

2.8 Novel Raised Band Configurations

The BEM simulation was applied to a novel electrode configuration, consisting of an insulating block above a raised electrode. Such a system may be manufactured by lithographic techniques. The two sides of the raised geometry are electroactive, as described in figure 2.36. This configuration was compared to raised microband of type 'All' (see previous section) and a inlaid double microband.

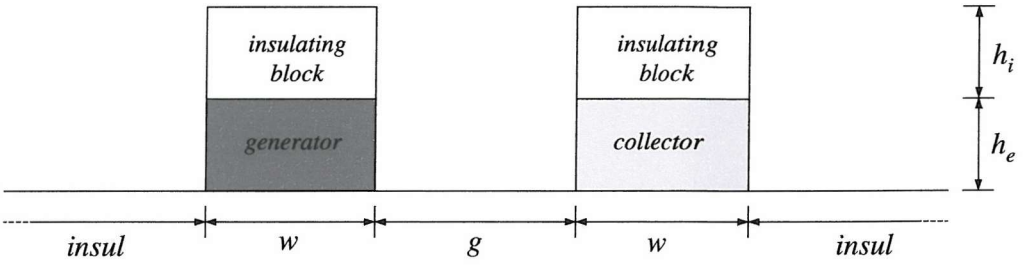

Figure 2.36: A description of electrode type 'sides'. Parameters used for all simulation in this section are identical to those used in the previous section, table 2.15 on page 111. Discretisation over the insulating block was equal(A) spaced, as described in that table.

Two variations of electrode type 'sides' were simulated; firstly an insulating block of equal height to the electrode, $h_e = h_i$, secondly a fixed block height of one, $h_i = 1$. The variation of current with increasing electrode height for a raised double microband is shown in figure 2.37 on the next page.

As expected the current for a raised electrode with only electroactive sides is lower than when the entire surface is electroactive. Despite initial appearances the curve is not directly proportional to h_e. Both electrode types approach direct proportionality of i_{norm} vs h_e, as h_e increases and linear diffusion between sides dominates. At very large values of h_e one would expect types 'all' and 'sides' to converge as non-linear diffusion becomes negligible. However, at small values of h_e, when non-linear diffusion is significant, proportionality does not hold. Simulation of $h_e < 0.1$ was not possible due to discretisation restraints; sufficient elements must be allocated over the electrode sides and top.

The difference in current response between the two 'sides' type of electrode is rel-

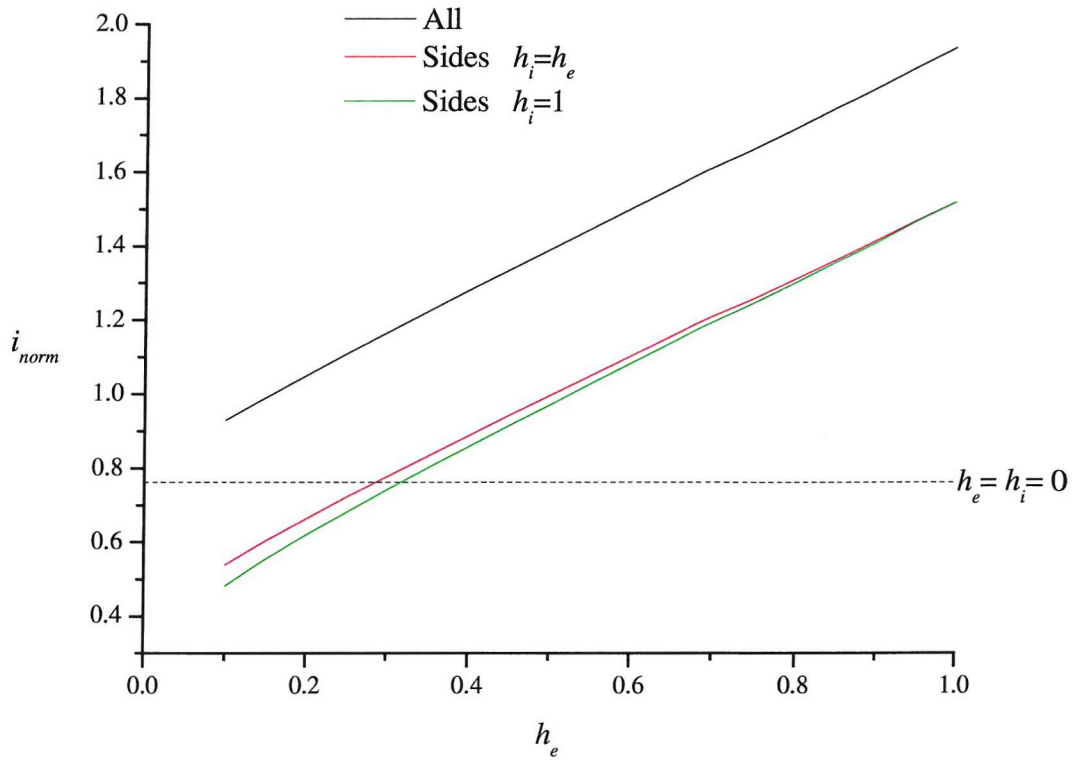

Figure 2.37: The variation of current with increasing electrode height for three configurations of double raised microbands. Electrode types and domain discretisation are described in figure 2.36 on the page before.

atively small, becoming more pronounced as h_e decreases. This is due to hindered diffusion from the outer sides of the electrodes. Table 2.16 on the following page shows the contribution to current from different areas of the generator electrode surface. The major contribution may be seen to arise from the electrode side facing the collector. When a larger insulating block is present the facing electrode side flux is virtually unchanged, however the far side decreases.

Total electrode flux at raised 'sides' electrodes is greater than flat geometries with the same surface area. This is true even when an insulating block hinders diffusion to half the raised area, and is due to the much greater flux present at facing surfaces than coplanar ones.

Electrode Type	h_e	h_i	Electrode area			Total Flux
			Left side	Centre	Right side	
inlaid	0.0	0.0	–	0.780	–	0.78
All Sides	0.5	0.0	0.185	0.606	0.600	1.39
	0.5	0.5	0.291	–	0.717	1.01
	0.5	1.0	0.263	–	0.719	0.98
All Sides	1.0	0.0	0.244	0.593	1.100	1.94
	1.0	1.0	0.317	–	1.218	1.54

Table 2.16: Components of the total flux at different configurations of raised microbands, from figure 2.37 on the preceding page.

2.8.1 Multiple Bands

Results were also obtained for two pairs of generator-collector microbands, for the three configurations. The variation of current with increasing electrode height for four raised microbands is shown in figure 2.38 on the next page. The behaviour is analagous to the raised double microband system, with higher currents due to the larger number of electrodes.

These simulations show the flexibility and versatility of the Boundary Element Method. To extend the simulation to multiple raised band configuration required alteration of only the input data describing the geometry of the domain and the boundary conditions.

The method enables solution of novel complex electrode geometry systems which are otherwise intractable with established techniques.

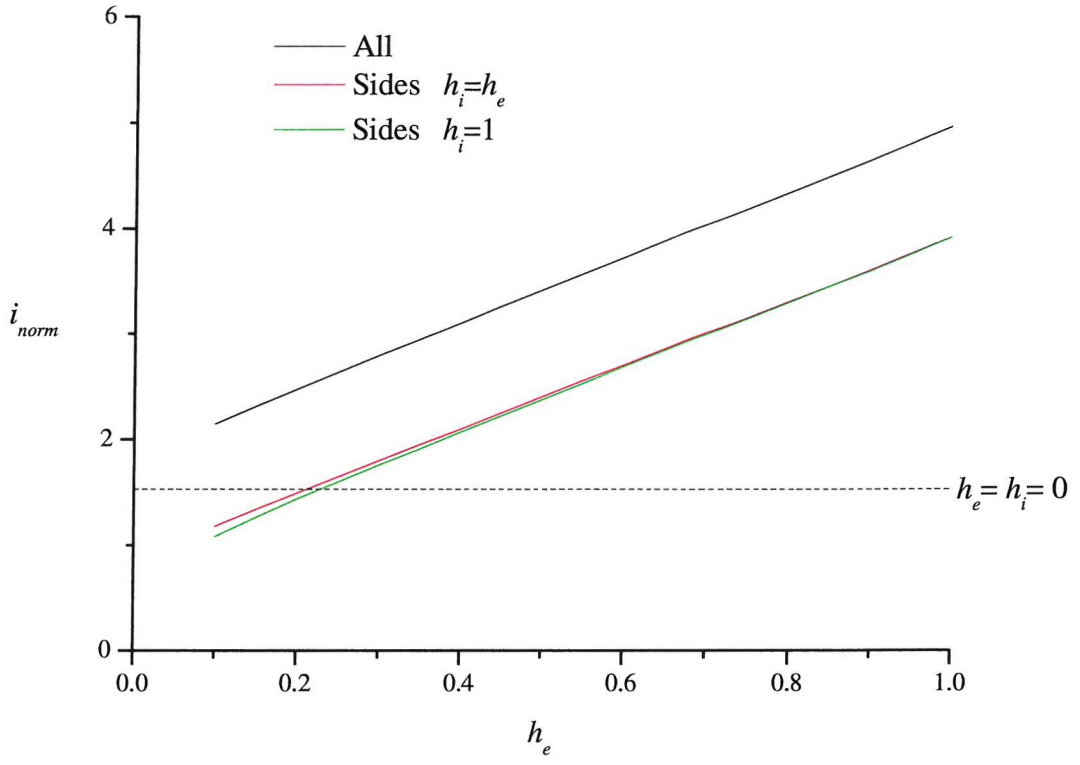

Figure 2.38: The variation of current with increasing electrode height for three configurations of four raised microbands. N_{pairs} = 2. Electrode types and domain discretisation are described in figure 2.36 on page 116.

2.9 Double Microband Scan

A scanning probe may be used to image a double microband substrate. If the probe is moved slowly, then the system is allowed to reach a steady state and convection is assumed to be negligible. A feedback loop between probe (generator) and substrate features (collector) is achieved, figure 2.39. Diffusion is physically inhibited by the presence of the substrate, therefore the geometry and proximity of the substrate is important. This is analogous to a Scanning Electrochemical Microscope[11] (SECM), here using a microband instead of a microdisc. This system demonstrates the power and flexibility of the BEM method. Each position of the probe along the scan represents one simulation, which for the BEM simply requires a shift in the definition of electrode coordinates. Concentration maps are easily obtained using an equally spaced rectangular mesh of internal points.

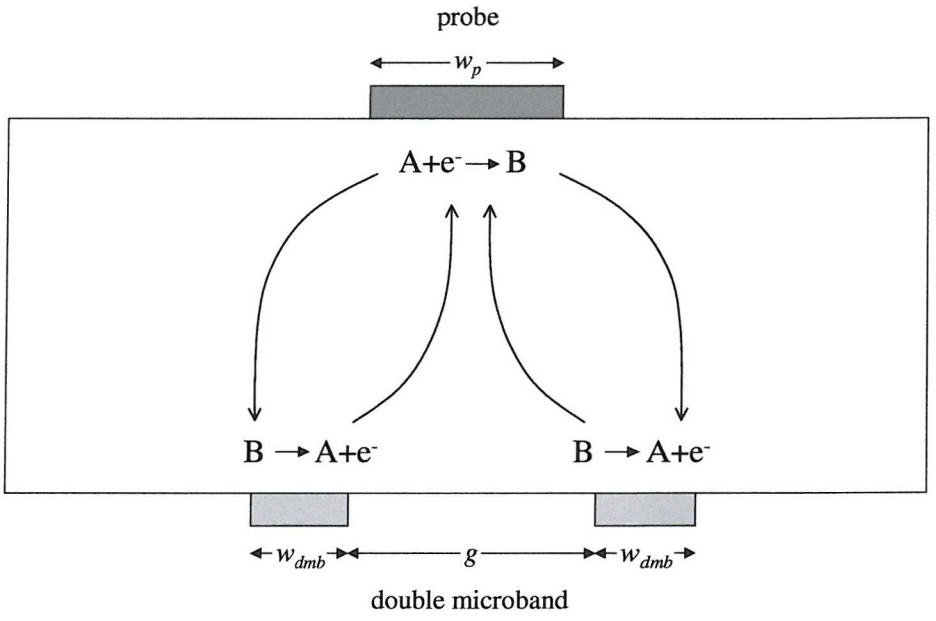

Figure 2.39: The scanning probe domain showing the feedback loop between the probe and the conducting substrate features, in this case a double microband.

Figure 2.40 on the next page shows the current response of the probe for parameters $w_p = 1$, $w_{dmb} = 1$, $g = 2$, $h = 0.5$. As it passes over the double microband two bands are clearly discernible.

A concentration map of the domain may be generated by interpolating the bound-

ary and internal mesh data, figure 2.41. The influence of the substrate features is significant at this close range of $h = 0.5w$. Lines between concentration values are due to the limited number of colours.

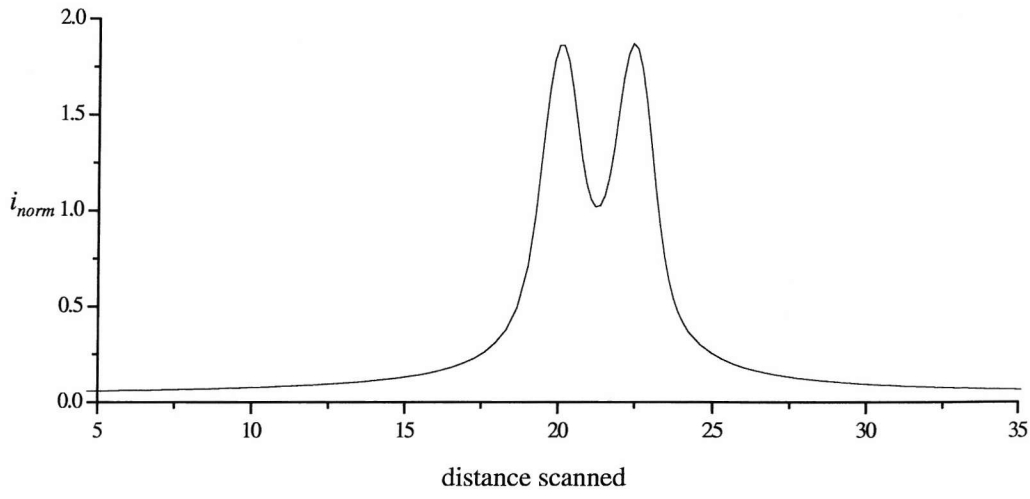

Figure 2.40: The current response of the probe. A total of 120 simulations are plotted. $w_p = 1$, $w_{dmb} = 1$, $g = 2$, $h = 0.5$.

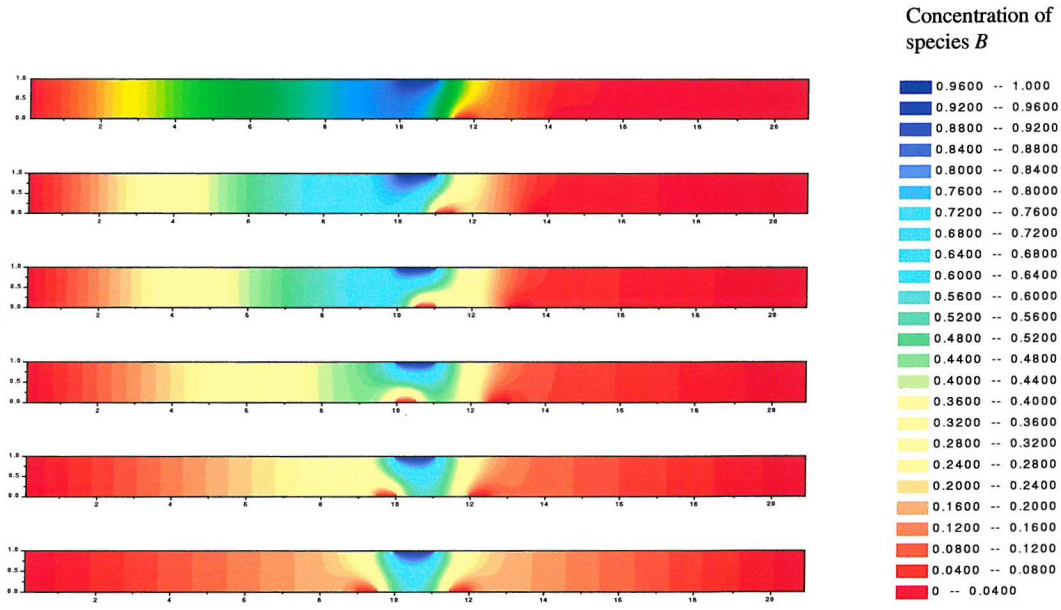

Figure 2.41: A series of concentration maps for a probe scanned over a double microband. $w_p = 1$,$w_{dmb} = 1$,$g = 2$,$h = 0.5$. The map is centered on the scanning probe. The blue region corresponds to the region below the tip where the product species is generated, the two red spots correspond to the two microbands where the redox mediator is regenerated.

In practice it would be difficult to perform this experiment with a microband. If the band is not lined up exactly parallel to the substrate, one end of the band would pass over before the other, leading to a blurred image and decreasing resolution. A microdisc electrode would be better suited to this task. The size of the surrounding sheath has been shown to have an effect on the current obtained,[66] and would be expected to have an analogous effect for the microband.

2.10 Refinements and Limitations

The basic Boundary Element Method may be enhanced when considering accuracy and speed of computation. Linear elements, where concentration and flux vary linearly along the length of the element, increase accuracy or allow fewer elements giving faster simulation times. The theoretical aspects of applying linear element types to the BEM is described in the next section. Implementation of alternative linear algebra routines, described in section 2.4.1 on page 70, does not affect the accuracy of the method, but does increase the speed of computation.

2.10.1 Linear Elements

One of the approximations made in section 2.2 on page 54 was to assume that concentration and flux values were constant over the entire length of a given element. Elements of higher order variation, which are more accurate, may be defined. Typical element types are shown in figure 2.42 on the next page.

Linear elements were implemented for the two dimensional Laplace equation. Differences in implementation from section 2.2 on page 54 are outlined below.

BEM Theory

As concentration and flux are no longer constant they cannot be removed from the Boundary Integral Equation integrals. The discrete BIE is therefore

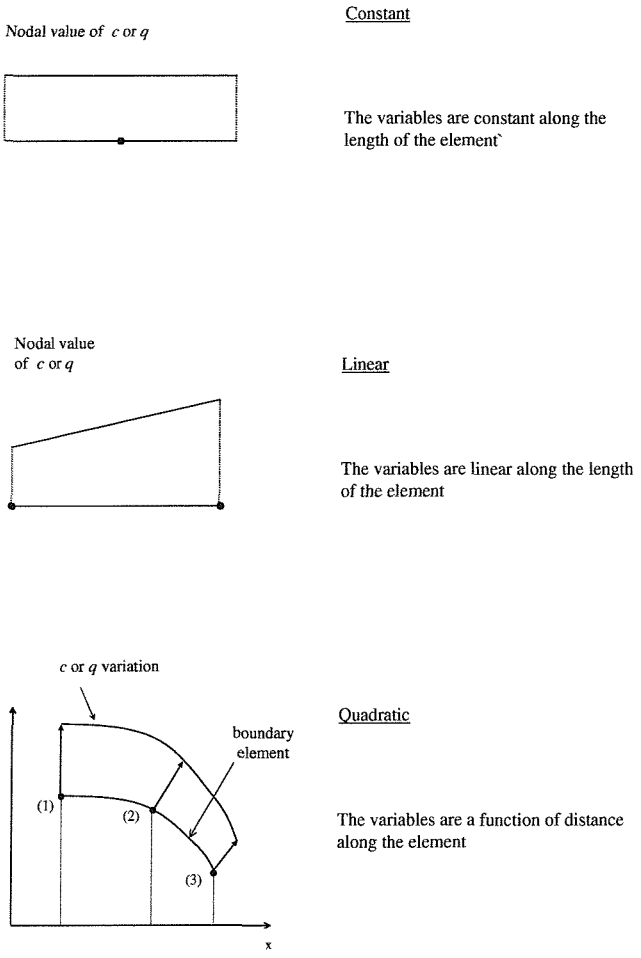

Figure 2.42: Increasing order of variation of concentration and flux along the boundary element. Both constant and linear types were implemented.

$$d_s c_s + \sum_{j=1}^{N} \int_{\Gamma j} c_j q^*_{sj} \, \mathrm{d}\Gamma = \sum_{j=1}^{N} \int_{\Gamma j} q_j W_{sj} \, \mathrm{d}\Gamma \tag{2.47}$$

where
- d is the geometry coefficient
- c is concentration
- q is flux
- Γ_j is an element boundary
- W is the fundamental solution
- q^* is the derivative of the fundamental solution
- ξ_1,ξ_2 are source point coordinates.
- s is the source point integer counter
- j is the field point integer counter

A local coordinate system, η, is used for integration over each element. This is defined as

$$-1 \leq \eta \leq 1 \tag{2.48}$$

Concentration and flux over each element vary linearly, analogous to linear interpolation. The variations are defined as follows

$$c = \phi_1 c_1 + \phi_2 c_2 \tag{2.49}$$

$$q = \phi_1 q_1 + \phi_2 q_2 \tag{2.50}$$

where c is concentration, q is flux and ϕ are basis functions. These functions are defined

$$\phi_1 = \frac{1}{2}(1 - \eta) \tag{2.51}$$

$$\phi_2 = \frac{1}{2}(1 + \eta) \tag{2.52}$$

where η is a local coordinate.

Linear elements have nodes at each end of the element[¶]. A comparison of linear and constant element discretisation is given in figure 2.43 on the next page.

The integrals in equation 2.47 may be written in matrix notation by defining

$$\hat{l}^n_{sj} = \int_{\Gamma j} \phi_n q^* \, \mathrm{d}\Gamma \tag{2.53}$$

$$m^n_{sj} = \int_{\Gamma j} \phi_n W \, \mathrm{d}\Gamma \tag{2.54}$$

[¶]Linear elements may also have one or both nodes offset from the end of the element, known as a discontinuous element. This variation may be used to avoid integrating at a boundary singularity.[22]

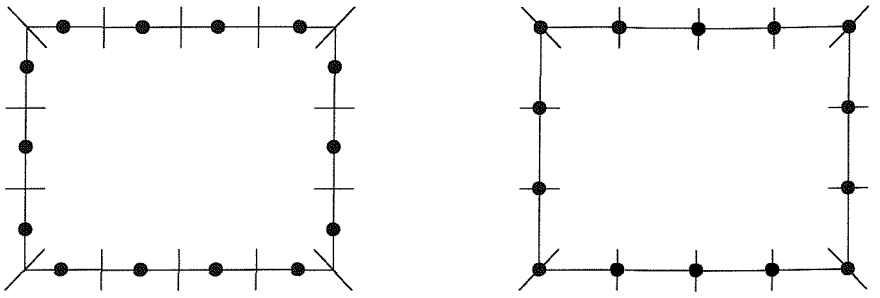

Figure 2.43: A comparison of constant and linear element discretisation. Constant elements have one node per element, linear elements have two nodes per element. However, as linear element nodes coincide with each other the total number of nodes is identical.

where
$\hat{l}, m$	are influence coefficients
W	is the fundamental solution
q^*	is the derivative of the fundamental solution
ϕ	are basis functions
n	is the interpolation node number, for linear elements $n = 1, 2$
Γ_j	is an element boundary
s	is the source point integer counter
j	is the field point integer counter

The expression $d = \frac{1}{2}$ is valid only if the boundary is smooth about the source point. This may no longer be true as source points are located at the ends of the element. As defined in section 2.2 on page 54 the geometry coefficient, d, is given by

$$d = \frac{\theta}{2\pi} \tag{2.14}$$

where θ is the internal angle. However there is an easier way to calculate this term, without reference to the element geometry. When a uniform concentration is applied over a bounded region, the sum of all the derivatives must be zero. Therefore d may be calculated by summation of the non-singular $\hat{l}_{sj}$ terms.

The summation is thus

$$l_{ss} = \sum_{\substack{j=1 \\ j \neq s}}^{N} \hat{l}_{sj} \tag{2.55}$$

where N is the number of elements. This only applies to internal Laplace regions. External regions have a summation of one

$$l_{ss} = 1 - \sum_{\substack{j=1 \\ j \neq s}}^{N} \hat{l}_{sj} \tag{2.56}$$

The use of the term l_{sj} (without the hat) indicates the summation rule for singular terms is incorporated.

These terms may be substituted into the Boundary Integral Equation, equation 2.47,

$$\sum_{j=1}^{N} \begin{pmatrix} l_{sj}^1 & l_{sj}^2 \end{pmatrix} \begin{pmatrix} c_{n1} \\ c_{n2} \end{pmatrix} = \sum_{j=1}^{N} \begin{pmatrix} m_{sj}^1 & m_{sj}^2 \end{pmatrix} \begin{pmatrix} q_{n1} \\ q_{n2} \end{pmatrix} \tag{2.57}$$

where $n1$ and $n2$ are nodes 1 and 2 respectively, of element j.

When written in matrix form this equation reduces to equation 2.32, identical to the constant element formulation,

$$\mathsf{L}\boldsymbol{c} = \mathsf{M}\boldsymbol{q} \tag{2.32}$$

which may be solved with standard linear algebra techniques.

Corner Nodes

A single value for flux is inadequate at corner junctions in the boundary. The two perpendicular components of flux must be calculated separately, figure 2.44 on the next page. Thus matrix L has dimensions Nx$2N$ and vector q is of length $2N$.

Alternative singular integration is required, solutions for which are available in the literature.[22,103]

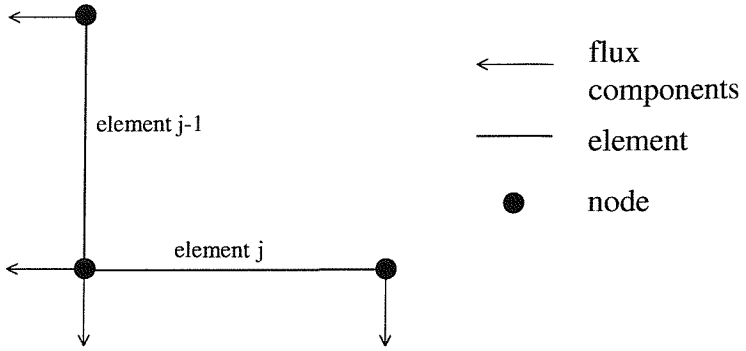

Figure 2.44: Components of flux must be calculated separately for linear elements. The components are defined perpendicular to the element, facing outward form the boundary.

Comparison of Element Types

Linear elements were implemented for the direct BEM simulation. Figure 2.45 on the following page shows that convergence is faster than for constant elements. Using a linear variation of variables increases accuracy, requiring fewer elements.

The effort involved in implementing linear element types is substantial, mostly due to the increased programming complexity involved. The benefits of linear elements are limited by the behaviour of boundary discretisation, when applied to electrochemical problems. These discretisation effects, described in detail in section 2.5.2 on page 77, have a far greater influence than the element type.

2.10.2 Limitations

A detailed analysis of the BEM for the one and two dimensional Laplace equation has been given in this chapter. However, to model a different geometry, for instance axisymmetric or three dimensional, requires implementation of a suitable fundamental solution and derivative, and suitable elements types. Also to account for additional terms in the original partial differential equation, such as convection or homogeneous chemical reactions, requires implementation of a suitable fundamental solution.

Although various fundamental solutions are available[22,23,103] these changes involve

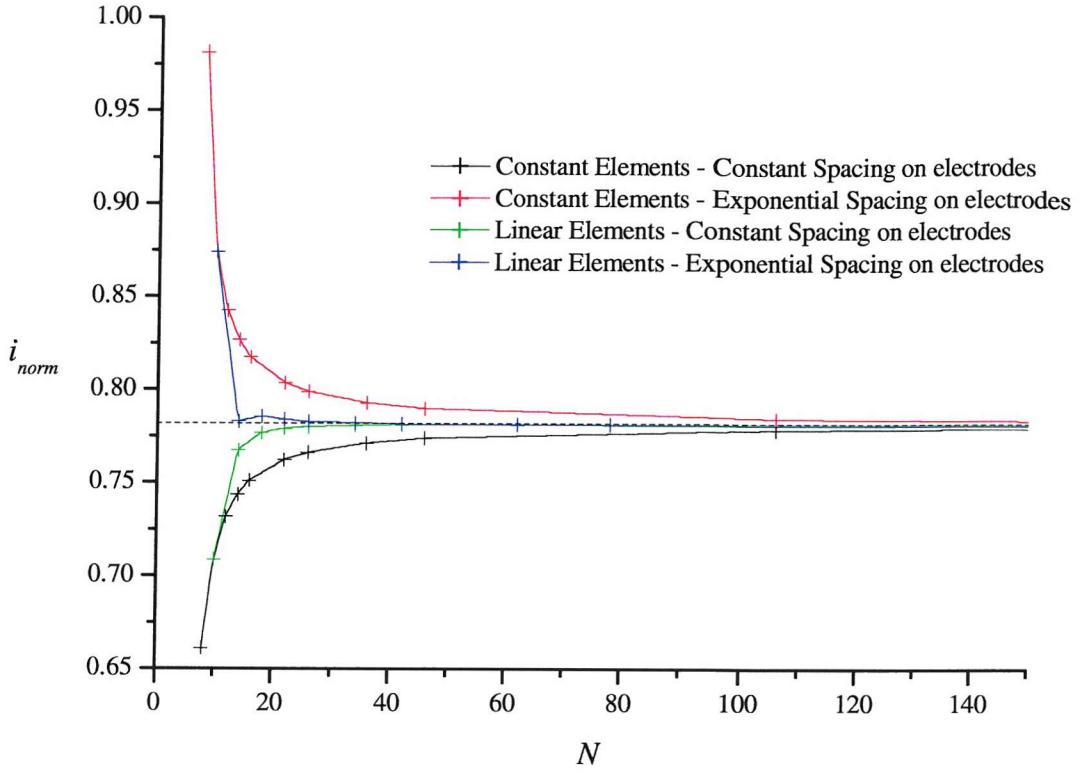

Figure 2.45: A comparison of the effect linear and constant element types, for the double microband. Discretisation used was a constanst number of elements over each boundary section. Within each section elements were equally spaced. N is the total number of elements around the entire boundary. $w = g = 1$, $insul = wall = 200$.

substantial effort. An appealing alternative is a technique which allows simulation of a wide variety of additional terms, based on the Laplace fundamental solution. This is known as the Dual Reciprocity Method and is described in the following chapter.

Chapter 3

Chapter Three - The Dual Reciprocity Method

3.1 Introduction

The standard Boundary Element Method requires a fundamental solution to be derived for each partial differential equation modelled. It would be advantageous to apply the BEM principles to different partial differential equations without recourse to new fundamental solutions, whether for reasons of difficulty of derivation or the complexity of implementing a function already obtained.

An advanced addition to the BEM, the Dual Reciprocity Method (DRM) enables just such a generalisation. This has significant potential for application to electrochemical problems which are otherwise intractable. The vast majority of BEM and related research has taken place in various fields of engineering. However, electrochemical systems represent a unique class of often complex problems, with features such as mixed boundary conditions, convection and diffusion combined with reactions in solution. Although simplified electrochemical problems have direct analogies in some engineering fields, the majority do not. With its extensible nature, the DRM offers the opportunity to solve a range of complex electrochemical problems.

The Dual Reciprocity Method allows evaluation of a variety of partial differential equations using a formulation based on the fundamental solution to the Laplace

equation. This is achieved by approximating the remaining derivatives (non-Laplacian terms) with a series of interpolation functions. Some internal points are used, however discretisation of the internal domain is not required, thus retaining the geometrical advantages of the Boundary Element Method.

3.1.1 Historical Background

The Dual Reciprocity Method was first introduced in 1982 by Nardini and Brebbia.[157] A steady stream of advances were made in the 1980's including transient diffusion,[158] axisymmetric diffusion[159] and others.[160,161] Further investigations were carried out in the following decade,[101] the 1990's, with significant improvements in understanding the approximating functions used,[162,163] a wider variety of applications and efficiency of implementation.[164,165] At this time alternative related methods such as the Multiple Reciprocity Method[166] and the Method of Fundamental Solutions[167] were developed.

During the period of study of the author the Dual Reciprocity Method was a novel method to electrochemists. It has since been applied by Fisher *et al.*[102]

There are still a number of areas with regard to aspects of the DRM formulation which need to be addressed, including combining the DRM with closely related methods. These are currently active areas of research.[167–170]

3.1.2 The DRM Applied to Electrochemistry

In the following two sections the procedure for solving the steady state diffusion-convection equation, in two dimensions, is outlined. An example of an electrochemical application which is governed by this equation is the channel flow system,[171] described in section 3.5 on page 147. This is a suitable example to test and validate the DRM as approximate analytical solutions are available, in addition to results from alternative simulation methods, for comparison.

A fundamental solution to the diffusion-convection equation, assuming a constant flow velocity, has been derived.[172] However, this assumption is not valid for the channel flow system due to its flow profile; this is described in section 3.5 on page 147.

The general DRM formulation is described in the next section, the specific application of the DRM to the diffusion-convection equation is covered in the following section.

3.2 Dual Reciprocity Method Formulation

In terms of the BEM formulation, if the additional convection term in the governing partial differential equation cannot be moved to the boundary, through derivation of a suitable fundamental solution, it introduces internal domain integrals. These must be approximated by domain discretisation.

The DRM formulation is an alternative approach which removes the need to discretise the domain by approximating the convection term using a linear interpolation formulation. These integrals may then be moved to the boundary, without requiring a fundamental solution, via the Inverse Form of the partial differential equation, in an analogous manner to the standard BEM.

3.2.1 Governing Partial Differential Equation

The Dual Reciprocity Method solves partial differential equations of the general form

$$\frac{\partial^2 c(x,y)}{\partial x^2} + \frac{\partial^2 c(x,y)}{\partial y^2} = b(x,y,c,t) \tag{3.1}$$

where c is concentration, x, y are cartesian coordinates and t is time. The term on the right hand side is known as an internal domain term, as it will not be described by the boundary terms of the standard BEM. Note that the right hand term may include a time derivative and a convection term.

Writing the governing partial differential equation in this form allows the fundamental solution of the Laplace equation to be utilized to solve the left hand side of equation 3.1, while using an approximating function to account for the right hand side and still retain the boundary method characteristics.

As an example for this derivation the dimensionless steady state diffusion-convection equation is used. This equation is described in detail in section 3.5.1 on page 148. However, the procedure applies to any domain integral term from equation 3.1.

The governing partial differential equation for diffusion-convection is

$$\frac{\partial^2 c(x,y)}{\partial x^2} + \frac{\partial^2 c(x,y)}{\partial y^2} - \nu(x,y)\frac{\partial c(x,y)}{\partial x} = 0 \tag{3.2}$$

where ν is the dimensionless flow rate coefficient. Refer to section 3.5.1 on page 148 for the model and assumptions used to derive this equation.

Equation 3.2 may be rearranged and written in a form suitable for the DRM

$$\frac{\partial^2 c(x,y)}{\partial x^2} + \frac{\partial^2 c(x,y)}{\partial y^2} = \nu(x,y)\frac{\partial c(x,y)}{\partial x} \tag{3.3}$$

where the left hand side may be recognised as part of the Laplace equation.

A solution to equation 3.3 may be written as

$$\frac{\partial^2 \hat{c}(x,y)}{\partial x^2} + \frac{\partial^2 \hat{c}(x,y)}{\partial y^2} = \nu(x,y)\frac{\partial c(x,y)}{\partial x} \tag{3.4}$$

where $\hat{c}$ is a series of particular solutions. An approximating function for the internal domain term, which is valid over the entire domain, may be defined by this series of particular solutions. Calling this function f, gives

$$\nu(x,y)\frac{\partial c(x,y)}{\partial x} \approx \sum_k \alpha_k f_k(x,y) \tag{3.5}$$

where α are initially unknown coefficients, k are DRM summation points (see figure 3.2 on page 139) and f is an approximating function, defined by

$$f_k(x,y) = \frac{\partial^2 \hat{c}_k(x,y)}{\partial x^2} + \frac{\partial^2 \hat{c}_k(x,y)}{\partial y^2} \tag{3.6}$$

3.2.2 The f Approximating Function

The choice of a suitable approximating function is important as the basis of the DRM is the approximation of domain integrals by these interpolation functions. Therefore which function is used will have a direct effect on accuracy.

There were a variety of functions originally proposed,[157] including elements of Pascal's triangle, sine series and radial basis functions. For example

$$1, x, y, x^2, xy, y^2, \ldots \tag{3.7}$$

$$1, \sin x, \sin y, \sin 2x, \sin xy, \ldots \tag{3.8}$$

and

$$1 + r + r^2 + r^3 + \ldots \tag{3.9}$$

where

$$r = \sqrt{(x - \xi_1)^2 + (y - \xi_2)^2} \tag{3.10}$$

ξ_1, ξ_2 are the cartesian coordinates of the source point, s while x, y are the cartesian coordinates of the field point, k. r is thus the distance from the source to field points.

Some of these original functions include r, the same parameter as that used in the Laplace fundamental solution. These were later found to be a form of Radial Basis Functions (RBF).[162] Strictly, RBF's of the series, equation 3.9, are odd powers of r only. If even powers are included in the function it does not seem to affect the solution, but they should be avoided.[173]

The function $f = 1 + r$ became the most widely used from the introduction of the method until the mid 1990's. At this time, with increasing interest in the Dual Reciprocity technique, investigations of the behaviour, accuracy and mathematical basis[162] of a variety of approximating functions were performed.[163,174] Convergence of the r series was proved[175] and a variety of functions were proposed,[176] some of which are summarised in table 3.1 on the next page.

The functions tested in this work were the radial basis functions of equation 3.9. Variation of concentration and flux with increasing series terms was found to be very small. The function $f = 1 + r + r^2 + r^3$ was selected for use throughout this work.

Name	Example Function
Thin Plate Spline (TPS)	$r^2 \log r$
Higher Order Thin Plate Spline	$r^4 \log r$
Augmented Thin Plate Spline (ATPS)	$1 + r^2 \log r$
Multiquadric*	$(r^2 + a^2)^{\frac{1}{2}}$

* a is a user defined constant dependent on the specific mesh used.[173]

Table 3.1: A variety of approximating functions have been proposed, some of which are summarised here.

To understand the behaviour and significance of the approximating function, f may be thought of in terms of an interpolation function which describes the variation of a variable, for example the concentration gradient, over the entire domain. A number of nodes are required in the interior of the domain to calculate this interpolation. This is in contrast to the standard BEM which only required nodes on the boundaries.

A recent by paper by Partridge,[173] published after the DRM studies reported here, suggests optimal functions for various types of partial differential equations. It is found that a single r function is often least accurate, although higher order RBF series are accurate. The reader is referred to this text when choosing a specific approximation function. The optimal functions for a range of electrochemical problems are summarised in table 3.2 on the following page. Two dimensional DRM only is covered, although three dimensional equivalents exist for most functions, optimal two dimensional versions are not necessarily optimal in three dimensions.

Note that in the literature radial basis functions are often referred to as 'local' functions, whereas other functions such as sine expansions are 'global' functions.[176]

3.2.3 Formation of the Boundary Integral Equation

The inverse form of the modified partial differential equation is used to obtain a Boundary Integral Equation in an analogous manner to the standard BEM. Substi-

Problem Type	Optimal f functions
steady state convection	$1 + r^3$ $r^4 \log r$
transient diffusion	no optimal function
transient diffusion and convection	no optimal function
simple homogeneous reaction, e.g. $E_r C_i$	$1 + r^3$ $r^4 \log r$

Table 3.2: Optimal functions for various electrochemical related problems. Reference[173] describes optimal functions for a range of engineering partial differential equation systems.

tuting equations 3.5 and 3.6 into equation 3.3 gives

$$\frac{\partial^2 c(x,y)}{\partial x^2} + \frac{\partial^2 c(x,y)}{\partial y^2} = \sum_k \alpha_k \left(\frac{\partial^2 \hat{c}_k(x,y)}{\partial x^2} + \frac{\partial^2 \hat{c}_k(x,y)}{\partial y^2} \right) \tag{3.11}$$

where α is an unknown coefficient, $\hat{c}$ and $\hat{q}$ are particular solutions.

The weighted residual form of this equation is integrated twice, and applied at a source point on the boundary producing the Boundary Integral Equation

$$dc(\xi_1,\xi_2) + \int_\Gamma q^*(x,y,\xi_1,\xi_2) c(x,y)\, \mathrm{d}\Gamma - \int_\Gamma W(x,y,\xi_1,\xi_2) q(x,y)\, \mathrm{d}\Gamma =$$
$$\sum_k \alpha_k \left(d_k \hat{c}_k(x,y) + \int_\Gamma q^*(x,y,\xi_1,\xi_2) \hat{c}_k(x,y)\, \mathrm{d}\Gamma - \int_\Gamma W(x,y,\xi_1,\xi_2) \hat{q}_k(x,y)\, \mathrm{d}\Gamma \right) \tag{3.12}$$

where
- W is the fundamental solution to the Laplace equation
- q^* equals $\partial W/\partial n$ (n is the unit outward normal)
- $\hat{c}$ is a series of particular solutions
- $\hat{q}$ equals $\partial \hat{c}/\partial n$
- d is the geometry coefficient (defined in section 2.2)
- k is the DRM summation point number
- Γ is the domain boundary

This equation contains no explicit internal domain integral; the three terms on the left hand side are all boundary terms, recognisable from standard BEM, the domain integral term now has equivalent boundary integrals, the terms on the right hand

side.

The discrete Boundary Integral Equation is obtained by defining I internal points and discretising the boundary into N elements, as shown in figure 3.1.

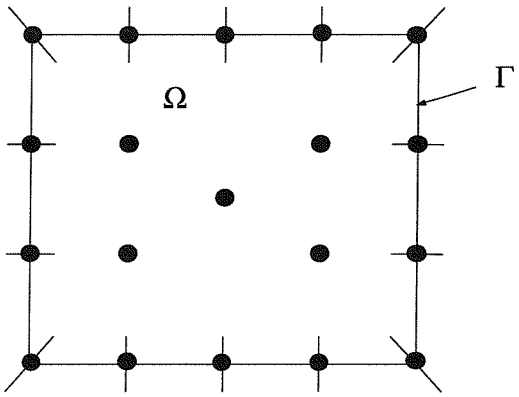

Figure 3.1: Discretisation of the domain for the DRM formulation. Boundary discretisation is the same as in the standard BEM but additional internal points are added to approximate domain integrals. Linear elements are shown here; alternatively constant elements may also be used. Ω is the internal domain and Γ is the boundary.

The discrete form of equation 3.5 including summation limits is thus

$$\nu(x,y)\frac{\partial c(x,y)}{\partial x} \approx \sum_{k=1}^{N+I} \alpha_k f_k(x,y) \tag{3.13}$$

where α are initially unknown coefficients and f is an approximating function and k are DRM summation points.

The Boundary Integral Equation is applied at each source point to give the discrete

Boundary Integral Equation

$$d_s c_s(\xi_1,\xi_2) + \sum_{j=1}^{N} \int_{\Gamma j} q^*_{sj}(x,y,\xi_1,\xi_2) c_{sj}(x,y)\, \mathrm{d}\Gamma - \sum_{j=1}^{N} \int_{\Gamma j} W_{sj}(x,y,\xi_1,\xi_2) q_{sj}(x,y)\, \mathrm{d}\Gamma = \sum_{k=1}^{N+I} \alpha_k \Bigg(d_s \hat{c}_{sk}(x,y) + \sum_{j=1}^{N} \int_{\Gamma j} q^*_{sj}(x,y,\xi_1,\xi_2) \hat{c}_{jk}(x,y)\, \mathrm{d}\Gamma - \sum_{j=1}^{N} \int_{\Gamma j} W_{sj}(x,y,\xi_1,\xi_2) \hat{q}_{jk}(x,y)\, \mathrm{d}\Gamma \Bigg) \quad (3.14)$$

where N is the number of boundary elements, I is the number of internal points, j is the element number and all other terms are defined in the equation 3.12 on page 137.

The difference between source points, s and DRM summation points, k is emphasised in figure 3.2.

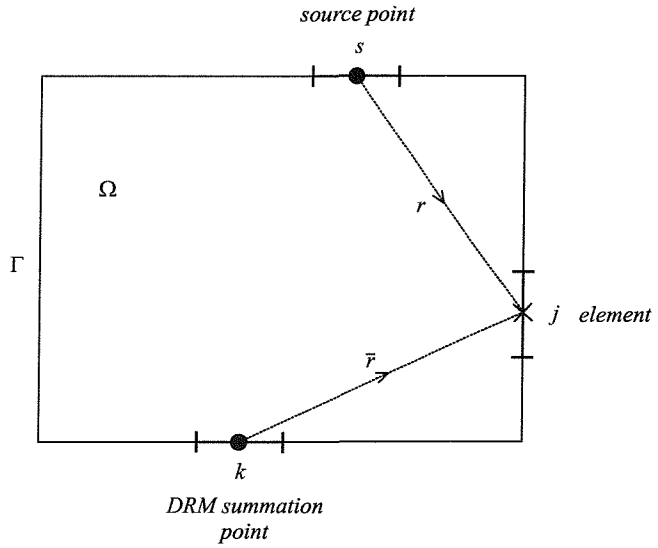

Figure 3.2: A schematic showing the difference in source point, s and DRM summation point, k. The vector $\bar{\boldsymbol{r}}$ is used for calculation of $\hat{u}_{kj}$ and $\hat{q}_{kj}$. However the influence coefficients l_{sj} and m_{sj} use the vector $\boldsymbol{r}$. Letting $k = s$ it may be seen that vector $\boldsymbol{r}$ may be used for calculation of $\hat{u}$ and $\hat{q}$ provided the sign of the vector is changed. Note that for simplicity constant elements are shown here although linear elements were implemented. Ω is the internal domain and Γ is the boundary.

It is more efficient to approximate $\hat{c}$ and $\hat{q}$ over each element with interpolation functions dependent on the element type. For example, if linear elements are used to discretise the boundary, using linear interpolation functions for the particular solutions allow identical functions to be used on both sides of equation 3.14. Constant element types are used in the following derivation. Linear elements, which were implemented, require similar alterations to the formulation as described for the standard BEM in section 2.10.1 on page 123.

The same definitions as used previously in section 2.2.4 for matrix elements enable a more concise version of equation 3.14 to be written in matrix form. They are repeated here to maintain continuity

$$l_{sj} = \int_{\Gamma j} q^*(x, y, \xi_1, \xi_2)\, \mathrm{d}\Gamma \tag{3.15}$$

$$m_{sj} = \int_{\Gamma j} W(x, y, \xi_1, \xi_2)\, \mathrm{d}\Gamma \tag{2.28}$$

where l, m are matrix elements and Γj is the length of the element.

The use of l (as opposed to $\hat{l}$) indicates the $d_s c_s$ term has been incorporated in the leading diagonal of matrix L as described in section 2.2.4 on page 63.

Applying this notation to equation 3.14 gives

$$\sum_{j=1}^{N} L_{sj} c_j - \sum_{j=1}^{N} M_{sj} q_j = \sum_{k=1}^{N+I} \alpha_k \left(\sum_{j=1}^{N} L_{sj} \hat{c}_{jk} - \sum_{j=1}^{N} M_{sj} \hat{q}_{jk} \right) \tag{3.16}$$

which may be written in matrix form

$$\mathsf{L}\boldsymbol{c} - \mathsf{M}\boldsymbol{q} = \sum_{k=1}^{N+I} \alpha_k \left(\mathsf{L}\hat{\boldsymbol{c}}_k - \mathsf{M}\hat{\boldsymbol{q}}_k \right) \tag{3.17}$$

where L, M are influence coefficient matrices.

One may write this in a more compact form by placing vectors $\hat{\boldsymbol{c}}_k$ and $\hat{\boldsymbol{q}}_k$ as columns

of matrices $\hat{\mathsf{C}}$ and $\hat{\mathsf{Q}}$ respectively to give

$$\mathsf{L}\boldsymbol{c} - \mathsf{M}\boldsymbol{q} = \boldsymbol{\alpha}\left(\mathsf{L}\hat{\mathsf{C}} - \mathsf{M}\hat{\mathsf{Q}}\right) \tag{3.18}$$

This is the general DRM formulation. The right hand side of equation 3.18 is the domain integral approximation and is dealt with differently depending on the specific domain integral term of the governing partial differential equation.

The vector $\boldsymbol{\alpha}$ may be found from equation 3.5. The general form of this is

$$b(x, y, c, t) = \sum_k \alpha_k f_k(x, y) \tag{3.19}$$

This equation may be applied at each source point to give a vector of domain values, $\boldsymbol{b}$. Note that F is a matrix because b_s and f_k have different subscripts, as shown in figure 3.2 on page 139.

$$\boldsymbol{b} = \mathsf{F}\boldsymbol{\alpha} \tag{3.20}$$

This allows the initially unknown vector $\boldsymbol{\alpha}$ to be found

$$\boldsymbol{\alpha} = \mathsf{F}^{-1}\boldsymbol{b} \tag{3.21}$$

The specific form of equation 3.21 will depend on the domain terms of $b(x, y, c, t)$. For the case of the diffusion-convection equation this form is described in the following section

3.3 Application to the Steady State Diffusion-Convection Equation

The formulation derived thus far is general and may by applied to any function $b(x, y, c, t)$. For each form of function b it is necessary to find a way of expressing this function in terms of the approximating function f_k, to enable α_k to be found. This section describes how to include a convection term which contains a flow profile which is a function of x and y.

The following procedure allows the convection term to be expressed in terms of $c(x, y)$ and $f_k(x, y)$. The domain integral term is approximated by equation 3.19. In an analogous way an additional approximation may be defined for concentration

$$c(x, y) \approx \sum_k f_k(x, y)\beta_k \tag{3.22}$$

where f is the approximating function, and β an unknown coefficient. Differentiating this equation gives

$$\frac{\partial c(x, y)}{\partial x} \approx \sum_k \frac{\partial f_k(x, y)}{\partial x}\beta_k \tag{3.23}$$

Rearranging equation 3.22 and substituting into equation 3.23 gives

$$\frac{\partial c(x, y)}{\partial x} \approx c(x, y) \sum_k \frac{\partial f_k(x, y)}{\partial x} \frac{1}{f_k(x, y)} \tag{3.24}$$

where $\partial f/\partial x$ may be obtained by differentiating the specific f function used.

The coefficient α may be found by rearranging equation 3.5, in which the general term $b(x, y, c, t)$ has been replaced by the convection term, giving

$$\alpha_k \approx \nu(x, y) \frac{\partial c(x, y)}{\partial x} \sum_k \frac{1}{f_k(x, y)} \tag{3.25}$$

Substituting equation 3.24 yields

$$\alpha_k \approx \nu(x,y)c(x,y)\sum_k \frac{1}{f_k(x,y)}\frac{\partial f_k(x,y)}{\partial x}\frac{1}{f_k(x,y)} \tag{3.26}$$

Applying this equation to each source point gives the required vector $\boldsymbol{\alpha}$

$$\boldsymbol{\alpha} = \mathsf{F}^{-1}\frac{\partial \mathsf{F}}{\partial x}\mathsf{F}^{-1}\boldsymbol{\nu c} \tag{3.27}$$

Substituting for α in the general DRM equation, equation 3.12 gives

$$\mathsf{L}\boldsymbol{c} - \mathsf{M}\boldsymbol{q} = \left(\mathsf{L}\hat{\mathsf{C}} - \mathsf{M}\hat{\mathsf{Q}}\right)\mathsf{F}^{-1}\frac{\partial \mathsf{F}}{\partial x}\mathsf{F}^{-1}\boldsymbol{\nu c} \tag{3.28}$$

Defining the domain part as D

$$\mathsf{D} = \left(\mathsf{L}\hat{\mathsf{C}} - \mathsf{M}\hat{\mathsf{Q}}\right)\mathsf{F}^{-1}\frac{\partial \mathsf{F}}{\partial x}\mathsf{F}^{-1}\boldsymbol{\nu} \tag{3.29}$$

and substituting equation 3.29 into equation 3.28 gives

$$(\mathsf{L} - \mathsf{D})\,\boldsymbol{c} = \mathsf{M}\boldsymbol{q} \tag{3.30}$$

This equation has the same form as that derived for the boundary element method, and may be solved by applying prescribed boundary conditions and standard matrix solving techniques.

3.4 Program Structure

The structure of a DRM program is similar to the standard BEM algorithm with the addition of several sub-routines to account for integral approximation. A diagram of the program structure is given in figure 3.3 on the next page.

3.4.1 Efficiency and Performance

Computational efficiency of the BEM, which highlights that the matrix solving routine is the slowest step, was covered in section 2.4 on page 70. The DRM requires extra calculations therefore it is slower than an equivalent standard BEM formulation. The approximating functions matrix F must be inverted, in addition to the solution of the final linear matrix equation. These are the two slowest steps in the procedure; the efficiency of matrix solving is addressed in the next section.

It is important to use maximum precision floating point variables especially when dealing with matrix equations where round off error may accumulate and become significant.[124]

Internal points are required, and in the case of convection a substantial number of points are required to approximate the domain integral behaviour. For alternative terms, such as the time derivative from the diffusion equation, significantly fewer points are required.[102,158]

3.4.2 DRM Linear Matrix Solving Routines

The time taken to solve the matrix equation $\mathsf{A}\boldsymbol{x} = \boldsymbol{b}$ for a fully populated unsymmetrical matrix A is of the order $O(e^3)$, where e is the number of elements for an e x e matrix. For the DRM formulation the internal points must be calculated as part of the boundary solution, thus the number of matrix elements is $e = N + I$ where N is the number of boundary elements and I the number of internal points. In contrast to the BEM increasing the number of internal points has a dramatic effect on the speed of the simulation.

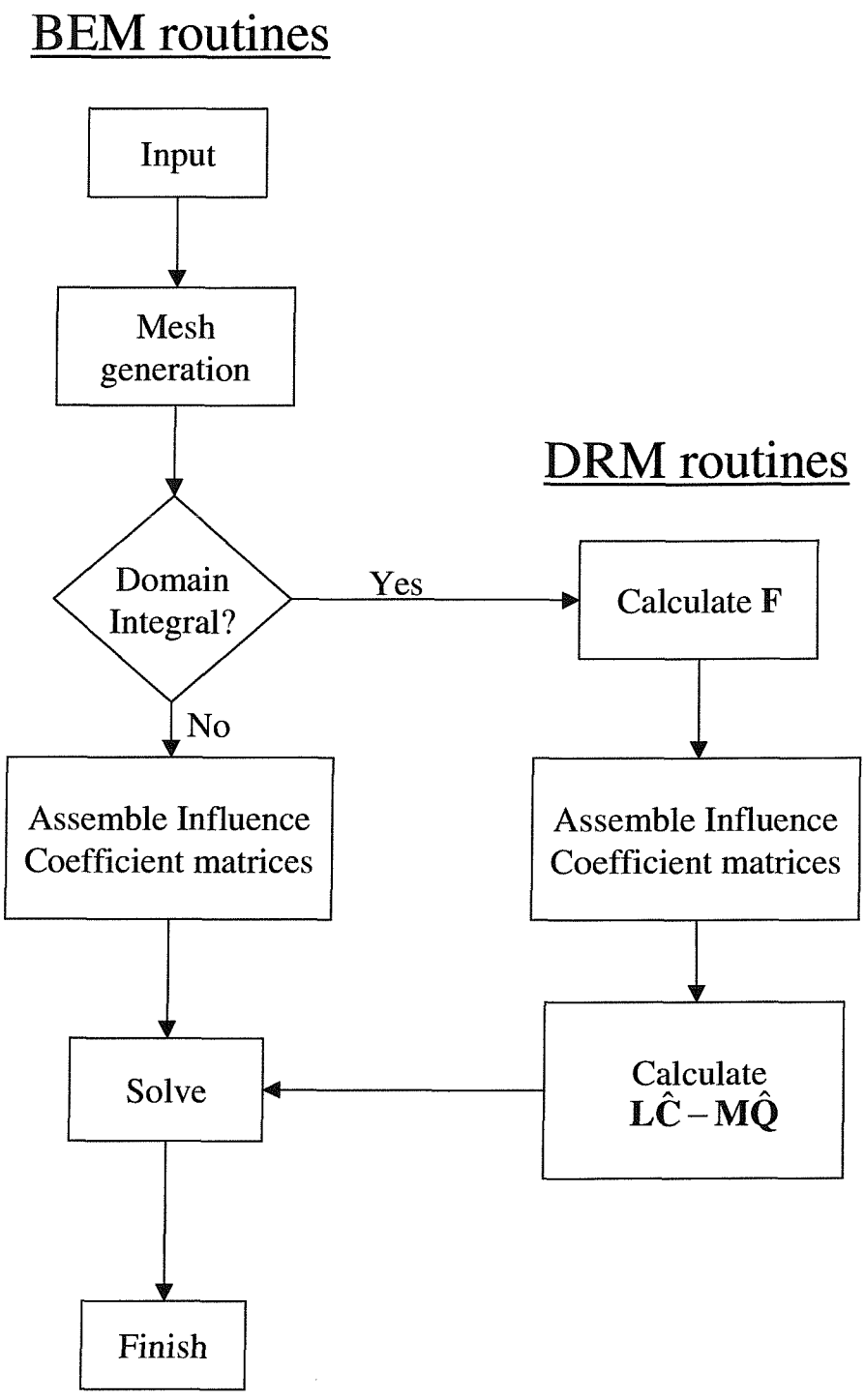

Figure 3.3: Schematic of the DRM program, emphasizing the similarities to the standard BEM program. However, implementation of the DRM procedure is a complex effort.

The DRM leads to two significant matrix calculations with direct relevance to the speed of computation. Firstly the inversion of matrix F. Secondly the calculation of $\mathsf{A}\boldsymbol{x} = \boldsymbol{b}$. Both matrices are fully populated and unsymmetrical.

For this work an LU decomposition routine was used.[143] However, it is possible to implement faster routines,[124] such as Conjugant Gradient Squared[177] and Generalised Minimum Residual.[178] When implemented for the DRM[170] these resulted in simulations an order of magnitude faster than LU decomposition. These methods also required pre-conditioners, which alter the matrix in some way, such as exchanging rows, to improve its solvability and aid convergence.

3.5 Channel Flow Electrodes

A group of electrochemical techniques which has been the focus of considerable efforts towards theoretical understanding in recent years is that of hydrodynamic electrodes, in particular the channel flow electrode. These are especially useful for mechanistic analysis, allowing simple alterations of mass transport parameters by controlling the flow rate.

This class of electrodes originated with the Rotating Disc Electrode (RDE). The technique may be modelled by a one dimensional diffusion-convection equation. The solution flow rate is determined by the rate of rotation of the disc, and parameters such as the rate of mass transport and rate of electron transfer may be obtained.

The maximum flow rate that may be attained is restricted by the requirement to maintain laminar flow, which is assumed in the theoretical treatment.

Alternative hydrodynamic methods, such as tube and channel flow, wall jet and wall pipe, which overcome some of the disadvantages of the rotating disc electrode, have been developed.[171]

A typical channel flow cell is shown in figure 3.4. Channel flow systems often utilize microband electrodes which provide an additional means to control the mass transport regime to be studied by altering the characteristic electrode dimension; in this case the electrode width.

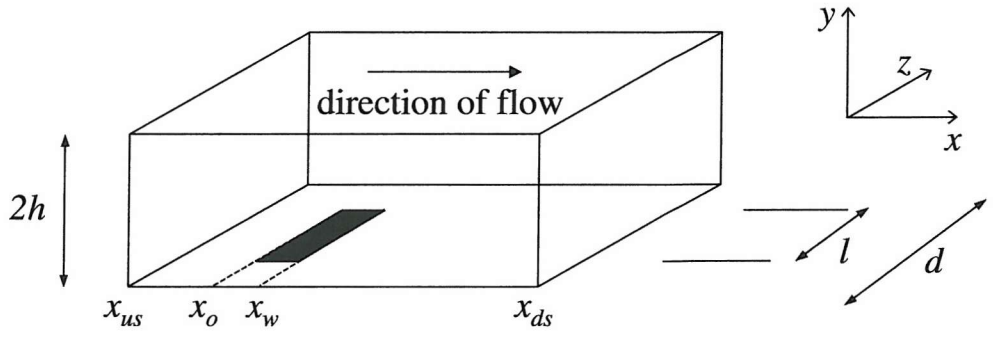

Figure 3.4: A typical channel flow cell.

The cell is designed to eliminate the possibility of convection in the direction perpen-

dicular to the electrode (the yz plane in figure 3.4). Also, by ensuring the electrode length is sufficient to ignore effects from the ends and sufficient separation from the walls of the cell, the mathematical description is reduced to a two dimensional diffusion-convection equation with only one convection term.

Idealised channel flow systems are particularly amenable to finite difference simulation[179,180] due to their rectangular geometry. A considerable number of advances have been made in this area.[72,74,75]

3.5.1 Governing Partial Differential Equation

The steady state diffusion-convection equation with a flow of species in the x direction is[1]

$$-D\frac{\partial^2 C(X,Y)}{\partial X^2} - D\frac{\partial^2 C(X,Y)}{\partial Y^2} + v_x(Y)\frac{\partial C(X,Y)}{\partial X} = 0 \tag{3.31}$$

where C is dimensional concentration, D is the diffusion coefficient and v_x is the solution flow rate.

The flow is assumed to be laminar, thus the flow profile is parabolic in the xy plane, as shown in figure 3.5 on the following page. This is also known as Poiseuille flow, with the flow rate defined by

$$v_x(Y) = v_0\left(1 - \frac{(h-Y)^2}{h^2}\right) \tag{3.32}$$

where $2h$ is the height of the channel and v_0 is the flow rate at the centre of the channel (at $Y = h$).

Dimensionless Form of the Diffusion-Convection Equation

To generalise simulation results the dimensionless form of the diffusion-convection equation is used. The velocity coefficient is normalised with respect to the diffusion coefficient and electrode width. In line with standard procedure in the literature a further dimensionless parameter, the Peclet number is defined. This is a ratio of

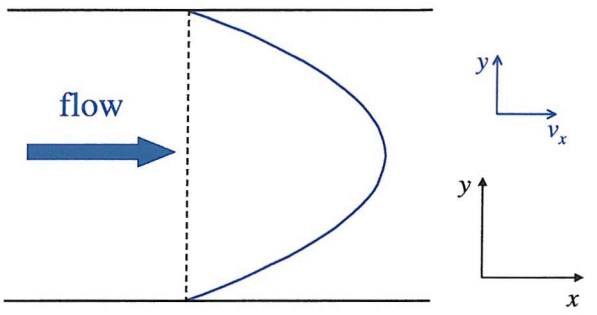

Figure 3.5: The parabolic flow profile of a channel flow technique. The blue lines represent solution flow velocity, v_x. The flow is assumed to be laminar.

the rates of diffusion and convection, which simplifies the dimensionless treatment when approximations are made.

One may define

$$c(x,y) = \frac{C(x,y)}{C^*}, \quad x = \frac{X}{x_w}, \quad y = \frac{Y}{x_w} \quad \nu_x(y) = \frac{v_x(Y)x_w}{D} \tag{3.33}$$

where			
	c	dimensionless concentration	no units
	C	dimensional concentration	mol cm^{-3}
	C^*	bulk concentration	mol cm^{-3}
	x	dimensionless distance along the x axis	no units
	X	actual distance along x axis	cm
	y	dimensionless distance along the y axis	no units
	Y	actual distance along y axis	cm
	x_w	width of the electrode	cm
	ν	dimensionless velocity coefficient	no units
	v_x	velocity coefficient	cm s^{-1}
	D	diffusion coefficient	cm^2 s^{-1}

The dimensionless diffusion-convection equation is therefore

$$-\frac{\partial^2 c}{\partial x^2} - \frac{\partial^2 c}{\partial y^2} + \nu_x(y)\frac{\partial c}{\partial x} = 0 \tag{3.34}$$

Peclet Number The Peclet number, P_s is an indication of the relative importance of diffusion and convection. It is defined as

$$P_s = \frac{3}{2} p_1^2 p_2 \tag{3.35}$$

where p_1, p_2 are defined below.

Following the standard form in the literature,[120] the additional normalising parameters are defined

$$v_f = \frac{4dhv_0}{3} \tag{3.36}$$

and

$$p_1 = \frac{x_w}{h} \quad p_2 = \frac{v_f}{dD} \tag{3.37}$$

where d is the width of the channel.

The dimensionless flow rate parameter may be defined in terms of the Peclet number

$$\nu_x = \frac{1}{2} P_s y(2 - p_1 y) \tag{3.38}$$

When $P_s < 1$ diffusion dominates. At larger values then convection dominates.

Approximations

To simplify the solution of the two dimensional convection diffusion equation, two approximations may be made. The first is often used with two dimensional finite difference simulations, the second allows an analytical solution to be found.

Leveque Approximation Close to the floor of the cell the parabolic flow profile may be approximated by a linear dependence of velocity with y. This assumption is valid when the diffusion layer is small with respect to h; for example using a

microelectrode

$$x_w \ll h \tag{3.39}$$

This is known as the Leveque approximation[181] and leads to

$$v_x \approx \frac{2v_0(Y)Y}{h} \tag{3.40}$$

equation 3.38 becomes

$$\nu_x = \frac{1}{2}P_s y(2 - p_1 y) \approx P_s y \tag{3.41}$$

Dominant Axial Diffusion To simplify further one may assume convection dominates flow in the x direction. In this case equation 3.31 reduces to one dimensional diffusion

$$-D\frac{\partial^2 C}{\partial y^2} + v_x(Y)\frac{\partial C}{\partial x} = 0 \tag{3.42}$$

This approximation is valid with reasonably fast flow rates and large electrodes, where edge effects are negligible. However, it often does not hold for microbands.

Applying both these approximations leads to an analytical solution analogous to the Levich equation[1] for rotating disc electrodes.

Dual Reciprocity Method When the Leveque approximation is made, the velocity coefficient, ν_x, is still a function of y, hence the fundamental solution available for the BEM cannot be used. The DRM is capable of modelling any function $b(x, y, c, t)$, thus it is possible to simulate the channel flow model with and without the Leveque approximation.

3.5.2 Simulation Domain and Boundary Conditions

The simulation domain is shown in figure 3.6.

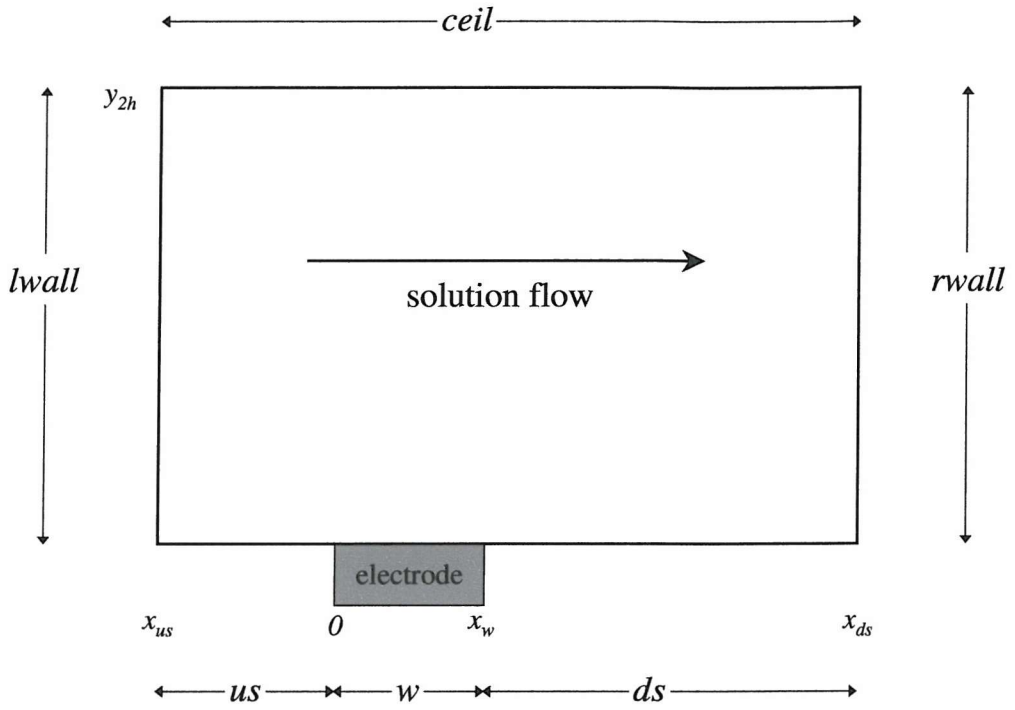

Figure 3.6: The channel microband simulation domain. N_{int} is defined as the number of internal points. These may have a distribution over the *entire domain* or in a *local* region near the electrode. These terms are defined in figure 3.8 on page 159 of section 3.6.3.

The boundary conditions for the channel flow cell are as follows

$$x_{\mathrm{us}} < x < x_0 \qquad y = 0 \qquad \frac{\partial c}{\partial y} = 0 \tag{3.43a}$$

$$x_0 < x < x_{\mathrm{w}} \qquad y = 0 \qquad c = 0 \tag{3.43b}$$

$$x_{\mathrm{w}} < x < x_{\mathrm{ds}} \qquad y = 0 \qquad \frac{\partial c}{\partial y} = 0 \tag{3.43c}$$

$$x = x_{\mathrm{ds}} \qquad 0 < y < 2\mathrm{h} \qquad \frac{\partial c}{\partial x} = 0 \tag{3.43d}$$

$$x_{\mathrm{us}} < x < x_{\mathrm{ds}} \qquad y = 2\mathrm{h} \qquad \frac{\partial c}{\partial y} = 0 \tag{3.43e}$$

$$x = x_{\mathrm{us}} \qquad 0 < y < 2\mathrm{h} \qquad c = 1 \tag{3.43f}$$

Current

The dimensionless form of the current equation used throughtout this chapter is

$$i_{norm} = \int_0^w \left. \frac{\partial c(x,y)}{\partial y} \right|_{y=0} \mathrm{d}x \tag{3.44}$$

where i_{norm} is current and w is the width of the electrode.

3.6 Validation of the Dual Reciprocity Method Applied to Convection

The Dual Reciprocity Method program was validated against a one dimensional heat flow test case[101] with a known analytical solution. This enabled individual concentration and flux values, at both boundary and internal nodes, to be checked.

The method was then applied to a channel flow simulation for which analytical approximations, described in the next section, and previous simulation results[120] are available. Unfortunately, the method proved unstable and boundary discretisations could not be found for which concentration and flux values would converge.

Results for diffusion-dominated flow (low P_s values) using the Leveque approximation are presented. For convection-dominated flow meaningful results could not be found. Possible reasons for the behaviour of the DRM applied to the channel flow technique are also given.

3.6.1 Analytical Approximations

Several analytical approximations have been derived for the channel flow cell, making use of the Leveque approximation to simplify the partial differential equation. Solutions have been found for the low and high flow rate cases, however no single approximation describes the current accurately over the entire range of practical flow rates.

Ackerberg used asymptotic expressions[182] to obtain an approximation valid for $P_s < 1$

$$i = \pi g(P_s)\,(1 - 0.04633 P_s g(P_s)) \tag{3.45}$$

where

$$g(P_s) = \frac{1}{\log\left(\frac{4}{\sqrt{P_s}}\right) + 1.0559} \tag{3.46}$$

and i is the steady state current to the band electrode.

Two expressions for high speed flow have been derived. Newman[183] takes into account both upstream and downstream edge effects to give an expression valid for $P_s > 1$

$$i = 0.8075P_s^{\frac{2}{3}} + 0.7085P_s^{-\frac{1}{6}} - 0.1984P_s^{-\frac{1}{3}} \tag{3.47}$$

Aoki *et al*[184] decided that downstream edge effects were small compared to upstream edge effects, and obtained

$$i = 0.8075P_s^{\frac{2}{3}} + 0.4558P_s^{-\frac{1}{6}} - 0.1984P_s^{-\frac{1}{3}} \tag{3.48}$$

They also gave a correction term for the downstream edge effect.

3.6.2 Semi-Infinite Boundary Distances

The effect of the distance of semi-infinite boundaries is an important indicator of simulation properties. Feedback from boundaries which are positioned too closely to electrodes is a common feature of electrochemical simulation methods, as described in section 2.5.1 on page 76. The behaviour of each boundary must be observed individually to ensure effects are not cancelled out.

The current response as a function of semi-infinite boundary distance for the channel microband domain is shown in figure 3.7. The errors for these results are given in table 3.3 on the following page.

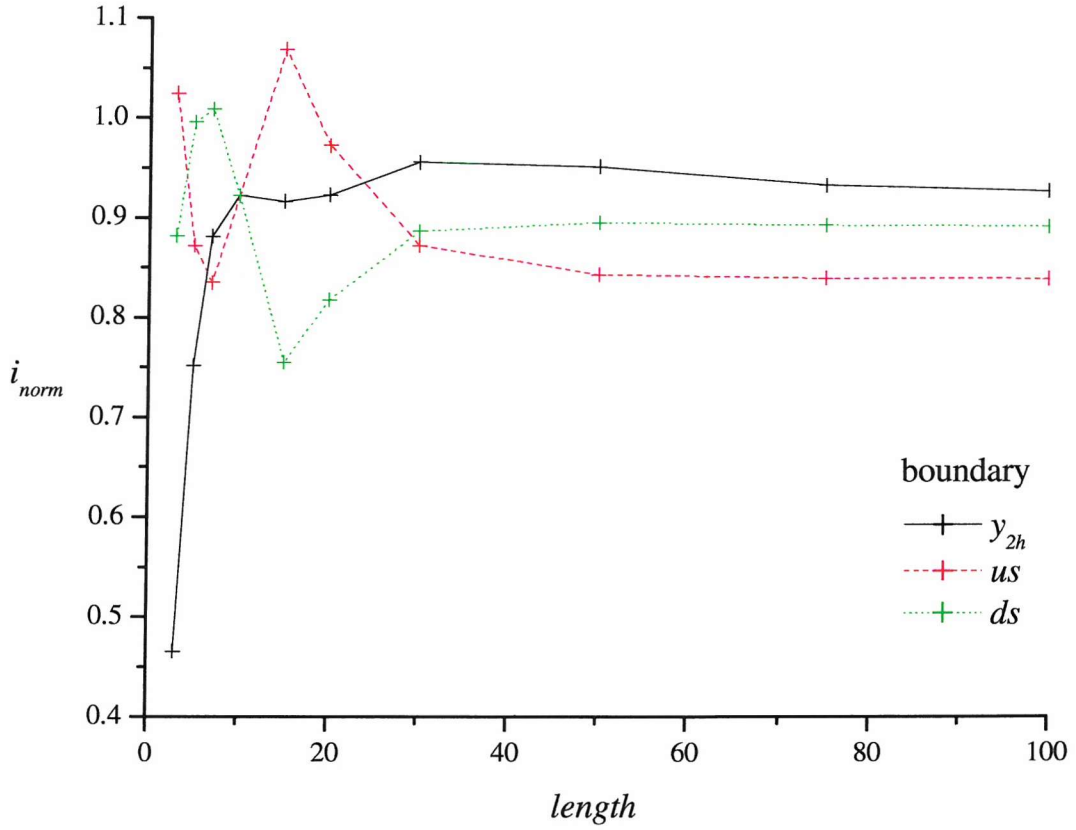

Figure 3.7: The current response when increasing semi-infinite boundary length. The remaining two semi-infinite boundaries were kept at a fixed distance of $10w$. Elements were equally spaced around the entire boundary, therefore as the length of the semi-infinite boundary increases the number of elements increases proportionally. Parameters were $w = 1$, $us = ds = y_{2h} = 10$. Internal points had a *local* distribution (see figure 3.8 on page 159 for definition). $NE_{elec} = 2$, $NE_{us} = NE_{ds} = NE_{lwall} = NE_{rwall} = 20$, $NE_{ceil} = 42$ and $NE_{int} = 9$. $P_s = 0.1$.

length	y_{2h}		
	i_{norm}	% change	Δ% change
3	0.4652	−49.55	–
5	0.7515	−18.50	31.05
7	0.8813	−4.43	14.07
10	0.9221	0.00	4.43
15	0.9161	−0.65	−0.65
20	0.9225	0.04	0.69
30	0.9553	3.60	3.56
50	0.9511	3.15	−0.45
75	0.9327	1.15	−2.00
100	0.9268	0.50	−0.64

a)

length	x_{us}			x_{ds}		
	i_{norm}	% change	Δ% change	i_{norm}	% change	Δ% change
3	1.0245	11.14	–	0.8821	−4.34	–
5	0.872	−5.40	−16.54	0.9963	8.04	12.38
7	0.8352	−9.42	−4.02	1.0089	9.41	1.37
10	0.9221	0.00	9.42	0.9221	0.00	−9.41
15	1.0689	15.92	15.92	0.7551	−18.11	−18.11
20	0.9725	5.47	−10.45	0.8177	−11.32	6.79
30	0.8723	−5.41	−10.87	0.8865	−3.86	7.46
50	0.8429	−8.59	−3.18	0.8951	−2.94	0.92
75	0.8396	−8.95	−0.36	0.8928	−3.18	−0.24
100	0.8390	−9.01	−0.06	0.8915	−3.33	−0.15

b)

Table 3.3: The effect of increasing the semi-infinite boundaries of the channel flow cell. The value for current should converge to a small Δ% change value when a sufficient distance to ensure negligible feedback is reached. However none of these boundaries converge satisfactorily. Parameters used for these results are defined in figure 3.7 on the preceding page.

Upstream x_{us} Severe oscillations are observed initially, followed by dampened oscillations at larger distances. The expected behaviour would be significant positive feedback at small distances, leading to smooth convergence to a current value where the boundary influence is negligible. This kind of current response is an indication

of an inherent problem with the simulation, rather than simply an insufficient semi-infinite boundary distance.

Downstream x_{ds} Increasing distance also shows severe oscillations, whereas negative feedback at small distances would be expected because $Ps < 1$.

Relation between Upstream and Downstream Effects The current responses due to the upstream and downstream boundaries appear to be mirroring one another. The suspected cause of this is the distance between the semi-infinite boundary and internal points, which are fixed above the electrode. The effect of internal points is discussed in section 3.6.3 on the next page.

Height y_{2h} The behaviour of increasing the height of the channel flow cell is closer to the expected response; at small distances negative feedback is observed as would be predicted. However, the curve also exhibits oscillations throughout the distance range simulated. This also implies a flaw within the method's ability to model convection. If the distance between semi-infinite boundary and internal points is causing this instability one might expect the behaviour of the cell height to be linked to upstream and downstream effects, as they are to one another. However, convection occurs only in the x direction, thus the inaccuracy of response due to the y axis boundary may be independent.

Concentration Values Concentration values, both on the boundary and at internal points were also found to oscillate. At times they gave completely erroneous results; values larger than one or less than zero.

In summary, the current response does not converge with increasing semi-infinite boundary distances. Additionally erroneous concentration values were found. This suggests that the DRM is unable to interpolate the convection term of the governing differential equation satisfactorily. The effect of internal points distribution was investigated in detail to clarify the behaviour of the method.

3.6.3 Internal Points

The basis of the treatment of convection is interpolation across the domain using both boundary and internal points. Thus the placement of internal points has the potential to be of significant importance to the accuracy of the Dual Reciprocity Method. At least one point is required for the method to function, however a larger number of points would be expected to increase the accuracy of the interpolation.

There are a number of strategies which may be used to define the position of points.

1) The points may be spread equally across the entire domain
2) They may be distributed randomly
3) A mesh may be positioned locally in the region of the electrode

These meshes may be equally spaced or follow a predicted diffusion field. For the following results the first and third strategies were used, with equally spaced points, as shown in figure 3.8.

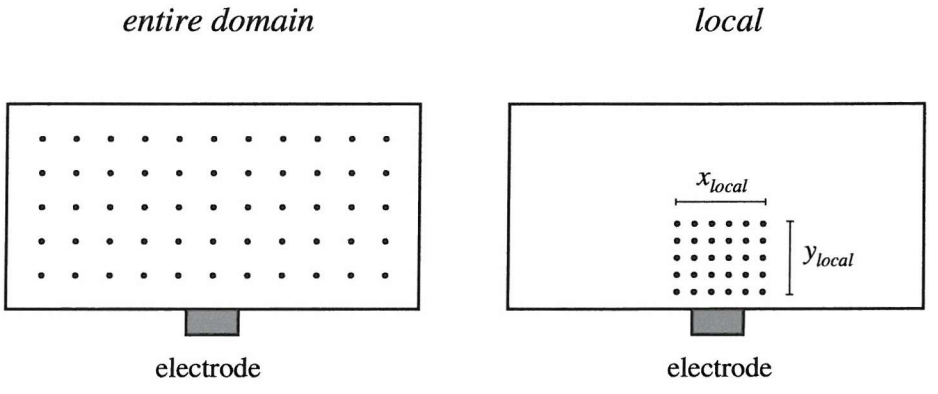

Figure 3.8: The two types of internal point distribution tested. The local mesh distribution routine enabled a variable rectangular mesh, of dimensions x_{local} and y_{local}.

The placement of internal points is an area that has received limited investigation within the DRM field; most authors preferring to distribute them equally across the entire domain.[101,125,164,173]

Number of points As the number of internal points is increased one would expect an increase in accuracy as more points are used for interpolation. The current response should converge. In contrast to the standard BEM, DRM internal points are inherent in the method and as such are incorporated as part of the boundary solution. Thus increasing the number of internal points also increases the time required to calculate boundary values, placing an upper limit on the number of points that may be used.

The effect of increasing the number of internal points, for a mesh distributed over the entire domain and local to the electrode is shown in figure 3.9.

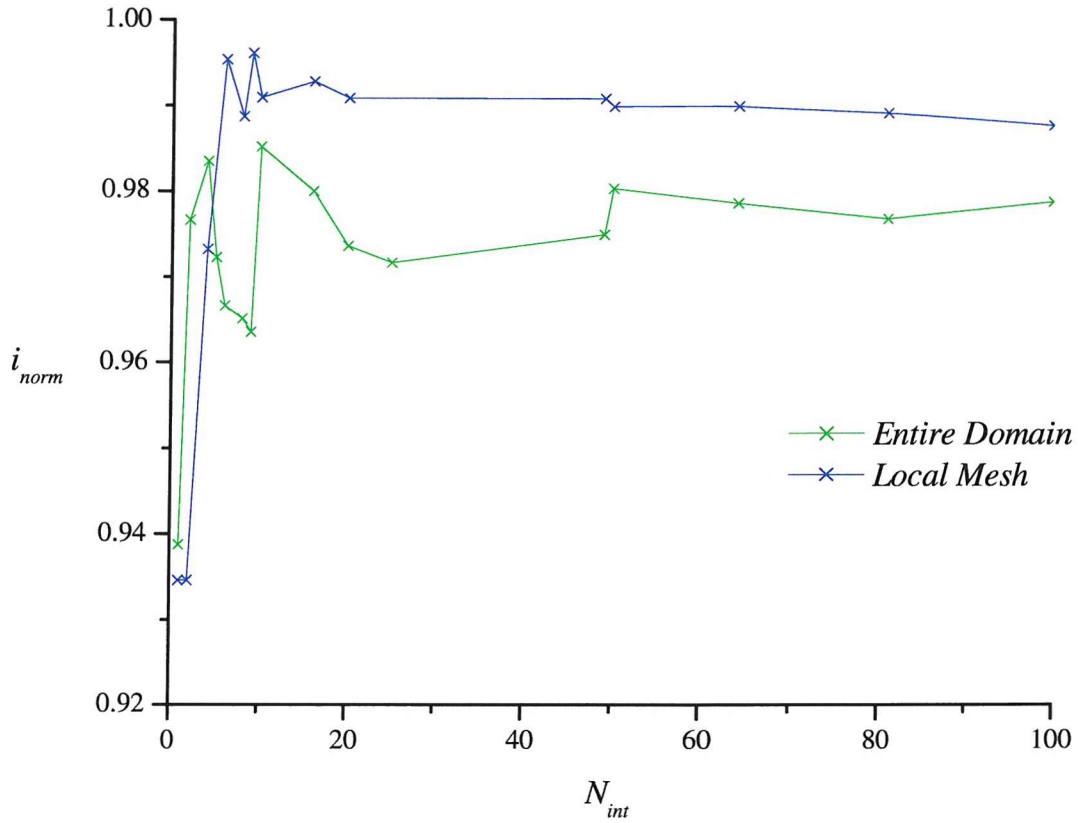

Figure 3.9: The current response produced by increasing the number of internal points, N_{int}. The types of point distribution are shown in figure 3.8 on the page before. Parameters used for these results were $w = 1$, $us = ds = y_{2h} = 10$. $NE_{elec} = 2$, $NE_{us} = NE_{ds} = NE_{lwall} = NE_{rwall} = 20$, $NE_{ceil} = 42$ and $NE_{int} = 9$. $P_s = 0.1$.

The number of points has an enormous influence on current response. Severe oscillations are observed for both types of distribution, with neither converging to a value. These results confirm that the DRM interpolation is inadequate to describe the

convection term in the governing differential equation of the channel flow electrode, even for low flow rates. Increasing the number of internal points, for instance by improving the performance of the program, is unlikely to provide sufficient accuracy as there is no indication of convergence.

Varying *local* Mesh Distribution The local distribution of points was altered by varying the size of the mesh rectangle, table 3.4.

x_{local}	y_{local}	i_{norm}
1	0.5	0.9369
2	1	0.9536
4	2	0.9788
5	2.5	0.9854
6	3	0.9887
7	3.5	0.9895
8	4	0.9884
9	4.5	0.9861
10	5	0.9833

Table 3.4: The effect of varying *local* internal point distribution. This is defined in figure 3.8 on page 159. Simulation parameters used were as described in figure 3.9 on the preceding page.

The size of the local mesh is seen to have a significant effect on current response.

For all internal point distributions tested erroneous concentration and flux values occurred within the domain.

Collectively these results show that it does not appear possible to find an internal point distribution that accurately simulates the convection term in the diffusion-convection equation using the DRM.

3.6.4 The f Approximating Function

The effect of using different approximating functions for interpolation was investigated. The results, in table 3.5 on the next page, show a wide variation of current response, depending on the f function used. All functions result in oscillating currents and erroneous concentration and flux values. Note that using even terms in

radial basis functions (refer to section 3.2.2 on page 134) produces very small changes in the current, which concurs with the behaviour found by Partridge.[173] It is not possible to select an optimum approximating function, considering the inaccuracy of the model.

f function		Mesh Discretisation			
	NE_{elec}	2	2	4	6
	NE_{total}	244	244	488	732
	N_{int}	9	25	25	25
$1+r$	i_{norm}	0.8778	0.8928	0.8695	0.8617
	% error	0.536	2.259	−0.419	−1.307
$1+r+r^2$	i_{norm}	0.8771	0.8942	0.8705	0.8626
	% error	0.456	2.412	−0.305	−1.202
$1+r+r^2+r^3$	i_{norm}	0.0270	0.5842	0.8850	0.8346
	% error	−96.906	−33.096	1.362	−4.412
$1+r^3$	i_{norm}	0.8230	0.8749	0.8494	0.8508
	% error	−5.739	0.198	−2.717	−2.552
r^3	i_{norm}	0.8229	0.8748	0.8526	0.8451
	% error	−5.749	0.198	−2.352	−3.205
$1+r+r^3$	i_{norm}	0.0430	0.5867	0.8843	0.8344
	% error	−95.070	−32.808	1.286	−4.438

Table 3.5: The behaviour of several f approximating functions, for a selection of mesh discretisations. Values are compared to the approximate analytical function of Ackerberg *et al*;[182] for Ps=0.1, i=0.87312. Parameters used were $w = 1$, $us = ds = y_{2h} = 20$. Boundary elements were equal spaced. $P_s = 0.1$.

3.6.5 Parabolic Flow and High Flow Rates

The behaviour of the simulation was also investigated for a parabolic flow profile. As expected only small variations occurred in current response compared to results using the Leveque approximation. However, as values oscillate in exactly the same manner as those obtained with the Leveque approximation, parabolic flow results are omitted.

Similarly, high flow velocities (large P_s values) gave meaningless concentration and flux values and results are not presented.

3.7 Conclusions

A summary is given in the next section of pertinent aspects of the results of the channel flow model and possible explanations for simulation behaviour. The following section discusses the validity and relevance of the general DRM method.

3.7.1 Channel Flow Cell Model

The Dual Reciprocity Method is unable to model the channel flow microband accurately for either low or high flow rates, with or without the Leveque approximation.

The position of the DRM internal points was found to have a significant effect on boundary values. The model suffered from severe instability and erroneous concentration and flux values. Altering the boundary discretisation affects the field point-internal point distance, thus mesh optimisation investigation is not possible due to this instability.

The channel flow electrode attains a steady state due to the influx of material from the bulk solution arriving upstream of the microband. Species generated at the electrode are swept away by convection; thus for a given flow rate a static concentration profile and a steady state current are achieved.

However, at low flow rates diffusion is the dominant mass transfer process. For the generator-collector, diffusion only, microband system in section 2.5.2 of chapter 2, when a bulk concentration semi-infinite boundary condition was used, the electrode pair did not have equal currents when a steady state was imposed. Therefore for the convection system, at a diffusion-dominated flow rate, feedback may occur with the upstream boundary. In this case one would expect the microband current to decrease as the upstream boundary recedes. It was not possible to observe whether this occurred however, due to instability and erroneous results.

The particular solution interpolation was inadequate to describe the convection term, despite testing a variety of radial basis functions. Although not tested for this work, the use of global approximation functions does not appear to increase the accuracy of the DRM for convection systems.[176]

The diffusion-convection partial differential equation is complex to model using numerical methods as the nature of the equation changes depending upon the flow rate. At low flow rates (diffusion dominated flow) the equation is parabolic, at high flow rates (convection dominated flow) the equation becomes hyperbolic.

There are some additional techniques available to improve the behaviour of the DRM applied to convection. Zhang and Zhu[126,185] suggest a Laplace transform of the partial differential equation to obtain an internal domain term that is a function of x, y only. This improves concentration values by an order of magnitude, however, flux values, which are also of importance to electrochemists, are not improved.

Wrobel *et al*[125] split the convection term into a constant velocity component and a variational component; using the fundamental solution for the constant velocity diffusion-convection equation and applying the DRM to the variational part. This has the advantage of transforming at least some of the convection term to a boundary integral. However, they found a domain discretisation was still required for high flow rates.

3.7.2 General Dual Reciprocity Method

The Dual Reciprocity technique enables Boundary Element principles to be applied to a wide variety of partial differential equations, without requiring a specific fundamental solution.

There are a number of approximate particular solutions which have been applied to the method and research continues to prove convergence and find the optimum function for different classes of differential equations.

The DRM, using a variety of radial basis functions, has proven inadequate to model electrochemical diffusion-convection domains accurately. However, this is only one application of the method, from which conclusions cannot be drawn as to the validity of the technique for alternative partial differential equations.

The method has been successfully applied to model the time derivative in the diffusion equation.[102,158,186] Usually a time stepping scheme, for instance Galerkin[19] or Crank-Nicolson,[6] is utilised in conjunction with the DRM. This greatly simpli-

fies mesh generation for complex domains, removing the requirement for internal domain discretisation.

The extension of the DRM for three dimensional domains is comparatively simple, *provided* a suitable approximating function is found. The mesh generation advantages of BEM become especially advantageous for three dimensional systems. However, the majority of research into the properties of approximating functions has been for two dimensional domains. There is no guarantee that for functions that converge in two dimensions the analogous three dimensional version will also converge.

In conclusion, the Dual Reciprocity Method provides a flexible advanced addition to the Boundary Element Method. However, accurate integral domain term interpolation is found for only a proportion of possible partial differential equations; care must be taken to ensure the accuracy of the technique is established for a particular governing differential equation and domain.

Chapter 4

Conclusion: The Future of BEM in Electrochemistry

The Boundary Element Method was described in detail in the first part of chapter 2. In the second part it was applied to various flat and irregular multiple microband geometries. These domains, which contain large numbers of microelectrodes, could not be simulated using domain techniques such as FDM or FEM due to practical considerations; for each electrode there are two boundary singularities, and domain techniques require optimisation for each of these. Thus the computational time required becomes prohibitive.

The Boundary Element Method has proved to be a flexible simulation technique capable of successfully simulating these systems.

An advanced formulation, the Dual Reciprocity Method, showed the potential to model a wider variety of governing partial differential equations. This was implemented and described in chapter 3. It was applied to steady state diffusion-convection systems, however, it proved unstable and inadequate. Subsequently, it has been shown to be successful when applied to time dependent systems.[102] A description of relatively simple alterations to the formulation given in chapter 3 to model these systems, is included in the following section.

The most notable feature of the BEM is the potential to model complex three-dimensional systems. Initial investigations were made in this area and a success-

ful test program developed. The implementation of three dimensional BEM and preliminary results are presented in section 4.2 on page 173.

The majority of practical electrochemistry systems involve more than two species and one or more chemical reactions; in section 4.4 on page 183 incorporation of these factors into the BEM is considered. Finally, the distinguishing features of the BEM which are of particular interest to electrochemists are summarised.

4.1 Time-Dependent Systems

The majority of electrochemical techniques are time dependent, thus the capability to model partial differential equations containing a time derivative is important for numerical methods applied to electrochemistry. To apply the standard Boundary Element Method, as outlined in chapter 2, a suitable weighting function (the fundamental solution) must be found. Additionally, a time integration strategy is required.[187] For simple equations, such as the diffusion equation, it may be possible to derive a fundamental solution;[22] this depends upon the individual governing equation in question. Assuming a fundamental solution is found the standard Boundary Element Method, depending upon the time integration scheme used, may require internal discretisation.

The Dual Reciprocity Method represents a viable alternative, requiring only minor modifications to incorporate a time derivative term. The domain integrals are transferred to the boundary, retaining a boundary-only formulation. The original partial differential equation may also contain additional terms, assuming these can be approximated accurately using the DRM method. However, considering the poor performance of the method applied to convection (see chapter 3), a direct BEM approach, if possible, is preferable.

Research into the behaviour of different f approximating functions is currently ongoing.[173,176] Singh and Kalra[186] have investigated optimal time integration schemes for various domains. Qiu and Fisher[102] have recently applied the DRM to diffusion at microelectrodes.

The DRM procedure is described in detail in chapter 3 and an outline of additional details required for the diffusion equation is given below.

4.1.1 The DRM Applied to the Diffusion Equation

The procedure for time dependent terms is analogous to that described for a convection term in chapter 3, and is outlined below.

The DRM may be used to approximate non-Laplacian terms by posing the governing equation in a suitable form; separating the Laplacian terms. This gives the general

form

$$\frac{\partial^2 c(x,y,t)}{\partial x^2} + \frac{\partial^2 c(x,y,t)}{\partial y^2} = b(x,y,c,t) \tag{3.1}$$

where b is any internal domain term, c is concentration, x, y are cartesian coordinates and t is time.

The diffusion equation, in two dimensions, is

$$\frac{\partial^2 c(x,y,t)}{\partial x^2} + \frac{\partial^2 c(x,y,t)}{\partial y^2} = \frac{\partial c(x,y,t)}{\partial t} \tag{4.1}$$

The generic DRM equation, before application to a specific b term, is given by equation 3.18 in section 3.2.3 on page 136

$$\mathsf{L}\boldsymbol{c} - \mathsf{M}\boldsymbol{q} = \left(\mathsf{L}\hat{\mathsf{C}} - \mathsf{M}\hat{\mathsf{Q}}\right)\boldsymbol{\alpha} \tag{3.18}$$

where
- L, M are influence coefficient matrices
- $\boldsymbol{c}$ is a concentration vector
- $\boldsymbol{q}$ is a flux vector
- $\hat{\mathsf{C}}, \hat{\mathsf{Q}}$ are vectors of particular solution vectors
- $\boldsymbol{\alpha}$ is a vector of initially unknown coefficients

A series of approximating functions is defined for the time derivative term

$$\frac{\partial c(x,y,t)}{\partial t} = \dot{c}(x,y,t) = \sum_{k=1}^{N+L} f_k(x,y)\alpha_k \tag{4.2}$$

where $\dot{c}$ is a time derivative, f are approximating functions and α are initially unknown coefficients.

Using matrix notation equation 4.2 becomes

$$\dot{\boldsymbol{c}} = \mathsf{F}\boldsymbol{\alpha} \tag{4.3}$$

which is substituted into equation 3.18

$$\mathsf{L}\boldsymbol{c} - \mathsf{M}\boldsymbol{q} = \left(\mathsf{L}\hat{\mathsf{C}} - \mathsf{M}\hat{\mathsf{Q}}\right)\mathsf{F}^{-1}\dot{\boldsymbol{c}} \tag{4.4}$$

Defining the term A as follows

$$\mathsf{A} = -\left(\mathsf{L}\hat{\mathsf{C}} - \mathsf{M}\hat{\mathsf{Q}}\right)\mathsf{F}^{-1} \tag{4.5}$$

then equation 4.4 may be rearranged to form

$$\mathsf{A}\dot{\boldsymbol{c}} + \mathsf{L}\boldsymbol{c} = \mathsf{M}\boldsymbol{q} \tag{4.6}$$

Finite Difference Time Approximation A one dimensional finite difference scheme may be applied to approximate the time derivative term. Standard θ notation[186] is used here and is defined as follows

$$c = (1 - \theta_c)\, c^j + \theta_c c^{j+1} \tag{4.7}$$

$$q = (1 - \theta_q)\, q^j + \theta_q q^{j+1} \tag{4.8}$$

where θ is a constant whose value determines the type of finite difference scheme. For example, $\theta = 1/2$ gives the Crank-Nicolson algorithm[6] and $\theta = 2/3$ gives the Galerkin algorithm.[19]

A forward difference is used for the time derivative

$$\frac{\partial c(x, y, t)}{\partial t} = \frac{1}{\Delta t}\left(c^{j+1} - c^j\right) \tag{4.9}$$

When applied to equation 4.6 this gives

$$\frac{\mathsf{A}}{\Delta t}\left(\boldsymbol{c}^{j+1} - \boldsymbol{c}^j\right) + \mathsf{L}\left((1 - \theta_c)\boldsymbol{c}^j + \theta_c \boldsymbol{c}^{j+1}\right) = \mathsf{M}\left((1 - \theta_q)\boldsymbol{q}^j + \theta_q \boldsymbol{q}^{j+1}\right) \tag{4.10}$$

Taking a two-step scheme as an example, where $\theta_c = 0.5$ and $\theta_q = 1$ gives

$$\left(\frac{\mathsf{A}}{\Delta t} + \frac{\mathsf{L}}{2}\right)\boldsymbol{c}^{j+1} - \mathsf{M}\boldsymbol{q}^{j+1} = \left(\frac{\mathsf{A}}{\Delta t} - \frac{\mathsf{L}}{2}\right)\boldsymbol{c}^j \tag{4.11}$$

Summary The DRM applied to transient governing equations has proved successful. However, the approximation of domain terms by an interpolation function (the basis of the DRM technique) is inferior to the exact representation obtained through use of a fundamental solution. Thus, for transient systems, a direct BEM approach is likely to yield more accurate results.

4.2 Three Dimensional Boundary Element Method

The Boundary Element Method formulation may be applied in three dimensional space. The Boundary Integral Equation obtained contains only surface integrals, and is exact within the interior domain. A description of the three dimensional BEM is given below.

The boundary may be discretised using suitable surface elements, also known as primitives; basic element types are given in figure 4.1. Thus domain meshing is greatly simplified when compared to volume discretisation, however, elements must be orientated correctly within three spatial dimensions so mesh generation is more complex than for a two dimensional domain.

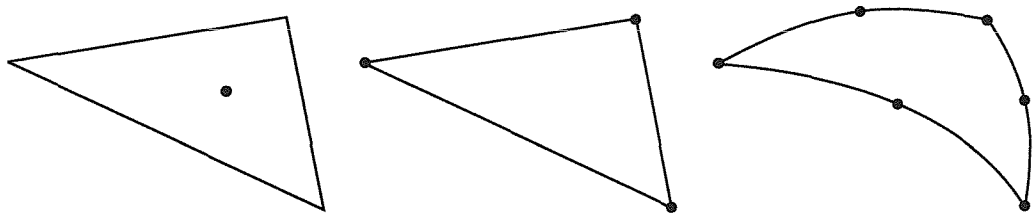

Figure 4.1: Boundary element types for three-dimensional surface discretisation. Concentration and flux variation over the element is a) constant b) linear c) quadratic. The quadratic element shown is curvilinear, using quadratic shape functions.

4.2.1 Three Dimensional BEM Formulation

The formulation of the Boundary Element Method for three dimensions is analogous to the two dimensional procedure, explained in chapter 2. Differences and alternative equations required are described below for the Laplace equation.

The Laplace equation in three dimensions is

$$\frac{\partial^2 c(x,y,z)}{\partial x^2} + \frac{\partial^2 c(x,y,z)}{\partial y^2} + \frac{\partial^2 c(x,y,z)}{\partial z^{2^2}} = 0 \tag{4.12}$$

The Boundary Integral Equation (BIE) is derived by integrating the weighted residual form of the Laplace equation twice. It is identical to equation 2.13 in section 2.2

on page 54, although parameters are now functions of three spatial dimensions

$$dc(\xi_1,\xi_2,\xi_3) + \int_\Gamma c(x,y,z)\frac{\partial W(x,y,z,\xi_1,\xi_2,\xi_3)}{\partial n}\,\mathrm{d}\Gamma = \int_\Gamma \frac{\partial c(x,y,z)}{\partial n} W(x,y,z,\xi_1,\xi_2,\xi_3)\,\mathrm{d}\Gamma \quad (4.13)$$

where	d	is a geometry coefficient
	c	is the concentration at the source point
	Γ	is the domain boundary
	c	is the concentration around the boundary
	W	is the fundamental solution
	n	the element unit outward normal
	ξ_1, ξ_2, ξ_3	are source point coordinates.
	Γ	is a surface integral

This BIE may be discretised in an analogous fashion to section 2.2, using any of the element types described above.

A definition of the fundamental solution and a technique for boundary integration are required to proceed to assembly of the influence coefficient matrices. These are described in the following two sections.

Fundamental Solution

The fundamental solution for the three dimensional Laplace equation[22] is

$$W(x,y,z,\xi_1,\xi_2,\xi_3) = \frac{1}{4\pi r} \quad (4.14)$$

where W is the fundamental solution, ξ are source point coordinates and r is the distance between source and field points;

$$r = \sqrt{(x-\xi_1)^2 + (y-\xi_2)^2 + (z-\xi_3)^2} \quad (4.15)$$

The element outward normal is defined as perpendicular to the element surface, in a direction exterior to the domain. The derivative of the fundamental solution with

respect to the outward normal is

$$q^* = \frac{\partial W}{\partial n} = \frac{p}{4\pi r^3} \tag{4.16}$$

where p is the perpendicular distance from the source point to the plane passing through the field point element. Thus $p = \boldsymbol{r}.\hat{\boldsymbol{n}}$, where $\hat{\boldsymbol{n}}$ is the element unit outward normal.

Boundary Integration

To simplify boundary integration a local coordinate transform is performed which is dependent upon the type of element. Triangular elements with constant field variables are considered here.

The transformation of coordinates requires a parameter known as a Jacobian

$$\mathrm{d}\Gamma = |J|\,\mathrm{d}\eta_1\,\mathrm{d}\eta_2 \tag{4.17}$$

where Γ is the surface boundary, J is the Jacobian and η is the local coordinate system.

For a triangle the Jacobian is equal to twice the area of the triangle.[103]

Applying this transformation to the boundary integrals from equation 4.13, and removing the concentration and flux parameters (which are constant) from their respective integrals gives

$$\int_{\Gamma j} W\,\mathrm{d}\Gamma = |J| \int_0^1 \left(\int_0^{1-\eta_2} W(\eta)\,\mathrm{d}\eta_1 \right) \mathrm{d}\eta_2 \tag{4.18}$$

$$\int_{\Gamma j} q^*\,\mathrm{d}\Gamma = |J| \int_0^1 \left(\int_0^{1-\eta_2} q^*(\eta)\,\mathrm{d}\eta_1 \right) \mathrm{d}\eta_2 \tag{4.19}$$

The element unit normal, $\hat{n}$, required for calculation of $q^* = \partial W/\partial \hat{n}$ may be calculated from the cross-product of two sides of the element, which are vectors in three dimensional space.

Non-Singular Integration ($s \neq j$) When the boundary integrals are not singular, numerical integration may be used; in the case of constant triangular elements a suitable scheme is Hammer's quadrature.[188] This is defined as

$$\int_0^1 \left(\int_0^{1-\eta_2} f(\eta_1, \eta_2, \eta_3)\, \mathrm{d}\eta_1 \right) \mathrm{d}\eta_2 \approx \sum_{h=1}^{NI} f(\eta_1^h, \eta_2^h, \eta_3^h)\omega_h \tag{4.20}$$

where f is an arbitrary function, h is an integer counter, ω are quadrature weighting factors and NI are the number of integration points.

Specific coordinates and weighting factors may be found in the literature.[22,188]

The notation of section 2.2.4 on page 63 is used to define influence coefficient matrices. Their components, applying Hammer's quadrature are

$$L_{sj} = \frac{A_j p_{sj}}{2\pi} \sum_{h=1}^{NI} \frac{1}{r_{sh}^3} \omega_h \tag{4.21}$$

$$M_{sj} = \frac{A_j}{2\pi} \sum_{h=1}^{NI} \frac{1}{r_{sh}} \omega_h \tag{4.22}$$

where A_j is the area of triangular element j, p is the perpendicular distance from the source point, s, to the plane passing through element j and other terms are defined above.

Singular Integration ($s = j$) The two boundary integrals are considered separately: The derivative of the fundamental solution is equal to zero, leaving only the contribution of the geometry coefficient, d. This is equal to a half because the element is smooth; L_{ss} (see *'The Geometry Coefficient'* paragraph in section 2.2 of chapter 2). For integration of M_{ss} an analytical solution may be derived using polar coordinates.[22]

The assembled influence coefficient matrices are of identical size to those obtained with two dimensional elements. After application of boundary conditions, they may be solved in the same way with standard matrix solvers. As this is the slowest step in the BEM procedure, the three dimensional BEM is as efficient as a two dimensional version with the same number of elements.

To solve for concentration and flux values at internal points, after the boundary solution is known, an analogous procedure to section 2.2.6 on page 64 may be used.

4.2.2 Results

The results presented here validate the three dimensional BEM using a simple planar diffusion test case. Constant elements were used and a typical discretisation is shown in figure 4.2.

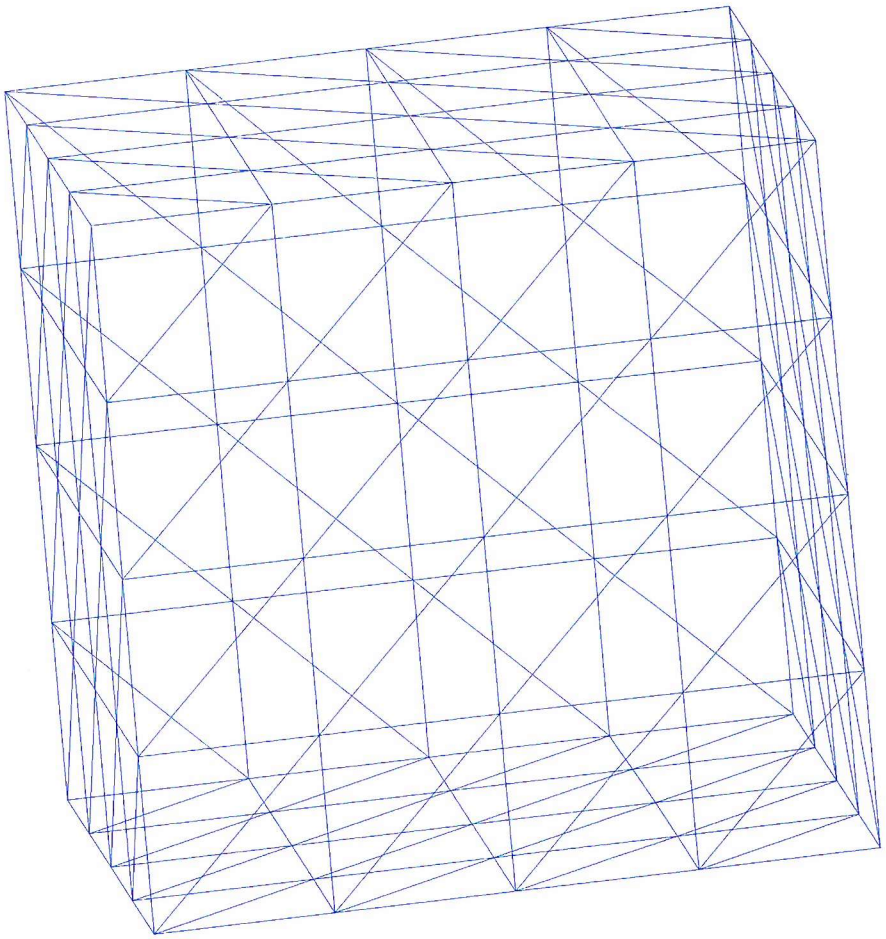

Figure 4.2: A typical mesh discretisation for the planar diffusion test case. The surface is divided into equal size triangular elements.

It is important that boundary elements are defined in a consistent manner to ensure

that element normals are correctly aligned. For the planar diffusion case outward element normals and boundary conditions are shown in figure 4.3. For constant element types field variables may be discontinuous in adjoining elements, thus elements may be defined in any order and are unconnected.

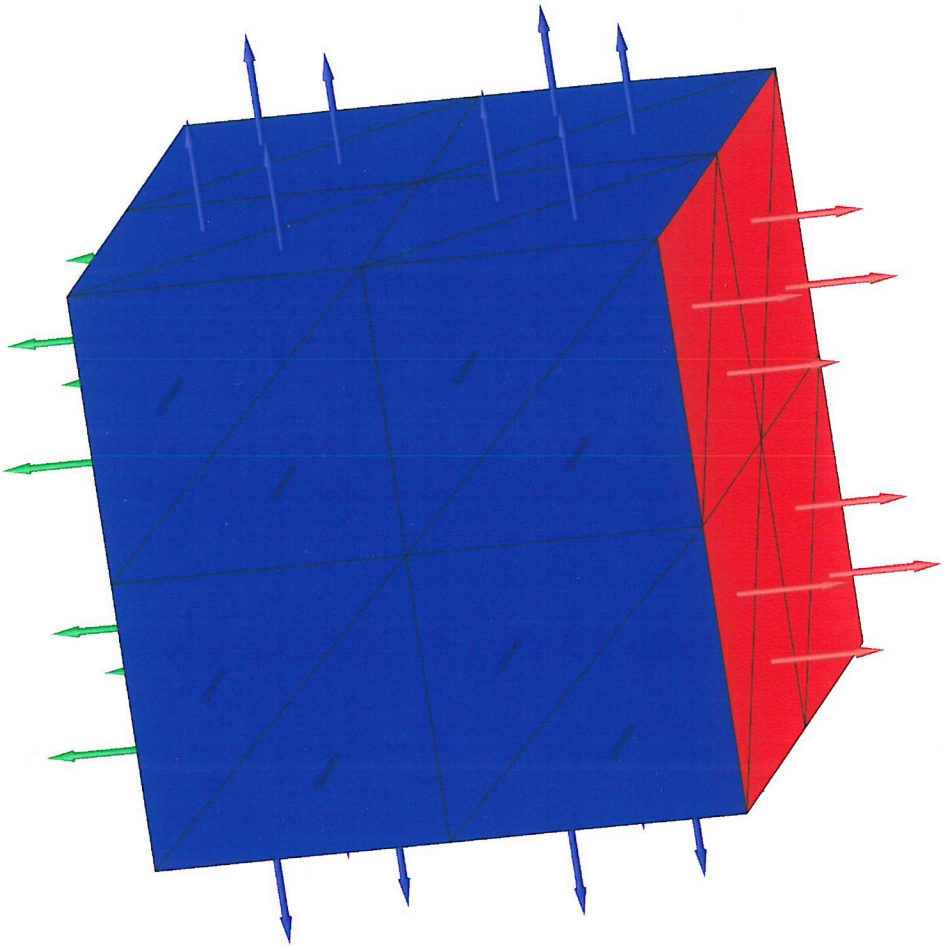

Figure 4.3: Simple discretisation of the cube domain used for the planar diffusion test case. The direction of element outward normals are depicted by arrows, which originate from the element centroid. The colours show boundary conditions; blue is $q = 0$, red is $c = 1$ and green is $c = 0$.

The concentration and flux values for nodes covering two faces of the cube are evaluated for a discretisation of 8 triangular elements per face; a total of 48 elements. The nodal coordinates are defined in table 4.1, and table 4.2 on page 180 shows BEM results and error analysis.

The accuracy of the results is remarkably good considering the sparsity of the mesh

Node	Centroid		
n	x	y	z
9	0.3333	0.0000	0.1667
10	0.1667	0.0000	0.3333
11	0.8333	0.0000	0.1667
12	0.6667	0.0000	0.3333
13	0.3333	0.0000	0.6667
14	0.1667	0.0000	0.8333
15	0.8333	0.0000	0.6667
16	0.6667	0.0000	0.8333
17	1.0000	0.3333	0.1667
18	1.0000	0.1667	0.3333
19	1.0000	0.8333	0.1667
20	1.0000	0.6667	0.3333
21	1.0000	0.3333	0.6667
22	1.0000	0.1667	0.8333
23	1.0000	0.8333	0.6667
24	1.0000	0.6667	0.8333

Table 4.1: The coordinates of the centroids of the triangles covering two faces of the cube modelled. These are shown in figure 4.3 on the preceding page

discretisation used. Note the error of concentration values are an order of magnitude better than corresponding flux values. Preliminary results showed convergence with increasing number of elements. Unfortunately, the three dimensional BEM simulation developed could not be applied to more complex domains due to study time constraints.

The BEM was applied to three dimensional SECM simulations by other research groups[100,189] during the course of this work. There is a huge variety of possibilities for application of a three-dimensional simulation in electrochemistry. BEM is ideally placed as a simulation method which has the capability to solve complex geometric domains.

However, incorporating reaction mechanisms is an involved task; this is discussed in section 4.4.1 on page 183.

Node	Analytical		BEM		Error /%	
n	c	q	c	q	c	q
9	0.3333	0.0000	0.3109	0.0000	6.72	–
10	0.1667	0.0000	0.1557	0.0000	6.59	–
11	0.8333	0.0000	0.8203	0.0000	1.56	–
12	0.6667	0.0000	0.6706	0.0000	−0.59	–
13	0.3333	0.0000	0.3323	0.0000	0.31	–
14	0.1667	0.0000	0.1751	0.0000	−5.01	–
15	0.8333	0.0000	0.8439	0.0000	−1.27	–
16	0.6667	0.0000	0.6879	0.0000	−3.18	–
17	1.0000	1.0000	1.0000	1.0913	–	−9.13
18	1.0000	1.0000	1.0000	1.1594	–	−15.94
19	1.0000	1.0000	1.0000	1.2366	–	−23.66
20	1.0000	1.0000	1.0000	0.9563	–	4.37
21	1.0000	1.0000	1.0000	0.9563	–	4.37
22	1.0000	1.0000	1.0000	1.2366	–	−23.66
23	1.0000	1.0000	1.0000	1.1594	–	−15.94
24	1.0000	1.0000	1.0000	1.0913	–	−9.13

Table 4.2: The concentration and flux values at triangle element centroids. Node coordinates are given in table 4.1 on the preceding page.

4.3 Computational Aspects of Numerical Methods

The implementation of numerical methods in electrochemical simulation is becoming increasingly involved. Therefore, the choice of programming paradigm is an important consideration. Additionally, the performance of algorithms is often a factor. The programming and computational aspects of the implementation of the Boundary Element Method are discussed in this section.

The use of modern programming techniques enable a program to be designed which is flexible and extensible. The advantages of object-oriented design, regression testing and format independent data are outlined below.

Object-Oriented Design The use of an object-oriented language,[137] such as C++[140] or Java,[142] encourages good program design; for example, separating interface and implementation. This allows alterations to be made to specific parts of a program, without interfering with the rest of the program. For instance, a Gaussian integration routine could be re-implemented as an adaptive routine completely independently from matrix formation. Additionally, some parts of the program, such as mesh generation, are simplified through the use of objects and class library resources.[141]

Testing Comprehensive testing increases confidence in results, in addition to reducing time spent debugging. There are two types of testing relevant to a BEM program such as described in this thesis: Firstly, functional tests; for example, simulation of a simple model with a known analytical solution. Secondly, at a lower level, unit tests; these verify that each individual method* behaves as expected. Automating these tests will save a significant amount of time. A variety of frameworks to automate testing, such as xUnit,[190] are available for several languages.

eXtensible Markup Language (XML) The use of XML[191] as a data format removes the problem of adhering to specific formatting conventions, which may

*The term *method* is used in the context of object-oriented languages. For the purposes of this discussion it may be thought of as analogous to a function or sub-routine.

require alteration as the program develops. Additionally, this simplifies importing files for use with data analysis software.

The Boundary Element Method program may be split into two primary components. Firstly, the mesh input data; either input directly or obtained from a mesh generation routine. Secondly, the core simulation; boundary integration, applying boundary conditions and reordering the matrices, and solving to obtain unknown values. Internal points, if required, are also calculated during this stage.

Mesh Generation The generation of specific boundary meshes, including boundary conditions, is a broad and varied topic, and a current area of research.[24] The time taken to calculate mesh generation is negligible compared to the core simulation, thus ease of use and flexibility is of greater importance than performance.

Core Simulation The most important consideration for the core simulation is optimal performance. Assuming a reasonably large number of boundary elements are simulated, the matrix solving routine is the slowest step. Several optimised routines are available in the literature.[124,143]

Due to the significant amount of effort involved in implementing a Boundary Element Method program, it would be advantageous if the program were accessible to electrochemists without requiring detailed knowledge of implementation of the technique. This is possible, to some degree, through the use of a clearly documented data format which allows direct input of boundary data. However, as mentioned in the previous paragraph, mesh generation is often an involved task. Thus a simplified generation routine is desirable. For example, the user defines boundary sections and coordinates, such as the ends of an electrode, and the discretisation of individual elements is then automatic. This allows easier convergence testing of various parameters.

4.4 The Boundary Element Method in Electrochemistry

The electrochemical technique simulated throughout this thesis was a diffusion controlled potential step, for a single redox reaction. This is the most common model in electrochemical simulation when considering complex geometrical domains. The electrochemical mechanism and experimental technique are kept simple, in order to investigate the behaviour of a particular numerical method, when altering the geometric features.

The behaviour of the Boundary Element Method for several different geometries was described in this and the preceding chapters. The method proved successful and flexible for modelling a range of complex geometries.

For a numerical method to be of relevance to a broad spectrum of the electrochemistry field, it must possess the ability to model a variety of electrochemical mechanisms and practical techniques. In the following sections the potential of the Boundary Element Method to model these considerations is addressed.

4.4.1 Electrochemical Mechanisms

A system involving several chemical species is described by a set of partial differential equations consisting of one equation for each species. A description of types of governing partial differential equations, and the basic terminology used to describe electrochemical mechanisms was covered in section 1.2.4 on page 14. Multiple equations which are coupled may be incorporated in the BEM in two ways. Firstly, a sequential solution; an approximate value is initially substituted for the first equation unknown and each equation solved sequentially using the previous result. Iteration is performed until a preset tolerance achieved. Secondly, using a method known as the Matrix of Fundamental Solutions (MFS); a fundamental solution is derived for each equation, forming a fundamental solution matrix which couples the equations. This method is only applicable to linear equations.[103] The two types of reactions common in electrochemical systems are now discussed.

Homogeneous Reactions These lead to extra terms of the form $\pm kc(x_i)$ in the governing equations. A fundamental solution may be derived which incorporates such a chemical term, however, the set of equations describing the system are usually coupled; to account for sets of coupled equations with BEM a method such as MFS must be used. Second-order reactions lead to non-linear partial differential equations. These may be modelled using quasi-linearisation or using a transformation and iterative solution.[103]

Heterogeneous Reactions Reactions on the surface of the electrode, for example electron transfer, are described by suitable boundary conditions along the electrode. Dirichlet and Neumann conditions have been described in chapter 1, boundary conditions of a third kind involving a concentration and flux, known as a Robin boundary condition, are of the form $\partial c/\partial n = f(c) + k$. These may easily be incorporated in the BEM formulation in an analogous manner to the former two conditions.

4.4.2 Electrochemical Techniques

There are a wide variety of electrochemical techniques for which an analytical solution does not exist, and a numerical solution is required. The application of the BEM to two common techniques is discussed below. Hydrodynamic systems were considered in chapter 3 on page 130.

Potentiostatic Control Simulation of the diffusion limited chronoamperometric potential step has been described in detail; the Boundary Element Method has been applied to simulate the steady state attained, and additional alterations for the transient case outlined. To model techniques which utilise other potential waveforms, for example cyclic voltammetry (CV), the boundary condition at the electrode is calculated according to the specific system under consideration. For instance, a reversible CV may be modelled using the Nernst equation to relate the ratio of concentrations on electrode surface to the potential at a particular moment in time. Finite Difference Methods use a conservation of flux property to obtain the surface

concentration in terms of adjacent concentrations on the finite difference mesh.[6] Thus, this technique is not applicable to the BEM.

Galvanostatic Control The current through an electrode is set, usually held constant, and the resulting potential observed. The flux at the electrode surface may be deduced from the current applied. For the BEM a Neumann boundary condition is thus prescribed along the electrode surface.

4.4.3 Distinguishing Features of the Boundary Element Method

In summary, electrochemical simulation techniques developed before the present period of study, mostly based on finite difference, proved insufficient to model complex electrochemical domains. Thus alternative numerical methods developed in related fields were investigated. The Boundary Element Method was shown to be a viable alternative numerical method for specific electrochemical applications. A comparison of BEM and FEM with finite difference was presented in chapter 1 on page 7. The former two methods exhibited potential benefit for electrochemical simulations.

BEM or FEM? The numerical method selected depends upon the particular electrochemical system under consideration. For three dimensional domains, and two dimensional systems with many boundary singularities, the BEM requires less complex meshing and offers possible performance advantages. However, incorporation of multiple species is currently a significant limitation; these aspects are discussed in detail below. For two dimensional domains FEM can model a variety of electrochemical mechanisms and practical techniques. Advanced automatic mesh generation allows optimisation for boundary singularities and complex shapes.

The Boundary Element Method possesses several properties of interest to electrochemists. Three of these, of a particular importance for electrochemical simulation are discussed below. For each a description of the practical consequence of the property is given, followed by an explanation of the origin of the property.

Less Complex Meshing

Only the domain boundary is described using a mesh of simple elements. No elements or points are required in the domain interior.

The use of the inverse form and a suitable weighting function (the fundamental solution) produces a formulation containing only boundary integrals. The formulation is exact in the domain interior.

Accurate Simulation of Boundary Singularities

Boundary singularities are often described accurately without mesh optimisation. When optimisation is required, the process is relatively easy due to less complex meshing, described above, and the fact that globally continuous mesh spacing is not required.

The Laplacian operator is transferred to the weighting function, thus the dependent variable (concentration) is not required to be continuous between elements. Boundary singularities are often discontinuities in the concentration gradient, and therefore may be accurately described.

Infinite Domains and Multiple Regions

An infinite domain may be described simply by discretising the boundary of the object in question; the domain is thus external to this boundary. The element outward normal must be defined in the correct direction.

The infinite boundary is incorporated in the BEM formulation. By ensuring that certain regularity conditions[22] are fulfilled these extra terms cancel out. The boundary conditions at infinity are usually $c = 0$ and $q = 0$, however, non-zero values may also be incorporated in the formulation.[22]

In an infinite domain, multiple boundary regions may be modelled. For constant elements this is achieved simply by ensuring each region is closed when the mesh is defined.

Field variables may be discontinuous between constant elements, thus by defining each end point of the element and ensuring the boundary is closed, data connecting elements is not required and multiple regions may be defined.

Present Limitations

The Boundary Element Method shows significant potential for application to electrochemical simulation. However, the incorporation of multiple species, described in section 4.4.1, has received limited attention within the engineering field.[103] This is of particular importance for electrochemical simulation; the ability to model multiple species and various mechanisms are likely to be the most challenging future developments of the BEM in electrochemistry.

Appendix A

The Formulation of Weighted Residual Numerical Methods

A.1 Numerical Methods

The majority of physical problems expressed as differential equations can only be solved in an approximate manner. The most widely known techniques are Finite Difference (FDM) and Finite Element Method (FEM). The Finite Difference technique defines a series of nodes at which the discrete version of the differential equation is satisfied. For the Finite Element Method the differential equation, or rather its inner product formulation, is satisfied in an average sense over an element. These two techniques discretise the interior domain in addition to the boundaries of the region under consideration. The third technique considered here, the Boundary Element Method (BEM), satisfies the differential equation exactly over the interior domain, through use of the inverse form of the partial differential equation. Thus discretisation of the boundary only is required.

The three techniques are closely related if one focuses on the approximation involved.

This appendix relates the formulation of each of the three approaches in detail through the Method of Weighted Residuals (MWR). The discussion is initiated by defining an approximate solution and the properties of these types of function. We

proceed by stating the Weighted Residual, a technique used to distribute the error arising from the use of an approximate solution. A particular type of MWR is the collocation method, which is utilised for all three methods considered here. A simple form of the FDM may be derived as a special type of collocation method, although it is more often derived directly. The FEM and BEM methods may be derived through either one or two integrations of the MWR equation respectively.

The aim of this appendix is to emphasise the relation between the formulation of the three methods. Details of implementation are not considered.

A.2 Notation

To simplify the presentation of formulae the following notation is defined.

The Laplacian operator, $\mathcal{L}$,

$$\text{1D} \qquad \mathcal{L}() = \frac{\partial^2}{\partial x^2} \tag{A.1a}$$

$$\text{2D} \qquad \mathcal{L}() = \frac{\partial^2}{\partial x^2} + \frac{\partial^2}{\partial y^2} \tag{A.1b}$$

$$\text{3D} \qquad \mathcal{L}() = \frac{\partial^2}{\partial x^2} + \frac{\partial^2}{\partial y^2} + \frac{\partial^2}{\partial z^2} \tag{A.1c}$$

Einstein's summation of indices. The subscript, i, is the number of dimensions.

$$i \qquad x_i \qquad \frac{\partial}{\partial x_i}$$

$$1 \qquad x \qquad \frac{\partial}{\partial x} \tag{A.2a}$$

$$2 \qquad x + y \qquad \frac{\partial}{\partial x} + \frac{\partial}{\partial y} \tag{A.2b}$$

$$3 \qquad x + y + z \qquad \frac{\partial}{\partial x} + \frac{\partial}{\partial y} + \frac{\partial}{\partial z} \tag{A.2c}$$

A.3 Approximate Solutions

The following set of equations are defined

$$\mathcal{L}(c_0) = 0 \qquad \text{on} \quad \Omega \tag{A.3}$$

where $\mathcal{L}$ is the Laplacian operator, Ω is the domain under consideration, with boundary conditions

$$\text{Dirichlet} \qquad c_0 = d \qquad \text{on} \quad \Gamma_1 \tag{A.4}$$

$$\text{Neumann} \qquad q_0 = n \qquad \text{on} \quad \Gamma_2 \tag{A.5}$$

c_0 represents the *exact* solution of the problem which is usually impossible to find. q is a derivative of the dependent variable on the boundary; for instance, for one dimension $q = d/dx$, for two dimensions $q = \partial/\partial n$ where n is the outward normal to the boundary.

The function c_0 can be approximated by a set of functions $\phi_k(x)$ such that

$$c_0 \approx c = \sum_{k=1}^{n} \alpha_k \phi_k + \alpha_0 \tag{A.6}$$

α_k are undetermined parameters and ϕ_k are linearly independent functions taken from a complete sequence of functions (these terms are defined in the next section) such as

$$\phi_1(x_i), \phi_2(x_i), \ldots, \phi_n(x_i) \tag{A.7}$$

x_i represents the spatial coordinates in the Ω domain. These functions are usually chosen to satisfy certain given conditions relating to the boundary conditions and the degree of continuity (see section A.4.3 on page 195). They are known as basis functions or shape functions.

A.3.1 Linear Independence and Completeness

A sequence of functions such as the ones defined in equation A.7 is said to be linearly independent if $\alpha_1\phi_1 + \alpha_2\phi_2 + \cdots + \alpha_n\phi_n = 0$ is true only when all α_i are zero.

A sequence of linearly independent functions is said to be complete if a number of terms, n, and a corresponding set of constants, α_k, may be found for which the difference between an arbitrary function c_0 and its approximation can be made as small as one requires. This may be expressed

$$\left\{\int (c_0 - c)^2\, dx\right\}^{1/2} \leq \beta \tag{A.8}$$

where β is a small positive quantity.

A.4 Method of Weighted Residuals

Substituting an approximating function for c_0 into equation A.3 gives a Residual or error function R such that

$$R = \mathcal{L}(c) \neq 0 \tag{A.9}$$

If the function c does not satisfy all the boundary conditions one may define two additional residual functions, one for each boundary type

$$R_1 = c - \bar{c} \neq 0 \qquad \text{on} \quad \Gamma_1 \tag{A.10}$$

$$R_2 = q - \bar{q} \neq 0 \qquad \text{on} \quad \Gamma_2 \tag{A.11}$$

where $\Gamma_1 + \Gamma_2 = \Gamma$, $\bar{c}$ and $\bar{q}$ are known concentration and flux boundary values respectively.

The aim is to make errors as small as possible over the domain and on the boundary. These errors will be forced to be zero in an average sense. To achieve this errors will be distributed; and the way in which this is done produces different types of approximate methods.

We now define another set of linearly independent functions Ψ_k such as

$$\psi_1(x_i),\psi_2(x_i),\psi_3(x_i),\ldots,\psi_k(x_i) \tag{A.12}$$

One can now define a set of arbitrary coefficients β_k which allow us to write the set ψ_k in a compact form as a function w;

$$w = \beta_1\psi_1 + \beta_2\psi_2 + \beta_3\psi_3 + \cdots \tag{A.13}$$

Assuming for simplicity that c identically satisfies all the boundary conditions of the problem (i.e. $R_1 = R_2 \equiv 0$), one can distribute the error R in Ω by multiplying it by a weighting function w and integrating over the domain.

$$\int_\Omega Rw \, \mathrm{d}\Omega = 0 \tag{A.14}$$

This ensures the error R is distributed with the functions in w. This equation (an inner product) may be written in compact form as

$$\langle R, w\rangle \equiv \int_\Omega Rw \, \mathrm{d}\Omega \tag{A.15}$$

A.4.1 The Collocation Method

Instead of satisfying the equations in an average form we try to satisfy them at a series of chosen points.

Defining an approximating function

$$c = \sum_{k=1}^{n} \alpha_k\phi_k \tag{A.16}$$

In principle the number of α_k has to be the same as the number of collocation points chosen. We have a residual function, equation A.9, which must be satisfied at n points in the domain Ω. One can express this condition in a weighted residual form by defining the ψ_i functions as Dirac delta functions. The collocation method

at a series of points i can now be represented by equation A.14

$$\int_{\Omega} Rw \, d\Omega = 0 \tag{A.14}$$

where the weighting function

$$w = \beta_1\delta_1 + \beta_2\delta_2 + \beta_3\delta_3 + \cdots + \beta_k\delta_k \tag{A.17}$$

δ_i represents the Dirac delta functions at the collocation points.

Relation to the Finite Difference Method

A special type of collocation method produces the finite difference method. Consider a region around the node i under consideration. One can propose a local approximating function over each region as follows:

$$c = c_{k-1}\phi_1 + c_k\phi_2 + c_{k+1}\phi_3 \tag{A.18}$$

c_k are the values of the function at the nodes of the finite difference grid. The functions ϕ_k are quadratic functions, such that referring to the dimensionless system of coordinates η one can write

$$\phi_1 = \frac{1}{2}\eta(\eta - 1) \tag{A.19}$$

$$\phi_2 = (1 - \eta)(1 + \eta) \tag{A.20}$$

$$\phi_3 = \frac{1}{2}\eta(1 + \eta) \tag{A.21}$$

Differentiating equation A.18 twice for the one dimensional Laplace equation, taking into consideration the above shape functions, and collocating at k gives

$$R_k = \frac{d^2c}{dx^2} = \frac{1}{l^2}(c_{k-1} - 2c_k + c_{k+1}) = 0 \tag{A.22}$$

known as the central finite difference expression.

A.4.2 Galerkin's Method

Galerkin's Method is a particular weighted residual method for which the weighting functions belong to the same set as the approximating functions.

As the same functions are used for c and w and the β's are arbitrary it is common to write the w function as a variation of c, i.e.

$$w = \delta c = \delta\alpha_1\phi_1 + \delta\alpha_2\phi_2 + \delta\alpha_3\phi_3 + \cdots \tag{A.23}$$

where $\delta\alpha_k \equiv \beta_k$.

The property of having the same functions for the weighting and approximating functions is important in practice as it produces symmetrical coefficients in many cases. Most finite element models are based on Galerkin type techniques.

A.4.3 Properties of Approximating Functions and Weighting Functions

The approximating and weighting functions chosen must possess two properties: Firstly, as previously stated, they must be linearly independent from a complete set. Secondly, they must have a sufficient order of continuity.

Consider the 1-D Laplace equation, which is second order

$$\mathcal{L}(c) = \frac{d^2c}{dx^2} = 0 \qquad \text{for} \quad 0 < x < 1 \tag{A.24}$$

and its weighted residual statement

$$\int_0^1 \frac{d^2c}{dx^2} w \, dx = 0 \tag{A.25}$$

A different order of continuity is required for c than for w. To define these continuity requirements we need to introduce a classification for the degree of continuity of a function.

Order of Continuity

Assume a function f is discontinuous at discrete points but is finite throughout the region, its norm satisfying the following condition

$$\int f^2 \, dx < \infty \tag{A.26}$$

The function f is then said to be *square integrable*. If we impose conditions on the first derivative, the function is said to be a *first derivative square integrable* function and the following norm has to be bounded

$$\int \left\{ f^2 + \left(\frac{df}{dx} \right)^2 \right\} dx < \infty \tag{A.27}$$

We can continue defining higher order continuity. For example, functions whose *second derivative* is *square integrable* have the following norm

$$\int \left\{ f^2 + \left(\frac{df}{dx} \right)^2 + \left(\frac{d^2 f}{dx^2} \right)^2 \right\} dx < \infty \tag{A.28}$$

The above definitions can be extended to two and three dimensional problems by replacing the scalar products with vector products.

Thus the approximating function c in equation A.25 needs to be second derivative square integrable while the weighting function w is required only to be square integrable. In many cases it is preferable to reduce the order of continuity required for c and this can be done by integrating by parts. Consider equation A.25 and integrate by parts

$$\int_0^1 \frac{d^2 c}{dx^2} w \, dx = - \int_0^1 \frac{dc}{dx} \frac{dw}{dx} \, dx + \left[\frac{dc}{dx} w \right]_0^1 \tag{A.29}$$

This is the weak formulation. Now both functions c and w need to be continuous up to their first derivatives. Therefore we can take a set of first derivative square

integrable basis functions for c and dc/dx

$$c = c_1\phi_1 + c_2\phi_2 + \cdots \tag{A.30}$$

$$w = \delta c = \delta c_1\phi_1 + \delta c_2\phi_2 + \cdots \tag{A.31}$$

The weak formulation is the basis for the Finite Element Method. The generalized weak formulation, and additional concepts to obtain the FEM formulation are given in following section.

A.5 The Weak Formulation

The finite element method is based upon the weak formulation of the governing partial differential equation. The weak formulation is obtained by integrating the original equation. If Dirichlet boundary conditions are given and the approximate functions satisfy them the functions w also identically satisfy these conditions. One must take into account the remaining two residual functions

$$R = \mathcal{L}(c) \quad \text{in the domain } \Omega \tag{A.9}$$

$$R_2 = q - \bar{q} \quad \text{on the } \Gamma_2 \text{ part of the boundary} \tag{A.11}$$

A general weighted residual for a Laplacian operator, for any number of dimensions, is

$$\int_\Omega (\mathcal{L}(c))w \, \mathrm{d}\Omega = \int_{\Gamma_2} (q - \bar{q})w \, \mathrm{d}\Gamma \tag{A.32}$$

Integrating the operator $\mathcal{L}(\,)$ gives

$$\int_\Omega \frac{\partial c}{\partial x_i}\frac{\partial w}{\partial x_i} \, \mathrm{d}\Omega = \int_\Gamma qw \, \mathrm{d}\Gamma \tag{A.33}$$

where the operator of c and w is of a reduced order, q is a derivative of the dependent variable on the boundary, Ω is the interior domain and Γ the boundary. x_i are the Einstein summation indices defined in equations A.2

The right hand side of the equation is a boundary flux term. On the left hand side are interior domain terms, which are integrated through domain discretisation. Integration is performed over each individual element at collocation points. The values at overlapping nodes on adjacent elements are combined to assemble a global matrix. The matrix equation obtained may be solved using standard methods. Details of FEM implementation may be found in the text by Reddy.[19]

The method considered so far utilises an approximate function which satisfies the Dirichlet boundary conditions of the system and is approximate in the domain, not satisfying exactly the governing equations. The remaining Neumann boundary condition is also approximate. This is the most common method used in FEM, although it is alternatively possible to use a solution which satisfies the Neumann condition.

In contrast, the Boundary Element Method is a formulation which is exact in the domain, using an approximate function for both boundary conditions. This is briefly outlined in the following section.

A.6 The Inverse Formulation

The Boundary Element Method is based upon the inverse formulation (also known as the strong formulation) of the governing partial differential equation; where the equation is integrated twice. This process has the effect of transferring the Laplacian operator from the problem variable (the concentration in electrochemistry problems) to the weighting function. Both boundary conditions are approximate and three residuals are considered

$$R = \mathcal{L}(c) \quad \text{in the domain } \Omega \tag{A.9}$$

$$R_1 = c - \bar{c} \quad \text{on the } \Gamma_1 \text{ part of the boundary} \tag{A.10}$$

$$R_2 = q - \bar{q} \quad \text{on the } \Gamma_2 \text{ part of the boundary} \tag{A.11}$$

Taking a weighted residual approach for any dimension Laplace equation over an arbitrary domain gives

$$\int_{\Omega}(\mathcal{L}(c))w\,\mathrm{d}\Omega = \int_{\Gamma_2}(q-\bar{q})w\,\mathrm{d}\Gamma - \int_{\Gamma_1}(c-\bar{c})\frac{\partial w}{\partial n}\,\mathrm{d}\Gamma \tag{A.34}$$

This generalised equation uses residual approximations for the domain, Ω, and both boundaries, Γ_1, Γ_2. Integrating twice produces the inverse form

$$\int_{\Omega}\mathcal{L}(w)c\,\mathrm{d}\Omega = \int_{\Gamma_1}\bar{c}\frac{\partial w}{\partial n}\,\mathrm{d}\Gamma + \int_{\Gamma_2}c\frac{\partial w}{\partial n}\,\mathrm{d}\Gamma - \int_{\Gamma_1}qw\,\mathrm{d}\Gamma - \int_{\Gamma_2}\bar{q}w\,\mathrm{d}\Gamma \tag{A.35}$$

The right-hand side terms may be combined to give

$$\int_{\Omega}\mathcal{L}(w)c\,\mathrm{d}\Omega = \int_{\Gamma}c\frac{\partial w}{\partial n}\,\mathrm{d}\Gamma - \int_{\Gamma}qw\,\mathrm{d}\Gamma \tag{A.36}$$

where it is implicitly assumed that $\bar{c}$ and $\bar{q}$ are substituted on their respective boundaries.

This is the inverse form used in the BEM derivation in chapter 2.

The resulting operator which acts on $w(x)$ is called the adjoint operator, $\mathcal{L}^*$. In this case $\mathcal{L} = \mathcal{L}^*$, therefore $\mathcal{L}$ is self-adjoint or symmetric.

It is common in BEM literature to see the inverse form written in a more concise manner using inner product notation. An inner product is defined as

$$< a, b >= \int_{\Omega} ab\,\mathrm{d}\Omega \tag{A.37}$$

where a and b arbitrary functions.

We also define

$$B = \int_{\Gamma}c\frac{\partial w}{\partial n}\,\mathrm{d}\Gamma - \int_{\Gamma}qw\,\mathrm{d}\Gamma \tag{A.38}$$

which gives

$$< W(x), \mathcal{L}c(x) > = B + < c(x), \mathcal{L}^*W(x) > \tag{A.39}$$

where B are the boundary integrals.

This equation is the basis of the Boundary Element Method. To obtain the direct BEM formulation (also known as the singular BEM) the weighting function is chosen such that it satisfies the governing partial differential equation and the residual over the domain, R, is zero. Thus the formulation is exact over the domain. This type of weighting function is known as a fundamental solution.

The implementation of the direct BEM is described in detail in chapter 2 on page 48.

A.7 Classification of Approximate Methods

The mathematical aspects of the formulation of three approximate methods has been compared in this appendix. The fundamental difference between all these methods may be summarised based upon the initial treatment of the governing partial differential equation.

Taking the Poisson equation as an example

$$\mathcal{L}(c) - b = 0 \tag{A.40}$$

the weighted residual statements can be classified as follows:

i Weighted Residual Statement

$$\int_\Omega (\nabla^2 c - b) w \, \mathrm{d}\Omega = \int_{\Gamma_2} (q - \overline{q}) w \, \mathrm{d}\Gamma - \int_{\Gamma_1} (c - \overline{c}) \frac{\partial w}{\partial n} \, \mathrm{d}\Gamma \tag{A.41}$$

ii Weak Formulation

$$\int_\Omega \frac{\partial c}{\partial x_k} \frac{\partial w}{\partial x_k} \, \mathrm{d}\Omega + \int_\Omega b w \, \mathrm{d}\Omega = \int_{\Gamma_2} \overline{q} w \, \mathrm{d}\Gamma + \int_{\Gamma_1} q w \, \mathrm{d}\Gamma + \int_{\Gamma_1} (c - \overline{c}) \frac{\partial w}{\partial n} \, \mathrm{d}\Gamma \tag{A.42}$$

iii Inverse Statement

$$\int_{\Omega}(\nabla^2 w)c\,\mathrm{d}\Omega - \int_{\Omega} bw\,\mathrm{d}\Omega = -\int_{\Gamma_2}\overline{q}w\,\mathrm{d}\Gamma - \int_{\Gamma_1} qw\,\mathrm{d}\Gamma + \int_{\Gamma_2} c\frac{\partial w}{\partial n}\,\mathrm{d}\Gamma + \int_{\Gamma_1}\overline{c}\frac{\partial w}{\partial n}\,\mathrm{d}\Gamma \tag{A.43}$$

Another essential difference between techniques lies in the type of basis function used for the approximation c and for the weighting w. We can divide numerical methods according to those for which the same basis functions are used for c and w and those for which they are different.

1. *Finite Differences* Normally one has different basis functions for c and w, the latter being taken in the form of Dirac delta functions. Most FDM schemes are based on statement (i).

2. *Finite Elements* Usually the same basis functions for c and w are taken to obtain symmetric matrices. FEM schemes are based on weak formulations (ii).

3. *Boundary Elements* Boundary element schemes are based on inverse statement (iii). For weighting functions w they use a set of basis functions which enable elimination of the domain integrals and reduce the problem to a boundary only system. These functions (for the direct BEM technique) are known as fundamental solutions.

References

[1] Bard, A. J.; Faulkner, L. R. *Electrochemical Methods.* Wiley, New York, 1980.

[2] Greef, R.; *et al. Instrumental Methods in Electrochemistry.* Wiley, New York, 1985.

[3] Mackerle, J.; Brebbia, C. A. (Eds.). *The Boundary Element Reference Book.* Computational Mechanics Publications, 1988.

[4] Tuckerman, M.; Martyna, G. *J. Electroanal. Chem.*, **104**, (2000), 159.

[5] Feldberg, S. W. *Anal. Chem.*, **3**, (1964), 199.

[6] Britz, D. *Digital Simulation in Electrochemistry.* 2nd edition. Springer-Verlag, Berlin, 1988.

[7] Speiser, B. *J. Electroanal. Chem.*, **19**, (1996), 1.

[8] Bieniasz, L. *Computers Chem.*, **21**, (1997), 1.

[9] Rudolph, M.; Reddy, D. P. *Anal. Chem.*, **66**, (1994), 589A.

[10] Dai, W.; Nassar, R. *Numer. Meth. Partial Differ. Equations*, **14**(2), (1998), 159.

[11] Rubenstein, I. (Ed.). *Physical Electrochemistry*, pp. 209–242. Marcel Dekker, New York, 1995.

[12] Gavaghan, D. J. *J. Electroanal. Chem.*, **420**, (1997), 147.

[13] Foster, I. *Designing and Building Parallel Programs.* Addison-Wesley, Reading Mass., 1995.

[14] Gropp, W.; Lusk, E.; Skjellum, A. *Using MPI: Portable Parallel Programming with the Message Passing Interface.* MIT Press, Cambridge, MA, 1995.

[15] Pacheco. *Parallel Programming with MPI.* Morgan Kaufmann, San Diego, CA, 1996.

[16] Gavaghan, D. J. *J. Electroanal. Chem.*, **456**, (1998), 1.

[17] Mastin, C. W. *J. Comput. Phys.*, **47**, (1982), 1.

[18] Angus, J. N. Internal report. Chemistry Department, University of Southampton, Southampton, United Kingdom., 1998.

[19] Reddy, J. N. *An Introduction to the Finite Element Method.* 2nd edition. McGraw-Hill, New York, 1993.

[20] Penczek, M.; Stojek, Z.; Osteryoung, J. *J. Electroanal. Chem.*, **181**, (1984), 83.

[21] Moorhead, E. D.; Stephens, M. M. *J. Electroanal. Chem.*, **282**, (1990), 1.

[22] Brebbia, C. A.; Wrobel, L. C.; Telles, J. C. F. *Boundary Element Techniques.* Springer-Verlag, 1984.

[23] Brebbia, C. A.; Walker, S. *Boundary Element Techniques in Engineering.* Newnes-Butterworths, London, 1980.

[24] Frey, P. J.; George, P. L. *Mesh Generation. Application to Finite Elements.* Hermes Science, Oxford, 2000.

[25] Brebbia, C. A. (Ed.). *Adaptive Finite and Boundary Elements.* Computational Mechanics Publications, 1988.

[26] Sladek, V.; Sladek, J. *Singular Integrals in Boundary Element Methods.* Computational Mechanics Publications, 1998.

[27] Brebbia, C. A.; Wrobel, L. C. *Boundary Element Methods in Heat Transfer.* Computational Mechanics Publications, Southampton, 1992.

[28] Hall, W. S. *The Boundary Element Method.* Kluwer, 1994.

[29] Paris, F.; Canas, J. *Boundary Element Method, Fundamentals and Applications.* Oxford University Press, Oxford, 1997.

[30] Queiros, M. A.; Daschbach, J. L. (Eds.). *Microelectrodes: Theory and Applications*, volume 197 of *NATO ASI Series E.* Kluwer Academic, Dordrecht, 1991.

[31] Denuault, G. *Chemistry and Industry*, **18**, (1996), 678.

[32] *Encyclopaedia Britannica.* 10 edition. Merriam-Webster, 1994.

[33] Fraleigh, J. B. *Calculus with Analytical Geometry.* 3rd edition. Addison-Wesley, Reading Mass., 1990.

[34] Crank, J. *Mathematics of Diffusion.* Oxford University Press, Oxford, 1975.

[35] Kreyszig, E. *Advanced Engineering Mathematics.* 8th edition. Wiley, New York, 1999.

[36] Weltner, K.; *et al. Mathematics for Engineers and Scientists.* Stanley Thornes, Cheltenham, 1986.

[37] Widder, D. V. *The Laplace Transform.* Princeton University Press, New Jersey, 1941.

[38] Smith, G. D. *Numerical Solution of Partial Differential Equations: Finite Difference Methods.* 2nd edition. Clarendon, Oxford, 1979.

[39] Doetsch, G. *Laplace Transformation.* Dover, New York, 1953.

[40] Roberts, G. E.; Kaufman, H. *Tables of Laplace Transforms.* Saunders, Philadelphia, 1966.

[41] Erdelyi, A.; Magnus, W. *Tables of Integral Transforms.* McGraw-Hill, New York, 1954.

[42] Bieniasz, L. K. *J. Electroanal. Chem.*, **345**, (1993), 13.

[43] Nagy, G.; Sugimoto, Y.; Denuault, G. *J. Electroanal. Chem.*, **433**, (1997), 167.

[44] Brebbia, C. A.; Dominguez, J. *Boundary Elements, An Introductory Course.* 2nd edition. Computational Mechanics Publications, 1992.

[45] Ruzic, I. *J. Electroanal. Chem.*, **189**, (1986), 432.

[46] Shoup, D.; Szabo, A. *J. Electroanal. Chem.*, **199**, (1986), 437.

[47] Bieniasz, L. K.; Osterby, O.; Britz, D. *J. Electroanal. Chem.*, **21**(6), (1998), 391.

[48] Heinze, J.; Storzbach, M.; Mortensen, J. *J. Electroanal. Chem.*, **165**, (1984), 61.

[49] Britz, D.; *et al. J. Electroanal. Chem.*, **240**, (1988), 27.

[50] Marques da Silva, B.; Avaca, L. A. *J. Electroanal. Chem.*, **269**, (1989), 1.

[51] Feldberg, S. W. *J. Electroanal. Chem.*, **290**, (1990), 49.

[52] Lerke, S. A.; Evans, D. H.; Feldberg, S. W. *J. Electroanal. Chem.*, **296**, (1990), 299.

[53] Compton, R.; Pilkington, M. B. G.; Stearn, G. M. *J. Chem. Soc. Faraday. Trans.*, **84**, (1988), 2155.

[54] Fisher, A. C.; Compton, R. G. *J. Phys. Chem.*, **95**, (1991), 7538.

[55] Rudolph, M. *J. Electroanal. Chem.*, **314**, (1991), 13.

[56] Rudolph, M. *J. Electroanal. Chem.*, **338**, (1992), 85.

[57] Mocak, J.; Feldberg, S. W. *J. Electroanal. Chem.*, **378**, (1994), 17.

[58] Rudolph, M. *J. Electroanal. Chem.*, **503**, (2001), 15.

[59] Heinze, J. *J. Electroanal. Chem.*, **124**, (1981), 73.

[60] Amphlett, J. L. *Numerical Simulation of Microelectrodes.* Ph.D. thesis, University of Southampton, United Kingdom, 2000.

[61] Unwin, P.; Bard, A. J. *J. Phys. Chem.*, **96**, (1991), 7814.

[62] Unwin, P.; Bard, A. J. *J. Phys. Chem.*, **96**, (1991), 5035.

[63] Unwin, P.; Mirkin, M.; Bard, A. J. *J. Phys. Chem.*, **96**, (1992), 1861.

[64] Demaille, C.; Unwin, P.; Bard, A. J. *J. Phys. Chem.*, **100**, (1996), 14137.

[65] Taylor, G.; Girault, H. *J. Electroanal. Chem.*, **293**, (1990), 19.

[66] Amphlett, J. L. *J. Phys. Chem. B.*, **102**(49), (1998), 9946.

[67] Stone, H. L. *J. Numer. Anal.*, **5**, (1968), 530.

[68] Compton, R. G.; *et al. J. Electroanal. Chem.*, **383**, (1995), 13.

[69] Alden, J. A.; *et al. J. Electroanal. Chem.*, **389**, (1995), 45.

[70] Alden, J. A.; Compton, R. G. *J. Electroanal. Chem.*, **402**, (1996), 1.

[71] Paddon, D. J.; Holstein, H. *Multigrid methods for integral and differential equations.* Clarendon Press, Oxford, 1983.

[72] Alden, J. A.; Compton, R. G. *J. Electroanal. Chem.*, **415**, (1996), 1.

[73] Bard, A.; Denuault, G.; *et al. Anal. Chem.*, **63**, (1991), 1282.

[74] Alden, J. A.; Compton, R. G. *J. Phys. Chem. B.*, **101**, (1997), 8941.

[75] Alden, J. A.; Compton, R. G. *J. Phys. Chem. B.*, **101**, (1997), 9606.

[76] Nagy, G.; Denuault, G. *J. Electroanal. Chem.*, **433**, (1997), 175.

[77] Abercrombie, S. C. B. Chemistry Department, University of Southampton, Southampton, United Kingdom. Personal Communication.

[78] Whiting, L.; Carr, P. J. *J. Electroanal. Chem.*, **81**, (1977), 1.

[79] Villadsen, J. V.; Stewart, W. E. *Chem. Eng. Sci.*, **22**, (1967), 1483.

[80] Hertl, P.; Speiser, B. *J. Electroanal. Chem.*, **217**, (1987), 225.

[81] Urban, P.; Speiser, B. *J. Electroanal. Chem.*, **241**, (1988), 17.

[82] Villadsen, J. V.; Michelsen, M. L. *Solution of Differential Equation Models by Polynomial Approximation.* Prentice-Hall, New Jersey, 1987.

[83] Bieniasz, L. K.; Britz, D. *Acta Chem. Scand.*, **47**, (1993), 757.

[84] Ferrigno, R.; Brevet, P. F.; Girault, H. H. *Electrochemica Acta.*, **42**, (1997), 1895.

[85] Fleig, J.; Maier, J. *Solid State Ionics*, **94**, (1997), 199.

[86] Fulian, Q.; Fisher, A. C. *J. Phys. Chem. B.*, **102**, (1998), 9647.

[87] Alden, J.; Compton, R. *Anal. Chem.*, **72**(5), (2000), 198A.

[88] Alden, J.; Compton, R. *J. Electroanal. Chem.*, **402**, (1996), 1.

[89] Amatore, C. A.; Fosset, B. *J. Electroanal. Chem.*, **328**, (1992), 21.

[90] Tait, R. J.; *et al. J. Electroanal. Chem.*, **256**, (1993), 25.

[91] Gavaghan, D. J. *J. Electroanal. Chem.*, **456**, (1998), 13.

[92] Gavaghan, D. J. *J. Electroanal. Chem.*, **456**, (1998), 25.

[93] Bartlett, P.; Taylor, S. *J. Electroanal. Chem.*, **453**, (1998), 49.

[94] Nann, T.; Heinze, J. *Electrochem. Commun.*, **1**, (1999), 289.

[95] Harriman, K.; *et al. Electrochem. Commun.*, **2**, (2000), 150.

[96] Harriman, K.; *et al. Electrochem. Commun.*, **2**, (2000), 163.

[97] Reddy, J. N.; Gartling, D. K. *The Finite element method in heat transfer and fluid dynamics.* CRC Press, London, 1994.

[98] Banerjee, P.; Butterfield, R. *Boundary Element Methods in Engineering Science.* McGraw-Hill, London, 1981.

[99] Fulian, Q.; Fisher, A. C.; Denuault, G. *J. Phys. Chem. B.*, **103**, (1999), 4387.

[100] Fulian, Q.; Fisher, A. C.; Denuault, G. *J. Phys. Chem. B.*, **103**, (1999), 4393.

[101] Partridge, P. W.; Brebbia, C. A.; Wrobel, L. C. *The Dual Reciprocity Boundary Element Method.* Computational Mechanics Publications, Southampton, 1992.

[102] Qiu, F. L.; Fisher, A. C. *Electrochem. Commun.*, **2**, (2000), 738.

[103] Ramachandran, P. A. *Boundary Element Methods in Transport Phenomena.* Computational Mechanics Publications, Southampton, 1994.

[104] Joslin, T.; Pletcher, D. *J. Electroanal. Chem.*, **49**, (1974), 171.

[105] Fleischmann, M.; *et al. J. Electroanal. Chem.*, **263**(2), (1989), 225.

[106] Denuault, G.; *et al. J. Electroanal. Chem.*, **280**(2), (1990), 243.

[107] Denuault, G.; Pletcher, D. *J. Electroanal. Chem.*, **305**(1), (1991), 131.

[108] Gavaghan, D. J.; Rollett, J. S. *J. Electroanal. Chem.*, **295**, (1990), 1.

[109] Michael, A. C.; Wightman, R. M.; Amatore, C. A. *J. Electroanal. Chem.*, **267**, (1989), 33.

[110] Deakin, M. R.; Wightman, R. M.; Amatore, C. A. *J. Electroanal. Chem.*, **215**, (1986), 49.

[111] Safford, L. K.; Weaver, M. J. *J. Electroanal. Chem.*, **312**, (1991), 69.

[112] Verbrugge, M. W.; Baker, D. R. *J. Phys. Chem.*, **96**, (1992), 4572.

[113] Diao, G.; Zhang, Z. *J. Electroanal. Chem.*, **437**, (1997), 17.

[114] Papamichael, N. *J. Comput. Appl. Math.*, **28**, (1989), 63.

[115] Howell, L. H. *J. Comput. Appl. Math.*, **46**, (1993), 7.

[116] Delillo, T. K. *SIAM J. Numer. Anal.*, **31**(3), (1994), 788.

[117] Sparis, P. D. *J. Comput. Phys.*, **61**, (1985), 445.

[118] Papamichael, N.; Stylianopoulos, N. S. *Constr. Approx.*, **7**, (1991), 349.

[119] Harriman, K.; *et al. Electrochem. Commun.*, **2**, (2000), 157.

[120] Harriman, K.; *et al. Electrochem. Commun.*, **2**, (2000), 567.

[121] Ruppert, J. *Journal of Algorithms*, **18**(3), (1995), 548.

[122] Shewchuk, J. R. In Lin, M. C.; Manocha, D. (Eds.), *Applied Computational Geometry: Towards Geometric Engineering*, volume 1148 of *Lecture Notes in Computer Science*, p. 203. Springer-Verlag, 1996.

[123] Kita, E.; Kamiya, N. *Eng. Anal. Bound. Elem.*, **25**, (2001), 479.

[124] Kincaid, D.; Cheney, W. *Numerical Analysis, Mathematics of Scientific Computing.* 2nd edition. Brooks Cole, Pacific Grove, CA, 1996.

[125] Wrobel, L. C.; DeFigueiredo, D. B. *Eng. Anal. Bound. Elem.*, **8**(6), (1991), 312.

[126] Chen, K. *Eng. Anal. Bound. Elem.*, **23**, (1999), 639.

[127] Harriman, K.; *et al. Electrochem. Commun.*, **2**, (2000), 576.

[128] Galceran, J.; Taylor, S.; Bartlett, P. *J. Electroanal. Chem.*, **476**(2), (1999), 132.

[129] Galceran, J.; Taylor, S.; Bartlett, P. *J. Electroanal. Chem.*, **506**(2), (2001), 65.

[130] Stroud, A. H.; Secrest, D. *Gaussian Quadrature Formulas.* Prentice-Hall, New York, 1966.

[131] Telles, J. C. F. *Int. J. Numer. Meth. Eng.*, **24**, (1989), 959.

[132] Galceran, J.; Gavaghan, D.; Rollett, J. *J. Electroanal. Chem.*, **394**, (1995), 17.

[133] Liapis, S. *Eng. Anal. Bound. Elem.*, **14**, (1994), 315.

[134] Kita, E.; Kamiya, N. *Advances in Engineering Software*, **19**, (1994), 21.

[135] Yu, D. *Comput. Meth. Appl. Mech. Eng.*, **91**, (1991), 1237.

[136] Babuska, I.; *et al. Modeling, Mesh Generation, and Adaptive Numerical Methods for Partial Differential Equations.* Springer-Verlag, New York, 1995.

[137] Budd, T. *An Introduction to Object-oriented Programming.* 2nd edition. Addison-Wesley, Reading Mass., 1996.

[138] Riel, A. J. *Object-Oriented Design Heuristics.* Addison-Wesley, Reading Mass., 1996.

[139] Coplien, J. *Multi-Paradigm Design for C++.* Addison-Wesley, Reading Mass., 1998.

[140] Stroustrup, B. *The C++ Programming Language.* 3rd edition. Addison-Wesley, Reading Mass., 1997.

[141] Josuttis, N. M. *The C++ Standard Library.* Addison-Wesley, Reading Mass., 1999.

[142] Flanagan, D. *Java in a Nutshell.* 2nd edition. O'Reilly, Sebastopol, CA, 1997.

[143] Press, W. H.; *et al. Numerical Recipes in C: The Art of Scientific Computing.* 2nd edition. Cambridge University Press, Cambridge, 1993.

[144] Perry, G. *C by Example.* Que, Indianapolis, 1993.

[145] Amatore, C.; *et al. J. Electroanal. Chem.*, **500**, (2001), 62.

[146] Amatore, C. A.; Fosset, B.; *et al. Anal. Chem.*, **63**, (1991), 306.

[147] Taylor, S. L. *Modelling microelectrode and microbiosensor responses through computer simulation.* Ph.D. thesis, University of Southampton, United Kingdom, 1998.

[148] Origin 6.0. OriginLab Corporation, www.originlab.com. Software used for contour map interpolation.

[149] Rubenstein, I. (Ed.). *Physical Electrochemistry*, pp. 131–207. Marcel Dekker, New York, 1995.

[150] Prieto, F.; *et al. Electroanalysis*, **11**(8), (1999), 541.

[151] Alden, J. A.; *et al. Anal. Chem.*, **70**, (1998), 1707.

[152] Windsor Scientific. www.windsor-ltd.co.uk.

[153] Amatore, C. A.; Fosset, B.; *et al. Anal. Chem.*, **63**, (1991), 1403.

[154] Niwa, O.; Morita, M.; Tabei, H. *J. Electroanal. Chem.*, **267**, (1989), 291.

[155] Amatore, C.; *et al. Anal. Chem.*, **68**(17), (1996), 2951.

[156] Aoki, K.; *et al. J. Electroanal. Chem.*, **256**, (1988), 269.

[157] Brebbia, C. A. (Ed.). *Boundary Element Methods in Engineering.* Springer-Verlag, Berlin, 1982.

[158] Wrobel, L. C.; Berbbia, C. A.; Nardini, D. *Finite Elements in Water Resources VI.* Computational Mechanics Publications, Southampton, 1986.

[159] Wrobel, L. C.; Telles, J. C. F.; Berbbia, C. A. *Boundary Elements VIII.* Computational Mechanics Publications, Southampton, 1986.

[160] Nardini, D.; Brebbia, C. A. *Topics in Boundary Element Research.* Springer-Verlag, Berlin, 1985.

[161] Wrobel, L. C.; Brebbia, C. A. *Comp. Meth. Appl. Mech. Eng.*, **65**, (1987), 147.

[162] Golberg, M. A.; Chen, C. S. *Boundary Elements Comm.*, **5**, (1994), 57.

[163] Karur, S. R.; Ramachandran, P. A. *Mathematical and Computer Modelling*, **20**, (1994), 59.

[164] Partridge, P. W.; Berbbia, C. A. *Comm. Appl. Numer. Meth.*, **6**(2), (1990), 83.

[165] Partridge, P. W.; Berbbia, C. A. *Computational Methods in Water Resources VIII.* Computational Mechanics Publications, Southampton, 1990.

[166] Nowak, A. J.; Partridge, P. W. *Eng. Anal. Bound. Elem.*, **10**, (1992), 155.

[167] Partridge, P. W.; Sensale, B. *Eng. Anal. Bound. Elem.*, **24**, (2000), 633.

[168] Ramachandran, P. A.; Balakrishnan, K. *Eng. Anal. Bound. Elem.*, **24**, (2000), 575.

[169] Balakrishnan, K.; Ramachandran, P. A. *Math. Comput. Model.*, **31**, (2000), 221.

[170] Bulgakov, V.; Sarler, B.; Kuhn, G. *Int. J. Numer. Meth. Engng.*, **43**, (1998), 713.

[171] Cooper, J. A.; Compton, R. G. *Electroanalysis*, **10**(3), (1998), 141.

[172] Ikeuchi, M.; Onishi, K. *Appl. Math. Model.*, **7**, (1983), 115.

[173] Partridge, P. W. *Eng. Anal. Bound. Elem.*, **24**, (2000), 519.

[174] Cheng, A. H.; Lafe, O.; Grilli, S. *Eng. Anal. Bound. Elem.*, p. 14.

[175] Yamada, T.; Wrobel, L. C.; Power, H. *Eng. Anal. Bound. Elem.*, **13**, (1994), 291.

[176] Partridge, P. W. *Eng. Anal. Bound. Elem.*, **14**, (1994), 349.

[177] Paddon, D. J.; Holstein, H. (Eds.). *Multigrid Methods for Integral and Differential Equations.* Clarendon Press, Oxford, 1985.

[178] Saad, Y.; Schultz, M. H. *SIAM J. Scient. Statist. Comput.*, **7**, (1986), 856.

[179] Compton, R. G.; *et al. J. Phys. Chem.*, **98**, (1994), 1270.

[180] Alden, J. A.; Compton, R. G.; Dryfe, R. A. W. *J. Appl. Electrochem.*, **26**, (1996), 865.

[181] Leveque, V. G. *Ann. Mines. Mem. Ser.*, **12**, (1928), 201.

[182] Ackerberg, R. C.; Patel, R. D.; Gupta, S. K. *J. Fluid. Mech.*, **86**, (1977), 49.

[183] Newman, J. *Electroanalytic Chemistry*, **6**, (1973), 187.

[184] Aoki, K. *J. Electroanal. Chem.*, **217**, (1987), 33.

[185] Zhu, S.; Zhang, Y. *Communications in Numerical Methods In Engineering*, **10**(5), (1994), 361.

[186] Singh, K. M.; Kalra, M. S. *Eng. Anal. Bound. Elem.*, **18**(2), (1996), 73.

[187] Lewis, R. W.; Morgan, K.; Zienkiewicz, O. C. (Eds.). *Numerical Methods in Heat Transfer*, chapter 5. Wiley, 1981.

[188] Hammer, P. C.; Marlowe, O. J.; Stroud, A. H. *Math. Comput.*, **10**, (1956), 130.

[189] Skylar, O.; Wittstock, G. Presentation. 2nd International Workshop on Scanning Electrochemical Microscopy, Southampton, United Kingdom, 2001.

[190] xUnit. www.xunit.org.

[191] Harold, E. R.; Means, W. S. *XML in a Nutshell.* O'Reilly, Sebastopol, CA, 2001.

Index

A

accuracy, 68, 85, 86, **123**, 134, 159, 160, 164
Ackerberg, 154
adaptive mesh, 6, 68, 112
adjoint, 50
adsorption, 48
Alternating Direction Implicit, 30
analytical
  approximation, 1
  solution, 1, 18, 19
Aoki, 155
approximate
  analytical solution, 2
  numerical method, 4, 8
approximating function, 133, **134**, 136, 142, 161, 169
  optimal, 136, 162
  proposed, 135
approximation
  function, 43
    global, 164
  theorem, 13
array, *see* microband, array
asymptotic expressions, 154
Augmented Thin Plate Spline, 135

B

backward difference, 23, 24
Backward Difference Method, 30
Backward Implicit Method, 46
basis function, 45, 125
bilinear interpolation, 89
boundary, 11
  downstream, 158
  upstream, 157
boundary condition, **11**, 18, 74, 78, 98, 152, 178
  abrupt change, 3
  Dirichlet, 12, 77
  double microband, 74, 77
  Neumann, 12, 77, 185
  Robin, 2, 12
  semi-infinite, 89
boundary element, 58
Boundary Element Method, 5, 33, 47, **48**
  accuracy, 85, 123
  adaptive mesh, 41
  analytical element, 42
  application to a simple case, 65
  background, 5
  chemical reaction, 36
  comparison with FDM and FEM, 34
  computational aspects, 70
  discretisation, 38
    optimisation, 110, 111
  formulation, 45
    three-dimensional, 173
  higher-order element, 42
  implementation, 54, 123
  infinite domain, 186
  input, 68
  introduction, 35
  limitations, 128, 187
  mesh, 186
  microband arrays, 100
  multiple region, 186
  optimisation, 41
  procedure, 48
  program, 70
  refinement, 123
  simulation, 8
  three-dimensional, 173
  transient, 8, 36, 169
  validation, 73, 98
Boundary Integral Equation, **53**, 55, 56, 137, 173
  discrete, 59, 123, 138, 139, 174
  formulation, 136
  three-dimensional, 173
boundary integration, 58
boundary layer, 98
boundary singularity, 2, 3, 35, 36, 38, 42, **68**, 186, *see* singularity
boundary value problem, 18

C

C, 72
C++, 70, 72, 181
central difference, 23, 24

channel flow, 15, 30, **147**, 151, 152, 154, 164
characteristic
  dimension, 100
  length, 8, 26
charging current, 8
chemical reaction term, 2
collector, 48, 76, 77, 102
commercial software, 2
complex
  geometry, 4, 5, 8
  system, 5
concentration, 64
  distribution, 10
  flux, *see* flux
  gradient, 10, 12, 22
  map, 120
  profile, 17, 23
concentration gradient, *see* flux
conformal
  mapping, 3, **40**, 68, 76, 93
Conjugant Gradient method, 45
conservation of matter, 75
constant
  element, **56**, 59, 125, 177
continuous, **17**, 80, 86, *see* discontinuous
contour map, 93
convection, 10–12, 15, 46, 133
convergence, 77, 84, 110
corner nodes, 127
Cottrell equation, 18
Crank-Nicolson, 29, 165, 171
current, 10, 11, **18**, 75, 77, 111, 153, 164
  dimensionless, 27
cyclic voltammetry, 184

D

degree of freedom, 2
Delauney triangulation, 41
density
  gradient, 11
  of elements, 88
  of points, 3, 68
diagonally dominant, 70
diffusion, 10
  controlled, 8, 74, 75, 183
  equation, **12**, 19, 21, 24, 43, 165
  non-linear, 116
  steady state, *see* steady state
diffusion-convection
  analytical approximations, 154
  equation, dimensionless, 148
Digisim, 30
dimensionless parameters, 26, 75
Dirac delta function, 51, 60
directional cosine, 60
Dirichlet, *see* boundary condition, Dirichlet
discontinuous, 125, 178, *see* continuous
discretisation, 36, **58**, 68, 77, 87, 88, 133
  optimisation, 110, 111
domain, 11
  discretisation, 36, 46, 133
  external, 127, 186
  mesh, 173
domain integral term, 141
double microband, **73**, 74–76, 78, 92, 93, 100, 107, 120
  domain, 73
  raised, 116
  raised/recessed, 109, 110
    discretisation, 110
    electrode height, 112
  scan, 120
Du-Fort Frankel, 30
Dual Reciprocity Method, **130**, 165
  application to diffusion-convection equation, 142
  approximating function, 161
  background, 131
  boundary conditions, 152
  computational aspects, 144
  current, 153
  diffusion equation, 169
  formulation, 133, 141
  general method, 165
  internal point, 164
  introduction, 130
  mesh optimisation, 164
  program structure, 144
  simulation domain, 152
  three-dimensional, 166
  transient, 169
  validation, 154

E

electric field, 11
electroanalytical, 8, 11
electrochemical
  mechanism, 7, 14
  model, 1
  reaction, 74, *see* mechanism
  simulation, 2
    review, 29
  system, 2, 7
  technique, 7
electrochemistry
  theoretical, 1
electrode
  geometry, 8
  surface, 11
electrodeposition, 48

electron transfer, 9, 11
element, 58
elliptic integral, 77
engineering, 2, 5, 130
  mechanical, 5
equal spacing, 79
error-bounding, 40
excess electrolyte, 11
expanding mesh, *see* exponential mesh
experiment, 11
experimental technique, 7, 183
explicit, 24
Explicit Finite Difference, 22, 24, 25, 29
exponential
  mesh, **68**, 81, 85, 86
  spacing, 4, 80
extensible, 181
eXtensible Markup Language, 181

F

far field, 74, 80, 89
Fast Implicit Finite Difference, 30
Fast Quasi-Explicit Finite Difference, 30
feedback, **76**, 89, 95, 98, 107, 120, 156, 157, 164
Fick
  first law of diffusion, 12
  second law of diffusion, 12–14, 17, *see* diffusion equation
field point, 55
finite difference, 171, *see* Finite Difference Method
  simulation of DMB and TMB, 100
Finite Difference Method, 3, 5, **22**, 29, 47
  accuracy, 36
  algorithms, 29–31
  chemical reaction, 35
  comparison with FEM and BEM, 34
  conformal mapping, 40
  discretisation, 36
  distribution of points, 36
  exponential mesh, 39
  formulation, 44
  introduction, 34
  local approximation, 40
  matrix solvers, 31
  mesh, 68
  optimisation, 39
  three-dimensional, 3
    transient, 4
  transient, 35
  two-dimensional, 3
Finite Element Method, 4, 5, 32, **35**, 47
  adaptive mesh, 40
  chemical reaction, 35
  comparison with FDM and BEM, 34
  discretisation, 37
  formulation, 45
  higher order element, 41
  introduction, 35
  mesh, 68
  optimisation, 40
  transient, 35
fixed ratio, 81, 82
fixed shape, 81, 82
flow rate, **147**, 148, 150, 154, 162, 164
flux, 18, 64, *see* concentration gradient
  component, 127
  error, 66
  infinite, 3, 68
  internal point, 65
forced convection, 11
forward difference, **23**, 24, 171
free software, 2
free space Green's function, 45, *see* fundamental solution
fully populated, 144, 146
functional test, 181
fundamental solution, 36, 45, **51**, 52, 55, 151, 172
  diffusion-convection, 131, 165
  Laplace equation, 133
  one dimensional Laplace equation, 52
  three-dimensional, 174
  two dimensional, 60

G

Galerkin, 165, 171
  method, 45
galvanostatic, 7, 185
Gaussian
  elimination, 70
  quadrature, 61, 62
general solution, 18
generator, 48, 76, 77, 102
geometry coefficient, **55**, 126, 176
global
  approximating function, 136, 164
  matrix, 35, 45
grid, *see* mesh

H

Hammer's quadrature, 176
Heaviside step function, 51
hemi-cylindrical, 97, 107
heterogeneous reaction, 9, 10, **184**
higher order element, 70
Higher Order Thin Plate Spline, 135

hindered diffusion, 76, 117, *see* feedback
homogeneous reaction, 9–11, 15, 16, 38, 46, **184**
Hopscotch, 29
hydrodynamic, 11, 147

I

ideal geometry, 109
ill-conditioning, 70, 86
imaging, 120, *see* Scanning Electrochemical Microscope
implicit, 24
infinite
  array, 101
  diffusion field, 107
  domain, 42
  element, 41
  time, 107
influence coefficient, 63, 64
  matrix, 36, 45, **63**, 140, 176
    formulation, 63
initial condition, 12, 18
initial value problem, 18
inlaid, **74**, 88, 98, 109
instability, 154, 164, *see* stability
insulating block, 116, 117
insulator surface
  boundary condition, 78
integration, 175
Interdigitated Array, 100, *see* microband, array
interior, 11
  domain, 64
  nodes, 136
internal
  angle, 56
  domain integral, 133
  domain term, 133, 134
  point, **64**, 120, 144, 158–160, 164
    DRM distribution, 159
interpolation, 120, 131, **134**, 136, 140, 158, 161, 164, 172
inverse form, 45, **50**, 52, 133, 136
iR drop, 8

J

Jacobian, 175
Java, 70, 181

L

laminar flow, 147, 148
Laplace equation, 17, 75
  two dimensional, 55
Laplace Transform, 19–21, 165
Leveque approximation, **150**, 151, 154, 162, 164
Levich, 151
linear algebra solver, 64, **70**, 127, 144
linear element, 70, **123**, 125
lithography, 116, *see* manufacture, lithography
load vector, 45
local
  approximating function, 136
  mesh refinement, 86
logarithmic
  expansion, 80, *see* exponential mesh
  Gaussian quadrature, 60
LU decomposition, 45, 70, 146

M

manufacture, 109, 116
  lithography, 109
  sandwich, 109
manufacturing technique, 8
mass transport, 7, **10**, 147, 164
mass transport controlled, 11
mathematical model, 10–28
matrix
  inversion, 144, 146
  pre-conditioner, 146
  solver, *see* linear algebra solver
Matrix of Fundamental Solutions, 183
mechanism, 46, 183
mesh, 3, 68
  generation, 68, 69, 166, 173
  optimisation, 68
Method of Weighted Residuals, 43, *see* weighted residual
microband, 122, 147
  array, 100, 106
    collector surrounding a generator, 106
    collector-generator, 101
    infinite, 100
  multiple, 100
  novel configuration, 116, 118
  realistic geometry, 109
microdisc, 3, 8, 122
microelectrode, 8, 68, 101, 151, 169
migration, 10–12
mixed boundary condition, *see* boundary condition, Robin
model, 1
  electrochemical, *see* electrochemical, model
Multi Grid Method, 30
Multiquadric, 135

N
natural convection, 11, 97, 98
near-steady-state, 25
Nernst, 184
Nernst-Planck equation, 10, 12
Neumann, *see* boundary condition, Neumann
Newman, 155
non-linear, 2, 116
novel domain, 110
numerical
  integration, 60–62, 112, 176
  method, 1, 2, 181
    computational aspects, 181
  method formulation, 42

O
object-oriented, 70, 181
Orthogonal Collocation, 32
oscillation, 157, 158, 160, *see* instability
outward normal, 56, 175, 178

P
parabolic flow, **148**, 150, 162, 165
paradigm, 181
parallel computing, 4
partial differential equation, 14–17, 133
  analytical solution, 19
  coupled, 2
  diffusion-convection, 148, 165
  domain integral term, 141
  DRM form, 133, 169
  homogeneous, 14
  hyperbolic, 46, 165
  inverse form, *see* inverse form
  linear, 14
  method formulation, 42
  non-linear, 17
  parabolic, 46, 165
  second order, 14
  solution, 17–18
  strong form, *see* inverse form
  three-dimensional, 14
  weak form, *see* weak form
particular solution, 18, **134**, 164, 165
  series of, 134
Pascal's triangle, 135
Peclet number, 148, 150
planar diffusion, 14, 48, 177, 178
point collocation, 22
Poiseuille flow, 148
potential, 11
  gradient, 11
  step, 4, **7**, 11, 48, 74, 97, 183
  sweep, 7, 48
  waveform, 184
potentiostatic, 7, 100, 184
Pre-conditioned Krylov Subspace, 31
primitive, 173
  element, 32, 37
  shapes, 4
probe, 120

Q
quadrature, 60–62, 176
quasi-steady-state, 74, 76, 97

R
radial basis function, **135**, 136, 164, 165
Random Walk, 31
reaction
  heterogeneous reaction, *see* heterogeneous
  homogeneous reaction, *see* homogeneous
  layer, 4, 38
  second order, 16
rectangular mesh, 39
redox reaction, 4
reduction in dimensionality, 5, 36
regression testing, 181
regularity conditions, 186
Residual, 43
Robin, 184
rotating disc electrode, 8, 15, **147**, 151
roundoff, 98

S
sandwich manufacture, *see* manufacture, sandwich
Scanning Electrochemical Microscope, 3, 8, **76**, 98, 120
section element ratio, 82
self-adjoint, 50
semi-analytical solution, 2
semi-implicit, 30
semi-infinite boundary, 76, 78, 95, 156
series of particular solutions, *see* particular solution, series of
sifting property, 51, 52
simulation, 22
  electrochemical, *see* electrochemical, simulation
sine series, 135
singular integration, 60, 62, 111, 176
singularity, 60, *see* boundary singularity
sink, 78, 89

smooth, 56
source, 78, 89
source point, **52**, 55, 58
sparse matrix, 31, 34, 45
spectrochemistry, 48
stability, 25, *see* instability
    coefficient, 25, 29, 30
standard matrix solver, *see* linear algebra solver
steady state, 7, 8, 17, 25, 30, **48**, 76, 78, 97, 164
    diffusion-convection, 133
stiffness matrix, 45
Streamline-Diffusion Finite Element Method, 46
Strongly Implicit Procedure, 30, 46
substrate, 120, 121
surface
    element, 36, 173
    primitive, 5
symmetry, 3, 8, 107
system, 1
    electrochemical, *see* electrochemical, system

T

Taylor approximation, 34, 44
Telles transformation, 61
testing framework, 181
thermal gradient, 11
Thin Layer Cell, 8, **48**, 50, 54, 65, 75, 92, 93
    discretisation, 58
    domain, 54
Thin Plate Spline, 135
time integration, 169
timescale, 11
timestep, 24
transient, **7**, 12, 17, 24, 133, 169, 172
triple microband, 106, 107
true steady state, 74

U

unit test, 181

V

velocity coefficient, 148, 151
Von Neumann analysis, 26

W

weak form, 45
weighted residual, **32**, 42, 44, 50, 55, *see* Method of Weighted Residuals
Weighted Residual Method, 32, *see* Method of Weighted Residuals

X

XML, *see* eXtensible Markup Language
xUnit, 181